Dynamical Dark Energy Models

Christine Farrugia

University of Malta
Faculty of Science
Department of Mathematics

Supervisor:

Prof. Joseph Sultana

THESIS

submitted to the University of Malta
in accordance with the regulations for
admittance to the Degree of

DOCTOR OF PHILOSOPHY

2020

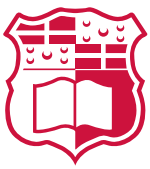

L-Università
ta' Malta

L-Università ta' Malta

FACULTY/INSTITUTE/CENTRE/SCHOOL Science

DECLARATION OF AUTHENTICITY FOR DOCTORAL STUDENTS

Student's Code _____

Student's Name & Surname Christine Farrugia

Course Doctor of Philosophy

Title of Dissertation/Thesis

Dynamical Dark Energy Models

(a) Authenticity of Thesis/Dissertation

I hereby declare that I am the legitimate author of this Thesis/Dissertation and that it is my original work.

No portion of this work has been submitted in support of an application for another degree or qualification of this or any other university or institution of higher education.

I hold the University of Malta harmless against any third party claims with regard to copyright violation, breach of confidentiality, defamation and any other third party right infringement.

(b) Research Code of Practice and Ethics Review Procedure

I declare that I have abided by the University's Research Ethics Review Procedures. Research Ethics & Data Protection form code _____.

☑As a Ph.D. student, as per Regulation 49 of the Doctor of Philosophy Regulations, I accept that my thesis be made publicly available on the University of Malta Institutional Repository.

□As a Doctor of Sacred Theology student, as per Regulation 17 of the Doctor of Sacred Theology Regulations, I accept that my thesis be made publicly available on the University of Malta Institutional Repository.

□As a Doctor of Music student, as per Regulation 26 of the Doctor of Music Regulations, I accept that my dissertation be made publicly available on the University of Malta Institutional Repository.

□As a Professional Doctorate student, as per Regulation 55 of the Professional Doctorate Regulations, I accept that my dissertation be made publicly available on the University of Malta Institutional Repository.

_____	CHRISTINE FARRUGIA	12 Oct. 2020
Signature of Student	Name in Full (in Caps)	Date

The research work disclosed in this publication is partially funded by the Endeavour Scholarship Scheme (Malta). Scholarships are part-financed by the European Union - European Social Fund (ESF) - Operational Programme II – Cohesion Policy 2014-2020 "*Investing in human capital to create more opportunities and promote the well-being of society*".

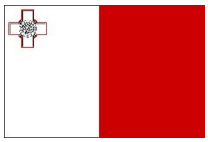

European Union – European Structural and Investment Funds
Operational Programme II – Cohesion Policy 2014-2020
"Investing in human capital to create more opportunities and promote the well-being of society"
Scholarships are part financed by the European Union - European Social Funds (ESF)
Co-financing rate: 80% EU Funds;20% National Funds

Abstract

Ever since it was discovered that the Universe is expanding at an accelerated rate, cosmologists have been searching for an explanation in the form of *dark energy*: a mechanism or physical component capable of producing this effect. The study presented here focuses on *dynamical dark energy* models, in which the observed acceleration arises as a result of either a cosmic component whose pressure is negative, or as a modification to the General Relativistic description of the geometry of the space-time manifold. The word 'dynamical' sets these models apart from the ΛCDM cosmology, in which the density of dark energy remains constant as the Universe expands.

Many works in the literature are based on the premise of a spatially flat Universe, and indeed this is what observational data appears to point to in a ΛCDM framework. The question naturally arises, however, whether the assumption of flatness continues to hold in the case of dynamical dark energy models, especially since spatial curvature is often correlated with dark energy parameters, and so any wrong assumptions about it could greatly distort our understanding of dark energy. The aim of this thesis is precisely to look for an answer to that question.

For the first part of the study, dark energy is modelled as a scalar field that can either be minimally or non-minimally coupled to the Ricci scalar, and a number of exact solutions to the cosmological field equations are presented. Each corresponds to a particular geometry – flat, open or closed. In the next part, analytical methods are combined with numerical techniques to analyse several models from the literature, chosen for their ability to represent the complete cosmic history. The aim is to investigate how spatial curvature influences the main features of the evolution. Initially, the Universe is assumed to consist of a Van der Waals fluid, but this alone cannot provide an explanation for the acceleration at late times, despite the fact that it accounts for the inflationary and matter-dominated epochs. Hence, dark energy is introduced as Quintessence, a Chaplygin gas or dynamical vacuum energy. It turns out that the transition from the inflationary epoch to the matter-dominated one would occur first for the open universe, and last for the closed one. The onset of late-time acceleration would also take place in this order. Furthermore, positive curvature is found to

enhance inflationary acceleration and the deceleration that follows. Among the fluid characteristics considered are the customary proportionality between energy density and pressure, and bulk viscosity.

The effects of spatial curvature on cosmic evolution are then investigated in the context of the *generalised running vacuum model* (GRVM) and its sub-cases. In the GRVM, the cosmological constant is replaced by a function of the Hubble parameter and its time derivative: $\Lambda(H) = A + BH^2 + C\dot{H}$ (A, B and C being constants). Two-parameter models are obtained by setting B or C equal to zero. The main goal is to find out if the models best describe observations when one assumes spatial flatness, or if the presence of curvature improves the fit. This is accomplished via a Markov Chain Monte Carlo (MCMC) analysis. The data set used comprises measurements of observables related to Type-Ia supernovae, cosmic clocks, baryon acoustic oscillations, the cosmic microwave background and redshift-space distortions (RSDs). Since it is well known that the data itself (rather than just the particular model) plays an important part in determining whether curvature is ruled out, the chapter draws comparisons between the constraints obtained in various scenarios, such as when RSD measurements are excluded (in contrast to when the full data set is employed). The lack of consensus within the scientific community about the value of the Hubble constant (H_0) is also taken into account. Two different values of H_0 from the literature are introduced and their effects on the results are investigated.

In the last part, the focus is shifted to an alternative theory of gravity – namely, $f(R)$ gravity, constructed by generalising the Ricci scalar in the Einstein-Hilbert action to a function thereof. Four $f(R)$ models are considered, all of which appear to be compatible with Solar-System and cosmological constraints: the Hu-Sawicki, Starobinsky, Exponential and Tsujikawa models. The idea is to see whether these models are able to accommodate non-zero spatial curvature (while still being consistent with cosmological observations). Since they all reduce to ΛCDM at high redshifts, any differences from ΛCDM are most likely to emerge at the level of perturbations. Therefore, the perturbation equations (in the sub-Hubble, quasi-static regime) are derived and incorporated into the analysis, which is again carried out using MCMC sampling techniques. Given that matter density perturbations are scale-dependent in $f(R)$ gravity, the results obtained for different values of $k_\dagger$ (the comoving wave number) are compared.

Conventions

- The metric signature is $(-,+,+,+)$;
- The unit system employed has $c = 1$ (c being the speed of light in vacuum);
- An overdot denotes differentiation with respect to cosmic time t;
- A prime denotes differentiation with respect to the argument;
- Plots are produced with $8\pi G/3$ set to unity (G is the Newtonian constant of gravitation). G is assigned standard units anywhere else;
- The Riemann curvature tensor takes the form

$$R^{\rho}{}_{\sigma\mu\nu} = \partial_\mu \Gamma^{\rho}_{\nu\sigma} - \partial_\nu \Gamma^{\rho}_{\mu\sigma} + \Gamma^{\rho}_{\mu\lambda}\Gamma^{\lambda}_{\nu\sigma} - \Gamma^{\rho}_{\nu\lambda}\Gamma^{\lambda}_{\mu\sigma} \ ;$$

- The Ricci tensor is derived from the Riemann tensor by summing over its first and third indices: $R_{\mu\nu} = R^{\lambda}{}_{\mu\lambda\nu}$.

Declaration

The work described in this thesis was carried out in the years $2015 - 2020$, when the author was a postgraduate research student at the Mathematics department of the Faculty of Science, University of Malta, under the supervision of Prof. Joseph Sultana.

The author declares that no part of the thesis has been submitted for any other degree. All research results and figures – unless explicitly marked with external references – are original, and the published material arising from the work presented here is indicated below.

Chapters 3 and 4 share content with the publications

- C. R. Farrugia and J. Sultana, *The effects of spatial curvature on cosmic evolution*, Int. J. Mod. Phys. D **26**, 1750115 (2017);
- C. R. Farrugia, J. Sultana and J. Mifsud, *Endowing Λ with a dynamic nature: Constraints in a spatially curved universe*, Phys. Rev. D **102**, 024013 (2020),

respectively.

Christine Farrugia
Candidate

Prof. Joseph Sultana
Supervisor

Acknowledgements

The journey has finally come to an end. And what a journey it's been! It has taught me to wonder at the boundlessness of knowledge, allowing me to appreciate the intricate scientific framework that humankind has constructed over the years, one equation at a time... and even bringing me face-to-face with its limitations.

A big thank-you goes to my travel companions – firstly, my supervisor, Prof. Joseph Sultana, for the opportunity to carry out research under his guidance, and especially for the insight he has given me into the subject. I am grateful for his unwavering professionalism and dedication.

I am also indebted to Prof. David Buhagiar, Head of the Department of Mathematics. He is one of the people to whom I owe my lecturing experience, and I truly admire his integrity.

Two colleagues I am obliged to are Jurgen Mifsud and Kris Grixti. Jurgen's help in getting to grips with Class and Monte Python was invaluable (as were the long Skype calls during which we tried to make head or tail of some unexpected result), and Kris assisted me with any problems encountered when running simulations on the super-computing cluster.

I am forever grateful to my family: my mum and dad, for financial (and emotional!) support, and my sisters, Katia and Marija, for making my life that much brighter. I did, indeed, stand on the shoulders of giants to get to this point.

Support came from my closest friends, too: Deandra, Jessica, Kimberly and Arielle (thank you for being genuine and caring!) Here I must also mention the significant number of people who at some time or other worked in the Advanced Physics Research Room (a.k.a. *Il-Kantina*). Although they are too many to include by name, I am indebted to you all for the shared laughter, the pranks, the conversations... and the memories I will treasure forever.

Last but definitely not least: my sincere thanks go to Jascha Schewtschenko, who always had time to help with code, or to offer insight into MCMC characteristics, or simply to hear me out, and who ranks among the smartest people I've encountered

so far (your ability to think outside the box is impressive!) But mostly, thank you for turning the journey into an adventure.

And finally, I cannot move on without mentioning two fluffy bundles of joy: Miċu, who spent so many hours sleeping by my side while I worked, and Milton, who generally slept as well but at times preferred to eat my notes.

The research work disclosed in this thesis was partially funded by the Endeavour Scholarship Scheme (Malta). Scholarships are part-financed by the European Union - European Social Fund (ESF) - Operational Programme II – Cohesion Policy 2014-2020, 'Investing in human capital to create more opportunities and promote the well-being of society'.

The research presented in Chapter 4 was carried out using computational facilities procured through the European Regional Development Fund, Project ERDF-080, 'A supercomputing laboratory for the University of Malta'.

The numerical part of the analysis for Chapter 5 was conducted with computing resources provided on the Sciama High Performance Compute (HPC) cluster, which is supported by the ICG, SEPNet and the University of Portsmouth.

'The most beautiful experience we can have is the mysterious.'

Albert Einstein

'Research is to see what everybody else has seen, and to think what nobody else has thought.'

Albert Szent-Györgyi

Contents

List of Figures

Symbols

t	Cosmic time
τ	Conformal time
x^i	Spatial coordinates; for an N-dimensional space-time manifold, $i = \{1, 2, \dots N-1\}$
x^μ	Temporal + spatial coordinates; $\mu = \{0, 1, \dots N-1\}$
$\vec{x}$	Spatial vector
d^4x	4-volume element
$\mathrm{d}s$	Line element
$g_{\mu\nu}$	Metric tensor
g	Determinant of metric tensor
$R^\sigma{}_{\mu\tau\nu}$	Riemann tensor
$R_{\mu\nu}$	Ricci tensor
R	Ricci scalar
δ^μ_ν	Kronecker delta
∂_μ	Partial derivative with respect to x^μ ($\partial_\mu = \partial/\partial x^\mu$)
∇_μ	Covariant derivative (along the tangent vector $\boldsymbol{e}_\mu = \partial/\partial x^\mu$)
$\vec{\nabla}_i$	Spatial covariant derivative
$\vec{\nabla}^2$	Laplace-Beltrami operator ($\vec{\nabla}^2 = \vec{\nabla}_i\vec{\nabla}^i$)
$\Box$	D'Alembert operator ($\Box = \nabla^\mu\nabla_\mu$)
S	Action
L	Field Lagrangian ($S = \int L\,\mathrm{d}t$)
$\mathcal{L}$	Lagrangian density ($L = \int \mathcal{L}\,\mathrm{d}^3x$)
$T_{\mu\nu}$	Energy-momentum tensor (with trace T)
$G_{\mu\nu}$	Einstein tensor ($G_{\mu\nu} = R_{\mu\nu} - Rg_{\mu\nu}/2$)
G	Newtonian constant of gravitation
$\mathcal{R}$	Cosmological scale factor
a	Normalised scale factor ($a = \mathcal{R}/\mathcal{R}_0$, where $\mathcal{R}_0$ is the present-day value of $\mathcal{R}$)
z	Cosmological redshift
H	Hubble parameter

H_0	Hubble constant (present-day value of H)
$\mathcal{H}$	Conformal/comoving Hubble parameter ($\mathcal{H} = aH$)
k	Normalised spatial curvature parameter ($k = \pm 1$ or 0)
κ	Spatial curvature parameter ($\kappa = k/\mathcal{R}_0^2$)
Λ	Cosmological constant
Ω_i	Density parameter; $i = \{$b (baryons), cdm (cold dark matter), r (radiation), Λ (vacuum energy), $\Lambda(H)$ (dynamical vacuum energy), k (spatial curvature)$\}$
Ω_i^0	Present-day value of the density parameter Ω_i
ρ_i	Rest-frame energy density of fluid i
p_i	Isotropic rest-frame pressure of fluid i
w_i	Equation-of-state parameter of fluid i ($w_i = p_i/\rho_i$)
$k_\dagger$	Comoving wave number

CHAPTER 1

Introducing Dark Energy

1.1 Evidence for Dark Energy

A few decades ago, the present-day Universe was thought to be mainly composed of matter. This would then have explained the supposedly decelerating cosmic expansion. In 1998, however, the High-z Supernova Search Team reported that luminosity distance measurements to a sample of Type Ia Supernovae (SNeIa) favoured an accelerating universe [1, 2]. The next year, the Supernova Cosmology Project published a study [3] which made use of the magnitude-redshift data for a number of SNeIa to constrain cosmological parameters. The team also found evidence of cosmic acceleration. For their leading role in 'the discovery of the accelerating expansion of the Universe through observations of distant supernovae', Saul Perlmutter, Brian P. Schmidt and Adam G. Riess were awarded the 2011 Nobel Prize in Physics [4].

Supernovae classified as Type Ia have optical spectra with two distinctive features: the absence of hydrogen lines, and the occurrence of a singly ionised silicon Si II absorption line at 615 nm [6]. They are thought to be thermonuclear explosions of white dwarf stars, with ignition taking place either when one of these stars has accreted enough mass from a nearby companion to exceed the Chandrasekhar limit, or when two white dwarfs collide [7]. SNeIa make it possible to probe the expansion history of the Universe by looking at how their (luminosity) distance[1] from us is related to their redshift. Whenever this relation departs from a pure Hubble law,[2] the difference (to lowest order in z) is proportional to the deceleration parameter, and can thus yield important information about the rate at which the Universe is expanding [2]. SNeIa are ideal in this regard because they act as *standard candles* – in the sense that their

[1] Refer to subsection 1.3.4.

[2] Hubble's law states that the observed recession velocity v of a galaxy is directly proportional to its distance d from us: $v = H_0 d$, where H_0 is the Hubble constant [8]. This law only holds for redshifts $z \ll 1$ [9].

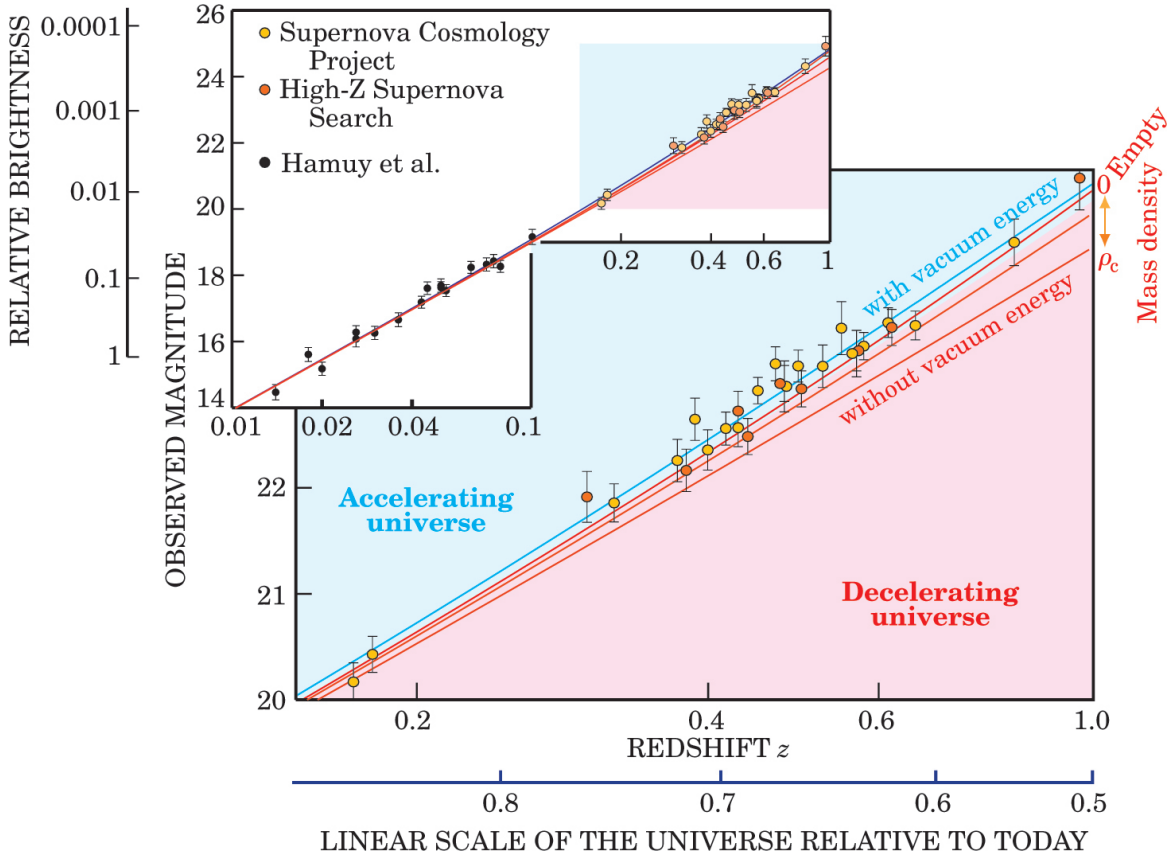

FIGURE 1.1: Observed magnitude versus redshift for distant and (in the inset) nearby Type Ia Supernovae. For clarity, measurements at the same redshift are combined. At redshifts beyond $z = 0.1$, the cosmological predictions (indicated by the curves) begin to diverge, depending on the assumed cosmic densities of matter and vacuum energy. The red curves represent models with zero vacuum energy and matter densities ranging from the critical density ρ_c (refer to subsection 1.3.4) down to zero (an empty cosmos). The model that best fits the data is represented by the blue line; it has a matter density of about $\rho_c/3$ plus a vacuum energy density that's twice as large, and hence corresponds to an accelerating universe.

homogeneity as a group means their intrinsic luminosity (or *absolute magnitude*) can be calibrated [7], and hence astronomers may readily find how distant they are by measuring their observed luminosity (called the *apparent magnitude*) [10].

The discovery that the Universe is currently accelerating ushered in the concept of *dark energy*. This is a form of energy which (unlike matter and radiation) is not gravitationally attractive, but instead gives rise to a repulsive effect. Furthermore, dark energy is thought to be homogeneously distributed, with a density of only about $10^{-27}\,\mathrm{kg\,m^{-3}}$ [11], so the prospect of detecting it directly is very low. The fact that it only interacts gravitationally, and not via any of the other fundamental forces, makes it even more elusive.

Additional evidence for dark energy comes directly from the cosmic microwave background (CMB). Fluctuations in the temperature of the CMB usually follow a Gaussian distribution. Recently, however, astronomers analysing data from the Atacama Cosmology Telescope in Chile discovered CMB fluctuations which deviate from this distribution. The phenomenon was attributed to gravitational lensing by large-scale structure (LSS). It was proposed that the degree of non-Gaussianity could shed light on whether dark energy really exists, because in its absence the lensing signal would be enhanced (mainly due to three reasons: firstly, CMB photons would spend a longer time at lower redshifts, where there is more LSS; secondly, the growth rate of LSS is higher in a universe with positive curvature and no dark energy, and thirdly, when no dark energy is present, projection effects tend to pick out fluctuations with longer wavelengths, which are larger for most lensing scales). Consequently, lensing data is able to break the geometric degeneracy of models that, despite having different expansion rates and spatial curvature, give rise to similar temperature power spectra and so cannot be distinguished using only primordial CMB measurements. The amount of lensing detected was found to favour cosmologies with dark energy over those that had none [12, 13].

The existence of dark energy is further evidenced by the Integrated Sachs-Wolfe (ISW) effect [15]. This is an effect experienced by CMB photons due to the temporal variation of the cosmic gravitational potential, and translates into a secondary anisotropy of the CMB [16]. Let us suppose that a CMB photon travelling across the Universe passes through a region where there is a galactic super-cluster. As it falls into the gravitational potential 'well' created by the strong gravity of the super-cluster, the photon's energy increases, and it is blue-shifted. If the gravitational potential is static, this energy gain is compensated for by the loss that occurs when the photon has to

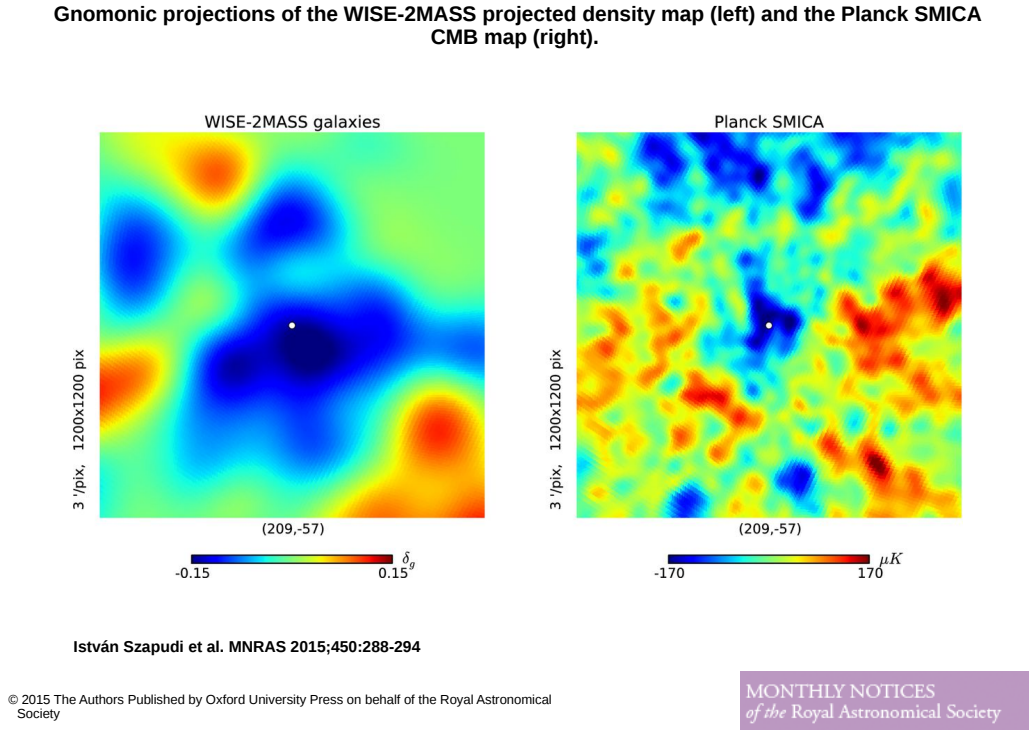

FIGURE 1.2: Comparison of the projected *WISE*-2MASS galaxy density field *(left)* with the *Planck* SMICA CMB map *(right)* reveals that one of the most significant cold spots of the CMB is aligned with a prominent large-scale under-density [14].

'climb out' of the well. However, the expansion of the Universe – driven by dark energy – causes the super-cluster to become less dense during the time it takes for the photon to travel through it. Consequently, the well becomes shallower, meaning that the energy the photon loses during exit is a little less than the amount gained on the way in. The light we receive from the corresponding region of the sky is thus slightly warmer than it would have been in the absence of the super-cluster [17].

As a result of successive additions and subtractions of energy (due to the presence of over- and under-dense regions), the path a photon travels from the last scattering surface to Earth may be characterised by a net rise or fall in temperature. This explains why *hot spots* in the CMB – regions with a higher-than-average temperature – correlate well with peaks in matter density. On the other hand, areas where the temperature is lower than average, called *cold spots*, are correlated with under-dense regions [17]. A typical example is depicted in Fig. 1.2.

1.2 Different Dark Energy Models

1.2.1 ΛCDM

Given the above-mentioned evidence, dark energy has to be somehow incorporated into a successful cosmological model, either as an actual component of the cosmic fluid or as a mechanism which arises from the geometry of the space-time manifold. One of the first dark energy models to be proposed was ΛCDM, constructed by adding a cosmological constant Λ – also known as *vacuum energy* – to Einstein's theory of General Relativity (GR).

As the name implies, the cosmological constant has an associated energy density ρ_Λ with fixed value: $\rho_\Lambda = -p_\Lambda = \Lambda/8\pi G$ [18], where p_Λ denotes the corresponding pressure. While the matter and radiation components are diluted by cosmic expansion, therefore, dark energy is not, and it eventually starts to dominate. This would then explain why we seem to be living in a dark-energy dominated epoch: the *WMAP* nine-year results suggest that in a flat ΛCDM universe, baryonic and dark matter only make up 28.65% of the cosmic fluid, with dark energy accounting for 71.35% [19]. Also assuming a flat ΛCDM cosmology, the *Planck* collaboration report a cosmic composition of 68.47% dark energy and 31.53% matter [20].

The addition of a cosmological constant was, in fact, initially considered by Einstein himself, albeit for a different purpose. At the time, observations of the Universe were mainly limited to the stars in our galaxy, and the available evidence suggested that the Universe was in a state of static equilibrium. In 1917, therefore, Einstein published a paper entitled 'Cosmological Considerations in the General Theory of Relativity', in which he proposed the addition of a new term to the field equations of GR as a means of counteracting the attractive force of gravity. Five years later, however, Friedmann derived a solution to Einstein's equations that appeared to imply an expanding universe. When Edwin Hubble verified this prediction observationally, Einstein dismissed the cosmological constant completely (refer to [21] and works cited therein). Indeed, he is reputed to have called it his 'biggest blunder'. Little did he know that it would be re-introduced many years later.

Despite providing a reasonably good fit to observational data,[3] ΛCDM is not without its shortcomings, especially on scales larger than the Solar System. Prominent among

[3] See, for instance, Refs. [19, 22] and [23].

these is the *smallness problem*, which refers to the fact that the theoretical value for Λ deduced in the framework of Quantum Field Theory is larger than the one derived from observations by a factor of $\sim 10^{120}$. This stems from the fact that zero-point energy calculations based on the assumption of a Planck-scale cutoff yield a vacuum energy density for bosonic fields [24] of $\sim 10^{111}\,\mathrm{J\,m^{-3}}$. On the other hand, the upper bound consistent with observations is of $\sim 10^{-9}\,\mathrm{J\,m^{-3}}$ [25]. Interestingly, Klauber mentions that if fermions are also taken into consideration when computing the theoretical estimate, the total vacuum energy density would be negative and of the same order as the observed value [24].

Another difficulty with ΛCDM is encountered when one considers that the matter energy density, notwithstanding the fact that it is a function of redshift, appears to be comparable to the density of dark energy at present. It is rather implausible that this should have happened purely by coincidence. However, ΛCDM offers no better explanation, a limitation which we term the *coincidence problem*. There is also the tension between the local value of the Hubble constant [26] and the result obtained by the *Planck* collaboration [20] in the context of a ΛCDM cosmology. A fourth example is the challenge posed by the 'small-scale crisis' (see Ref. [27] and works cited therein), which refers to the discrepancies between sub-galactic-scale observations and the predictions resulting from N-body simulations of structure formation in the standard model.

The above-mentioned shortcomings have led the scientific community to propose and study alternative models of dark energy. Most are constructed by modifying either side of Einstein's field equations [8]:

$$R_{\mu\nu} - \frac{1}{2} R g_{\mu\nu} = 8\pi G\, T_{\mu\nu} - \Lambda g_{\mu\nu} \ . \tag{1.1}$$

Here, $R_{\mu\nu}$, $g_{\mu\nu}$ and $T_{\mu\nu}$ are the Ricci, metric and energy-momentum tensors, respectively, while R denotes the Ricci scalar. We shall also take a look at a few models which are based on a completely different approach.

The next three sections summarise the main features of a number of models from each category. The list is extensive, but by no means exhaustive. The reader is directed to [28] for references and more information.

Before proceeding, however, let us make a small detour to introduce the equation of state (EoS) parameter. This is often denoted by w, and is defined as the ratio of p to ρ, where ρ is the energy density of the relevant cosmic fluid component and p the

associated pressure. For the cosmological constant, we thus get that $w_\Lambda = p_\Lambda/\rho_\Lambda = -1$. The EoS parameter of dark energy need not be constant, though, and in many models alternative to ΛCDM it is not. In such cases, it is more appropriate to refer to an 'effective' equation of state.

1.2.2 Modified matter models

In *Modified Matter models*, the energy-momentum tensor is altered to include a component whose negative pressure drives the late-time cosmic acceleration [29]. One class of such models is based upon the replacement of the cosmological constant with a dynamical Λ which, as the name implies, is allowed to vary throughout the cosmic history, although the EoS parameter is kept fixed at -1. The decay of vacuum energy to its present small value consequently provides a natural solution to the smallness problem. These dynamical-Λ cosmologies are further explored in Chapter 4.

When the modified model incorporates a rolling scalar field, the resultant cosmology can be thought of as a generalisation of ΛCDM: if the field rolls slowly, its potential energy behaves like the cosmological constant [28]. Prominent examples are *Quintessence* and *Phantom* (or *Ghost*) models. The main characteristics of each are briefly outlined below. A number of other Modified Matter models are also included.

Quintessence

The word *quintessence* means 'fifth element'. In fact, Quintessence models [30,31] are founded on the postulate of a fifth cosmic component – the other four being baryons, dark matter, radiation and spatial curvature. The new addition is a time-varying scalar field ϕ [29] which has a canonical kinetic energy term[4] and is minimally coupled to gravity. It provides the negative pressure required to explain the accelerating expansion of the Universe [28].

Quintessence models may be classified as either *freezing* or *thawing*. In the former case, w_ϕ decreases with time and approaches the phantom divide ($w_\phi = -1$), whereas in thawing scenarios the scalar field gradually 'thaws out' of its frozen state and causes w_ϕ to increase away from -1. Freezing models may additionally be subdivided into two

[4]This refers to a term of the form $-1/2\ g^{\mu\nu}\nabla_\mu\phi\nabla_\nu\phi$. The presence of a minus sign is made necessary by the choice of metric signature – given a scalar field that depends only on time, its kinetic energy density then works out to be positive [and equal to $1/2\ (\mathrm{d}\phi/\mathrm{d}t)^2$, where t is cosmic time] [32].

classes. In *tracking* freezing models, the evolution converges to a common solution for a wide range of initial conditions – a feature which could solve the coincidence problem. *Scaling* freezing models earn their name from the fact that the equation of state for ϕ scales as the one for matter during the early matter-dominated epoch [33, 34].

It should be emphasised, however, that the name 'quintessence' is often regarded simply as an indication of a phenomenological approach [35]. One need only mention that models based on non-minimally coupled scalar fields or bulk-viscous fluids, or even on networks of non-intercommuting topological defects, are among the many that may classify as 'Quintessence' [36].[5]

Phantom models

Phantom scalar fields [37] have negative kinetic energy. Consequently, they tend to roll up the potential 'hill' (and not down, like conventional fields do), so that their energy density ρ_ϕ grows in the process. Given that ρ_ϕ goes as $a^{-3(1+w_\phi)}$, where a is the cosmological scale factor, an increase implies that the EoS parameter w_ϕ must be less than -1 [38]. The fact that phantom energy violates the dominant-energy condition is perhaps unpalatable but not necessarily problematic [39].

If w_ϕ is constant, ρ_ϕ keeps on growing and causes the cosmic expansion rate to diverge in finite proper time, ultimately leading to a point at which the Universe is ripped apart and physical laws break down (the *Big Rip singularity*) [39]. A disadvantage of ghost models is the vacuum instability that results from interactions (gravitational or otherwise) of the phantom quanta with other fields [28].

Recently, K. J. Ludwick suggested that phantom models need not have negative kinetic energy on all relevant length scales at all times. He also concluded that the kinetic energy of Quintessence may not always be positive [40].

We now turn to dark energy models based on fields with modified kinetic terms.

K-essence

K-essence models are constructed by replacing the conventional kinetic term in the action with the pressure of the field, which is a function of both the field itself and also of the said canonical kinetic term. At the same time, it is made sure that

[5] Such models are sometimes referred to as *extended* Quintessence.

Lorentz symmetry is preserved [28]. As the name implies – K-essence is short for *Kinetically-Driven Quintessence* – in this class of models the particular behaviour of the scalar field derives from the presence of non-canonical kinetic terms [41], rather than on precise functional forms for the field potential (as is usually the case with Quintessence). While it is not generally possible to rewrite K-essence models in terms of Quintessence parameters, Malquarti et al. report that an equivalence can be made in certain dynamical regimes [42].

K-essence may lead to a unified cosmological framework in which a single scalar field accounts for both the inflation of the early Universe and the late-time accelerated expansion [43]. Indeed, the proposal that cosmic dynamics are kinetically-driven first appeared in the context of inflation [44].

Kinetic Gravity Braiding

The action for Kinetic Gravity Braiding is constructed by adding a term of the form $\sqrt{-g}\, f(\phi, X)\Box\phi$ to the Lagrangian density of K-essence, where $\Box$ is the covariant d'Alembertian and f is a generic function of the scalar field ϕ and the associated canonical kinetic energy X. Due to the presence of the $f\,\Box\phi$ interaction term, the energy-momentum tensor of the scalar field does not take the perfect-fluid form; ϕ is therefore termed an *imperfect* scalar. Furthermore, this same term encodes a coupling between ϕ and the metric tensor $g_{\mu\nu}$, giving rise to a mixing of the associated kinetic terms and thus earning the theory its name. The key feature of models with kinetic braiding is the dependence of the Einstein equations and the equation of motion for ϕ on the second derivatives of both the scalar field and metric – and this despite the fact that one starts off with a scalar field whose coupling to gravity is seemingly minimal [45]. The literature contains several examples of different forms that $f(\phi, X)$ may take [46, 47].

As a consequence of kinetic braiding, ϕ couples to other kinds of matter in a rather peculiar manner. In the absence of an additional, direct interaction between matter and the scalar field, this coupling has a one-way nature, in the sense that the matter distribution itself does not become coupled to the scalar and can thus only be affected gravitationally by it [45]. On the other hand, the sensitivity of ϕ to the presence of matter opens up the possibility that the former takes on the role of dark energy, so that under certain conditions the resulting cosmology approaches a de Sitter space asymptotically at late times. The scalar field may additionally cross the phantom

divide $w_\phi = -1$ without generating ghosts or gradient instabilities [45].

Ghost Condensation

The Ghost Condensation model is another generalisation of K-essence. It originated as a solution to the problem posed by the quantum instability of phantom dark energy [28].

Like the cosmological constant, a ghost condensate is endowed with the equation of state $p_\phi = -\rho_\phi$ (where p_ϕ stands for the pressure and ρ_ϕ the energy density of the condensate). It enables the Universe to admit a de Sitter phase, and is also similar to Λ in that it does not get diluted as the Universe expands. Contrary to vacuum energy, however, the ghost condensate is modelled as an actual physical fluid with a physical scalar excitation. The underlying concept stems from a theory based on a real scalar field ϕ whose Lagrangian has the 'wrong-sign' kinetic term characteristic of ghost fields. Additionally, ϕ is shift-symmetric and has a constant velocity [48].

The ability of the ghost condensate to give rise to a de Sitter phase suggests that it might be driving the current acceleration, and that it could have been responsible for the early inflationary epoch of the Universe. It has also been suggested that the ghost condensate may be able to produce the effects usually attributed to dark matter [48]. Furthermore, a recent study reports that the Galileon ghost condensate model (of which the model described here is a sub-case) is observationally favoured over ΛCDM [49].

We shall now take a look at a modified matter model which is not based on scalar field theory.

Chaplygin gas model

Most models of dark energy have a fluid description. Some, however, originate from the direct modification of hydrodynamical equations. Prominent among these is the *Chaplygin gas* (CG) model, so-called because it incorporates dark energy as a Chaplygin gas. The equations governing this fluid were originally used in aerodynamics to model the flow of air around the wings of an aircraft [28]. The Chaplygin gas EoS reads:

$$p_{\mathrm{CG}} = -\frac{A}{\rho_{\mathrm{CG}}} \ , \tag{1.2}$$

where $p_{\rm CG}$ and $\rho_{\rm CG}$ are the pressure and energy density of the fluid in a comoving reference frame, respectively, and A stands for a positive constant [50]. Generalised versions of Eq. (1.2) have also been explored in the literature. One of these, which gives rise to the *generalised Chaplygin gas* (GCG) model [28], includes a second constant (denoted by α) and takes the form [51]:

$$p_{\rm GCG} = -\frac{A}{\rho^{\alpha}_{\rm GCG}} \ . \tag{1.3}$$

Interestingly, despite the fact that the representation of dark energy as a Chaplygin gas did not originate as a scalar field theory, the resulting dynamics may alternatively be ascribed to the presence of a scalar with a simple potential during the matter- or dark energy-dominated epochs [28].

The CG and GCG models have been thoroughly investigated using observational data from numerous sources, such as SNeIa, baryon acoustic oscillations (BAOs), and the CMB. Most studies have shown that the CG model is not compatible with observations [28]. In particular, the combination of X-ray, SNeIa and Fanaroff-Riley type IIb radio galaxy data, when used to test the GCG model, yielded the constraint

$$\alpha = -0.09^{+0.54}_{-0.33} \tag{1.4}$$

at a 95% confidence level. This study thus rules out the CG model, which corresponds to $\alpha = 1$ [52].

An attractive feature of GCG is its ability to incorporate dark energy and dark matter as a single component. In fact, GCG is sometimes called the *Unified Dark Matter model*[6] (UDM). However, when α is positive, the dark matter power spectrum in the UDM scenario is characterised by oscillations which turn out to be incompatible with observations. On the other hand, negative values of α make the perturbations grow exponentially, but these are also ruled out. Studies have shown that most of the parameter space of α is excluded by observational constraints. The values still allowed are those extremely close to zero – which essentially means that only the ΛCDM limit can satisfy the said constraints [53].

[6]The reader is referred to [28] and works cited therein.

1.2.3 Modified gravity models

Modified Gravity models are constructed from altered versions of the action that forms the basis of General Relativity. The GR action reads [8]:

$$S = \int \left[\frac{\sqrt{-g}}{16\pi G}(R - 2\Lambda) \right] \mathrm{d}^4x \ . \tag{1.5}$$

Changes to Eq. (1.5) are made with a view to providing an alternative description of the geometry of space-time – one that gives rise to the effects usually attributed to dark energy. We will thus be concerned with the left-hand side of Eq. (1.1).

A number of Modified Gravity models are reviewed in more detail below.

$f(R)$ and $f(\mathcal{T})$ gravity

As the name suggests, the idea behind $f(R)$ gravity models is the generalisation of the Ricci scalar R in the gravitational action of GR [Eq. (1.5)] to a function $f(R)$. The action is then varied either with respect to the metric itself (an approach known as the *metric formalism*), or by treating the metric and connection[7] as independent variables and varying the action with respect to both. In the latter case, one gets the *Palatini formalism* of $f(R)$ gravity, in which the matter part of the action must be

[7]The *connection* is a mathematical construct that defines the notion of *parallel transport* along a curve on a manifold [54]. Parallel transport can be loosely understood as the curved-space generalisation of the concept of 'keeping a vector constant' while moving it along a path [8]. There is an important difference, however, between what happens in a flat space and a curved one: in the latter case, the result of parallel transport depends on the path taken.
An *affine connection* is essentially a set of linear transformations which enable us to compare tangent vectors lying at different points on a manifold [55]. To make the basic principles more intuitive, we may picture a pseudo-Riemannian manifold embedded in a pseudo-Euclidean space of higher dimension. Then, starting with the vector $\boldsymbol{v}$ belonging to the tangent space of a point P, we shift it to a neighbouring point Q, keeping it parallel to itself in the process. This amounts to transporting the vector within the Euclidean embedding space while keeping its length and direction fixed. At Q, $\boldsymbol{v}$ will not in general be tangential to the surface. That is why we need to equip the manifold with an affine connection. It enables us to shift $\boldsymbol{v}$ from P to Q in such a way that the end result is a vector lying in the tangent space of Q [18].
In mathematical terms, a vector $\boldsymbol{v}$ is said to be parallel transported along the path $x^\mu(\zeta)$ if the condition [8]

$$\frac{\mathrm{d}x^\mu}{\mathrm{d}\zeta} \nabla_\mu v^\sigma = 0$$

holds at every point along the path. The quantity $\nabla_\mu v^\sigma$ stands for the covariant derivative of $\boldsymbol{v}$ and is given by:

$$\nabla_\mu v^\sigma = \partial_\mu v^\sigma + \Gamma^\sigma_{\mu\rho} v^\rho \ .$$

assumed independent of the connection. If the assumption in question is relaxed, the resulting version is called *metric-affine* $f(R)$ *gravity* [56].

The recent discovery that the Universe is accelerating motivated a surge of interest in this class of models [56]. Indeed, like other Modified Gravity theories, $f(R)$ gravity opens up the possibility that the effects attributed to dark energy may be arising naturally from the geometry of the space-time manifold, and is an endeavour to make dark energy redundant. We shall be reviewing metric $f(R)$ in greater detail in Chapter 5. The metric-affine formalism is as yet relatively unpopular, and the Palatini class of theories has 'suffered multiple deaths' [57]; its problematic features include a non-dynamical scalar field, an ill-posed Cauchy problem, and curvature singularities arising from discontinuities in the matter distribution [57].

In GR, the geometric quantity that can be said to 'describe gravity' is the Riemann curvature tensor. This tensor embodies a description of the geometry that matter induces in the space-time manifold, and which in turn determines the trajectories of test particles – a role commonly attributed to 'gravity'. The Riemann curvature tensor is constructed from the torsionless *Levi-Civita* (or *Christoffel*) connection. In 1928, however, Einstein tried using the Weitzenböck connection instead. This has no associated curvature but is characterised by non-zero torsion. Consequently, in the resulting model (called *Teleparallelism*) the prominent role that the Riemann curvature tensor plays in GR is assigned to the torsion tensor. Nonetheless, Teleparallelism shares many features with standard GR [58].

The basis of the Lagrangian density for the *Teleparallel Equivalent of GR* (TEGR) is the torsion scalar $\mathcal{T}$ [58, 59]:

$$\mathcal{L} = \frac{\sqrt{-g}}{16\pi G}\mathcal{T} \ , \tag{1.6}$$

which is itself defined as the product $\mathcal{S}_\rho{}^{\mu\nu}\mathcal{T}^\rho{}_{\mu\nu}$. The torsion tensor $\mathcal{T}^\rho{}_{\mu\nu}$ is constructed

The connection is specified by the set of coefficients $\Gamma^\sigma_{\mu\rho}$. It is possible to construct many connections on a given manifold, but one is of particular significance: the (torsion-free) *metric compatible connection*, so-called because the associated covariant derivative operator gives zero when it acts upon the metric [8]. The coefficients that define this connection are known as the *Christoffel symbols* and may be computed from the metric as follows:

$$\Gamma^\sigma_{\mu\nu} = \frac{1}{2}g^{\sigma\rho}\left(\partial_\mu g_{\nu\rho} + \partial_\nu g_{\rho\mu} - \partial_\rho g_{\mu\nu}\right) \ .$$

Although we have focused exclusively on vectors, the concept of parallel transport can be extended to any tensor of arbitrary rank.

from the Weitzenböck connection, ${}^{\mathrm{w}}\Gamma^{\lambda}_{\nu\mu}$:

$$\mathcal{T}^{\lambda}{}_{\mu\nu} = {}^{\mathrm{w}}\Gamma^{\lambda}_{\mu\nu} - {}^{\mathrm{w}}\Gamma^{\lambda}_{\nu\mu} \ , \tag{1.7}$$

whereas $\mathcal{S}_{\rho}{}^{\mu\nu}$ takes the form:

$$\mathcal{S}_{\rho}{}^{\mu\nu} = \frac{1}{2}(\mathcal{K}^{\mu\nu}{}_{\rho} + \delta^{\mu}_{\rho}\mathcal{T}^{\theta\nu}{}_{\theta} - \delta^{\nu}_{\rho}\mathcal{T}^{\theta\mu}{}_{\theta}) \ . \tag{1.8}$$

Here, $\mathcal{K}^{\mu\nu}{}_{\rho}$ represents the contortion tensor:

$$\mathcal{K}^{\mu\nu}{}_{\rho} = -\frac{1}{2}(\mathcal{T}^{\mu\nu}{}_{\rho} - \mathcal{T}^{\nu\mu}{}_{\rho} - \mathcal{T}_{\rho}{}^{\mu\nu}) \ , \tag{1.9}$$

and δ^{μ}_{ν} is the familiar Kronecker delta [58, 59].

Just as $f(R)$ theory generalises the Ricci scalar in the GR action to functions thereof,[8] so $f(\mathcal{T})$ Lagrangian densities are non-linear functions of the above-mentioned TEGR scalar $\mathcal{T}$. One advantage of $f(\mathcal{T})$ models is the fact that the field equations, being second-order, avoid the pitfalls associated with the higher-order equations of the $f(R)$ metric formalism [58].

In $f(\mathcal{T})$ gravity, the non-zero torsion of the connection is responsible for the observed cosmic acceleration [59]. The theory can also accommodate the radiation- and matter-dominated epochs, and there is the possibility for inflation to be achieved without an inflaton field. The reader is directed to [60] for references and a comprehensive review.

MOND and TeVeS theories

The Modified Newtonian Dynamics (MOND) theory was proposed as a means of erasing the need for dark matter. It involves the modification of Newtonian dynamics on very large scales [28]. MOND can provide an explanation for several observational aspects of galaxies and galaxy clusters without invoking any 'hidden' mass [61].

[8] It should be noted, however, that in the Palatini and metric-affine approaches, R derives from the non-metric connection [56].

The basic assumption of MOND is concisely summarised by the equation

$$\begin{aligned} \mathbf{F} &= m_{\mathrm{g}}\, f(|\mathbf{a}|/\varsigma)\mathbf{a}\ ; \\ f(y \gg 1) &\approx 1\ ; \quad f(y \ll 1) \approx y\ , \end{aligned} \tag{1.10}$$

where m_{g} is the gravitational mass of an object that moves in a static force field $\mathbf{F}$ with acceleration $\mathbf{a}$. The constant ς was determined to be approximately 2×10^{-10} $\mathrm{m\,s^{-2}}$. When $|\mathbf{a}| \gg \varsigma$, the function f tends to unity, and Newtonian gravity is recovered [61]. The assumptions underlying MOND can be interpreted in two ways: either as a modification of Newton's second law ($\mathbf{F} = m_{\mathrm{g}}\mathbf{a}$) or as an alternative description of the gravitational field [62].

Bekenstein and Milgrom have shown that the basic principles of MOND may be incorporated into a theory with a Lagrangian formalism. The main feature of the Lagrangian density they propose is the fact that it contains a function of $(\nabla\Phi)^2$ (Φ being the potential responsible for the acceleration of test bodies) [62]. This property is reflected in the name given to the resulting theory: AQUAL, which is short for A QUadratic Lagrangian [28].

The relativistic version of AQUAL is based on the Lagrangian density:

$$\mathcal{L} = \frac{\sqrt{-g}}{16\pi G}\left[R - \frac{2}{U^2} f\left(U^2 g^{\mu\nu}\nabla_\mu\psi\nabla_\nu\psi\right)\right]\ . \tag{1.11}$$

Here, U is a constant introduced for dimensional consistency, ψ represents a real scalar field,[9] and $g_{\mu\nu}$ is conformal to the physical metric (which is given by $g_{\mu\nu}\mathrm{e}^{2\psi}$). Unfortunately, relativistic AQUAL has been empirically falsified, mainly because of two major shortcomings: the violation of causality by ψ-waves and the failure to properly account for light deflection, which in GR requires the presence of dark matter [63].

TeVeS is arguably the most complicated in the MOND family of models. Indeed, the name is an acronym for *Tensor-Vector-Scalar*, because the theory incorporates three dynamical fields: the Einstein metric tensor $g_{\mu\nu}$, a timelike four-vector field v^μ and a scalar field ϕ, together with a non-dynamical scalar field ξ. Unlike some of the other MOND-like models, TeVeS makes it possible to avoid causality violations and to comply with the constraints imposed by gravitational lensing experiments.

[9] To a good approximation, relativistic AQUAL reduces to MOND when the acceleration is weak, and (subject to certain conditions) the field ψ takes the role of Φ [63].

Nonetheless, it has its share of problems. For instance, the effects that in GR are attributed to dark energy do not emerge as a natural consequence of the theoretical framework [28].

Gauss-Bonnet gravity and Lovelock gravity

For *Gauss-Bonnet* (GB) gravity [64], the Einstein-Hilbert action of Eq. (1.5) is modified to include a ghost-free correction proportional to $R^{\mu\nu\rho\sigma}R_{\mu\nu\rho\sigma} - 4R^{\mu\nu}R_{\mu\nu} + R^2$. This expression is called the GB term $\mathcal{G}$ [28].

GB theory was proposed with the aim of deriving a ghost-free gravitational action from the low-energy limits of string theory [28, 64]. When $\mathcal{G}$ is coupled to a scalar field ϕ whose potential takes the form $V(\phi) = V_0 \exp(-\lambda\phi)$, and the GB coupling – in other words, the factor which scales $\mathcal{G}$ in the action – is proportional to $\exp(\varrho\phi)$ ($\varrho > \lambda$; ϱ and λ are both contants), the matter-dominated era may be followed by a late-time de Sitter epoch. Yet despite being well-motivated by low-energy effective string theory, GB gravity is observationally disfavoured as a dark energy candidate model. Additionally, in order to prevent Solar System constraints from being violated, the energy contribution of the GB correction must be strongly suppressed. This suppression may in turn render the GB term insufficient to account for the late-time accelerated cosmic expansion. However, it is possible to get the required acceleration by replacing $\mathcal{G}$ with a function $f(\mathcal{G})$. A number of models that result from this approach are able to satisfy local gravity constraints, but have been found lacking in other ways. In particular, density perturbations in perfect fluids are subject to negative instabilities during both the radiation- and matter- dominated epochs (refer to [65] and works cited therein).

A more general version of GB theory is known as *Lovelock gravity* [66]. In a $D-$dimensional space-time, the action for *pure* Lovelock gravity takes the form[10] [67]:

$$S_{(q)} = \int \frac{\sqrt{-g}}{16\pi G}\, c_{(q)} \eta^{\mathrm{L}}_{(q)}\, \mathrm{d}^D x \ , \tag{1.12}$$

where q is an integer, $c_{(q)}$ denotes a parameter with dimensions of $(\text{length})^{2(q-1)}$ and $\eta^{\mathrm{L}}_{(q)}$ represents the Lovelock invariant:

$$\eta^{\mathrm{L}}_{(q)} = \frac{1}{2^q}\, \delta^{\mu_1\nu_1\ldots\mu_q\nu_q}_{\sigma_1\lambda_1\ldots\sigma_q\lambda_q}\, R_{\mu_1\nu_1}{}^{\sigma_1\lambda_1} \ldots R_{\mu_q\nu_q}{}^{\sigma_q\lambda_q} \ ; \qquad \eta^{\mathrm{L}}_{(0)} = 1 \ . \tag{1.13}$$

[10] A general Lovelock action would contain a sum of Lovelock invariants [67].

In the above, $R_{\mu\nu}{}^{\sigma\lambda}$ is the Riemann tensor, while the indices μ, ν, σ and λ can take values in the range $[0, D-1]$ and serve to label the D spacetime coordinates. The generalized Kronecker delta is defined in terms of the Levi-Civita symbol[11] [67]:

$$\delta^{\mu_1\ldots\mu_n}_{\nu_1\ldots\nu_n} \equiv \epsilon^{\mu_1\ldots\mu_n}\epsilon_{\nu_1\ldots\nu_n} = n!\delta^{\mu_1}_{[\nu_1}\ldots\delta^{\mu_n}_{\nu_n]} \ . \tag{1.14}$$

Although Lovelock gravity cannot directly yield a cosmology dominated by dark energy, dimensional reduction techniques have made it possible for third-order Lovelock dark energy models to be proposed [28]. In Ref. [68], for instance, the authors consider the third-order Lovelock equations in a higher-order Kaluza-Klein space-time devoid of matter and without a cosmological constant. They show that dark energy and matter can be created out of the curvature of the Kaluza-Klein space-time.

Hořava-Lifshitz Gravity

Hořava-Lifshitz Gravity [69] tackles the problem of non-renormalisability, a major stumbling block encountered when attempting to quantise GR.[12] Hořava suggested that by giving up Lorentz invariance at high energies, it is possible to at least have power-counting renormalisability [28]. A theory is said to be *renormalisable by power counting* when the processes leading to divergences are finite in number and exclusive to Feynman graphs with only a few external lines [70].

The metric that arises within the Hořava-Lifshitz framework reads:

$$\mathrm{d}s^2 = -N^2\mathrm{d}t^2 + \mu_{ij}\left(\mathrm{d}x^i + N^i\mathrm{d}t\right)\left(\mathrm{d}x^j + N^j\mathrm{d}t\right) \ , \tag{1.15}$$

Here, N and N^i represent the lapse and shift functions, respectively, and μ_{ij} is the spatial metric [71]. An important and distinctive property of the theory is its UV fixed point, which is characterised by an anisotropic, Lifshitz scaling of the form $x^i \to bx^i, t \to b^\varepsilon t$ (b is the scaling factor and ε the dynamical critical exponent [71]. The latter must equal three for the theory to be power-counting renormalisable in a spacetime with $3+1$ dimensions [69].)

Hořava-Lifshitz cosmology is constructed by combining the modified gravitational

[11] The Levi-Civita symbol, denoted by $\epsilon_{\rho_1\rho_2\ldots\rho_n}$, evaluates to $+1$ if $\rho_1\rho_2\ldots\rho_n$ is an even permutation of $0, 1, 2\ldots n-1$. It is equal to -1 if the permutation is odd, and 0 otherwise [8].

[12] The appearance of loops in Feynman diagrams often implies unbounded transition amplitudes. In very simple terms, *renormalisability* refers to the process of redefining certain quantities in a way that makes the transition amplitudes finite [24].

background with a scalar field ϕ. The resulting model describes a universe with a cosmological constant and a so-called *dark radiation* term, as well as a dark matter distribution that ϕ is expressly introduced to account for [71]. In Ref. [71], the addition of a second scalar field gives rise to an effective dark energy component with a varying EoS parameter that may even cross the phantom divide.

Conformal Weyl Gravity

The action for Conformal Weyl Gravity (CWG) is constructed from the conformal Weyl tensor $C_{\lambda\mu\nu\kappa}$ [72]:

$$S = -\beta \int \sqrt{-g}\, C_{\lambda\mu\nu\kappa} C^{\lambda\mu\nu\kappa}\, \mathrm{d}^4x \equiv -\beta \int \sqrt{-g} \left(R_{\lambda\mu\nu\kappa} R^{\lambda\mu\nu\kappa} - 2R_{\mu\nu}R^{\mu\nu} + \frac{R^2}{3} \right) \mathrm{d}^4x; \tag{1.16}$$

$$C_{\lambda\mu\nu\kappa} = R_{\lambda\mu\nu\kappa} - \frac{1}{2}\left(g_{\lambda\nu}R_{\mu\kappa} - g_{\lambda\kappa}R_{\mu\nu} - g_{\mu\nu}R_{\lambda\kappa} + g_{\mu\kappa}R_{\lambda\nu}\right) + \frac{R}{6}\left(g_{\lambda\nu}g_{\mu\kappa} - g_{\lambda\kappa}g_{\mu\nu}\right). \tag{1.17}$$

In the above, β is a dimensionless coupling constant.

Eq. (1.16) may be simplified [72] by making use of the fact that the Lanczos Lagrangian density [73], which reads

$$\mathcal{L}_{\mathrm{L}} = \sqrt{-g}\left(R_{\lambda\mu\nu\kappa} R^{\lambda\mu\nu\kappa} - 4R_{\mu\nu}R^{\mu\nu} + R^2 \right) , \tag{1.18}$$

is a total divergence and hence does not contribute to the equations of motion; the conformal action consequently becomes [72]:

$$S = -2\beta \int \sqrt{-g} \left(R_{\mu\nu}R^{\mu\nu} - \frac{R^2}{3} \right) \mathrm{d}^4x \ . \tag{1.19}$$

Among the features that CWG shares with standard GR are general coordinate invariance and an equivalence principle structure. In addition, CWG is endowed with local conformal invariance, meaning that metric transformations of the type $g_{\mu\nu}(x^\lambda) \to \mathrm{e}^{2f(x^\lambda)} g_{\mu\nu}(x^\lambda)$ [where $f(x^\lambda)$ is an arbitrary local phase] leave the action invariant [74].

The strong point of CWG is that it provides an explanation for galactic rotation curves without any need for dark matter [74]. It can also serve as a dark energy model [72], but has its share of controversy, not least because conformal invariance constrains the

total energy-momentum tensor $T^{\text{tot}}_{\mu\nu}$ to have vanishing trace. Since cosmological fluids (with the exception of radiation) are in general described by an energy-momentum tensor with non-zero trace, this must mean that $T^{\text{tot}}_{\mu\nu}$ receives contributions from an additional source. According to Mannheim, the source in question is none other than the Higgs field [75]. However, some see this scenario as highly unlikely. For instance, Yoon underlines the difficulty of proposing a mechanism that would distribute the Higgs field in the way necessary to render $T^{\text{tot}}_{\mu\nu}$ traceless [76].

A further setback of CWG concerns the parameter γ. This parameter arises as an integration constant in the line element exterior to a static, spherically symmetric source[13] [77]:

$$\mathrm{d}s^2 = -B(r)\mathrm{d}t^2 + \frac{\mathrm{d}r^2}{B(r)} + r^2\left(\mathrm{d}\theta^2 + \sin^2\theta\,\mathrm{d}\phi^2\right) \ ; \tag{1.20}$$

$$B(r) = 1 - \frac{\nu(2-3\nu\gamma)}{r} - 3\nu\gamma + \gamma r - \vartheta r^2 \ . \tag{1.21}$$

Eq. (1.21) essentially represents a modification of the Newtonian gravitational potential, and is the reason why the features of galactic rotation curves may be explained without the need for dark matter. A good fit to the data is obtained if γ is approximately $10^{-28}\,\mathrm{cm}^{-1}$ [77]. Herein lies the problem: the given estimate is several orders of magnitude smaller than the value inferred from lensing data [78] or from considerations of quantum interference effects [79]. A recent study even argues that γ must be set to zero [80]. On the other hand, constraints from the perihelion precession of planetary orbits are compatible with those from galactic rotation curves [81]. There is also the fact that the sign of γ is itself a subject of debate[14] [83–85].

1.2.4 Other models of dark energy

Several other noteworthy dark energy models are introduced below.

Holographic dark energy

The *Holographic Principle* originated from black hole thermodynamics [28]. After Bekenstein proposed that a black hole has an entropy proportional to its horizon

[13] The quantities ν and ϑ are also integration constants.

[14] A number of works have attempted to explain why different studies disagree on the role that γ plays in strong lensing. Refer, for instance, to [80, 82] and [83].

area [86], and the Bekenstein-Hawking area-entropy relation was established [86–88], 't Hooft [89] and Susskind [90] realised the possibility of interpreting black hole entropy as a dimensional reduction [28]. In his book *The Black Hole War: My Battle with Stephen Hawking to Make the World Safe for Quantum Mechanics* [91], Leonard Susskind tells how he and Gerard 't Hooft 'waged war' against Hawking's claim that the information trapped inside a black hole (due to in-falling matter) gets obliterated when the black hole evaporates. In an effort to save the principle of information conservation – 'one of the most trusted principles of physics' [91] – they suggested that the surface of the black hole encodes information about the matter that has fallen inside. This information then leaks out when the black hole emits Hawking radiation.

The Holographic Principle takes this concept one step further. According to it, everything inside a region of space can be described by information that is restricted to the boundary [91]. The holographic entropy bounds resulting from this approach paved the way [92] for a relation to be established between the infrared and UV cutoffs of a system [93], here denoted by ℓ_{i} and ℓ_{uv}, respectively. The said relation guarantees that, assuming the system has size ℓ_{i}, the quantum zero-point energy $\rho_{\mathrm{zp}} = \ell_{\mathrm{uv}}^4$ cannot exceed the energy pertaining to a black hole of the same size (Ref. [93] as cited by Ref. [94]). This places bounds on ρ_{zp} [94]. When the holographic principle is applied to the dynamics of the Universe, the cutoff length ℓ_{i} must be of cosmological proportions, and interestingly, different infrared cutoffs give rise to different dark energy models [95]. For instance, Cohen et al. reported that choosing a value for ℓ_{i} comparable to the current horizon size (the Hubble radius H^{-1} [95]) results in a dark energy density – equivalent to ρ_{zp} – which is approximately equal to the observed effective cosmological constant [93]. It later turned out, however, that this choice of ℓ_{i} means that w_Λ is equal to zero (rather than -1) [92]. Li suggested that the infrared cutoff could be identified with the size of the event horizon[15] instead [96].

Sub- and Super- Hubble inhomogeneities

One of the most fundamental assumptions underlying modern cosmology is the *cosmological principle*, according to which the observable Universe is both homogeneous and isotropic. This principle lies at the very core of the Friedmann-Lemaître-Robertson-Walker (FLRW) metric and all its implications for cosmology, including the Friedmann equations. Although deviations from the cosmological principle have been investigated

[15]The *event horizon* is defined in subsection 1.3.4.

in the literature – for instance, a Bianchi-type universe is homogeneous but not necessarily isotropic [97] – the FLRW description of the Universe is arguably the most popular today.

The cosmological principle is, in fact, supported by CMB and LSS observations. However, on sub-Hubble scales the Universe is not homogeneous at all, but contains structures such as galaxy clusters. Neither can it be ascertained that homogeneity and isotropy hold on scales larger than the observable Universe (*super-Hubble scales*) [28].

Since gravity is non-linear, it is possible that any anisotropies and/or inhomogeneities back-react on the evolution of the observable Universe [28], giving rise to accelerated expansion at late times ([28, 98] and references therein).

Quantum Cosmology

It is as yet not possible to speak about quantum cosmology as one would of a well-established dark-energy model, because at present we do not have a theory of quantum gravity to provide the necessary framework. However, we can at least formulate a qualitative picture of such a cosmology [99]. One way in which this may be done is by assigning the Universe a wave function whose behaviour is described by the Wheeler-De Witt wave equation [100–102]. Under certain conditions, the cosmological constant term behaves effectively as a mass-squared term in the said equation. Consequently, just as second quantisation makes it possible for a particle to decay into another of a different mass (provided that interactions between the two kinds of particles are allowed), so the addition of interactions to the quantised Lagrangian density implies that a universe with a large cosmological constant may decay into one having a smaller Λ [103, 104]. Given two universes with a different cosmological constant but coupled wave equations, it is also possible to construct a 'mass matrix' analogous to the one used in neutrino physics. The seesaw mechanism can then be applied to cosmology. In the case of neutrinos, this mechanism aims to provide an explanation for their small, non-zero mass by introducing a seesaw-like relation between the eigenvalues of the mass matrix: when one eigenvalue increases, the other decreases [28].

In a similar way, the 'mass matrix' associated with the above-mentioned universes might hold the key to the solution for the smallness of the cosmological constant. The eigenvalues of the matrix would be determined by the two different values for the cosmological constant (one in each universe). If the vacuum energy of one universe is at the Planck scale, and that of the other is at the supersymmetry breaking scale,

the seesaw mechanism could result in the smaller eigenvalue being suppressed by the amount necessary for it to match the current observed value of Λ [104].

Another explanation of dark energy may arise from the mechanism of *efficient resonance tunnelling*, a well-established concept in quantum mechanics. It occurs when a wave function has to tunnel through multiple potential barriers. Although the process of tunnelling usually causes the wave function to decay exponentially, the presence of a second barrier alters the scenario considerably if the energy of the wave function matches that of a bound state in the intermediate region. Should this happen, the requirements of continuity may only be met at all the boundaries under a particular condition: the tunnelling amplitude must be exponentially enhanced by one of the barriers (while still being exponentially suppressed by the other) [28]. In certain situations, the probability of tunnelling through both barriers may actually become of order one, and efficient resonance tunnelling occurs [105].

It has been proposed that the Universe itself could have experienced resonant tunnelling. More specifically, it is possible – in the context of string theory – that the Universe might have tunnelled from an early era characterised by a large value for the cosmological constant to the current epoch, with its small value of Λ [105].

1.3 The FLRW Cosmology

The Friedmann-Lemaître-Robertson-Walker (FLRW) cosmology is based on three fundamental assumptions: the cosmological principle, Weyl's postulate, and the notion of a maximally symmetric three-space [18].

The *cosmological principle* states that all positions in space are equivalent at any given time. Additionally, the Universe as viewed from a general point looks the same in all directions. The former property is referred to as *homogeneity*, while the latter is called *isotropy* [18]. Although the idea that the Universe is roughly the same everywhere might seem counter-intuitive, especially when one considers inhomogeneities such as galaxies and galaxy clusters, the cosmological principle is only valid on scales large enough for density variations to be averaged over [8].

Weyl's postulate builds on the concept of space-time as a series of three-dimensional space-like hypersurfaces. In layman's terms, we 'slice' space-time into non-intersecting space-like surfaces and label each with a parameter t. Consequently, all events happening at a given time $\bar{t}$ must be confined to the surface bearing the

'label' $t = \bar{t}$. We then introduce the notion of *fundamental observers*, so called because they are assumed to be motionless relative to the cosmological fluid (this 'fluid' is the description we give to the 'smeared-out' motion of galaxy clusters and other matter). Weyl put forward the hypothesis that the time-like world lines of the fundamental observers link all of space-time. More specifically, they form a bundle which is assumed to diverge from a point in the past – or converge to one in the future – in such a way that there is a unique world line passing through every point, but no two intersect (except possibly at a singular point) [18].

The next postulate we consider is that of a maximally symmetric three-space. Before proceeding, it should be emphasised that each of the hypersurfaces mentioned above is a three-dimensional space – the idea of a 'surface' results from the fact that it is more intuitive to suppress a spatial dimension and imagine the Universe as a stack of two-dimensional 'sheets'. Now that the concept of space-time foliation has been established, we apply the cosmological principle by assuming that the three-spaces are homogeneous and isotropic. This in turn implies the highest degree of symmetry and renders them *maximally symmetric*. As a result, their Riemann and metric tensors are related thus:

$$R_{ijkl} = K\left(g_{ik}g_{jl} - g_{il}g_{jk}\right) \ . \tag{1.22}$$

The coordinate-independent *curvature* K is a constant that takes the same value for all hypersurfaces. It is more commonly expressed in normalised form as the ratio $K/|K|$, henceforth denoted by k [8, 18].

The above three propositions form the building blocks of the FLRW cosmology. When combined, they yield the line element [8]:

$$\mathrm{d}s^2 = -\mathrm{d}t^2 + a^2(t)\left[\frac{\mathrm{d}r^2}{1-\kappa r^2} + r^2(\mathrm{d}\theta^2 + \sin^2\theta\ \mathrm{d}\varphi^2)\right] \ , \tag{1.23}$$

where r has dimensions of distance and $a(t) = \mathcal{R}/\mathcal{R}_0$, $\mathcal{R}$ being the scale factor and $\mathcal{R}_0$ its-present day value [so that if we let t_0 denote the current time, we get that $a(t_0) = 1$]. The role of the scale factor is to account for the expansion or contraction of the Universe by scaling the spatial part of the metric accordingly. As for the parameter κ, this is defined as the ratio of k to $\mathcal{R}_0^2$. It thus follows that κ has dimensions of $(\text{length})^{-2}$ [8].

The spatial coordinates used in Eq. (1.23) are said to be *comoving*. In fact, these coordinates seem to move with the fundamental observers (who in actuality represent

individual galaxies), so that as long as peculiar velocities are negligible on cosmological scales, the world line of a galaxy has fixed values of (r, θ, φ). What about the parameter t? Space-time may be foliated in such a way that the world lines of the fundamental observers intersect the space-like hypersurfaces orthogonally. Consequently, t can be identified with the proper time of these observers, and is hence called the *synchronous time coordinate* [18].

1.3.1 Spatial curvature and geometry

Let us consider the metric given by Eq. (1.23) and extract the spatial part [8]:

$$\mathrm{d}\sigma^2 = \frac{\mathrm{d}r^2}{1-\kappa r^2} + r^2 \mathrm{d}\Psi^2 \ . \tag{1.24}$$

Here, $\mathrm{d}\Psi^2 = \mathrm{d}\theta^2 + \sin^2\theta \ \mathrm{d}\varphi^2$. If we redefine the radial coordinate as follows [8]:

$$\mathrm{d}\chi = \frac{\mathrm{d}r}{\sqrt{1-\kappa r^2}} \ , \tag{1.25}$$

and then integrate Eq. (1.25), we get that $r = \mathcal{F}(\chi)$, with

$$\mathcal{F}(\chi) = \begin{cases} \chi & \text{if } \kappa = 0 \ ; \\ \sin\left(\sqrt{\kappa}\,\chi\right)/\sqrt{\kappa} & \text{if } \kappa > 0 \ ; \\ \sinh\left(\sqrt{|\kappa|}\,\chi\right)/\sqrt{|\kappa|} & \text{if } \kappa < 0 \ . \end{cases} \tag{1.26}$$

Consequently, the spatial line element may be written as [8]

$$\mathrm{d}\sigma^2 = \mathrm{d}\chi^2 + \mathcal{F}^2 \mathrm{d}\Psi^2 \ . \tag{1.27}$$

Zero spatial curvature

When $\kappa = 0$, Eq. (1.27) becomes [8]

$$\mathrm{d}\sigma^2 = \mathrm{d}\chi^2 + \chi^2 \mathrm{d}\Psi^2 = \mathrm{d}x^2 + \mathrm{d}y^2 + \mathrm{d}z^2 \ , \tag{1.28}$$

where the last equality follows from the coordinate transformation $x = \chi \sin\theta \cos\varphi$, $y = \chi \sin\theta \sin\varphi$, $z = \chi \cos\theta$ [18]. Eq. (1.28) is none other than the metric for three-dimensional Euclidean space.

Positive spatial curvature

Positive values of κ are associated with the line element

$$\mathrm{d}\sigma^2 = \mathrm{d}\chi^2 + \frac{1}{\kappa}\sin^2\left(\sqrt{\kappa}\,\chi\right)\mathrm{d}\Psi^2 = \frac{1}{\kappa}\left[\mathrm{d}\tilde{\chi}^2 + \sin^2\left(\tilde{\chi}\right)\mathrm{d}\Psi^2\right] \ . \tag{1.29}$$

The last equality is obtained by setting $\sqrt{\kappa}\,\chi$ equal to $\tilde{\chi}$, and puts the metric in a form that describes a three-sphere embedded in four-dimensional Euclidean space. We can hence deduce that a 3-space with positive curvature has finite volume [18]. Indeed, a universe having $\kappa > 0$ is often said to be *closed*.

Negative spatial curvature

In this case, Eq. (1.27) reads

$$\mathrm{d}\sigma^2 = \mathrm{d}\chi^2 + \frac{1}{|\kappa|}\sinh^2\left(\sqrt{|\kappa|}\,\chi\right)\mathrm{d}\Psi^2 = \frac{1}{|\kappa|}\left[\mathrm{d}\tilde{\chi}^2 + \sinh^2\left(\tilde{\chi}\right)\mathrm{d}\Psi^2\right] \ , \tag{1.30}$$

where $\tilde{\chi} = \sqrt{|\kappa|}\,\chi$. The properties of the resulting geometry emerge more clearly if we embed the metric (as expressed in terms of $\tilde{\chi}$) in four-dimensional Minkowski space. Here, the 3-dimensional hypersurface may be identified with a hyperboloid, which leads us to conclude that a 3-space with negative curvature has infinite volume [18]. It additionally explains why a universe having $\kappa < 0$ is commonly referred to as being *open* [8].

1.3.2 Spatial curvature in the literature

One of the main aims of this study is to shed light on the role that spatial curvature plays in the expansion history of the Universe. The possibility that the Universe is not spatially flat has been largely overlooked in the literature, mainly due to two reasons: the consistency of a flat geometry with the concept of inflation, which would conceptually have 'smoothed out' any curvature, and the support that observations seem to lend to a flat ΛCDM cosmology [19, 20, 106, 107]. With regards to the latter, the question naturally arises whether the assumption of flatness may be justifiably extended to dynamical dark energy models, since many of the studies that use cosmic data to constrain spatial curvature do so in the framework of a ΛCDM cosmology. One might be tempted to answer in the affirmative, especially in the light of a number

of studies which have obtained constraints in several modified matter scenarios, and whose results are indicative of a flat geometry [108–111]. Other studies, however, have shown that alternative dark energy models may accommodate a non-flat universe when tested with cosmological data [112–114]. It should be remembered that the dark energy EoS parameter is likely to become degenerate with spatial curvature when one attempts to constrain both simultaneously [115]. Indeed, if the density of dark energy is allowed to vary freely with time, constraints on the geometry of the Universe may become looser [116]. This degeneracy implies that making a wrong assumption about one of the parameters can severely distort results related to the other. For instance, data analysis of models with curvature and dynamical dark energy may produce results suggestive of flat ΛCDM should the dynamics of dark energy be overlooked. On the other hand, the assumption of flatness can result in cosmological observations being seemingly at odds with ΛCDM if the Universe is actually curved [115, 117]. There is the additional possibility that a closed universe consisting of dust and quintessence behaves as a flat, accelerating ΛCDM universe at late times [118].

Relativistic effects like cosmic magnification may also play a part. It has been suggested that unless these effects are accounted for in galaxy number counts, measurements of Ω_k^0 based on data from galaxy surveys can be significantly biased [119]. Another point of interest is the fact that recent SNeIa data appears to be in tension with the flat ΛCDM hypothesis [120], and may actually favour a non-flat universe [121,122].

Standard inflation predicts that any spatial curvature should be negligibly small. This follows from the exponential decrease of Ω_k^0 during inflation and the much smaller growth rate since then [22]. It may be argued, however, that one should look for the potential presence of curvature as a means of testing the inflationary paradigm, rather than setting Ω_k^0 to zero [112]. Moreover, Bolejko suggests that the spatial geometry of the Universe could have evolved from spatial flatness at early times to a slightly hyperbolic one today. The author reaches this conclusion by running a Simsilun simulation[16](a relativistic simulation of the large-scale structure of the Universe) [123], and finds that the emergence of spatial curvature might actually be the key to solving the Hubble constant problem. He reports that when the system enters the non-linear regime, Ω_k^0 begins to depart from zero, while the average expansion rate deviates from ΛCDM and ultimately yields a value of $72.5 \pm 2.1\,\mathrm{km\,s^{-1}\,Mpc^{-1}}$ for the Hubble constant. This despite the fact that the initial conditions are consistent with the Planck constraints [124].

[16]A ray-tracing algorithm is first incorporated into the simulation.

1.3.3 The Friedmann equations for ΛCDM

Let us return to Einstein's equation for GR, first introduced in subsection 4.6.5. It is reproduced below for ease of reference [8]:

$$R_{\mu\nu} - \frac{1}{2}Rg_{\mu\nu} = 8\pi G\, T_{\mu\nu} - \Lambda g_{\mu\nu} \ . \tag{1.31}$$

The left-hand side relates to the geometry of the space-time manifold and may be evaluated once $g_{\mu\nu}$ is known. Indeed, we have that [8]

$$R = g^{\mu\nu} R_{\mu\nu} \ ; \tag{1.32}$$

$$R_{\mu\nu} = R^{\lambda}{}_{\mu\lambda\nu} \ ; \tag{1.33}$$

$$R^{\rho}{}_{\sigma\mu\nu} = \partial_\mu \Gamma^{\rho}_{\nu\sigma} - \partial_\nu \Gamma^{\rho}_{\mu\sigma} + \Gamma^{\rho}_{\mu\lambda}\Gamma^{\lambda}_{\nu\sigma} - \Gamma^{\rho}_{\nu\lambda}\Gamma^{\lambda}_{\mu\sigma} \ ; \tag{1.34}$$

$$\Gamma^{\sigma}_{\mu\nu} = \frac{1}{2} g^{\sigma\rho} \left(\partial_\mu g_{\nu\rho} + \partial_\nu g_{\rho\mu} - \partial_\rho g_{\mu\nu} \right) \ , \tag{1.35}$$

where R is the Ricci scalar, $R_{\mu\nu}$ and $R^{\rho}{}_{\sigma\mu\nu}$ denote the Ricci and Riemann tensors, respectively, and $\Gamma^{\sigma}_{\mu\nu}$ represents the Christoffel symbols.

The right-hand side of Eq. (1.31) accounts for any sources of energy and/or momentum. In cosmology, the matter and radiation content of the Universe is usually modelled as a cosmic fluid. In other words, just as fluid mechanics deals with the bulk properties of liquids and gases – rather than with the behaviour of the constituent particles – so the approach in cosmology is to 'smear out' the individual galaxies and galaxy clusters, treating them as a whole and focusing instead on the attributes of the generalised distribution. To this end, it is common practice to adopt a *perfect fluid* description. Such a fluid is defined by the absence of heat conduction and viscosity in the instantaneous rest frame (IRF) [18]. Its energy-momentum tensor is completely characterised by the energy density ρ and isotropic pressure p:

$$T^{\mu\nu} = (\rho + p)\, u^\mu u^\nu + p g^{\mu\nu} \ , \tag{1.36}$$

with both quantities as measured in the IRF. The vector u^μ is the four-velocity of the fluid ($u^\mu u_\mu = -1$) [8].

We are now in a position to find out what specific form the Einstein field equations take. In an FLRW universe filled with a perfect fluid, the $\mu\nu = 00$ component of

Eq. (1.31) yields[17] [8, 18]:

$$\frac{\ddot{a}}{a} = -\frac{4\pi G}{3}(\rho + 3p) + \frac{\Lambda}{3} \ , \tag{1.37}$$

which, when combined with the equation for $\mu\nu = ij$, allows us to conclude that:

$$\left(\frac{\dot{a}}{a}\right)^2 = \frac{8\pi G}{3}\rho + \frac{\Lambda}{3} - \frac{\kappa}{a^2} \ . \tag{1.38}$$

The isotropic nature of the FLRW space-time implies that one may only obtain a single distinct equation from the $\mu\nu = ij$ components [8, 18].

The above two relations, (1.37) and (1.38), are collectively known as the *Friedmann equations.*[18]

1.3.4 Terminology

The Hubble parameter

The Hubble parameter H characterises the rate of expansion [8]. It is defined as the quantity

$$H = \frac{\dot{a}}{a} \ , \tag{1.39}$$

(or equivalently, as $\dot{\mathcal{R}}/\mathcal{R}$), and the value it takes at present is known as the *Hubble constant* (H_0). This value is currently a subject of some controversy. The reason is that in the context of a ΛCDM cosmology, measurements of CMB observables constrain H_0 to be approximately $67\,\mathrm{km\,s^{-1}\,Mpc^{-1}}$ [20], which is in tension at 4.4σ with the model-independent value inferred directly from Cepheid data ($H_0 = 74.03 \pm 1.42\,\mathrm{km\,s^{-1}Mpc^{-1}}$) [125].

The density parameters

The various components of the cosmic fluid all have an associated density ρ and pressure p that are generally functions of redshift. The way these quantities scale with z may be determined by invoking the principle of energy and momentum conservation.

[17] An overdot denotes differentiation with respect to t.

[18] When referring to them individually, we shall call (1.38) the *first Friedmann equation* and (1.37) the *second Friedmann equation.*

Provided the components do not interact, each of them must satisfy the condition [18]:

$$\nabla_\mu \left(T^{\mu\nu}\right)_i = 0 \ . \tag{1.40}$$

The action of the covariant derivative ∇_σ on an arbitrary tensor is as follows [8]:

$$\begin{aligned}
&\nabla_\sigma J^{\mu_1\mu_2\ldots\mu_n}{}_{\nu_1\nu_2\ldots\nu_m} = \partial_\sigma J^{\mu_1\mu_2\ldots\mu_n}{}_{\nu_1\nu_2\ldots\nu_m} \\
&+ \Gamma^{\mu_1}_{\sigma\rho} J^{\rho\mu_2\ldots\mu_n}{}_{\nu_1\nu_2\ldots\nu_m} + \Gamma^{\mu_2}_{\sigma\rho} J^{\mu_1\rho\ldots\mu_n}{}_{\nu_1\nu_2\ldots\nu_m} + \cdots + \Gamma^{\mu_n}_{\sigma\rho} J^{\mu_1\mu_2\ldots\rho}{}_{\nu_1\nu_2\ldots\nu_m} \\
&- \Gamma^{\rho}_{\sigma\nu_1} J^{\mu_1\mu_2\ldots\mu_n}{}_{\rho\nu_2\ldots\nu_m} - \Gamma^{\rho}_{\sigma\nu_2} J^{\mu_1\mu_2\ldots\mu_n}{}_{\nu_1\rho\ldots\nu_m} - \cdots - \Gamma^{\rho}_{\sigma\nu_m} J^{\mu_1\mu_2\ldots\mu_n}{}_{\nu_1\nu_2\ldots\rho} \ .
\end{aligned} \tag{1.41}$$

Eq. (1.40) may thus be expanded by making use of Eqs. (1.23), (1.35), (1.36) and (1.41). The result (for a generic component of the cosmic fluid) reads:

$$\dot{\rho}_i(t) = -3H(\rho_i + p_i) \ . \tag{1.42}$$

Next, we establish the relationship between ρ_i and p_i by choosing an appropriate equation of state. For the perfect fluids relevant to cosmology, this equation is particularly simple [8]:

$$p_i = w_i \rho_i \ . \tag{1.43}$$

Inserting the above relation into Eq. (1.42) allows us to solve for ρ_i:

$$\begin{aligned}
& \dot{\rho}_i = -3\frac{\dot{a}}{a}\rho_i(1+w_i) \ ; \\
\implies \quad & \frac{\mathrm{d}\rho}{\mathrm{d}a} = -\frac{3}{a}\rho_i(1+w_i) \ ; \\
\therefore \quad & \rho_i(a) = \rho_i^0 a^{-3(1+w_i)} \ .
\end{aligned} \tag{1.44}$$

Here, ρ_i^0 denotes the current density, while the equation-of-state parameter w_i is a constant whose value depends on the fluid being considered. It is equal to zero in the case of matter, $1/3$ for radiation and -1 for the cosmological constant. Thus we get that

$$\rho_\mathrm{m} = \rho_\mathrm{m}^0 a^{-3} \ ; \qquad \rho_\mathrm{r} = \rho_\mathrm{r}^0 a^{-4} \ ; \qquad \rho_\Lambda = \rho_\Lambda^0 \ . \tag{1.45}$$

In the above, the subscripts m, r and Λ respectively stand for matter (baryons and cold dark matter), radiation (photons and massless neutrinos) and a cosmological constant, while a superscript 0 indicates present-day values. The multi-component

cosmic fluid may itself be treated as a perfect fluid with energy-momentum tensor [18]

$$T^{\mu\nu} = (\rho + p)\, u^\mu u^\nu + p g^{\mu\nu} \ , \tag{1.46}$$

where

$$T^{\mu\nu} = \sum_i \left(T^{\mu\nu}\right)_i \ ; \quad \rho = \sum_i \rho_i \ ; \quad p = \sum_i p_i \ . \tag{1.47}$$

It is common practice to write the energy densities in terms of dimensionless quantities called *density parameters*. The density parameter Ω_i associated with ρ_i is defined as the ratio of ρ_i to the critical density $\rho_{\rm crit}$ [18]:

$$\Omega_i = \frac{\rho_i}{\rho_{\rm crit}} = \frac{\rho_i}{3H^2/(8\pi G)} = \frac{8\pi G}{3H^2}\rho_i = \Omega_i^0 \left(\frac{H_0}{H}\right)^2 a^{-3(1+w_i)} \ , \tag{1.48}$$

$\rho_{\rm crit}$ being the energy density of the cosmic fluid in a perfectly flat Universe. When we divide Eq. (1.38) by H^2 and express the energy densities as functions of the respective $\Omega_i s$ [while making use of the relation $\rho_\Lambda = \Lambda/(8\pi G)$], the first Friedmann equation takes the form:

$$1 = \Omega_{\rm m} + \Omega_{\rm r} + \Omega_\Lambda - \frac{\kappa}{H^2 a^2} \ . \tag{1.49}$$

It is customary to introduce a parameter Ω_k analogous to Ω_i [18]:

$$\Omega_k = -\frac{\kappa}{H^2 a^2} \ , \tag{1.50}$$

so that Eq. (1.49) becomes:

$$\Omega_{\rm m} + \Omega_{\rm r} + \Omega_\Lambda + \Omega_k = 1 \ . \tag{1.51}$$

By comparing model predictions to cosmological observations, the present-day values for the density parameters (in the framework of a ΛCDM cosmology) are estimated at 0.3 for the matter component and 0.7 for vacuum energy [20]. $\Omega_{\rm r}^0$ is found to be negligibly small[19] ($\approx 9 \times 10^{-5}$).

The cosmological redshift

As light from galaxies travels through space-time, the expansion of the Universe causes its wavelength to 'stretch' and thus shifts it closer to the red end of the spectrum. In

[19] This can be calculated from the current value of the matter density parameter ($\Omega_{\rm m}^0 \approx 0.3$) and the redshift at which the matter and radiation densities were equal, $z_{\rm eq} = 3349$ [20].

other words, the light is *red-shifted*.

Let us consider a photon emitted at point O and received at R. The cosmological redshift z is defined in terms of the change in frequency it undergoes along the way [8]:

$$z = \frac{\omega_{\mathrm{O}} - \omega_{\mathrm{R}}}{\omega_{\mathrm{R}}} \ . \tag{1.52}$$

Here, ω is the frequency of the photon at the point indicated by the subscript. We may write z as a function of the photon energy E by recalling that $E \propto \omega$:

$$z = \frac{E_{\mathrm{O}} - E_{\mathrm{R}}}{E_{\mathrm{R}}} \ . \tag{1.53}$$

E itself is determined from the momentum four-vector (p^μ) of the photon, and its value also depends on the four-velocity (u^ν) of the observer [8]:

$$E = -p_\mu u^\mu \ . \tag{1.54}$$

We shall parameterise the null geodesic along which the photon travels in such a way that $p^\mu = \mathrm{d}x^\mu/\mathrm{d}\varkappa$ ($\varkappa$ represents an affine parameter). If we furthermore pick an observer who co-moves with the cosmic flow – that is, one whose four-velocity u^μ is $(1, 0, 0, 0)$ – it may be deduced that [8]:

$$E = -g_{00}\frac{\mathrm{d}x^0}{\mathrm{d}\varkappa}u^0 = \frac{\mathrm{d}x^0}{\mathrm{d}\varkappa} = \frac{\mathrm{d}t}{\mathrm{d}\varkappa} \ , \tag{1.55}$$

since $g_{00} = -1$ for the FLRW metric [Eq. (1.23)].

The simplest definition of a geodesic is that it is a curve along which the tangent vector is parallel-transported. In other words, the directional covariant derivative of the tangent vector must be zero at every point on a geodesic. The condition for parallel transport is thus:

$$\frac{\mathrm{d}x^\mu}{\mathrm{d}\varkappa}\nabla_\mu\left(\frac{\mathrm{d}x^\mu}{\mathrm{d}\varkappa}\right) = 0 \ , \tag{1.56}$$

which can be expanded to give

$$\frac{\mathrm{d}^2x^\mu}{\mathrm{d}\varkappa^2} + \Gamma^\mu_{\rho\sigma}\frac{\mathrm{d}x^\rho}{\mathrm{d}\varkappa}\frac{\mathrm{d}x^\sigma}{\mathrm{d}\varkappa} = 0 \ , \tag{1.57}$$

where $\Gamma^\mu_{\rho\sigma}$ are the Christoffel symbols [8]. Without loss of generality, we may consider paths having $x^\mu(\varkappa) = \{t(\varkappa), r(\varkappa), 0, 0\}$. In an FLRW cosmology, then, the $\mu = 0$

component of the geodesic equation [Eq. (1.57)] would read:

$$\frac{\mathrm{d}^2 t}{\mathrm{d}\varkappa^2} + \frac{a\dot{a}}{1-\kappa r^2}\left(\frac{\mathrm{d}r}{\mathrm{d}\varkappa}\right)^2 = 0 \ , \tag{1.58}$$

and Eq. (1.23) would be reduced to

$$0 = -\mathrm{d}t^2 + a^2(t)\frac{\mathrm{d}r^2}{1-\kappa r^2} \ , \tag{1.59}$$

since photon geodesics have a null line element [8]. The above equation may be expressed as $\mathrm{d}r/\mathrm{d}\varkappa = a^{-1}\sqrt{1-\kappa r^2}\ \mathrm{d}t/\mathrm{d}\varkappa$. Inserting this into Eq. (1.58) yields the following relation:

$$\frac{\mathrm{d}^2 t}{\mathrm{d}\varkappa^2} + \frac{\dot{a}}{a}\left(\frac{\mathrm{d}t}{\mathrm{d}\varkappa}\right)^2 = 0 \ , \tag{1.60}$$

which admits the solution $\mathrm{d}t/\mathrm{d}\varkappa \propto a^{-1}$. Hence, going back to Eq. (1.55), we are able to deduce that $E \propto a^{-1}$. Eq. (1.53) consequently becomes [8]

$$z = \frac{a_{\mathrm{O}}^{-1} - a_{\mathrm{R}}^{-1}}{a_{\mathrm{R}}^{-1}} = \frac{a_{\mathrm{R}}}{a_{\mathrm{O}}} - 1 \ , \tag{1.61}$$

so that if the photon is detected at present (when $a_{\mathrm{R}} = 1$), the redshift of the source is

$$z = a^{-1} - 1 \ , \tag{1.62}$$

where $a = a_{\mathrm{O}}$, although the subscript is now redundant.

In conclusion, light undergoes a frequency shift as it travels through space-time, and this feature – a direct result of cosmic expansion – provides us with the value of the scale factor at the time the photon was emitted. It additionally serves as a measure of distance: the greater the redshift, the further away the source is from the detector [8]. The frequency shift itself is determined from the emission or absorption spectrum of the former.

Distance measures

Proper distance

The proper distance to an object is the radial separation between it and the origin of our coordinate system, as measured *instantaneously* i.e. when both origin and object

are contained within the same spatial hypersurface [8]. Before proceeding, let us make use of Eq. (1.27) and write Eq. (1.23) in a slightly different form:

$$\mathrm{d}s^2 = -\mathrm{d}t^2 + a(t)^2 \left(\mathrm{d}\chi^2 + \mathcal{F}^2 \left[\mathrm{d}\theta^2 + \sin^2\theta \, \mathrm{d}\phi^2\right]\right) \ . \tag{1.63}$$

The proper distance to an object positioned at χ is therefore:

$$d_{\mathrm{P}} = a(t) \int_0^{\chi} \mathrm{d}\bar{\chi} = a(t)\chi \ , \tag{1.64}$$

where χ is a comoving coordinate and so (provided the origin and observed object have no peculiar velocity) does not change with time.

Despite being a physical distance, d_{P} is not a quantity we can measure in practice. Anything we observe must be situated in our past light cone and not within our spatial hypersurface [8].

Comoving distance

This is simply the proper distance with the expansion of the Universe 'factored out':

$$d_{\mathrm{C}} = \int_0^{\chi} \mathrm{d}\bar{\chi} = \chi \ . \tag{1.65}$$

Since the scale factor a is normalised with respect to its present-day value, the proper and comoving distances are currently equivalent.

Angular diameter distance

In Euclidean space, an object of proper diameter $\mathcal{D}$ located at a distance d subtends an angle (or *angular diameter*) $\Delta\theta$ that is given by the ratio of $\mathcal{D}$ to d. To calculate the angular diameter distance d_{A}, the starting point is therefore the relation:

$$d_{\mathrm{A}} = \frac{\mathcal{D}}{\Delta\theta} \ . \tag{1.66}$$

An expression for $\mathcal{D}$ may be obtained from the FLRW metric [18]. To this end, we consider two rays of light that are emitted at $t = t_{\mathrm{e}}$ from a source having proper length (or diameter) $\mathcal{D}$ and positioned at a fixed value of χ (say χ_{e}). The rays travel along radial null geodesics and reach our observer at time t_{obs}, where they intersect at an angle $\Delta\theta$. We shall simplify the derivation by orienting the spatial axes in such

a way that ϕ does not change along the photon paths [18].

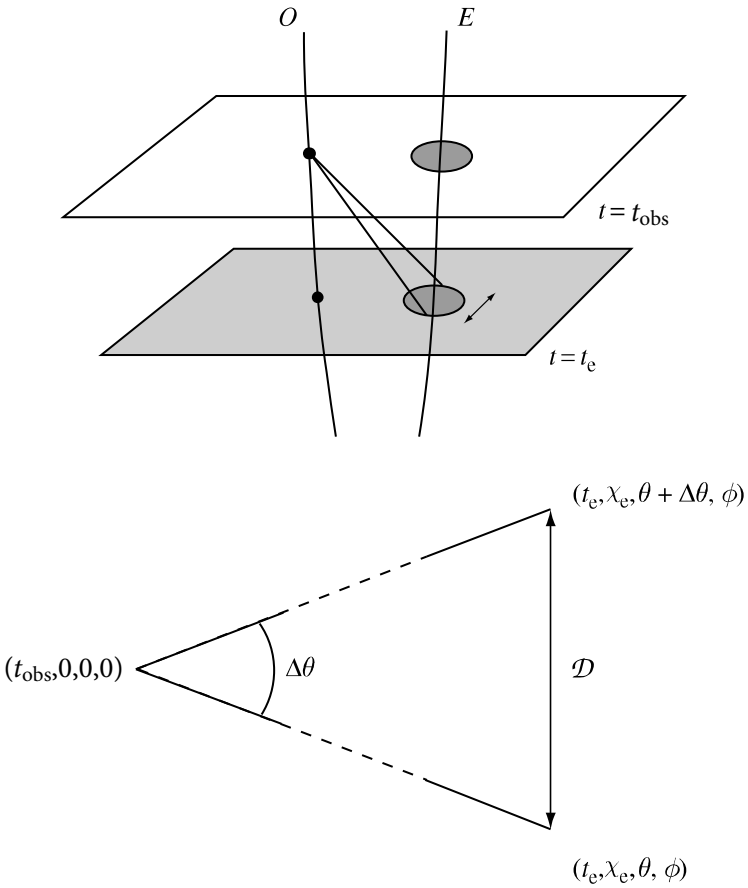

FIGURE 1.3: *(Top)* Geometry associated with the definition of angular diameter distance (one spatial dimension is suppressed), and *(bottom)* specification of coordinates. The observer is indicated with an O and the source (or emitter) with an E.

Figure and caption from Ref. [18].

As depicted in Fig. 1.3, the source has end-points with spatial coordinates $(\chi_e, \theta + \Delta\theta, \phi)$ and (χ_e, θ, ϕ), and the observer sees it the way it was at $t = t_e$. This information [in conjunction with Eq. (1.63)] allows us to deduce that:

$$\mathcal{D} = a(t_e)\mathcal{F}(\chi_e)\Delta\theta \ . \tag{1.67}$$

Inserting the above into Eq. (1.66) yields [18]:

$$d_A = \frac{a(t_e)\mathcal{F}(\chi_e)\Delta\theta}{\Delta\theta} = a(t_e)\mathcal{F}(\chi_e) \ , \tag{1.68}$$

and once $a(t_e)$ has been converted into the corresponding redshift via Eq. (1.62), the

expression for the angular diameter distance reads:

$$d_{\mathrm{A}} = \frac{\mathcal{F}(\chi_{\mathrm{e}})}{1+z_{\mathrm{e}}} \ , \tag{1.69}$$

with the function $\mathcal{F}$ defined as in Eq. (1.26). The comoving coordinate χ_{e} may be calculated from Eq. (1.63) by using the fact that $\mathrm{d}s = \mathrm{d}\theta = \mathrm{d}\phi$ along a photon path. Provided the origin is fixed at the position of the observer (i.e. the photon is assumed to be incoming), and the redshifts of the emitter and observer are denoted by z_{e} and z_{obs}, respectively, we can write [18]:

$$\chi_{\mathrm{e}} = \int_0^{\chi_{\mathrm{e}}} \mathrm{d}\chi = -\int_{t_{\mathrm{obs}}}^{t_{\mathrm{e}}} \frac{\mathrm{d}t}{a(t)} = \int_{t_{\mathrm{e}}}^{t_{\mathrm{obs}}} \frac{\mathrm{d}t}{a(t)} = \int_{z_{\mathrm{obs}}}^{z_{\mathrm{e}}} \frac{\mathrm{d}z}{H(z)} \ . \tag{1.70}$$

Luminosity distance

As before, it is best to start from an operational definition [18]. In Euclidean space, the flux F from a source of absolute luminosity L decreases in inverse proportion to the area over which the light spreads. In other words, we have that $F = L/(4\pi d^2)$ [8], and hence [18]

$$d_{\mathrm{L}} = \sqrt{\frac{L}{4\pi F}} \ . \tag{1.71}$$

What does Eq. (1.71) translate into for an FLRW geometry? Let us suppose that a source with χ-coordinate χ_{e} (relative to an observer at the origin) emits a signal at $t = t_{\mathrm{e}}$. At any given time $t > t_{\mathrm{e}}$, the photons would be spread evenly over a sphere centred at the point of emission. The area of the sphere may be determined from the metric [Eq. (1.63)] by considering that:

- $\mathrm{d}t = 0$, because the sphere exists within the same hypersurface;
- $\mathrm{d}\chi = 0$. To clarify why this is so, we may shift the origin to the position of the emitter. Then, by symmetry, the emitter would assign the coordinate χ_{e} to the observer. Detection occurs when the photons reach χ_{e} (i.e. the location of the observer). But since all points on the sphere of light are equidistant from the emitter, it follows that all have χ-coordinate χ_{e}, and so $\mathrm{d}\chi = 0$ along the surface of the sphere.

Consequently, at the time of observation (t_{obs}) the surface has line element:

$$\mathrm{d}s^2 = a^2(t_{\mathrm{obs}})\mathcal{F}^2(\chi_{\mathrm{e}})\left(\mathrm{d}\theta^2 + \sin^2\theta\,\mathrm{d}\phi^2\right) \ . \tag{1.72}$$

The above may be compared with the metric of a 2-sphere having radius r (and area $4\pi r^2$):

$$\mathrm{d}s^2 = r^2\left(\mathrm{d}\theta^2 + \sin^2\theta\,\mathrm{d}\phi^2\right) \ , \tag{1.73}$$

from which it can readily be deduced that the surface area A of the sphere of light is $4\pi a^2(t_{\rm obs})\mathcal{F}^2(\chi_{\rm e})$. However, the flux is not diluted simply because the light spreads out. Two additional effects come into play as a result of cosmic expansion [8]: firstly, the photons are redshifted by a factor $(1+z)$ on their way from the source,[20] and secondly, two photons emitted a time δt apart reach the detector with a temporal separation of $(1+z)\delta t$. Therefore, the flux observed at $t = t_{\rm obs}$ is [8]:

$$F(t_{\rm obs}) = \frac{L(t_{\rm e})}{4\pi d_{\rm L}^2} = \frac{L(t_{\rm e})}{A} \times \frac{1}{(1+z)^2} = \frac{L(t_{\rm e})}{4\pi a^2(t_{\rm obs})\mathcal{F}^2(\chi_{\rm e})}\frac{1}{(1+z)^2} \ , \tag{1.74}$$

and the luminosity distance is given by:

$$d_{\rm L} = a(t_{\rm obs})\mathcal{F}(\chi_{\rm e})(1+z) \ . \tag{1.75}$$

At this stage, it is convenient to introduce a function $\bar{\mathcal{F}}$ that is a slightly modified version of $\mathcal{F}$ [the latter is defined in Eq. (1.26)]:

$$\bar{\mathcal{F}}(x) = \begin{cases} x & \text{if } \kappa = 0 \ ; \\ \sin x & \text{if } \kappa > 0 \ ; \\ \sinh x & \text{if } \kappa < 0 \ . \end{cases} \tag{1.76}$$

Then Eq. (1.75) becomes:

$$d_{\rm L} = a(t_{\rm obs})\frac{1+z}{\sqrt{|\kappa|}}\,\bar{\mathcal{F}}\left(\sqrt{|\kappa|}\,\chi_{\rm e}\right) \ , \tag{1.77}$$

and inserting Eq. (1.70) into the above yields:

$$d_{\rm L} = a(t_{\rm obs})\frac{1+z}{H_0\sqrt{|\Omega_k^0|}}\,\bar{\mathcal{F}}\left(\sqrt{|\Omega_k^0|}\int_{z_{\rm obs}}^{z_{\rm e}}\frac{\mathrm{d}z}{H(z)/H_0}\right) \ , \tag{1.78}$$

where we have also made use of the relation $\kappa = -\Omega_k^0 H_0^2$ from Eq. (1.50). When $\kappa = 0$, Eq. (1.78) simplifies to

[20] As outlined in subsection 1.3.4, $1+z$ is defined as the ratio of the frequency at emission to the frequency at reception. We refer to z as the *redshift of the source*.

$$d_{\mathrm{L}} = a(t_{\mathrm{obs}})\frac{1+z}{H_0}\int_{z_{\mathrm{obs}}}^{z_{\mathrm{e}}}\frac{\mathrm{d}z}{H(z)/H_0}\ . \tag{1.79}$$

The horizons

The speed of light sets a limit on how far into the past we are able to look. To investigate the extent of the region from which an arbitrary comoving observer may receive light signals (at some given time t), we must first familiarise ourselves with the various horizons defined in cosmology.

The particle horizon

The particle horizon provides a measure of the distance that light could have travelled since the beginning of the Universe [126]. The concept can be simplified by considering the following scenario: a comoving observer E with χ coordinate χ_{e} emits a photon at $t = t_{\mathrm{e}}$, which travels through spacetime and reaches an observer O situated at $\chi = 0$. The arrival time of the photon shall be denoted by t_{obs}. Since information cannot be transmitted at a speed faster than that of light, the only signals emitted at t_{e} that O can detect at time t_{obs} are those originating from radial coordinates $\chi \leq \chi_{\mathrm{e}}$ [18].

We have already seen that χ_{e} can be expressed as the integral

$$\chi_{\mathrm{e}} = \int_{t_{\mathrm{e}}}^{t_{\mathrm{obs}}}\frac{\mathrm{d}t}{a(t)}\ . \tag{1.80}$$

It follows that if $\chi_{\mathrm{e}} \to \infty$ as $t_{\mathrm{e}} \to 0$, O is able to receive signals from any comoving particle[21] – no matter how far away it is – provided that they are emitted at a sufficiently early time. On the other hand, should the integral converge in this limit, it would mean that the χ-coordinate of the emitter has a finite, time-dependent upper bound $\chi_{\mathrm{P}}(t)$, and the region beyond is inaccessible to O. Simply put, the integral in Eq. (1.80) (with $t_{\mathrm{e}} \to 0$) determines where an emitter should be situated if a light pulse it sends out at the very beginning of time ($t = 0$) just reaches the observer at $t = t_{\mathrm{obs}}$. Signals from objects that are further away would still be 'in transit'. The fact that χ_{P} is a function which increases with t implies that as time passes, previously hidden parts of the Universe gradually come into view [18].

In conclusion, if the integral of Eq. (1.80) converges as $t_{\mathrm{e}} \to 0$, our vision of the Universe at time t is restricted by a *particle horizon* located at χ_{P}, where χ_P is given

[21] In this context, *particles* represent typical galaxies.

by:

$$\chi_{\rm P}(t) = \int_0^t \frac{{\rm d}\bar{t}}{a(\bar{t})} \ . \tag{1.81}$$

For instance, the proper distance to the particle horizon in a flat ΛCDM cosmology is $3t$ during the matter-dominated epoch, and $2t$ for a radiation-dominated Universe [18].

The presence of a particle horizon leads to an apparent contradiction known as the *horizon problem*. If the homogeneity of the Universe is due to the physical transport of energy and momentum from place to place, then at a given time t one would expect to find inhomogeneities on scales larger than $2a(t)\chi_{\rm P}(t)$, this being the maximum possible proper distance between any two particles that could have received the same signal by time t [127]. How, then, does one explain the nearly uniform temperature of the cosmic microwave background? The photons of the CMB were emitted from the surface of last scattering, and the particle horizon at the time would subtend an angle of around 1° in the sky today [128]. So how do regions so far apart that – according to standard cosmological models – they could never have been in causal contact display the same physical characteristics?

The horizon problem was one of the factors that motivated the introduction of *inflation*. This refers to a period of very rapid expansion that is thought to have taken place in the early Universe, and which caused the comoving Hubble distance (defined as the quantity H^{-1}/a) to shrink. Consequently, the observable Universe is at present much smaller than the region that was causally connected before inflation [121].

The event horizon

The event horizon is closely related to the particle horizon. We have seen that the latter grows with time, which raises the question: what happens as $t \to \infty$? This is where the event horizon comes in.

Let us return to Eq. (1.80) and take the limit $t_{\rm obs} \to t_{\rm max}$ [18]:

$$\chi_{\rm e} = \int_{t_{\rm e}}^{t_{\rm max}} \frac{{\rm d}t}{a(t)} \ . \tag{1.82}$$

Here, $\chi_{\rm e}$ is the $\chi-$coordinate of the source, $t_{\rm e}$ the time of emission, and $t_{\rm max}$ is either infinity or the time of the big crunch, depending on the model. Whether or not the model admits an *event horizon* is determined by the behaviour of the integral. If it diverges, the answer is no, because the χ-coordinate of the emitter is not subject to an

upper bound [18]. However, a finite value for $\chi_{\rm e}$ (say $\chi_{\rm E}$) indicates that a light pulse sent out at $t = t_{\rm e}$ from a source at $\chi_{\rm E}$ will reach the observer (positioned at $\chi = 0$) just as $t \to t_{\rm max}$. Signals emitted at $t = t_{\rm e}$ from particles with radial coordinate $\chi > \chi_{\rm E}$ would *never* be detected; there would simply not be enough time for them to travel all the way to the observer. Therefore, a convergent integral indicates that our view of the Universe is forever limited by an event horizon located at $\chi_{\rm E}$. The value of $\chi_{\rm E}$ depends on $t_{\rm e}$ and is given by:

$$\chi_{\rm E} = \int_{t_{\rm e}}^{t_{\rm max}} \frac{{\rm d}t}{a(t)} \ . \tag{1.83}$$

Symmetry considerations imply that a signal emitted from $\chi = 0$ at $t = t_{\rm e}$ would be unable to ever go beyond $\chi = \chi_{\rm E}$ [18].

The Hubble distance

The *Hubble distance* (or *radius*) is defined as the reciprocal of the Hubble parameter:

$$d_{\rm H}(t) = \frac{1}{H(t)} \ , \tag{1.84}$$

and serves as a measure of the size of the observable Universe. Since it approximates the distance that light can traverse while the Universe expands appreciably, it is commonly called 'the horizon' [126]. On scales much smaller than $d_{\rm H}(t)$, Newtonian theory is often adequate to describe gravitational phenomena [18], and provided the time intervals considered are sufficiently shorter than the Hubble time,[22] the expansion of the Universe can usually be treated as negligible on such scales [126].

[22]The *Hubble time* is the quantity H^{-1} (the Hubble distance is cH^{-1}, but becomes H^{-1} with our choice of units). It provides a rough estimate of the age of the Universe [126].

CHAPTER 2

Cosmology based on Scalar-Tensor Theory

2.1 Introduction

Without doubt, the simplest fields that can be invoked to explain physical phenomena are the scalar ones. A prominent example of the relevance and importance of scalar fields is their use in inflationary cosmic scenarios. Their significance, however, began to be realised long before Guth [129] proposed the concept of inflation in the 1980s. Indeed, the conformally flat scalar theory of gravity put forward by Nordström [130] is even older than General Relativity (GR). Another example is provided by the Newtonian constant of gravitation (G). It was Dirac [131], when working on his Large Number Hypothesis, who first explored the idea of making G time-dependent. He saw this as a means of establishing a relation between cosmological and fundamental physical constants. The following decade, Jordan [132] took Dirac's idea further and promoted G to the role of a gravitational scalar field [36].

The prototype of Scalar-Tensor Theory (STT) was published by Brans and Dicke [133] in 1961. Their theory makes use of the Friedmann-Lemaître-Robertson-Walker (FLRW) metric tensor, but they added a scalar field that can be identified with the inverse of the gravitational coupling G. In Brans-Dicke theory, G is a variable whose value is determined by all the matter in the Universe. Mach's principle is thus explicitly incorporated – the distribution of matter on cosmological scales affects local gravitational experiments [36][23].

The success of GR in accounting for Solar System observations means that any alternative model must have a GR limit on small scales. Significant deviations may only show up in cosmological scenarios. The fact that scalar fields in STT evolve over a cosmological time scale, therefore, makes Scalar-Tensor gravity especially relevant for

[23] Also refer to works cited therein.

cosmology [36].

The importance of scalar fields in modern unified theories has led to renewed interest in STT. After all, it is a scalar field (called the Higgs field) which allows the W and Z bosons and the fundamental fermions to acquire mass [134]. Quantum excitations of the Higgs field give rise to scalar bosons known as *Higgs particles* [135, 136]. The experimental verification of the bosons' existence by the ATLAS [137] and CMS [134] collaborations in 2012 was a pivotal moment for particle physics.

In cosmology, the relevance of STT becomes evident when one considers, for instance, that bosonic string theory has a low-energy limit similar to the Brans-Dicke model [138], and that STT bears a resemblance to supergravity and string theory. At the classical level, the extra spatial dimensions of Kaluza-Klein theory may be compactified to arrive at the Brans-Dicke theory [36][24].

This is not to say that Scalar-Tensor gravity is without its caveats. There was actually a time when its popularity began to decline, especially as Solar System experiments became more and more accurate and the resulting constraints more stringent. Conflict between observation and theory centred around the value of the parameter ω that features in Brans-Dicke theory. This parameter is expected to be of order unity, but the constraints imposed by Solar System observations were pointing to much larger values [139, 140]. Although the discrepancy did not disqualify the theory, the implied fine-tuning did not go down well with physicists. However, the dynamic nature of ω in generalised Brans-Dicke theory and STT means that it can vary from a parameter of order unity in the early Universe to attain the required larger value later on [36, 141, 142].

At present, the principles of STT provide the basis for some of the most prominent dark energy models. It may well be that the observed acceleration of the Universe is due to a long-range gravitational scalar field [36]. Part of the work leading to this thesis involved looking for solutions to the field equations of Scalar-Tensor gravity. We shall therefore proceed by going over the basic properties of STT, and then we shall analyse a number of solutions in which the scalar field produces the effects of dark energy at late times.

[24] Also refer to works cited therein.

2.1.1 Scalar fields in the literature

The detection of gravitational waves from a binary neutron star merger became a reality on August 17, 2017, when the LIGO-VIRGO collaboration picked up signals from the event later designated GW170817 [143]. The signature of a short gamma ray burst (GRB170817A) reached observatories a few seconds later [144].

This episode has had great implications for scalar-tensor theory. The extremely small probability that GW170817 and GRB170817A happened in such close proximity (both temporal and spatial) purely by chance led to the conclusion that they were both the result of the same event. The recorded electromagnetic and gravitational wave signals could thus be used to constrain the difference between their respective speeds, and the tight bound obtained implied a variation of less than $10^{-13}\,\%$ [144]. A significant number of scalar-tensor theories, however, predict a gravitational wave speed that differs from the speed of light, and consequently many of these are no longer deemed viable dark energy models [145]. The list includes Horndeski theories such as the Fab Four [146] and the quartic/quintic Galileon scenarios [147, 148], as well as several beyond Horndeski models [149–151]. Quintessence and K-essence, Brans-Dicke theory, $f(R)$ gravity and Kinetic Gravity Braiding are among the models that remain valid [145].

As may be deduced from the last two sentences, 'Scalar Tensor Theory' has become a kind of umbrella term for all the models in which cosmic dynamics are controlled by one or more scalar fields. Some of these models – $f(R)$ gravity, for instance – are not explicitly scalar-tensor theories, but may be recast as such [56, 152].

The GW170817 event appears to favour simple dark energy models. One of the simplest constructs in the context of STT is Quintessence – a family of models based on a canonical scalar field ϕ that is minimally coupled to gravity.[25] These models are usually classified as either freezing or thawing. The former accommodate very small departures from ΛCDM when tested with observational data, but thawing models appear to allow for more significant deviation [33][26]. The possibility that the same scalar field drives both inflation and the current accelerated expansion has also been considered in the literature [153–156], many times in the framework of braneworld cosmology. The resulting models are called *Quintessential Inflationary Scenarios*.[27]

[25] *Minimal* and non-minimal coupling are defined in the beginning of section 2.2.

[26] See also [34] and references therein.

[27] The word *quintessence* is usually taken to be synonymous with 'dark energy', while the scalar field responsible for inflation is referred to as an *inflaton*.

In standard models of Quintessence, however, the scalar field is only allowed to gain prominence at late times. This is motivated by the fact that a non-negligible (albeit sub-dominant) amount of Quintessence present during the period of structure formation would have left a detectable imprint on the cosmic microwave background (CMB). On the contrary, models in which the scalar field couples directly to matter can support the growth of density perturbations even when the scalar dominates. Such a coupling arises naturally if the STT equations are expressed in the Einstein frame.[28] The problem in this case is that the associated 'fifth force' may be difficult to reconcile with cosmological observations [36][29], although it does not preclude the existence of viable models. For instance, Tsujikawa et al. [157] consider models whose Einstein-frame version is characterised by a constant coupling Q between non-relativistic matter and the scalar field. Quintessence corresponds to the case $Q = 0$, but in general the scalar field is not minimally coupled, nor its kinetic term canonical. The authors conclude that these models may admit a matter-dominated era followed by a period of cosmic acceleration. Provided certain conditions are met, they are furthermore able to satisfy both cosmological and local gravity constraints [157]. Another study [158] has shown that a canonical scalar field conformally coupled[30] to dark matter – and evolving in a background identical to the one in ΛCDM – can alleviate the $f\sigma_{8,0}$ tension that is currently one of the major shortcomings of the standard model. This tension refers to the difference that emerges between the amount of clustering inferred from CMB data and that determined from redshift space distortions when estimates are made in a ΛCDM framework [158].

A phase of cosmic history during which scalar fields are thought to have been especially important is the primordial period of acceleration known as *inflation*. STT models meant to describe the early Universe may in fact not only incorporate a graceful exit from inflation [159,160], but the dynamics of the scalar field can also serve to suppress the nucleation of true vacuum bubbles until inflation reaches the final stages [141]. Inflationary scenarios modelled on the basis of STT are often termed *hyper-extended* [36]. This chapter, however, focuses on scalar fields whose properties resemble those of dark energy at late times.

In the context of Einstein gravity, a minimally-coupled scalar field cannot have an equation of state (EoS) with characteristic parameter $w_{\rm d} < -1$. Quintessence is a case in point. Yet the situation changes when the coupling is non-minimal – in this

[28] More details about the Einstein frame may be found in Chapter 5, subsection 5.2.3.
[29] Also refer to works cited therein.
[30] *Conformal coupling* is defined in the beginning of section 2.2.

case, an EoS parameter ($w_{\rm d}$) that crosses the phantom divide does not preclude the existence of attractor solutions [36][31], although the range of values it can take is currently a matter of dispute. Observational constraints on the present value often restrict it to the range $[-1, -1/3]$. Nonetheless, values less than -1 can also be compatible with observations [31, 161].

The advantages of non-minimal coupling go beyond the possibility of having $w_{\rm d} < -1$. For instance, the inclusion of a (non-zero) coupling constant ξ in the coupled Einstein-Klein-Gordon equations is necessary to renormalise the theory, and may be shown to arise from first-loop corrections [36][31]. It has additionally been proposed that non-minimal coupling may alleviate problems associated with primordial nucleosynthesis [162].

2.2 Field Equations[32]

Let us first recall the famous *Einstein-Hilbert action* on which GR is based:

$$S = \frac{1}{16\pi G} \int R\sqrt{-g}\ \mathrm{d}^4x\ . \tag{2.1}$$

The addition of a cosmological constant is effected by replacing R with $R - 2\Lambda$.

Eq. (2.1) emerges naturally if one considers the following: under the condition that metric derivatives higher than second order are excluded, R turns out to be the only independent scalar which can be constructed from the metric. This led Hilbert to realise that the simplest action based on $g_{\mu\nu}$ was the one given by Eq. (2.1) [8].

In contrast, the gravitational part of the STT action we adopt throughout this chapter reads:

$$S = \int \left[\left(\frac{1}{16\pi G} - \frac{\xi}{2}\phi^2 \right) R - \frac{1}{2}\nabla^\eta\phi\nabla_\eta\phi - V(\phi) \right] \sqrt{-g}\, \mathrm{d}^4x\ . \tag{2.2}$$

Here, $V(\phi)$ denotes the potential associated with the scalar field ϕ, and ξ is a dimensionless constant responsible for the explicit coupling between ϕ and the Ricci scalar. Setting $\xi = 0$ corresponds to what is known as *minimal* coupling. On the other hand, if ξ is non-zero we say we have *non-minimal* coupling. The choice $\xi = 1/6$ is especially popular. This is the case of *conformal coupling*, so called because putting the potential V either equal to zero or proportional to ϕ^4 renders the Klein-Gordon

[31] Also refer to works cited therein.

[32] Sec. 2.2 is based on parts of Ref. [36]. Any other sources are referenced explicitly.

equation (and hence the physics of ϕ) conformally invariant when $\xi = 1/6$.[33] Another important feature of models with conformal coupling is their adherence to the Einstein equivalence principle. Indeed, all other values of ξ lead to violations of this principle [163]. We note that the *strong coupling* scenario ($|\xi| >> 1$) is also given attention in the literature.

The next step consists in varying the action (2.2) with respect to the metric. The resulting field equation is:

$$(1 - 8\pi G\xi\phi^2)G_{\mu\nu} \; = 8\pi G\Big\{\nabla_\mu\phi\nabla_\nu\phi - \frac{1}{2}g_{\mu\nu}\nabla^\eta\phi\nabla_\eta\phi - Vg_{\mu\nu} + \xi\left[g_{\mu\nu}\,\Box(\phi^2) - \nabla_\mu\nabla_\nu(\phi^2)\right]\Big\}\,, \tag{2.3}$$

while variation with respect to ϕ yields:

$$\Box\phi - \frac{\mathrm{d}V}{\mathrm{d}\phi} - \xi R\phi \;=\; 0\;. \tag{2.4}$$

The latter can be thought of as the curved-space generalisation of the Klein-Gordon equation.

The energy-momentum tensor of a non-minimally coupled scalar field can be defined in various ways. Consequently, so can the energy density, pressure, and effective equation of state associated with ϕ. The differences arise from the way in which Eq. (2.3) is cast and reflect the fact that as yet, no general formulation for the energy density of the gravitational field has been established. There are three options available to us. If we follow the work of Callan, Coleman and Jackiw [164], for instance, the term $8\pi G\xi\phi^2 G_{\mu\nu}$ on the left-hand side of (2.3) is absorbed into the expression for $T^{\phi}_{\mu\nu}$:

$$G_{\mu\nu} = 8\pi G\left(T^{\phi,\,\mathrm{CCJ}}_{\mu\nu} + T^{\mathrm{m}}_{\mu\nu}\right)\;. \tag{2.5}$$

In the above, $T^{\mathrm{m}}_{\mu\nu}$ is the energy-momentum tensor for any matter distribution additional to the scalar field. $T^{\phi,\,\mathrm{CCJ}}_{\mu\nu}$ denotes the energy-momentum tensor of ϕ and is given by:

$$T^{\phi,\,\mathrm{CCJ}}_{\mu\nu} = \nabla_\mu\phi\nabla_\nu\phi - \frac{1}{2}g_{\mu\nu}\nabla^\eta\phi\nabla_\eta\phi - Vg_{\mu\nu} + \xi\left[g_{\mu\nu}\,\Box(\phi^2) - \nabla_\mu\nabla_\nu(\phi^2)\right] + \xi\phi^2 G_{\mu\nu}\;. \tag{2.6}$$

[33] A theory is said to be *conformally invariant* if the form of its action is not altered by conformal transformations [such as the one of Eq. (2.27)].

Alternatively, one may take the *effective coupling approach* and divide Eq. (2.3) by $(1-8\pi G\xi\phi^2)$, getting that

$$G_{\mu\nu} = \frac{8\pi G}{1-8\pi G\xi\phi^2}\left(T^{\phi,\,\mathrm{EC}}_{\mu\nu}+T^{\mathrm{m}}_{\mu\nu}\right) = \kappa_{\mathrm{eff}}(\phi)\left(T^{\phi,\,\mathrm{EC}}_{\mu\nu}+T^{\mathrm{m}}_{\mu\nu}\right), \tag{2.7}$$

with $T^{\phi,\,\mathrm{EC}}_{\mu\nu} = T^{\phi,\,\mathrm{CCJ}}_{\mu\nu} - \xi\phi^2 G_{\mu\nu}$. The parameter $\kappa_{\mathrm{eff}}(\phi)$ plays the role of an effective gravitational coupling for both $T^{\phi,\,\mathrm{EC}}_{\mu\nu}$ and $T^{\mathrm{m}}_{\mu\nu}$ and earns the procedure its name.

The so-called *mixed approach* on which this chapter is based entails rewriting Eq. (2.3) as:

$$G_{\mu\nu} \;=\; 8\pi G\left(T^{\phi,\,\mathrm{MIX}}_{\mu\nu}+\frac{T^{\mathrm{m}}_{\mu\nu}}{1-8\pi G\xi\phi^2}\right)\,. \tag{2.8}$$

Now the energy-momentum tensor for the scalar field takes the form

$$T^{\phi,\,\mathrm{MIX}}_{\mu\nu} = \frac{1}{1-8\pi G\xi\phi^2}\left[\nabla_\mu\phi\nabla_\nu\phi-\frac{1}{2}g_{\mu\nu}\nabla^\eta\phi\nabla_\eta\phi-Vg_{\mu\nu}+\xi\left(g_{\mu\nu}\Box-\nabla_\mu\nabla_\nu\right)\phi^2\right]. \tag{2.9}$$

One caveat of adopting this viewpoint is the potential loss of solutions for $\xi > 0$. Scalar fields which satisfy Eq. (2.3) but which attain one of the values $\pm(8\pi G\xi)^{-1/2}$ are missed when looking for solutions to Eq. (2.8). The mixed approach is nonetheless advantageous in other ways. A case in point is the fact that in the FLRW framework, it yields simpler expressions for the energy density and pressure of the scalar field. We shall henceforth take $T^{\phi}_{\mu\nu}$ to stand for $T^{\phi,\,\mathrm{MIX}}_{\mu\nu}$.

The total energy-momentum tensor, $T^{\mathrm{tot}}_{\mu\nu} \;=\; T^{\phi}_{\mu\nu}+T^{\mathrm{m}}_{\mu\nu}/(1-8\pi G\xi\phi^2)$, is conserved in the mixed approach (as is $T^{\mathrm{m}}_{\mu\nu}$). In other words, we have that $\nabla^\mu T^{\mathrm{tot}}_{\mu\nu} \;=\; 0$. However, $T^{\phi}_{\mu\nu}$ is not conserved separately unless $T^{\mathrm{m}}_{\mu\nu}=0$. Indeed, one gets the relation

$$\nabla^\nu T^{\phi}_{\mu\nu} \;=\; -\frac{16\pi G\xi\phi}{(1-8\pi G\xi\phi^2)^2}\left(\nabla^\nu\phi\right)T^{\mathrm{m}}_{\mu\nu}\,. \tag{2.10}$$

The total energy density is given by the sum of the individual densities, ρ_ϕ and ρ_{m}, with the latter rescaled by the factor $1/(1-8\pi G\xi\phi^2)$:

$$\rho_{\mathrm{tot}} = \rho_\phi + \frac{\rho_{\mathrm{m}}}{1-8\pi G\xi\phi^2}\,. \tag{2.11}$$

2.2.1 The field equations in an FLRW cosmology

The homogeneous nature of the FLRW universe precludes any spatial variation of the scalar field, restricting it to be solely a function of time. As is common practice, we shall be assuming that ϕ has the characteristics of a perfect fluid. This means that we shall cast the effective energy momentum tensor of Eq. (2.9) in the form:

$$T^{\phi}_{\mu\nu} = (p_\phi + \rho_\phi)u_\mu u_\nu + p_\phi g_{\mu\nu} \ , \tag{2.12}$$

where ρ_ϕ is the energy density of the scalar field and p_ϕ its pressure, while its four-velocity u^μ satisfies $g_{\mu\nu}u^\mu u^\nu = u_\nu u^\nu = -1$. An expression for ρ_ϕ may be obtained by considering that an observer comoving with the fluid (and thus also having velocity u^μ) measures its energy density to be $T^{\phi}_{\mu\nu}u^\mu u^\nu$, since $T^{\phi}_{\mu\nu}u^\mu u^\nu = (p_\phi + \rho_\phi)u_\mu u_\nu u^\mu u^\nu + p_\phi g_{\mu\nu}u^\mu u^\nu = (p_\phi + \rho_\phi)(-1)(-1) + p_\phi(-1) = p_\phi + \rho_\phi - p_\phi = \rho_\phi$. If $T^{\phi}_{\mu\nu}$ is written as specified in Eq. (2.9), therefore, it follows that

$$\begin{aligned}\rho_\phi &= \frac{1}{1-8\pi G\xi\phi^2}\left[\nabla_\mu\phi\nabla_\nu\phi - \frac{1}{2}g_{\mu\nu}\nabla^\eta\phi\nabla_\eta\phi - Vg_{\mu\nu} + \xi\left(g_{\mu\nu}\Box - \nabla_\mu\nabla_\nu\right)\phi^2\right]u^\mu u^\nu; \\ &= \frac{1}{1-8\pi G\xi\phi^2}\left[\dot{\phi}^2 - \frac{1}{2}(-1)\nabla^\eta\phi\nabla_\eta\phi - V(-1) - \xi\,\Box\phi^2 - \xi\left(\nabla_\mu\nabla_\nu\phi^2\right)u^\mu u^\nu\right] \ .\end{aligned}$$

In the second line, the first term in square brackets is a result of the fact that fundamental observers have $u^\mu = (1,0,0,0)$, and consequently $(\nabla_\mu\phi\nabla_\nu\phi)u^\mu u^\nu = (\partial_0\phi)^2u^0u^0 = \dot{\phi}^2$ (a dot denotes differentiation with respect to cosmic time t). The term next to it simplifies due to ϕ being a function of time only: $\nabla^\eta\phi\nabla_\eta\phi = g^{\eta\sigma}\nabla_\sigma\phi\nabla_\eta\phi = -(\partial_0\phi)^2$. At this stage, then, we have that

$$\begin{aligned}\rho_\phi &= \frac{1}{1-8\pi G\xi\phi^2}\left[\frac{\dot{\phi}^2}{2} + V - \xi g^{\mu\nu}\nabla_\mu(2\phi\nabla_\nu\phi) - \xi\nabla_0\left(2\phi\dot{\phi}\right)\right] \ ; \\ &= \frac{1}{1-8\pi G\xi\phi^2}\left[\frac{\dot{\phi}^2}{2} + V - 2\xi\phi\,\Box\phi - 2\xi g^{\mu\nu}\nabla_\mu\phi\nabla_\nu\phi - 2\xi\phi\ddot{\phi} - 2\xi\dot{\phi}^2\right] \ ,\end{aligned} \tag{2.13}$$

with $\Box\phi = g^{\mu\nu}\nabla_\mu\nabla_\nu\phi = g^{\mu\nu}(\partial_\mu\partial_\nu\phi - \Gamma^\sigma_{\mu\nu}\partial_\sigma\phi) = -\ddot{\phi} - g^{\mu\nu}\Gamma^0_{\mu\nu}\partial_0\phi = -\ddot{\phi} - (g^{11}\Gamma^0_{11} + g^{22}\Gamma^0_{22} + g^{33}\Gamma^0_{33})\dot{\phi}$. The FLRW metric tensor is diagonal, and so g^{11}, g^{22} and g^{33} are simply the reciprocals of the respective components from Eq. (1.23). Combining these with the connection coefficients $\Gamma^0_{11} = a\dot{a}/(1-\kappa r^2)$, $\Gamma^0_{22} = a\dot{a}r^2$ and $\Gamma^0_{33} = a\dot{a}r^2\sin^2\theta$ [18] allows us to conclude that $\Box\phi = -\ddot{\phi} - 3H\dot{\phi}$. Meanwhile, the quantity $g^{\mu\nu}\nabla_\mu\phi\nabla_\nu\phi$ that appears in (2.13) reduces to $-\dot{\phi}^2$, as explained above. These considerations mean that Eq. (2.13) becomes

$$\rho_\phi = \frac{1}{1-8\pi G\xi\phi^2}\left[\frac{\dot\phi^2}{2} + V + 2\xi\phi(\ddot\phi + 3H\dot\phi) - 2\xi\phi\ddot\phi\right] ;$$
$$= \frac{1}{1-8\pi G\xi\phi^2}\left[\frac{\dot\phi^2}{2} + V + 6\xi\phi\dot\phi H\right] . \tag{2.14}$$

An expression for the pressure of the scalar field may be obtained in similar fashion. We go back to Eq. (2.12) and find the trace of $T^\phi_{\mu\nu}$:

$$T^\phi = T^\phi_{\mu\nu}g^{\mu\nu} = (p_\phi + \rho_\phi)u_\mu u_\nu g^{\mu\nu} + p_\phi g_{\mu\nu}g^{\mu\nu}$$
$$= (p_\phi + \rho_\phi)(-1) + 4p_\phi = 3p_\phi - \rho_\phi . \tag{2.15}$$

The term $4p_\phi$ in the last row arises from the relation $g_{\mu\sigma}g^{\sigma\nu} = \delta^\nu_\mu$.

The quantity p_ϕ is therefore given by:

$$p_\phi = \frac{1}{3}\left(T^\phi + \rho_\phi\right) = \frac{1}{3}T^\phi_{\mu\nu}\left(g^{\mu\nu} + u^\mu u^\nu\right) , \tag{2.16}$$

and expanding this by following the principles outlined when deriving ρ_ϕ yields

$$p_\phi = \frac{1}{1-8\pi G\xi\phi^2}\left[\left(\frac{1}{2} - 2\xi\right)\dot\phi^2 - V - 2\xi\phi\ddot\phi - 4\xi H\phi\dot\phi\right] . \tag{2.17}$$

The reader is again reminded that measurements of energy density and pressure are observer-dependent. Both Eqs. (2.14) and (2.17) reflect the point of view of a fundamental observer, i.e. one who comoves with the cosmic fluid.

The scalar field is assumed to coexist with a matter distribution that also behaves as a perfect fluid. Thus its energy-momentum tensor reads:

$$T^{\rm m}_{\mu\nu} = (p_{\rm m} + \rho_{\rm m})u_\mu u_\nu + p_{\rm m}g_{\mu\nu} , \tag{2.18}$$

$\rho_{\rm m}$ and $p_{\rm m}$ being the corresponding energy density and pressure, respectively. Since $T^{\rm m}_{\mu\nu}$ is conserved separately of $T^\phi_{\mu\nu}$, the general relativistic conservation equation still holds:

$$\dot\rho_{\rm m} + 3H(\rho_{\rm m} + p_{\rm m}) = 0 . \tag{2.19}$$

Let us furthermore assume that ordinary matter has the customary barotropic EoS, $p_{\rm m} \propto \rho_{\rm m}$. Then the solution to Eq. (2.19) is a simple power law:

$$\rho_{\rm m} = \rho^0_{\rm m}a^{-3(1+w_{\rm m})} , \tag{2.20}$$

where the EoS parameter $w_{\rm m}$ is a constant and $\rho_{\rm m}^0$ denotes the present-day value of $\rho_{\rm m}$. The above relation can in turn be used in conjunction with Eqs. (2.11) and (2.14) to substitute for $\rho_{\rm tot}$ in the first Friedmann equation:[34]

$$H^2 = \frac{8\pi G}{3}\rho_{\rm tot} - \frac{\kappa}{a^2} \ , \tag{2.21}$$

which consequently takes the form:

$$H^2 + \frac{\kappa}{a^2} - \frac{8\pi G}{3\left(1-8\pi G\xi\phi^2\right)}\left(\frac{\dot{\phi}^2}{2} + V + 6\xi H\phi\dot{\phi} + \rho_{\rm m}^0 a^{-3(1+w_{\rm m})}\right) = 0 \ . \tag{2.22}$$

This corresponds to the time-time component of Eq. (2.8). As for the spatial components, isotropy implies that all non-trivial equations obtained by setting $\mu\nu = ij$ in Eq. (2.8) should be equivalent. In fact, one finds that both sides of Eq. (2.8) sum up to zero for $i \neq j$, while the three cases with $i = j$ all lead to the same conclusion:

$$\frac{\ddot{a}}{a} = \frac{8\pi G}{3(1-8\pi G\xi\phi^2)}\left[\dot{\phi}^2(3\xi-1) + V + 3\xi\phi\left(\ddot{\phi} + H\dot{\phi}\right) - \frac{1}{2}\rho_{\rm m}^0 a^{-3(1+w_{\rm m})}(3w_{\rm m}+1)\right] . \tag{2.23}$$

Eq. (2.23) may be written more compactly as

$$\frac{\ddot{a}}{a} = -\frac{4\pi G}{3}\left(\rho_{\rm tot} + 3p_{\rm tot}\right) \ , \tag{2.24}$$

where $\rho_{\rm tot}$ is given by Eqs. (2.11), (2.14) and (2.20), and $p_{\rm tot}$ is similarly defined:

$$p_{\rm tot} = p_\phi + \frac{p_{\rm m}}{1-8\pi G\xi\phi^2} \ . \tag{2.25}$$

The pressure of the scalar field is as specified in Eq. (2.17), while $p_{\rm m} = w_{\rm m}\rho_{\rm m}$.

The FLRW version of Eq. (2.4) reads:

$$\ddot{\phi} - \frac{8\pi G\xi\phi}{1-8\pi G\xi\phi^2}\left[\dot{\phi}^2 - 4V - 18\xi H\phi\dot{\phi} - 6\xi(\dot{\phi}^2 + \phi\ddot{\phi}) - \rho_{\rm m}^0 a^{-3(1+w_{\rm m})}(1-3w_{\rm m})\right] + \frac{{\rm d}V}{{\rm d}\phi} + 3H\dot{\phi} = 0 \ . \tag{2.26}$$

[34] Refer to Chapter 1, Eq. (1.38).

2.2.2 The Einstein and Jordan frames

In the absence of ordinary matter, the field equations on which STT is based can be greatly simplified by means of conformal transformation techniques. These make it possible to map the *Jordan frame* – in which the governing equations are usually expressed – into the *Einstein frame*, where the non-minimal coupling present between ϕ and R in the Jordan frame disappears, allowing us to write the equations in terms of a minimally-coupled scalar $\tilde{\phi}$. It should be emphasised that although it is standard practice to use rigid units in the Einstein frame, this is not what Dicke intended when he introduced the concept of conformal transformations for Brans-Dicke theory [165]. According to his interpretation, the units of time, mass and length should scale with appropriate powers of the Brans-Dicke scalar. However, the version with fixed units for the Einstein frame is by far the more popular, and it is therefore the one we shall be referring to (unless otherwise stated).

There is some disagreement in the literature on what exactly constitutes a *conformal transformation* [166]. In our case, such a transformation shall be defined as a point-dependent rescaling of the metric tensor $g_{\mu\nu}$:

$$g_{\mu\nu}(x) \longrightarrow \tilde{g}_{\mu\nu}(x) = \Omega^2(x)\, g_{\mu\nu}(x) \ , \tag{2.27}$$

where the conformal factor $\Omega(x)$ is given by:

$$\Omega = \sqrt{1 - 8\pi G\xi\phi^2} \ , \tag{2.28}$$

and the coordinates are held fixed. It should be noted, though, that some works refer to Eq. (2.27) as a Weyl transformation instead, and describe a conformal transformation as a change of coordinates [from x to $\tilde{x}$, with $x^\mu = f^\mu(\tilde{x}^\nu)$] that acts on the metric similarly to a Weyl transformation [167]:

$$g_{\mu\nu}(x) \longrightarrow \tilde{g}_{\mu\nu}(\tilde{x}) = \frac{\partial f^\rho}{\partial \tilde{x}^\mu}\frac{\partial f^\sigma}{\partial \tilde{x}^\nu} g_{\rho\sigma}(f(\tilde{x})) = \Omega^2(\tilde{x})\, g_{\mu\nu}(\tilde{x}) \ . \tag{2.29}$$

The relation between the transformed field $\left(\tilde{\phi}\right)$ and its Jordan-frame analogue takes the form

$$\mathrm{d}\tilde{\phi} = \frac{\sqrt{1 - 8\pi G\xi(1-6\xi)\phi^2}}{1 - 8\pi G\xi\phi^2}\,\mathrm{d}\phi \ . \tag{2.30}$$

Consequently, any non-minimally coupled scalar field which solves the field equations in the Jordan frame, but at some point attains either of the values $\pm(8\pi G\xi)^{-1/2}$,

does not turn up as a solution in the Einstein frame. This may constitute a serious limitation in certain cases.

As already mentioned, the conformal transformation renders the scalar field minimally coupled, and so the Einstein-frame version of the field equations is usually much simpler to solve (provided other forms of matter are absent). Any solutions one finds may then be rewritten in terms of the Jordan-frame metric and scalar field. There is, however, a caveat: solutions which are physically significant in one frame do not necessarily remain so in the other.

For the rest of this chapter, the cosmic fluid shall be assumed to consist of a scalar field and ordinary matter. In the Einstein frame, the direct coupling of the two means that the system is no simpler than its Jordan frame analogue. There is also the fact that the equation $\nabla^{\mu}T^{\mathrm{m}}_{\mu\nu} = 0$ is only conformally invariant (i.e. it only holds in the Einstein frame) if $T^{\mathrm{m}}_{\mu\nu}$ has vanishing trace. Otherwise, energy and momentum are exchanged between the conformally-transformed scalar field and matter component. Furthermore, since the general relativistic geodesic equation is a direct consequence of energy-momentum conservation, massive particles which fall freely in the Jordan frame experience a 'fifth force' proportional to[35] $\tilde{\nabla}^{\mu}\tilde{\phi}$ in the Einstein frame. This fifth force violates the universality of free fall – and hence the equivalence principle. Interestingly, on adopting running units of mass, time and length for the Einstein frame, one finds that the mass $\tilde{m}$ of a massive particle becomes a varying quantity (within the said frame), and that $\tilde{\nabla}^{\mu}\tilde{\phi}$ is essentially equivalent to $\tilde{\nabla}^{\mu}\tilde{m}$. Herein lies the crux of the matter: the two frames *are* physically equivalent, but only if one uses running units in the Einstein frame, as Dicke intended [165]. With his interpretation, the presence of matter no longer spoils conformal invariance [168].

This does not mean that the Einstein frame with fixed units has no merits. On the contrary, the energies it admits are always physically acceptable, which cannot be said for the Jordan frame. Then again, the latter emerges more naturally from physical considerations. The long and short of it is that neither frame can be seen as superior. In certain situations, the Jordan-frame version of the theory is acceptable while the Einstein-frame formulation (with fixed units) is not, and vice-versa.

[35] $\tilde{\nabla}_{\mu}$ denotes the covariant derivative operator constructed from $\tilde{g}_{\mu\nu}$, the Einstein frame metric.

2.3 Dark Energy as a Scalar Field

The main goal of this chapter is to present solutions to the equations set out in Sec. 2.2 that could correctly model the late-time expansion history of the Universe. Any solutions must therefore meet the following criteria:

- $\ddot{a} > 0$, implying an accelerated cosmic expansion (the models are thus valid at $z \lesssim 0.3$);
- $a > 0$ and $\dot{a} > 0$ – the scale factor should be positive, and must also increase with time;
- $\rho_{\rm m} \geq 0$ at all times, in line with the stipulations of the weak energy condition (which is discussed in detail in the next subsection). The requirement that $\rho_{\rm m} + p_{\rm m} \geq 0$ is then satisfied automatically, since we set $p_{\rm m} = w_{\rm m}\,\rho_{\rm m}$, $w_{\rm m}$ being a non-negative constant.
- $\rho_\phi \geq 0$ and $\rho_\phi + p_\phi \geq 0$, as necessitated by the weak energy condition;
- $p_\phi < 0$, allowing the scalar field to drive the cosmic acceleration that characterises the current epoch;
- $\rho_{\rm tot} < -3p_{\rm tot}$. This follows from Eq. (2.24) and the first two points mentioned above. The quantities $\rho_{\rm tot}$ and $p_{\rm tot}$ are as specified by Eqs. (2.11) and (2.25), respectively.

2.3.1 The Weak Energy Condition

A few comments about the Weak Energy Condition (WEC) are warranted before we move on to the said solutions. Let us start by noting that given any energy-momentum tensor $\boldsymbol{T}$ describing what is thought to be physically reasonable matter (though not a null fluid[36]), it is possible, at a general point P, to find a frame $\mathcal{S}$ in which $\boldsymbol{T}$ takes the form:

$$\boldsymbol{T} = \rho\ \boldsymbol{e}_0 \otimes \boldsymbol{e}_0 + p_1\ \boldsymbol{e}_1 \otimes \boldsymbol{e}_1 + p_2\ \boldsymbol{e}_2 \otimes \boldsymbol{e}_2 + p_3\ \boldsymbol{e}_3 \otimes \boldsymbol{e}_3\ , \tag{2.31}$$

[36]A null fluid is a field of directed massless radiation – an incoherent superpositioning of waves that have random phases and polarisations but the same direction of motion. Its energy-momentum tensor is $T_{\mu\nu} = \Phi\, k_\mu k_\nu$, where k_μ is a null vector ($k_\mu k^\mu = 0$) and Φ is often interpreted as the radiation density of the distribution. It is important to stress, however, that Φ is not uniquely defined. Examples of null fluids include massless neutrinos and null electro-magnetic fields [169,170].

where $(\boldsymbol{e}_0, \boldsymbol{e}_1, \boldsymbol{e}_2, \boldsymbol{e}_3)$ is an orthonormal basis with one time-like $(\boldsymbol{e}_0)$ and three space-like vectors, and $\otimes$ denotes the tensor product. The eigenvalue ρ may be identified with the rest energy density of the fluid, while the eigenvalues p_1, p_2 and p_3 are called the principal pressures [171].

In any other frame $\mathcal{S}'$ [assumed to have basis vectors $(\boldsymbol{\Pi}_0, \boldsymbol{\Pi}_1, \boldsymbol{\Pi}_2, \boldsymbol{\Pi}_3)$], the components of $\boldsymbol{T}$ can be expressed as:

$$T^{\mu\nu} = \rho\ e_0^\mu e_0^\nu + p_1\ e_1^\mu e_1^\nu + p_2\ e_2^\mu e_2^\nu + p_3\ e_3^\mu e_3^\nu\ , \tag{2.32}$$

with e_α^σ representing the component σ of the vector $\boldsymbol{e}_\alpha$ (since $\boldsymbol{e}_\alpha = e_\alpha^\sigma\, \boldsymbol{\Pi}_\sigma$).

Let us consider an observer in $\mathcal{S}$ with four-velocity:

$$\boldsymbol{u} = \gamma(\boldsymbol{e}_0 + y_1\boldsymbol{e}_1 + y_2\boldsymbol{e}_2 + y_3\boldsymbol{e}_3)\ . \tag{2.33}$$

Here, $\gamma = 1/\sqrt{1-v^2}$ and v denotes the magnitude of the three-velocity $\vec{v}$, so that $v^2 = y_1^2 + y_2^2 + y_3^2$. The parameters y_1, y_2 and y_3 are equivalent to the rate at which the respective spatial coordinates vary with cosmic time. Since $\boldsymbol{u}$ is time-like, we have that

$$y_1^2 + y_2^2 + y_3^2 < 1\ . \tag{2.34}$$

In $\mathcal{S}'$, the components of $\boldsymbol{u}$ read:

$$u^\mu = \gamma(e_0^\mu + y_1 e_1^\mu + y_2 e_2^\mu + y_3 e_3^\mu)\ . \tag{2.35}$$

The weak energy condition stipulates that a general observer always measures the energy density of any 'physically reasonable, classical matter' [171] to be non-negative. Now, according to an observer with four-velocity u^μ, the fluid described by the energy-momentum tensor $T_{\alpha\beta}$ has energy density equal to $T_{\alpha\beta}u^\alpha u^\beta$. Consequently, if all possible observers are to be taken into account, the condition $T_{\alpha\beta}u^\alpha u^\beta \geq 0$ must be satisfied *for all time-like vectors* $\boldsymbol{u}$. Let us put $T_{\alpha\beta} = g_{\alpha\mu}g_{\beta\nu}T^{\mu\nu}$ and write $T^{\mu\nu}$ and u^α as in Eqs. (2.32) and (2.35), respectively. Then it is straightforward to show that the orthonormality of the vectors $\boldsymbol{e}_0$, $\boldsymbol{e}_1$, $\boldsymbol{e}_2$ and $\boldsymbol{e}_3$ translates the requirement for $T_{\alpha\beta}u^\alpha u^\beta$ to be non-negative into:

$$\gamma^2(\rho + p_1 y_1^2 + p_2 y_2^2 + p_3 y_3^2) \geq 0\ . \tag{2.36}$$

If $\mathcal{S}'$ happens to be the rest-frame of the observer, y_1, y_2, and y_3 evaluate to zero,

and (2.36) reduces to a constraint on ρ: $\rho \geq 0$. Setting $y_2 = y_3 = 0$ implies that $\rho + p_1 y_1^2 \geq 0$, which when coupled with (2.34) yields the inequality[37] $\rho + p_1 \geq 0$. One can easily see that this may be generalised to $\rho + p_i \geq 0$ for $i = \{1, 2, 3\}$. To show that the conditions $\rho \geq 0$ and $p_i \geq -\rho$ are not only necessary, but also sufficient for $T_{\alpha\beta} u^\alpha u^\beta \geq 0$ to hold, it is enough to consider what happens when the relation $p_i \geq -\rho$ is combined with (2.36): we get that

$$\rho + p_1 y_1^2 + p_2 y_2^2 + p_3 y_3^2 \;\geq\; \rho - \rho(y_1^2 + y_2^2 + y_3^2) \;\geq\; 0 \;, \tag{2.37}$$

where the last inequality follows from (2.34). Hence, if $\rho \geq 0$ and $\rho + p_i \geq 0$, the WEC is satisfied.

Now that the physical significance of the WEC has been established, we may move to the STT solutions mentioned previously. They were obtained by first inserting a candidate function for a and/or ϕ into Eqs. (2.22) and (2.26),[38] then by looking for ways in which the equations could be satisfied (and trying to solve for a or ϕ if only one of them had been specified). This mainly involved deriving constraints for the model parameters. It was ensured that only solutions which met the conditions listed at the start of section 2.3 were retained for further analysis.

The work was carried out using Wolfram Mathematica® 11.3, and the code is provided in Appendix C.

2.3.2 Models in a flat universe

In this case, the spatial curvature parameter (κ) was set to zero. The letters A, B, C, D and n denote constants.

[37] If $p_i \neq 0$, the inequality in question becomes $\rho + p_i > 0$.

[38] In the process, the scalar potential V was replaced with the corresponding expression from Eq. (2.23).

Solution 1

The first solution we consider has the following characteristics:

$$a(t) = A\exp\left(Bt\right) ; \tag{2.38}$$

$$\phi(t) = C\exp\left(\frac{2B\xi}{4\xi-1}t\right) , \quad \xi \neq 1/4 ; \tag{2.39}$$

$$\rho_{\rm m}^0 = 0 .$$

Let us first redefine the time coordinate as $\bar{t} = H_0 t$. Then the Hubble parameter is automatically rescaled to $\bar{H} = H/H_0$, and at the present time ($t = t_0$) one gets that $\bar{t} = \bar{t}_0 = H_0 t_0$ and $\bar{H} = H_0/H_0 = 1$. The latter may in turn be combined with the fact that $a(\bar{t}_0) = 1$ to deduce that $\mathrm{d}a/\mathrm{d}\bar{t}$ $[= a'(\bar{t})]$ is currently equal to unity.

Equipped with the boundary conditions $a(\bar{t}_0) = a'(\bar{t}_0) = 1$, we may solve for A and B using Eq. (2.38) and its first derivative with respect to $\bar{t}$. It is found that $A = \exp\left(-\bar{t}_0\right)$ and $B = H_0$. Consequently, Eq. (2.38) can be rewritten as:

$$a(\bar{t}) = \exp\left(\bar{t} - \bar{t}_0\right) . \tag{2.40}$$

How does the resulting evolution compare with the (late-time) predictions of flat ΛCDM? One recalls that the dynamics in an FLRW cosmology are governed by the two Friedmann equations,[39] and in the presence of a cosmological constant the second one reads:

$$2a''(\bar{t}) + \Omega_{\rm m}^0 a^{-2} + 2\Omega_{\rm r}^0 a^{-3} - 2\Omega_\Lambda^0 a = 0 , \tag{2.41}$$

where $\Omega_{\rm m}^0$ and Ω_Λ^0 shall be fixed at 0.3153 and 0.6847 [20], respectively. As for $\Omega_{\rm r}^0$, this may be determined from the relation $\Omega_{\rm r}^0 = \Omega_{\rm m}^0/\left(1 + z_{\rm eq}\right)$ ($z_{\rm eq}$ being the redshift at matter-radiation equality). Putting $z_{\rm eq} = 3402$ [20] yields a value of approximately 9×10^{-5}. For practical purposes, therefore, the radiation component is negligible at low redshifts.

Fig. 2.1 depicts the variation of cosmic acceleration with time in the model under investigation and in flat ΛCDM. It was obtained by setting the age of the Universe, $\bar{t}_0$, equal to 0.95 – which is equivalent to around 13.8 Gyr [20]. The boundary conditions used to solve Eq. (2.41) numerically were thus fixed at $a(0.95) = a'(\bar{t} = 0.95) = 1$. It should be noted that Fig. 2.1 shows the acceleration as calculated with respect to the

[39] Refer to Chapter 1, Eqs. (1.37) and (1.38).

rescaled time [we denote this acceleration by $a''(\bar{t})$] – the axis label simply expresses it in terms of $\ddot{a}(t)$, its cosmic time counterpart. In other words, $a''(\bar{t}) = \ddot{a}(t)H_0^{-2}$.

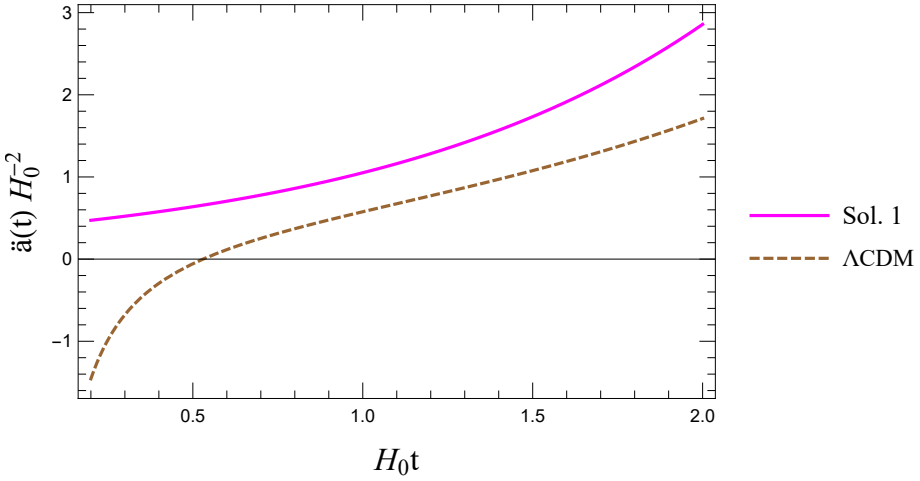

FIGURE 2.1: The variation of acceleration with time during the dark energy-dominated epoch, in a spatially flat universe devoid of matter and with a scalar field $\phi \propto \exp(Dt)$.

Our analysis of the solution outlined by Eqs. (2.38) and (2.39) ends here. This solution satisfies the WEC and is characterised by an accelerating cosmic expansion, but the absence of matter is a significant shortcoming. We shall therefore move on to more promising scenarios.

Solution 2

Here, the EoS parameter of the matter distribution ($w_{\rm m}$) and the coupling constant ξ equate to zero and $1/B^2$, respectively. The scale factor and scalar field vary with time as follows:

$$a(t) \;=\; A\, t^{6/5}\;; \tag{2.42}$$

$$\phi(t) \;=\; \frac{1}{\sqrt{8\pi G}}\left(B + Ct^{-4/5}\right)\;, \quad B^2 < 23/4\;, \tag{2.43}$$

while the present-day value of the matter density is given by:

$$\rho_{\rm m}^0 \;=\; \frac{A^3C^2(23-4B^2)}{50\pi G B^2}\;. \tag{2.44}$$

Redefining t as $\bar{t} = H_0 t$ and applying the constraints

$$a(\bar{t}_0) = a'(\bar{t}_0) = 1 \tag{2.45}$$

makes it possible to deduce that $\bar{t}_0 = 6/5$ and $A = (5H_0/6)^{6/5}$. Accordingly, Eq. (2.42) takes the form:

$$a(\bar{t}) = (5/6\ \bar{t}\ )^{6/5}\ . \tag{2.46}$$

The resulting acceleration is compared with the flat ΛCDM prediction in Fig. 2.2. We shall only use the value $6/5$ for $\bar{t}_0$ in relation to the STT solution, so Eq. (2.41) was again solved numerically subject to the conditions $a(0.95) = a'(\bar{t} = 0.95) = 1$.

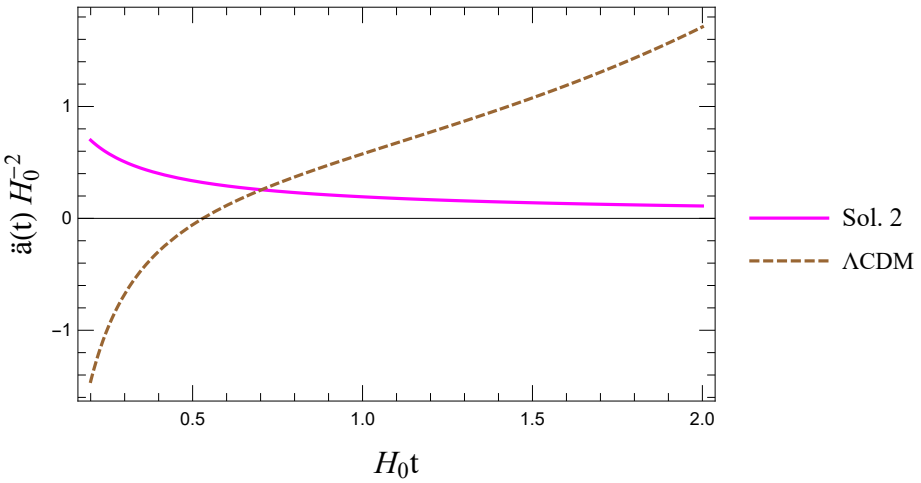

FIGURE 2.2: The variation of acceleration with time during the dark energy-dominated epoch, in a spatially flat universe consisting of dust and a scalar field $\phi \propto B + Ct^{-0.8}$.

Let us next consider the implications of having $\bar{t}_0 = H_0 t_0 = 6/5$. The first thing we note is that H_0 would have to be approximately $85\,\mathrm{km\,s^{-1}\,Mpc^{-1}}$ if one assumes a cosmic age of 13.8 Gyr [20], but this value for the Hubble constant is way too large in comparison to what is reported in the literature (see, for instance, Refs. [19,20,26]). If H_0 is instead set to the model-independent measurement of Riess et al. $\left(H_0 = 73.48 \pm 1.66\ \mathrm{km\,s^{-1}\,Mpc^{-1}}\right)$, one finds that t_0 amounts to about 16 Gyr, and using the upper bound for H_0 in place of the mean lowers the age of the Universe to 15.6 Gyr. The good news is that this value is not ruled out by constraints obtained from stellar dating. Nevertheless, it should be admitted that they do not accommodate it comfortably either [172].

Fig. 2.3 shows how the late-time evolution of ρ_ϕ [Eq. (2.14)] compares with that of ρ_m. Having $w_\mathrm{m} = 0$ is indicative of a dust distribution, so ρ_m equates to $\rho_\mathrm{m}^0 a^{-3}$, where ρ_m^0 is the present-day density given by Eq. (2.44). The constant B was set to unity and C to[40] $H_0^{-4/5}$. Additionally, for the sake of avoiding having to deal with very small

[40]The value of C was chosen with the aim of eliminating H_0 from the equation for $\rho_\phi(\bar{t})$. Note that Fig. 2.3 shows the rescaled energy densities, $\rho_\phi(\bar{t})$ and $\rho_\mathrm{m}(\bar{t})$, which are respectively equivalent to $\rho_\phi(t)H_0^{-2}$ and $\rho_\mathrm{m}(t)H_0^{-2}$.

numbers, the unit system was adjusted by putting $8\pi G/3 = 1$ when constructing figures.

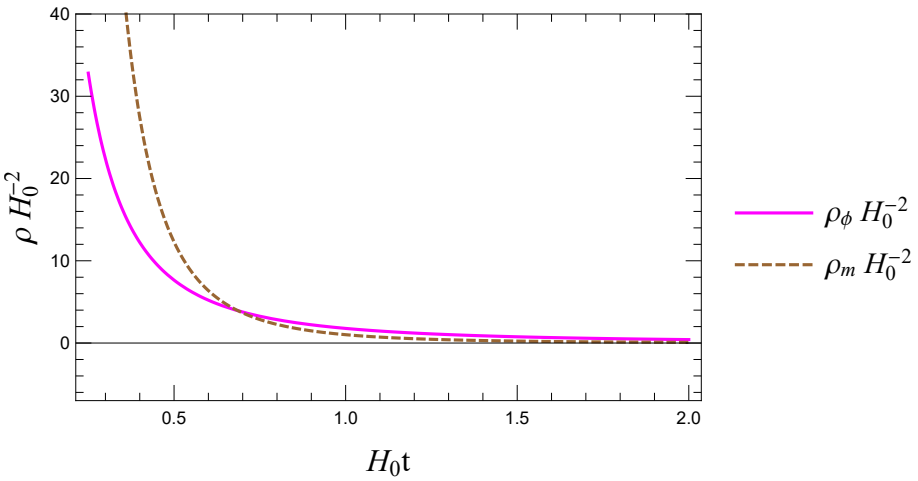

FIGURE 2.3: The dynamics of ρ_ϕ and $\rho_{\rm m}$ during the current epoch of acceleration, in a spatially flat universe consisting of dust and a scalar field $\phi \propto B + Ct^{-0.8}$.

As clearly shown in Fig. 2.3, the scalar field currently dominates over the matter component. This is the kind of behaviour we are looking for. It implies that we are living in an epoch during which the negative pressure associated with ϕ overcomes the attraction of dark and baryonic matter, causing the cosmic expansion to accelerate.

Solution 3

The final solution valid in a flat universe is given by

$$a(t) = At^{\lambda}\,, \qquad \lambda = \frac{2(1+n)}{3(1+w_{\rm m})}\,; \tag{2.47}$$

$$\phi(t) = \frac{1}{\sqrt{8\pi G}}\left(Bt^{n} + Ct^{-n}\right)\,. \tag{2.48}$$

Inserting the above (except the relation for λ) into Eq. (2.22) gives a polynomial in t with exponents that are functions of λ, n and $w_{\rm m}$; the coefficients of the different powers of t can be isolated by using the code provided in C.2. It turns out that no physically viable solution exists unless we equate two or more exponents. This explains the origin of the constraint on λ: $\lambda = 2(1+n)/3(1+w_{\rm m})$. Eq. (2.22) is re-evaluated for our particular choice of λ and the coefficients of different powers of t are again extracted. The aim is to try to obtain expressions for the model parameters that reduce all the coefficients to zero, so that the left-hand side of Eq. (2.22) matches the

right-hand side. It is found that terms in $t^{2(1+n)}$, t^2 and $t^{2(1+2n)}$ all go to zero if one assumes a flat universe, but the coefficient of $t^{4n+4(1+n)/3(1+w_\mathrm{m})}$ is $A^{3(1+w_\mathrm{m})}B^2\{4\xi + 2n\xi(7+3w_\mathrm{m}) - n^2[-3+8\xi+3w_\mathrm{m}(4\xi-1)]\}$, which equates to zero if

$$\xi \;=\; \frac{3n^2(1+w_\mathrm{m})}{2[-2-n(7+3w_\mathrm{m})+2n^2(2+3w_\mathrm{m})]} \;. \tag{2.49}$$

B and ρ^0_m may be inferred from the coefficients of $t^{2n+4(1+n)/3(1+w_\mathrm{m})}$ and $t^{4(1+n)/3(1+w_\mathrm{m})}$, respectively:

$$B \;=\; -\frac{2(1+n)[-2-n(7+3w_\mathrm{m})+2n^2(2+3w_\mathrm{m})]}{3Cn^2(1+w_\mathrm{m})[-4-3n(3+w_\mathrm{m})+2n^2(2+3w_\mathrm{m})]} \;; \tag{2.50}$$

$$\rho^0_\mathrm{m} \;=\; \frac{C^2A^{3(1+w_\mathrm{m})}n^3(5+2n+3w_\mathrm{m})}{4\pi G(1+w_\mathrm{m})(-2-7n+4n^2-3nw_\mathrm{m}+6n^2w_\mathrm{m})} \;. \tag{2.51}$$

Meanwhile, the constant n must satisfy:

$$n > \frac{1}{2}(1+3w_\mathrm{m}) \;; \qquad n > \frac{7+3w_\mathrm{m}+3\sqrt{9+10w_\mathrm{m}+w_\mathrm{m}^2}}{4(2+3w_\mathrm{m})} \;. \tag{2.52}$$

The first inequality follows from the requirement that $\ddot{a} > 0$ during the current epoch, and the second ensures that the matter distribution has positive energy density.

The constraints specified in Eq. (2.45) imply that Eq. (2.47) may alternatively be expressed as:

$$a(\bar{t}) = \left[\frac{3(1+w_\mathrm{m})}{2(1+n)}\bar{t}\right]^\lambda \;, \tag{2.53}$$

with $\bar{t}$ again equal to H_0t. The above relation was obtained by applying the condition $a(\bar{t}_0) = 1$ to determine A/H_0^λ as a function of $\bar{t}_0$, then using the fact that $a'(\bar{t}_0) = 1$ to write $\bar{t}_0$ in terms of n and w_m. As a further consequence of Eq. (2.45), one finds that

$$n = \frac{3(1+w_\mathrm{m})\bar{t}_0 - 2}{2} \;, \tag{2.54}$$

which, when combined with Eq. (2.52), allows us to deduce two lower bounds for $\bar{t}_0$:

$$\bar{t}_0 > 1 \;; \qquad \bar{t}_0 > \frac{1}{2(2+3w_\mathrm{m})}\left(5+\sqrt{\frac{9+w_\mathrm{m}}{1+w_\mathrm{m}}}\right) \;. \tag{2.55}$$

The first seems to be at odds with the *Planck* value for the age of the Universe (13.8 Gyr) [20], since this implies that $\bar{t}_0 \approx 0.95$. It should be kept in mind, however,

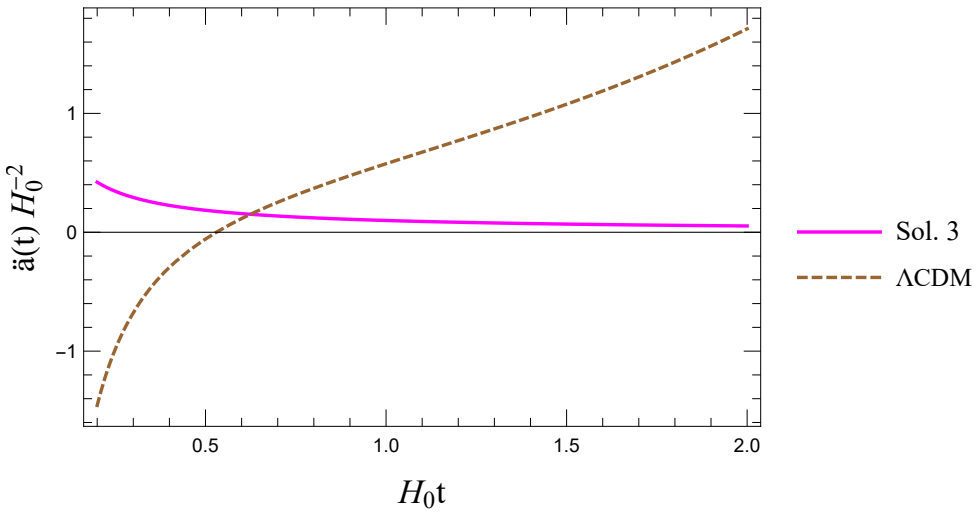

FIGURE 2.4: The variation of acceleration with time during the dark energy-dominated epoch, in a spatially flat universe consisting of a matter distribution (with $\rho_{\rm m} \propto a^{-4.8}$) and a scalar field $\phi \propto Bt^{1.64} + Ct^{-1.64}$.

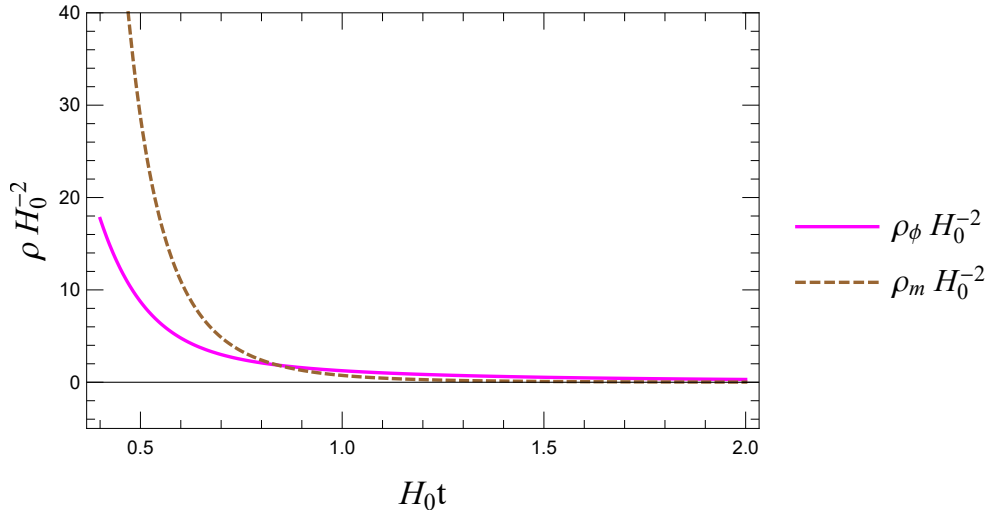

FIGURE 2.5: The dynamics of ρ_ϕ and $\rho_{\rm m}$ during the current epoch of acceleration, in a spatially flat universe consisting of a matter distribution (with $\rho_{\rm m} \propto a^{-4.8}$) and a scalar field $\phi \propto Bt^{1.64} + Ct^{-1.64}$.

that the conversion from t to $\bar{t}$ depends on H_0,[41] and the value of the Hubble constant is still a subject of controversy [26]. We should nonetheless ensure that the lower bound does not rise above unity. This may be achieved by specifying the constraint

$$\frac{1}{2(2+3w_{\rm m})}\left(5+\sqrt{\frac{9+w_{\rm m}}{1+w_{\rm m}}}\right) \leq 1\ , \tag{2.56}$$

[41]The estimate for $\bar{t}_0$ presented here was obtained using the *Planck* mean $\left(H_0 = 67.36\,{\rm km\,s^{-1}\,Mpc^{-1}}\right)$ [20].

which in turn means that $w_{\rm m} \geq 1/\sqrt{3}$.

The evolution of $a''(\bar{t})$ is compared with that of its flat ΛCDM counterpart in Fig. 2.4. The parameters $w_{\rm m}$ and $\bar{t}_0$ were assigned the values 0.6 and 1.1, respectively, while Eq. (2.41) was again solved subject to the constraints $a(0.95) = a'(\bar{t} = 0.95) = 1$. One may choose a value for the constant C in such a way that the end of the matter-dominated epoch occurs close to the transition redshift predicted by ΛCDM. Setting C equal to $0.4H_0^{-n}$ achieves this without excessive fine-tuning, and furthermore eliminates H_0 from the equations for the rescaled energy density and pressure of the scalar field.

Fig. 2.5 allows us to verify that the scalar field dominates the cosmic energy budget at late times. As a consequence of this imbalance, the negative pressure due to ϕ (Fig. 2.6) overcomes the attraction of matter and causes the cosmic expansion to accelerate, leading to the scenario depicted in Fig. 2.4.

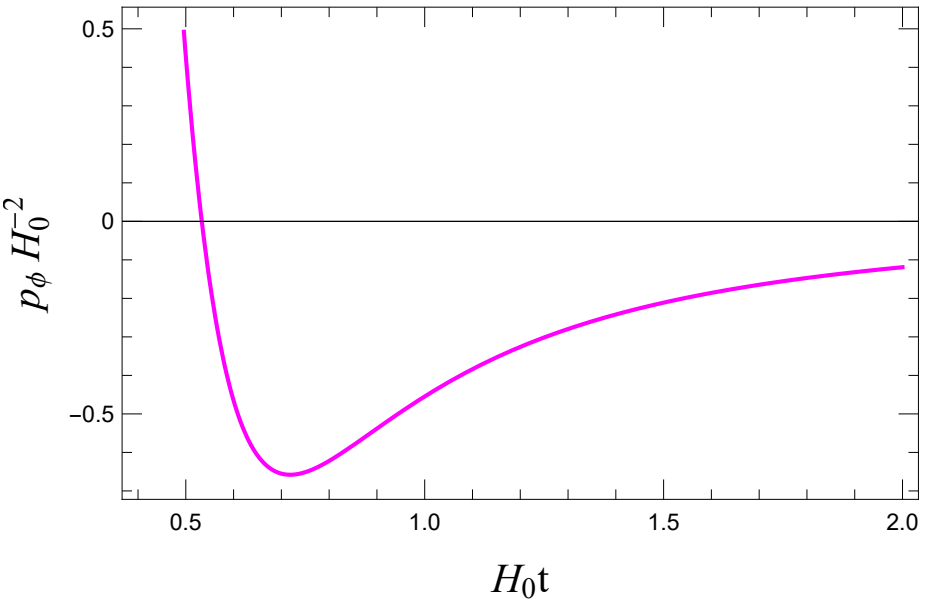

FIGURE 2.6: The dynamics of p_ϕ during the current epoch of acceleration, in a spatially flat universe consisting of a matter distribution (with $\rho_{\rm m} \propto a^{-4.8}$) and a scalar field $\phi \propto Bt^{1.64} + Ct^{-1.64}$.

2.3.3 Models in an open universe

Here we solve Eqs. (2.22), (2.23) and (2.26) in the context of a hyperbolic geometry. The spatial curvature, κ, is therefore equated to $-1/\mathcal{R}_0^2$ (equivalent to putting $k = -1$). The letters A, B, C, n and q represent constants.

Solution 4

This solution is characterised by the following expressions for a and ϕ:

$$a(t) \;=\; At^n \;; \tag{2.57}$$

$$\phi(t) \;=\; \frac{1}{\sqrt{8\pi G}}\left(Bt^q + Ct^{-q}\right) \;. \tag{2.58}$$

The constants n, q, A and B can be written in terms of $w_{\rm m}$, C and $\mathcal{R}_0$:

$$n \;=\; \frac{2}{1-3w_{\rm m}} \;; \qquad q \;=\; \frac{1+3w_{\rm m}}{1-3w_{\rm m}} \;; \tag{2.59}$$

$$A \;=\; \frac{1-3w_{\rm m}}{\mathcal{R}_0}\sqrt{\frac{\zeta\left[6\left(1-w_{\rm m}-6w_{\rm m}^2\right)+\eta\right]}{C^2(-1+w_{\rm m})(1+3w_{\rm m})^3(-13+30w_{\rm m}+63w_{\rm m}^2)}} \;; \tag{2.60}$$

$$B \;=\; \frac{3\zeta\left(-7+24w_{\rm m}+27w_{\rm m}^2+\eta\right)}{C(1+3w_{\rm m})^2(-13+30w_{\rm m}+63w_{\rm m}^2)} \;, \tag{2.61}$$

where $\eta = \sqrt{3}\sqrt{-1+w_{\rm m}[-20+3w_{\rm m}(10+60w_{\rm m}+81w_{\rm m}^2)]}$ and $\zeta = -1+4w_{\rm m}+9w_{\rm m}^2$. The coupling constant ξ is given by

$$\xi \;=\; \frac{1+6w_{\rm m}+9w_{\rm m}^2}{6\zeta} \;, \tag{2.62}$$

while $\rho_{\rm m}^0$ takes the form

$$\rho_{\rm m}^0 = \frac{C^2(1+3w_{\rm m})^2}{24\pi G\mathcal{R}_0^2(1+w_{\rm m})\zeta}\left\{\frac{\zeta(1-3w_{\rm m})^2\left[6\left(1-w_{\rm m}-6w_{\rm m}^2\right)+\eta\right]}{C^2\mathcal{R}_0^2(1+3w_{\rm m})^3\left(13-43w_{\rm m}-33w_{\rm m}^2+63w_{\rm m}^3\right)}\right\}^{q/n} \tag{2.63}$$

and the requirement that A is real restricts $w_{\rm m}$ to the range $[0.258, 0.275)$.

Substituting $\bar{t}/H_0$ for t and making use of Eq. (2.45) allows us to conclude that

$$a(\bar{t}) = \left[\frac{\bar{t}}{2}(1-3w_{\rm m})\right]^{2/(1-3w_{\rm m})} \;, \tag{2.64}$$

whereas $\bar{t}_0$ is found to equal $2/(1-3w_{\rm m})$. The range of values for $w_{\rm m}$ specified above consequently constrains $\bar{t}_0$ to vary between 8.8 and 11.4, a far cry from the values

found in the literature [1, 3, 19, 20, 173–175]. Solution 4 is thus effectively ruled out.

Solution 5

Here we have that

$$a(t) = At^{(5+\sqrt{13})/6} \; ; \tag{2.65}$$

$$\phi(t) = \frac{1}{\sqrt{8\pi G}} \left(B + Ct^{(1-\sqrt{13})/3} \right) \; . \tag{2.66}$$

B is related to A, C and $\mathcal{R}_0$ as follows:

$$B = \frac{-15 + 3\sqrt{13} + \sqrt{342 - 90\sqrt{13} - 8(-128 + 35\sqrt{13})C^2A^4\mathcal{R}_0^4}}{4(-4 + \sqrt{13})CA^2\mathcal{R}_0^2} \; , \tag{2.67}$$

while $\xi = 1/B^2$ and $w_{\rm m}$ must take the value $1/3(-7 + 2\sqrt{13}) \approx 0.07$. The density of matter at the present time depends on A, B and C:

$$\rho_{\rm m}^0 = \frac{C^3A^{-4+2\sqrt{13}} \left[14 - 11\sqrt{13} + 2(-5 + 2\sqrt{13})B^2 \right]}{72\pi G(5 - \sqrt{13})B^3} \; . \tag{2.68}$$

When t is redefined as $\bar{t} = H_0 t$ and the constraints specified in Eq. (2.45) are applied, Eq. (2.65) becomes:

$$a(\bar{t}) = \left(\frac{6\bar{t}}{5 + \sqrt{13}} \right)^{(5+\sqrt{13})/6} \; , \tag{2.69}$$

and $\bar{t}_0$ evaluates to $(5 + \sqrt{13})/6 \approx 1.43$. This allows us to deduce that H_0 must amount to approximately $102\,\mathrm{km\,s^{-1}\,Mpc^{-1}}$ if the age of the Universe is to be around 13.8 Gyr [20]. The fact that our estimate for H_0 is so at odds with the range of values found in the literature [19, 20, 26] means that Solution 5 cannot be considered a viable dark energy candidate model.

2.3.4 Models in a closed universe

When $\kappa = 1/\mathcal{R}_0^2$, the system of equations given by (2.22), (2.23) and (2.26) also admits a number of solutions. The two relevant ones found in this study are detailed below. A, B and C are again used to denote constants.

Solution 6

The first solution valid in a closed universe has an exponentially-increasing scale factor and a minimally-coupled scalar field:

$$a(t) \;=\; A\exp\left(Bt\right)\;; \tag{2.70}$$

$$\phi(t) \;=\; C\mathrm{e}^{3Bt}\left\{\mathrm{e}^{-3Bt}\left[\frac{2A}{\mathcal{R}_0^2}\mathrm{e}^{Bt}-\frac{1}{3BC(2\pi GA^3)^{1/2}}\right]\right\}^{3/2}\quad,\quad \xi=0\;, \tag{2.71}$$

while the matter distribution is dust-like ($w_{\rm m}=0$) and its density currently attains the value

$$\rho_{\rm m}^0 \;=\; \frac{2}{3BC(8\pi GA)^{3/2}}\;. \tag{2.72}$$

As already done when analysing Solution 1, the constants A and B may be determined by applying the conditions $a(\bar{t}_0)=a'(\bar{t}_0)=1$. One finds that $A=\exp\left(-\bar{t}_0\right)$ and $B=H_0$. With $\bar{t}/H_0$ in place of t, Eq. (2.70) then takes the form:

$$a(\bar{t}) = \exp\left(\bar{t}-\bar{t}_0\right)\;, \tag{2.73}$$

so that the variation of acceleration with time would be as shown in Fig. 2.1 (provided the age of the Universe, $\bar{t}_0$, is again equated to 0.95).

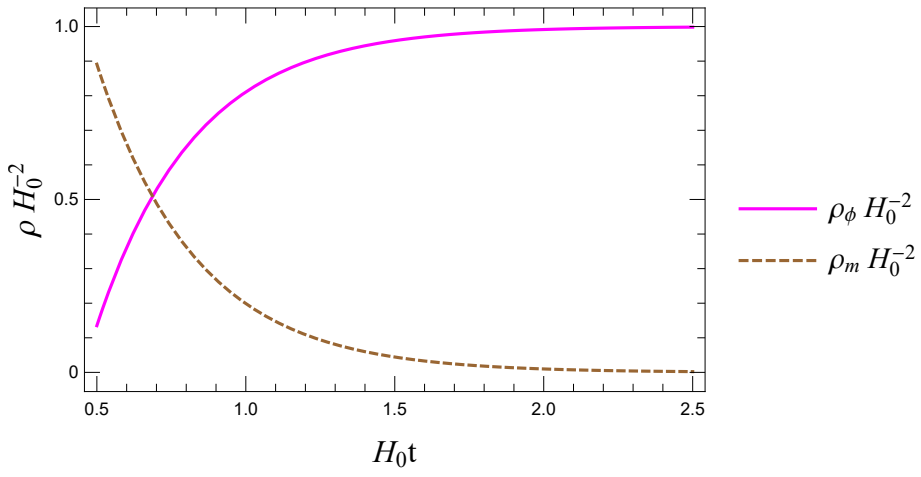

FIGURE 2.7: The dynamics of ρ_ϕ and $\rho_{\rm m}$ during the current epoch of acceleration, in a closed universe consisting of dust and the minimally-coupled scalar field $\phi = C\left(D_1 - D_2\,\mathrm{e}^{-Bt}\right)^{3/2}$ (D_1 and D_2 represent constants).

The next aim is to compare $\rho_{\rm m}$ and ρ_ϕ. To this end, the parameter $\mathcal{R}_0$ is expressed as $H_0^{-1}/|\Omega_k^0|^{1/2}$, with $\Omega_k^0=-0.0106$ [20], and C is set to $4H_0^{-3}/\sqrt{8\pi G}$. The resulting

evolution is portrayed in Fig. 2.7. Here, too, we note that the scalar field dominates the energy budget of the Universe during the time of interest. Additionally, the curve of $\rho_\phi H_0^{-2}$ gradually levels out, implying that at late times the scalar field effectively mimics a cosmological constant.

Solution 7

The scale factor and scalar field are now given by:

$$a(t) = At^2 + B \ , \tag{2.74}$$

$$A = \frac{C}{6\mathcal{R}_0} \quad \text{and} \quad B = \frac{1}{C\mathcal{R}_0} \tag{2.75}$$

$$or \quad A = \frac{C}{2\sqrt{3}\mathcal{R}_0} \quad \text{and} \quad B = \frac{\sqrt{3}}{2C\mathcal{R}_0}; \tag{2.76}$$

$$\phi(t) = \frac{C}{\sqrt{8\pi G}}t \ . \tag{2.77}$$

The coupling constant ξ takes the value $-1/6$ and $\rho_{\rm m}^0$ is equal to zero. The latter implies an unrealistic picture of the cosmos – we know that the Universe is not devoid of matter – and so this solution will not be analysed in detail. Let us nonetheless make the usual transformation from t to $\bar{t}$. Applying the constraints specified in Eq. (2.45) allows us to write Eq. (2.74) as:

$$a(\bar{t}) = \frac{\bar{t}^{\,2}}{2\bar{t}_0} + \frac{1}{2}(2 - \bar{t}_0) \ , \tag{2.78}$$

since A and B turn out to equal $H_0^2/(2\bar{t}_0)$ and $(2-\bar{t}_0)/2$, respectively. These may in turn be used to determine C. With A and B defined as in Eq. (2.75), we have that

$$C = H_0\sqrt{\frac{6}{\bar{t}_0(2-\bar{t}_0)}} \ , \tag{2.79}$$

whilst in the case of Eq. (2.76), the expression for C becomes:

$$C = H_0\sqrt{\frac{3}{\bar{t}_0(2-\bar{t}_0)}} \ . \tag{2.80}$$

2.4 In Brief...

In this chapter, dark energy takes the form of a scalar field that may be either minimally or non-minimally coupled to the Ricci scalar, and is considered in combination with a simple matter component having $p_{\mathrm{m}} \propto \rho_{\mathrm{m}}$. It is shown that such a scenario may indeed give rise to a period of late-time accelerated expansion.

All in all, the chapter serves to illustrate the challenge of finding exact analytical solutions that are in accord with cosmological observations. This is especially true when spatial curvature is introduced and the equations become more complicated, and underlines the important role played by numerical techniques. Nonetheless, a number of analytical solutions to the STT field equations (as expressed in an FLRW framework) were found and have been presented in section 2.3. Some hold in a cosmology with flat spatial sections, while others are valid when the Universe is either closed or open. Despite the appeal of their analytical nature, however, they have a number of shortcomings: several of them impose somewhat unconventional constraints on the equation-of-state parameter of dark matter, while others do not admit a matter component at all. Additionally, tensions with the observationally-established range of values for parameters like the Hubble constant or the age of the Universe have also been noted. One of the most promising solutions features an exponentially-increasing scale factor, a matter distribution with $w_{\mathrm{m}} = 0$ and a minimally-coupled scalar field that mimics a cosmological constant at late times.

CHAPTER 3

The Effects of Spatial Curvature on Cosmic Evolution

3.1 Introduction

As already discussed in Chapter 1, subsection 1.3.2, the importance of spatial curvature is greatly underrated. Indeed, the majority of works put forward continue to be based on the assumption that the Universe is flat. In this chapter, therefore, we shall investigate the consequences of introducing curvature into different cosmological models alternative to ΛCDM. The models in question provide a complete description of the cosmic expansion history: they start with an inflationary phase that evolves into an epoch of deceleration, which is in turn followed by the present period of acceleration. In particular, the Universe shall first be modelled as a dissipative mixture comprising a Van der Waals (VdW) fluid and a dark energy component, with the latter taking the form of either Quintessence or a Chaplygin gas. These models have been investigated in Ref. [176], but we shall extend the analysis by including spatial curvature and studying its effects on the evolution of the Universe. The versatility of the VdW fluid lies in the fact that its pressure can be either positive or negative, depending on its density. Consequently, it can slow down the cosmic expansion at certain times and speed it up at others.

In the last part of the chapter we shall consider two models in which the cosmological constant is replaced by a dynamic Λ. In this case, the matter component will be modelled in one of two ways: as a VdW fluid, or as a distribution with the customary direct proportionality between energy density and pressure. Spatial curvature will again be introduced and its role probed.

All numerical analysis presented in this chapter was carried out using Wolfram Mathematica® 12.0.

3.2 Matter as a Van der Waals Fluid

Let us first assume that the Universe consists solely of a matter distribution with the VdW equation of state (EoS). The aim is to build on Kremer's model [176], repeating his analysis but taking the possibility of non-zero spatial curvature into account. The starting point is the first Friedmann equation:

$$H^2 = \frac{8\pi G}{3}\rho_{\mathrm{m}} - \frac{\tilde{\kappa}}{\tilde{a}^2} \ , \tag{3.1}$$

where ρ_{m} represents the energy density of matter and $\tilde{a}$ is defined as the ratio $\mathcal{R}/\mathcal{R}_*$, $\mathcal{R}$ being the scale factor and $\mathcal{R}_*$ the value it takes when $H = 1$. The time at which this happens shall be denoted by t_* [i.e. $H(t_*) = H_* = 1$]. Next, we shift the time scale by putting $\tilde{t} = t - t_*$, so that at $\tilde{t} = 0$, $\mathcal{R} = \mathcal{R}_*$ and $\tilde{a} = \mathcal{R}_*/\mathcal{R}_* = 1$, while $\mathrm{d}\tilde{a}/\mathrm{d}\tilde{t} = H_* \times \tilde{a}(\tilde{t} = 0) = 1$. The spatial curvature $\tilde{\kappa}$ can be expressed in terms of the normalised spatial curvature k as $k/\mathcal{R}_*^2$ [8].

We proceed by differentiating Eq. (3.1) with respect to[42] $\tilde{t}$, then use the energy conservation equation:

$$\dot{\rho}_{\mathrm{m}} = -3H(\rho_{\mathrm{m}} + p_{\mathrm{m}}) \tag{3.2}$$

to substitute for $\dot{\rho}_{\mathrm{m}}$. After replacing H with $\dot{\tilde{a}}/\tilde{a}$ and discarding the solution $H = 0$, we get that

$$\tilde{\kappa} - 4\pi G\tilde{a}^2(\rho_{\mathrm{m}} + p_{\mathrm{m}}) + \dot{\tilde{a}}^2 - \tilde{a}\ddot{\tilde{a}} = 0 \ . \tag{3.3}$$

The relation between the pressure p_{m} of the matter content and its energy density takes the form of the VdW EoS [177]:

$$p_{\mathrm{m}} = \left[\frac{8w_{\mathrm{m}}\rho_{\mathrm{m}}}{3\rho_{\mathrm{m}}^{\mathrm{c}} - \rho_{\mathrm{m}}} - 3\left(\frac{\rho_{\mathrm{m}}}{\rho_{\mathrm{m}}^{\mathrm{c}}}\right)^2\right] p_{\mathrm{m}}^{\mathrm{c}} \ . \tag{3.4}$$

In classical thermodynamics, w_{m} is a dimensionless quantity equivalent to the ratio of T to T^{c}, where T is the temperature of the fluid and T^{c} its value at the critical point. This point is best described in the context of a pressure versus temperature plot. Here, it coincides with the high-temperature end of the gas-liquid coexistence curve; as one moves along the curve, the two phases grow more and more similar, finally becoming indistinguishable at the critical point [178].

[42] An overdot denotes differentiation with respect to t, but $\tilde{t} = t - t_*$, so $\mathrm{d}/\mathrm{d}t$ is equivalent to $\mathrm{d}/\mathrm{d}\tilde{t}$.

So what meaning does w_{m} have for us? In a cosmological setting, w_{m} is often identified with the constant of proportionality in the conventional barotropic relation $p_{\mathrm{m}} \propto \rho_{\mathrm{m}}$, because this is essentially the form that Eq. (3.4) takes for small values of $\rho_{\mathrm{m}}/\rho_{\mathrm{m}}^{\mathrm{c}}$ ($\rho_{\mathrm{m}}^{\mathrm{c}}$ and $p_{\mathrm{m}}^{\mathrm{c}}$ denote the critical energy density and pressure, respectively) [179]. Another common practice is to reduce the number of free parameters by setting $\rho_{\mathrm{m}}^{\mathrm{c}} = p_{\mathrm{m}}^{\mathrm{c}} = 1$. The VdW EoS can then be rewritten concisely as [179]:

$$p_{\mathrm{m}} = \frac{8 w_{\mathrm{m}} \rho_{\mathrm{m}}}{3 - \rho_{\mathrm{m}}} - 3\rho_{\mathrm{m}}^2 \ . \tag{3.5}$$

If p_{m} is replaced with the above expression and one uses Eq. (3.1) to substitute for ρ_{m}, Eq. (3.3) becomes:

$$\tilde{\kappa} + \dot{\tilde{a}}^2 - \frac{27(\tilde{\kappa} + \dot{\tilde{a}}^2)^2}{8\pi G \tilde{a}^2} - \frac{64\pi G w_{\mathrm{m}} \tilde{a}^2 (\tilde{\kappa} + \dot{\tilde{a}}^2)}{\tilde{\kappa} - 8\pi G \tilde{a}^2 + \dot{\tilde{a}}^2} + 2\tilde{a}\ddot{\tilde{a}} = 0 \ . \tag{3.6}$$

This reduces to Eq. (5) of Ref. [176] when $\tilde{\kappa} = 0$, although Eq. (3.6) would have to be written as a first-order differential equation in H to make a comparison.

Eq. (3.6) can be solved numerically by choosing appropriate parameter values and initial conditions. In line with Kremer's work, we have already established that $\tilde{a}(\tilde{t} = 0) = \dot{\tilde{a}}(\tilde{t} = 0) = 1$. Now we set w_{m} to 0.52, while $\tilde{\kappa}$ is assigned the values 0, 0.01 and -0.01. The resulting plots are shown in Figs. 3.1–3.4.

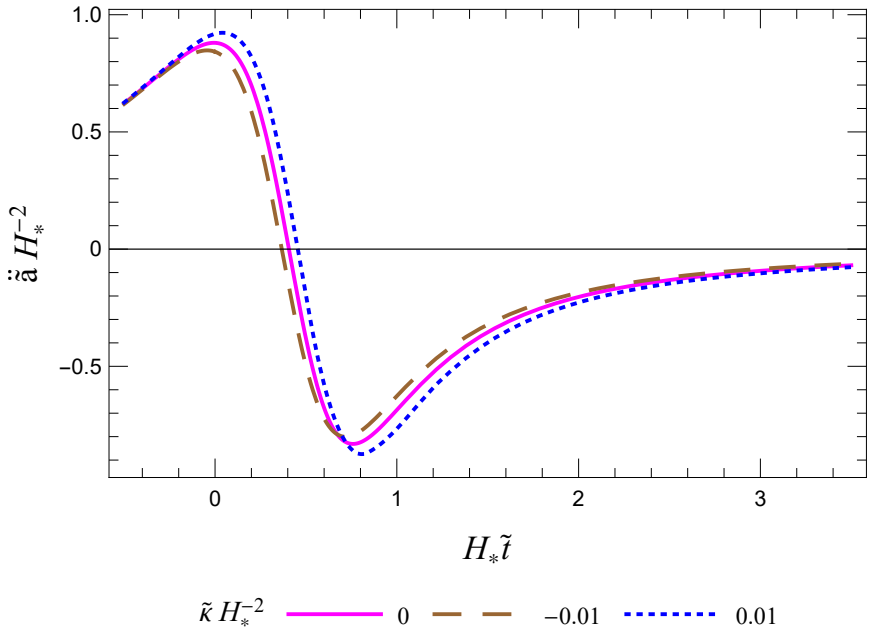

FIGURE 3.1: The variation of acceleration with time for a universe composed of a VdW fluid.

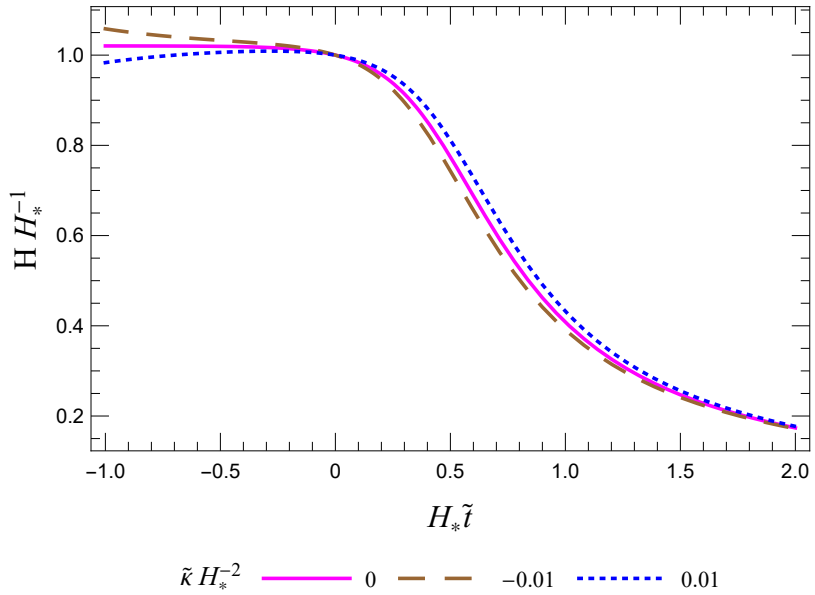

FIGURE 3.2: The variation of the Hubble parameter with time for a universe composed of a VdW fluid. It may be noted that in the flat case, H is constant at early times. This is suggestive of exponential inflation.

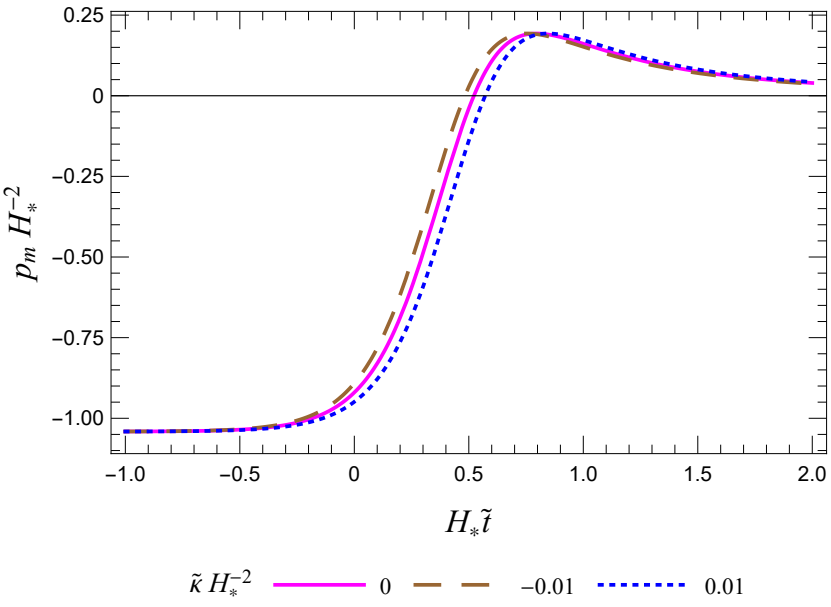

FIGURE 3.3: The variation of pressure with time for a universe composed of a VdW fluid.

The most widely-accepted view nowadays with regards to the different stages of cosmic evolution is that the Universe initially underwent a period of accelerated expansion known as *inflation* [129, 180, 181], and that a graceful exit then led to a radiation-dominated epoch (and a later matter-dominated one) during which deceleration occurred [182, 183]. This was followed by another phase of acceleration [1, 3, 184, 185]

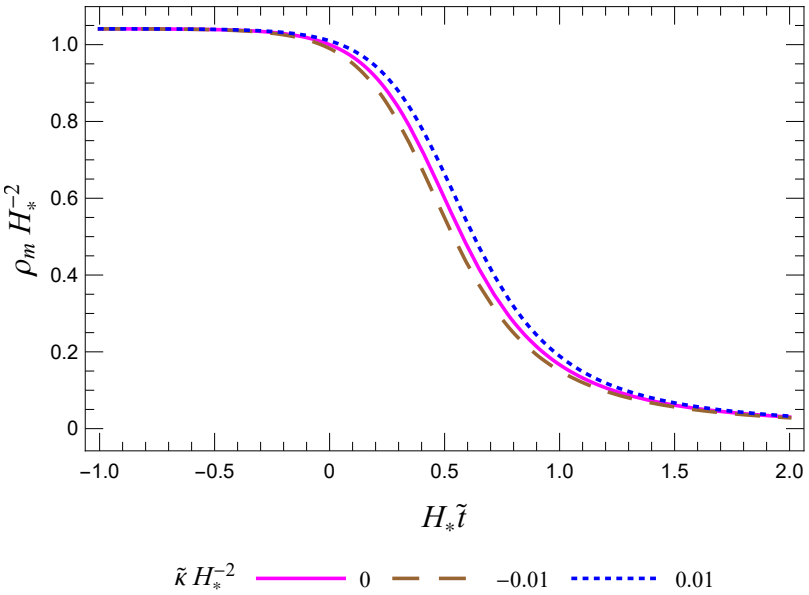

FIGURE 3.4: The variation of energy density with time for a universe composed of a VdW fluid.

– which extends to the present time and is thought to be one of the most notable sources of evidence for dark energy. As pointed out by Kremer, modelling the Universe as a VdW fluid can correctly describe the transition from the inflationary epoch to the subsequent deceleration, but fails to yield the proposed late-time acceleration (Fig. 3.1).

The evolution of the Universe is determined by the pressure of the cosmic fluid. In fact, Fig. 3.3 shows that when this fluid is described by the VdW EoS [Eq. (3.5)], p_{m} would initially be negative (resulting in inflation – Fig. 3.1). It would then start to increase and become positive (causing the acceleration to decrease and deceleration to set in), finally going asymptotically to zero (with deceleration following suit) rather than becoming negative again (which would cause the Universe to accelerate).

Another point of interest is the way the presence of curvature affects the evolution. From Fig. 3.1, it can be seen that positive curvature delays the onset of deceleration with respect to the flat case, while negative curvature causes it to occur earlier. The maximum acceleration and deceleration also change with $\tilde{\kappa}$: they are largest for the closed universe, and least for the open one. Furthermore, small variations in the parameters or the initial conditions only alter the magnitude of these effects, and not the behaviour of the evolution. The closed universe would still be characterised by the largest acceleration and deceleration, and the transition from one to the other would still occur later than it does for the flat and open geometries.

3.2.1 Dark energy as Quintessence or a Chaplygin gas

To alleviate the problem posed by the absence of late-time acceleration, Kremer [176] proposes adding a dark energy component to the VdW matter distribution. Thus Eq. (3.1) becomes

$$H^2 = \frac{8\pi G}{3}\left(\rho_{\rm m} + \rho_{\rm d}\right) - \frac{\tilde{\kappa}}{\tilde{a}^2} \ , \tag{3.7}$$

where $\rho_{\rm d}$ is the dark energy density and we shall denote the corresponding pressure by $p_{\rm d}$. Matter and dark energy are assumed to be non-interacting [176], so energy conservation may be expressed as two decoupled equations:

$$\dot{\rho}_{\rm d} = -3H(\rho_{\rm d} + p_{\rm d}) \ ; \tag{3.8}$$

$$\dot{\rho}_{\rm m} = -3H(\rho_{\rm m} + p_{\rm m} + \varpi) \ , \tag{3.9}$$

The term $-3H\varpi$ on the right-hand side of Eq. (3.9) represents the rate at which energy (density) is transferred irreversibly from the gravitational field to the VdW matter distribution, but may be equivalently described as the rate of change in $\rho_{\rm m}$ due to the bulk viscosity of the fluid. In other words, the decay of the gravitational field[43] can be accounted for by considering a bulk-viscous cosmic fluid. Before going on, let us note that the possibility of expressing energy conservation as two distinct equations [with the term in ϖ relegated to Eq. (3.9)] reflects the minimal nature of the coupling between dark energy and the gravitational field [176].

The quantity ϖ introduced in Eq. (3.9) is termed the *non-equilibrium pressure*. In second-order non-equilibrium thermodynamics, the relaxation of ϖ to its equilibrium value ($\varpi_0 = 0$) is described by the equation [189]:

$$\dot{\varpi} = -\frac{\varpi - \varpi_0}{\mathcal{T}} \ , \tag{3.10}$$

$\mathcal{T}$ being the *relaxation* or *characteristic* time [176]. Once we move to a cosmological setting and include the effects of an expanding universe, the above relation takes on an extra term:

$$\mathcal{T}\dot{\varpi} + \varpi = -3\eta H \ . \tag{3.11}$$

Here, η is the coefficient of bulk viscosity.[44] We shall proceed as in Ref. [176] and

[43] This decay happens due to particle production. More information may be found in Refs. [186,187] and [188].

[44] A derivation of Eq. (3.11) can be found in Ref. [186], where the authors make use of the seminal work of Israel and Stewart [190].

assume η to be directly proportional to the energy density [191] of the mixture ($\eta = \alpha\rho_{\rm tot}$, where $\rho_{\rm tot} = \rho_{\rm m} + \rho_{\rm d}$ and α is a constant). If $\mathcal{T}$ is equated to $\eta/\rho_{\rm tot}$ [192], it follows that $\mathcal{T} = \alpha$, and Eq. (3.11) becomes $\alpha\dot{\varpi} + \varpi = -3(\alpha\rho_{\rm tot})H$. Eq. (3.7) can then be utilised to eliminate $\rho_{\rm tot}$. One gets that:

$$\dot{\varpi} + \frac{1}{\alpha}\varpi = -\frac{9H}{8\pi G}\left(H^2 + \frac{\tilde{\kappa}}{\tilde{a}^2}\right) \ . \tag{3.12}$$

The presence of $\tilde{\kappa}$ suggests that the evolution of the non-equilibrium pressure is dependent on the geometry. In fact, this is the main reason why ϖ is introduced: it enhances the impact of spatial curvature. However, the main conclusions we reach would not be altered in its absence. The only effect to be expected – apart from the fact that differences due to $\tilde{\kappa}$ would be smaller – are changes to which of the three universes accelerates the most during the dark-energy dominated era. That said, the analysis presented in this chapter indicates that $\tilde{\kappa}$ does not play a significant role in the current epoch, so these slight variations are of no concern.

The pressure $p_{\rm m}$ and energy density $\rho_{\rm m}$ of the matter component are again related by the VdW EoS [Eq. (3.5)]. As for dark energy, we shall take Kremer's example and consider either Quintessence or a Chaplygin gas. A similar model consisting of Quintessence and a viscous VdW fluid in a Lyra manifold[45] is studied in Ref. [197]. There are some important differences, though: the authors also include a constant or dynamical Λ and restrict their analysis to a flat geometry, and furthermore assume dark energy and dark matter to be interacting, which is not the case in our work.

Quintessence

The EoS for Quintessence reads [176]

$$p_{\rm d} = w_{\rm d}\rho_{\rm d} \ ; \qquad w_{\rm d} < -1/3 \ , \tag{3.13}$$

[45] In 1918, Weyl [193] proposed a modification of Riemannian manifolds in order to fully geometrise gravitation and electromagnetism [194]. Another modification was put forward by Lyra [195] more than three decades later. Lyra's version serves as the framework for a unified field theory similar to Weyl's, but has the advantage that parallel transport leaves the length of a vector unaltered (this is not what happens in Weyl's theory). An important characteristic of Lyra's geometry is a gauge function (introduced into the structureless manifold) that gives rise to a gauge vector field $\phi_\mu(x^\nu)$ [194]. In cosmologies based on Lyra manifolds with constant ϕ_μ [$= (\beta, 0, 0, 0)$], the combination of ϕ_μ – which provides the necessary pressure – and a pressureless 'vacuum fluid' having $\rho_{\rm m} = -3\beta^2/2$ can be seen as analogous to a cosmological constant [196].

where $w_{\rm d}$ is a constant. When inserted into Eq. (3.8), Eq. (3.13) allows us to solve for $\rho_{\rm d}$. It is found that

$$\rho_{\rm d} = \rho_{\rm d}^0 \; \tilde{a}^{\,-3(1+w_{\rm d})} \; , \tag{3.14}$$

$\rho_{\rm d}^0$ being the dark energy density at $\tilde{t} = 0$. The next step entails taking the time derivative of Eq. (3.7), then substituting for $\dot{\rho}_{\rm d}$ and $\dot{\rho}_{\rm m}$ using the continuity equations, (3.8) and (3.9). These contain pressure terms, but $p_{\rm m}$ and $p_{\rm d}$ may easily be written as functions of the respective energy densities by means of Eqs. (3.5) and (3.13). Finally, the VdW energy density, $\rho_{\rm m}$, is replaced with the corresponding expression from Eq. (3.7), while the right-hand side of Eq. (3.14) serves to eliminate $\rho_{\rm d}$. The resulting equation is given by:

$$\begin{aligned} &8\pi G\left[\frac{8w_{\rm m}\tilde{a}^2 f(\tilde{t},\tilde{\kappa})}{3\tilde{a}^2 - f(\tilde{t},\tilde{\kappa})} - \frac{3}{\tilde{a}^2}f(\tilde{t},\tilde{\kappa})^2 + \frac{w_{\rm d}\rho_{\rm d}^0}{\tilde{a}^{1+3w_{\rm d}}} + \tilde{a}^2\varpi\right] + \tilde{\kappa} \; + \dot{\tilde{a}}^2 + 2\tilde{a}\ddot{\tilde{a}} = 0 \; ; \\ &f(\tilde{t},\tilde{\kappa}) = -\frac{\rho_{\rm d}^0}{\tilde{a}^{1+3w_{\rm d}}} + \frac{3}{8\pi G}\left(\tilde{\kappa} + \dot{\tilde{a}}^2\right) \; . \end{aligned} \tag{3.15}$$

Together with Eq. (3.12), Eq. (3.15) governs the evolution of a universe composed of a VdW matter distribution and Quintessence. It may be shown to reduce to Kremer's Eq. (13) [176] when $\tilde{\kappa} = 0$.

We thus have a system of two differential equations that can be solved numerically by again making use of the initial conditions $\tilde{a}(0) = \dot{\tilde{a}}(0) = 1$. This time, however, we also need an initial condition for Eq. (3.12), so we set $\varpi(\tilde{t} = 0) = 0$. The parameters are assigned values as follows: $\alpha = 0.4$, $w_{\rm m} = 0.6$, $w_{\rm d} = -0.9$, $\rho_{\rm d}^0 = 0.03 \times 3/(8\pi G)$ and $|\tilde{\kappa}| = 0.01$ (or zero), and the resulting plots are shown in Figs. 3.5–3.8. It immediately becomes evident that the negative pressure of dark energy is able to produce the late-time acceleration missing in the pure VdW model. Otherwise, the implications of a non-zero $\tilde{\kappa}$ for the epochs of inflation and deceleration are as before (albeit being more pronounced): with respect to a flat universe, positive $\tilde{\kappa}$ delays the onset of deceleration and increases the maximum acceleration and deceleration, while negative $\tilde{\kappa}$ does the contrary (Fig. 3.5). A similar pattern is observed in the onset of late-time acceleration. Once again, the closed universe is the last to undergo the transition.

As stated previously, changes in the acceleration/deceleration of the Universe are caused by variations in the pressure of the cosmic fluid. In fact, we note that the temporal shifts between the curves of total pressure against time (Fig. 3.7) complement those between the curves of acceleration versus time (Fig. 3.5). Provided that the

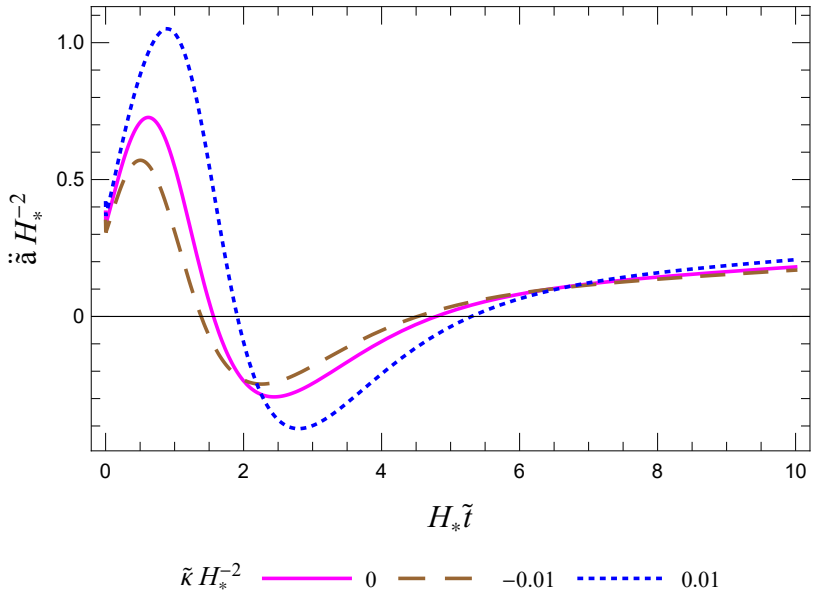

FIGURE 3.5: The variation of acceleration with time for a universe composed of a VdW matter distribution and Quintessence.

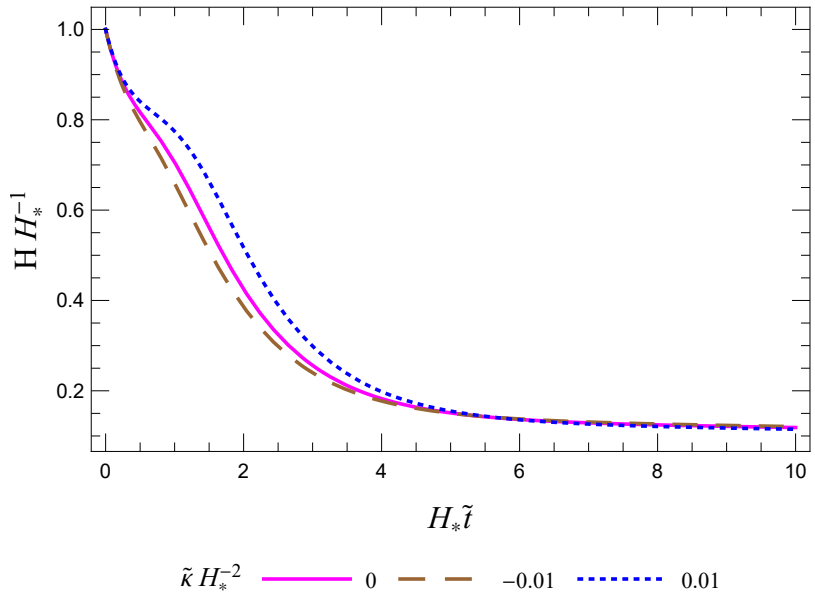

FIGURE 3.6: The variation of the Hubble parameter with time for a universe composed of a VdW matter distribution and Quintessence.

pressure of the VdW fluid evolves smoothly, small changes in the initial conditions or the parameters only alter the magnitude of the above-mentioned effects. Another point worthy of mention is the fact that the deviation from the flat universe is stronger for positive $\tilde{\kappa}$.

The results presented here are in line with the conclusions reached in Ref. [187].

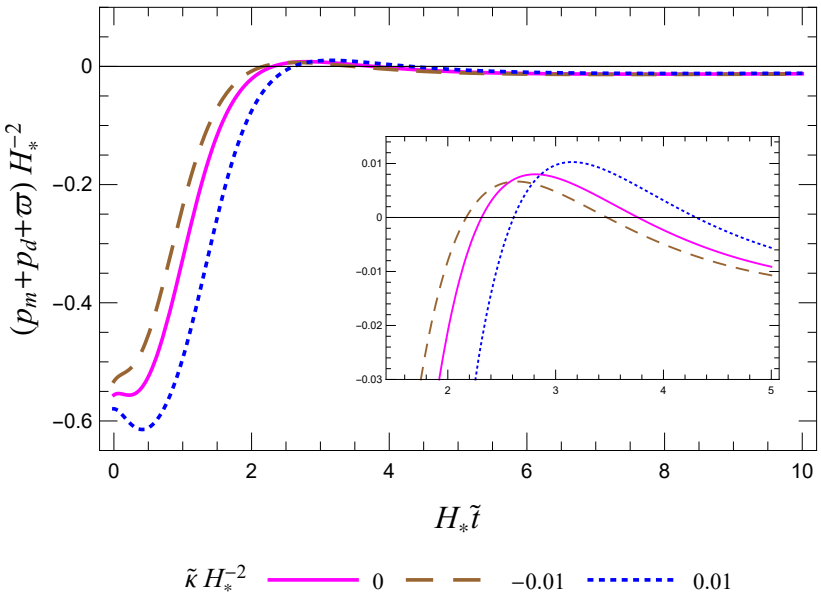

FIGURE 3.7: The variation of total pressure with time for a universe composed of a VdW matter distribution and Quintessence. The peaks of the curves are shown at greater resolution (inset).

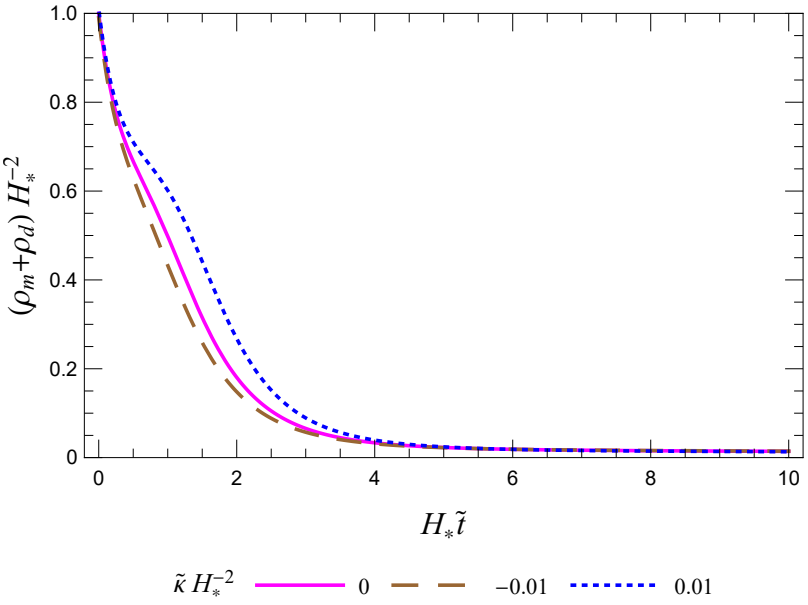

FIGURE 3.8: The variation of total energy density with time for a universe composed of a VdW matter distribution and Quintessence.

Kremer and Teixeira da Silva model the cosmic fluid as a scalar field mixed with a matter distribution, and likewise find that the inflationary acceleration and subsequent deceleration are most pronounced for $\tilde{\kappa} > 0$, while the transition to the present epoch of acceleration occurs first for the open universe. They suggest that the larger acceleration the closed universe undergoes during inflation is due to a greater $|\varpi|$

since, being negative, the non-equilibrium pressure ϖ is partly responsible for the said acceleration, as may be inferred from the second Friedmann equation:

$$\ddot{\tilde{a}} = -\frac{4\pi G}{3}\tilde{a}(\rho_{\rm tot} + 3p_{\rm eq} + 3\varpi) \ . \tag{3.16}$$

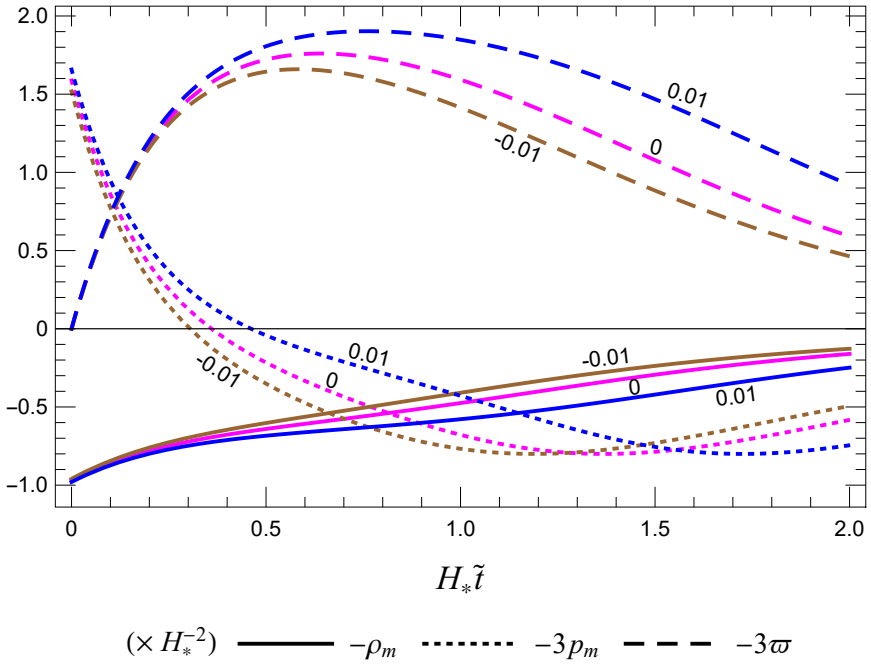

FIGURE 3.9: The two main factors contributing to the difference in the maximum inflationary acceleration of the flat, open and closed universes: the variation with $\tilde{\kappa}$ of the non-equilibrium pressure ϖ and the VdW pressure $p_{\rm m}$. The evolution of $-\rho_{\rm m}$ is also shown. The Universe is modelled as a bulk-viscous mixture of Quintessence and a VdW fluid and the value of $\tilde{\kappa}$ is denoted by the label on each curve. Quintessence is negligible at this stage.

Here, $\rho_{\rm tot} = \rho_{\rm m} + \rho_{\rm d}$ and $p_{\rm eq} = p_{\rm m} + p_{\rm d}$. It transpires that their conclusion is valid in our case, as may easily be deduced from Fig. 3.9. There is, however, an important difference: the VdW fluid also exerts a repulsive pressure ($p_{\rm m}$) at early times, and the fact that this is strongest in the closed universe [which is, in turn, a result of the fact that $\rho_{\rm m}$ is largest for $\tilde{\kappa} > 0$ at $\tilde{t} = 0$, as suggested by Eq. (3.7)] helps to boost its acceleration. Indeed, it is precisely the difference in $p_{\rm m}$ that initially causes the closed universe to have the greatest acceleration. The effects due to ϖ set in later (Fig. 3.9). After a while, the pressure $p_{\rm m}$ becomes attractive, and at first it is smallest for $\tilde{\kappa} > 0$ (Fig. 3.10). This is yet another factor which helps to enhance $\ddot{\tilde{a}}$.

There is a strong link between the variation of ϖ and $\tilde{a}$ with $\tilde{\kappa}$. As Eq. (3.12) suggests, $|\dot{\varpi}|$ is largest for positive $\tilde{\kappa}$ at the start of the evolution. Hence ϖ grows more rapidly in the closed universe, which (partly because of this) expands at the fastest rate.

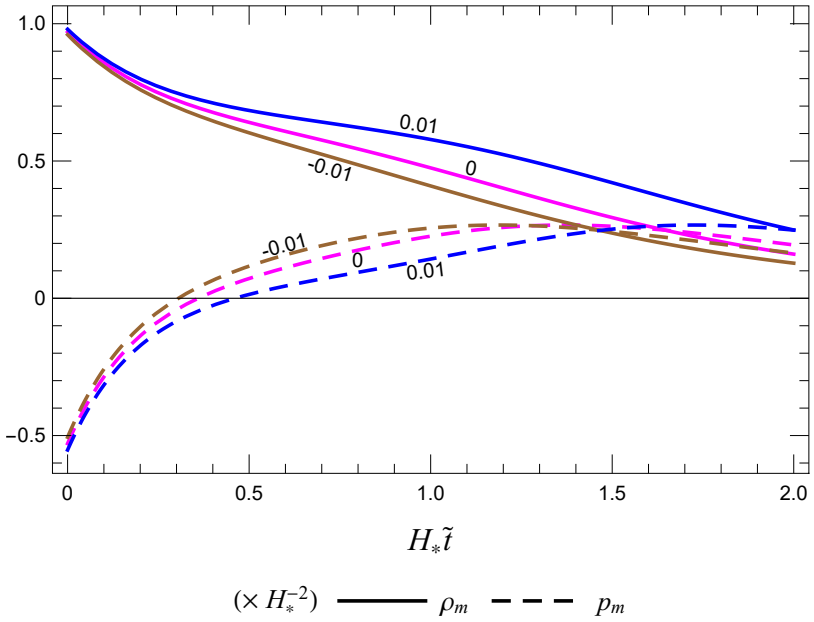

FIGURE 3.10: Curves showing how the energy density and pressure of matter vary with time. The Universe is modelled as a bulk-viscous mixture of Quintessence and a VdW fluid. The labels denote the respective values of $\tilde{\kappa}$.

Accordingly, the rapid expansion causes the gravitational field to decay more quickly than it does in the flat and open cases,[46] resulting in a higher rate of energy transfer to the VdW fluid and thus causing it to be diluted more slowly. The consequent decrease in $|\dot{\rho}_\mathrm{m}|$ may be deduced from Eq. 3.9 and emerges clearly in Fig. 3.10. Moreover, it explains why the total energy density in the closed universe soon becomes larger than that in the other scenarios, remaining this way well into the deceleration epoch (Fig. 3.8). In turn, a greater ρ_tot (and H) speeds up the growth of ϖ (Eq. 3.12), although not indefinitely – the non-equilibrium pressure acts to slow down its own build-up, as is evident from the same equation.

Until ρ_m has decayed by a sufficient amount, the right-hand side of Eq. (3.5) is dominated by the term $-3\rho_\mathrm{m}^2$. Initially, therefore, the matter component exerts a negative pressure whose magnitude is largest where the fluid is most dense (hence in the closed universe). The variation of ρ_m and p_m with time is depicted in Fig. 3.10.

The larger magnitude that ϖ has in the closed universe explains the delay in the transition from the first accelerated epoch to the subsequent deceleration. Eq. (3.16) implies that this transition occurs when $3|\varpi|$ is equal to the sum $\rho_\mathrm{m} + 3p_\mathrm{m}$ – in other words, when the repulsive non-equilibrium pressure (dark energy is negligible at this

[46]The rate of decay is given by $3H\varpi$ [see Eq. (3.9)].

point) is counterbalanced by the attractive force of matter. The smaller $|\varpi|$ in the open universe thus leads to an earlier onset of deceleration. This is illustrated in Fig. 3.11.

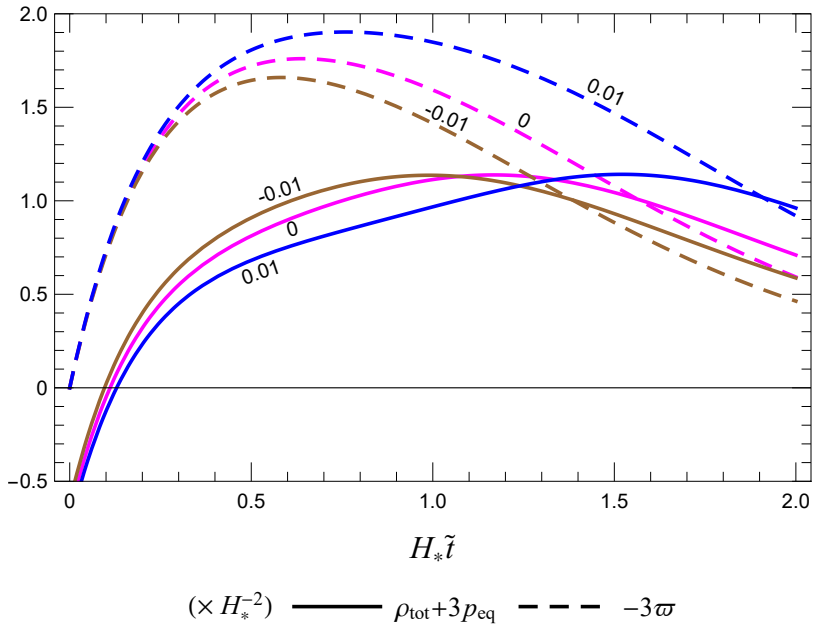

FIGURE 3.11: Curves depicting the evolution of the non-equilibrium pressure ϖ and of the sum $\rho_{\rm tot} + 3p_{\rm eq}$. The Universe is modelled as a bulk-viscous mixture of Quintessence and a VdW fluid, and labels denote the spatial curvature $\tilde{\kappa}$. The intersection between curves with the same $\tilde{\kappa}$ indicates the onset of deceleration for the respective universes.

As suggested above, Eq. (3.9) allows one to conclude that a negative non-equilibrium pressure reduces the magnitude of $\dot{\rho}_{\rm m}$. Kremer and Teixeira da Silva point out that, since $|\varpi|$ is greatest in the closed universe, this is also where the most matter is produced, hence leading to a larger deceleration [187]. Things are somewhat different in the case under consideration, however: although the non-equilibrium pressure decreases the rate at which matter is diluted during the first epoch of acceleration – an effect that is most pronounced in the closed universe – it is never large enough to yield an overall increase in $\rho_{\rm m}$. Indeed, Fig. 3.12 makes it clear that the closed universe undergoes the greatest deceleration mainly due to the larger value of its scale factor. This is because a scales the sum $\rho_{\rm tot} + 3p_{\rm eq} + 3\varpi$ in Eq. (3.16).

Ref. [187] invokes the greater production of matter for $\tilde{\kappa} > 0$ and the faster decay of the scalar field to explain why the onset of late-time acceleration is delayed when the geometry is closed. Here, the said delay is attributed to the fact that matter gets diluted more slowly in the closed universe,[47] which causes the evolution of $p_{\rm m}$

[47] This stops being the case at $\tilde{t} \approx 9$.

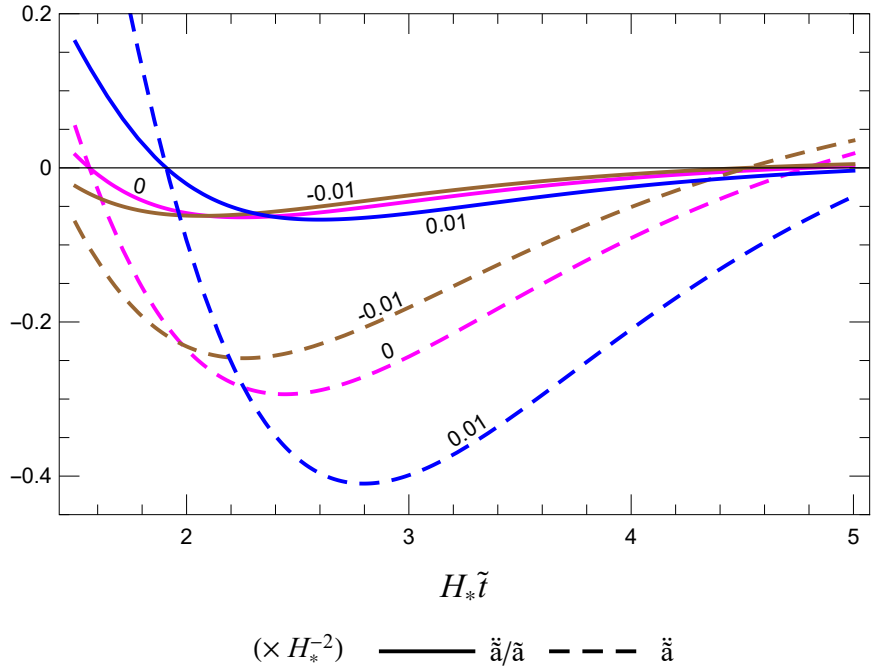

FIGURE 3.12: Curves showing the temporal variation of $\ddot{\tilde{a}}/\tilde{a}$ and $\ddot{\tilde{a}}$ for a universe composed of Quintessence and a VdW fluid. Labels denote the respective values of $\tilde{\kappa}$.

to lag behind that in the open and flat scenarios. One recalls that whether the Universe accelerates or decelerates is due to the interplay of pressures. Once the first term on the right-hand side of Eq. (3.5) dominates over the second one, the pressure $p_{\rm m}$ becomes positive, increases to a maximum and then starts to decay, until the repulsive pressure of dark energy takes over and the Universe enters a second phase of acceleration. Since $p_{\rm m}$ begins to decay at a later time when $\tilde{\kappa} > 0$, the transition to the final epoch of acceleration occurs last in the closed universe.

Chaplygin gas

Next, we model dark energy as a Chaplygin gas, whose pressure $p_{\rm d}$ is related to the energy density $\rho_{\rm d}$ by means of the EoS [176]:

$$p_{\rm d} = -\frac{A}{\rho_{\rm d}} \; ; \quad A > 0, \tag{3.17}$$

where A is a constant. Inserting this relation into Eq. (3.8) and solving for $\rho_{\rm d}$ as a function of $\tilde{a}$ yields:

$$\rho_{\rm d} = \frac{\sqrt{A\tilde{a}^6 + C}}{\tilde{a}^3} \; ; \quad C > 0. \tag{3.18}$$

In the above, C represents a constant of integration. If we write C/A as ψ and evaluate $\rho_{\rm d}$ at $\tilde{t}=0$, we get that $\rho_{\rm d}^0=\sqrt{A(1+\psi)}$, and so Eq. (3.18) may be expressed in the form:

$$\rho_{\rm d}=\frac{\rho_{\rm d}^0}{\tilde{a}^3}\sqrt{\frac{\tilde{a}^6+\psi}{1+\psi}}\ . \tag{3.19}$$

We repeat the procedure adopted in the case of Quintessence and take the time derivative of Eq. (3.7), then substitute for $\dot{\rho}_{\rm d}$ and $\dot{\rho}_{\rm m}$ from equations (3.8) and (3.9), respectively. The pressure of matter is determined by the VdW EoS [Eq. (3.5)], and that of dark energy by Eq. (3.17), with A written as $\left(\rho_{\rm d}^0\right)^2/(1+\psi)$. The matter energy density $\rho_{\rm m}$ is subsequently replaced with the corresponding expression from Eq. (3.7), while $\rho_{\rm d}$ takes the form specified in (3.19). The final equation reads:

$$\begin{aligned}
&8\pi G\left[\frac{8w_{\rm m}\tilde{a}^2h(\tilde{t},\tilde{\kappa})}{3\tilde{a}^2-h(\tilde{t},\tilde{\kappa})}-\frac{3h(\tilde{t},\tilde{\kappa})^2}{\tilde{a}^2}+\tilde{a}^2\varpi-\frac{\rho_{\rm d}^0\tilde{a}^5}{\mathcal{F}(\tilde{t})(1+\psi)}\right]+\tilde{\kappa}+\dot{\tilde{a}}^2+2\tilde{a}\ddot{\tilde{a}}=0\ ,\\
&\mathcal{F}(\tilde{t})=\sqrt{\frac{\tilde{a}^6+\psi}{1+\psi}}\ ;\qquad h(\tilde{t},\tilde{\kappa})=-\rho_{\rm d}^0\,\frac{\mathcal{F}(\tilde{t})}{\tilde{a}}+\frac{3}{8\pi G}(\dot{\tilde{a}}^2+\tilde{\kappa})\ ,
\end{aligned} \tag{3.20}$$

and reduces to Eq. (16) in Ref. [176] when $\tilde{\kappa}$ is set to zero and the necessary modifications in notation are made. Together with (3.12), Eq. (3.20) is solved by setting $\tilde{a}(0)=\dot{\tilde{a}}(0)=1$, $\varpi(0)=0$, $\alpha=0.4$, $w_{\rm m}=0.6$, $\psi=3$, $\rho_{\rm d}^0=0.03\times3/(8\pi G)$ and $|\tilde{\kappa}|=0.01$ or 0.

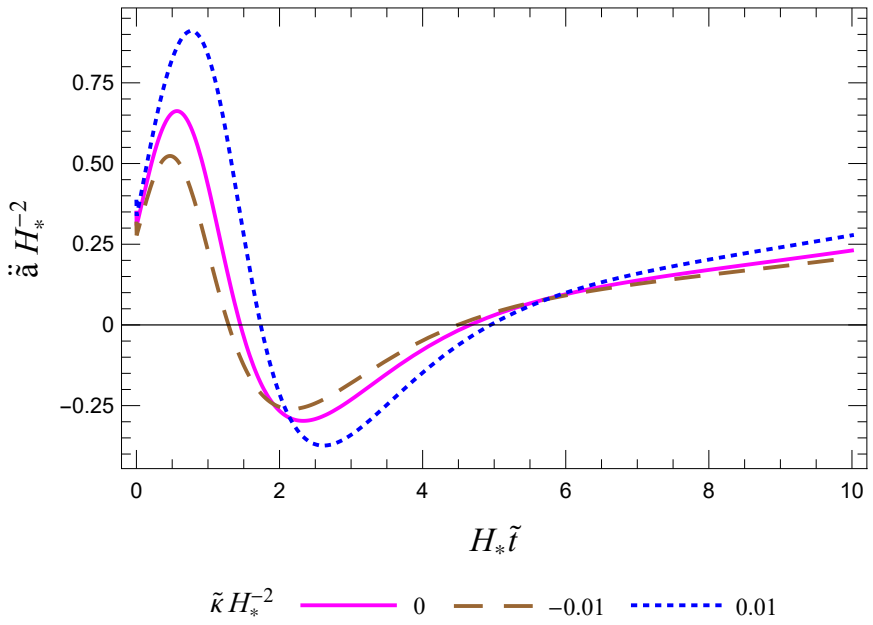

FIGURE 3.13: The variation of acceleration with time for a universe composed of a VdW matter distribution and a Chaplygin gas.

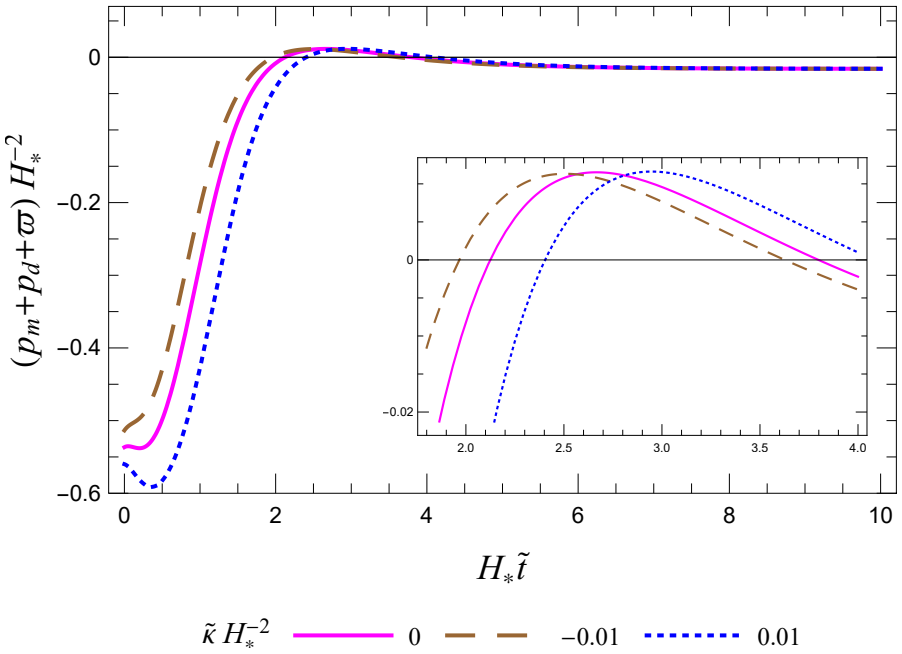

FIGURE 3.14: The variation of total pressure with time for a universe composed of a VdW matter distribution and a Chaplygin gas. The peaks of the curves are shown at greater resolution (inset).

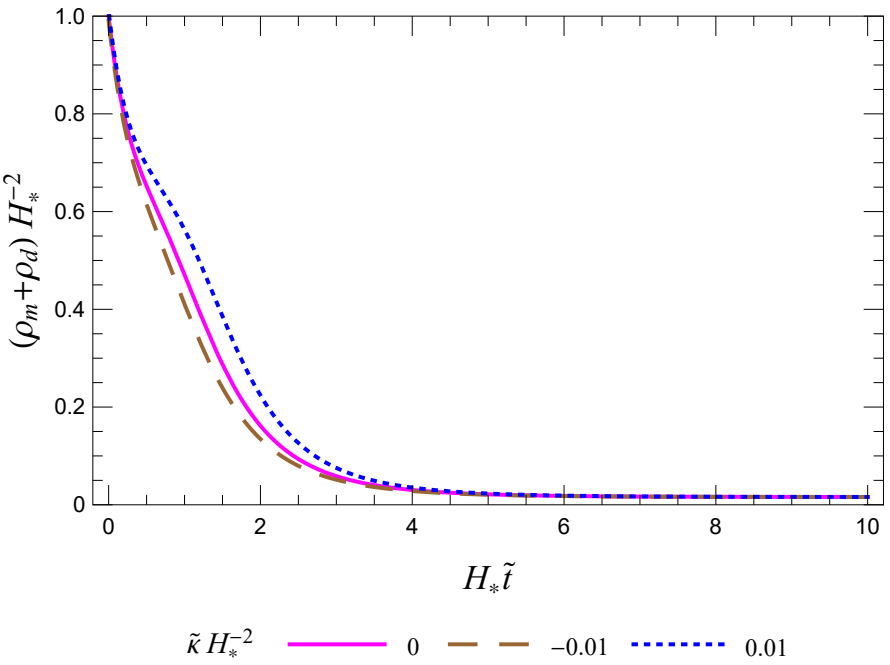

FIGURE 3.15: The variation of total energy density with time for a universe composed of a VdW matter distribution and a Chaplygin gas.

The evolution of a universe with a VdW fluid as the matter component and a Chaplygin gas as dark energy is illustrated in Figs. 3.13, 3.14 and 3.15. It can be seen that

the effects of curvature are similar to those noted when dark energy was modelled as Quintessence. Once again, small variations in the parameters or the initial conditions only change the magnitude of these effects.

3.2.2 Dark energy as a dynamical Λ

In this section, we again consider equilibrium pressures only, and model dark energy as a time-dependent cosmological term $\Lambda(\tilde{t})$ with EoS parameter $w_\Lambda = p_\Lambda/\rho_\Lambda = -1$ [p_Λ and ρ_Λ being, respectively, the pressure and energy density[48] associated with $\Lambda(\tilde{t})$]. Thus, Eq. (3.1) now reads:

$$H^2 = \frac{8\pi G}{3}\rho_\mathrm{m} - \frac{\tilde{\kappa}}{\tilde{a}^2} + \frac{\Lambda(\tilde{t})}{3} \ , \tag{3.21}$$

while energy conservation can be expressed as:

$$\dot{\rho}_\mathrm{m} = -3H(\rho_\mathrm{m} + p_\mathrm{m}) - \frac{\dot{\Lambda}(\tilde{t})}{8\pi G} \ . \tag{3.22}$$

In this case, the matter and dark energy components cannot be conserved separately, because Einstein's field equations take the form[49]

$$G_{\mu\nu} = R_{\mu\nu} - {}^1\!/_2 R g_{\mu\nu} = 8\pi G T^\mathrm{m}_{\mu\nu} - \Lambda(\tilde{t}) g_{\mu\nu} \ , \tag{3.23}$$

and hence the Bianchi identity, $\nabla^\mu G_{\mu\nu} = 0$, implies that $8\pi G \nabla^\mu T^\mathrm{m}_{\mu\nu} - g_{\mu\nu}\nabla^\mu \Lambda(\tilde{t}) = 0$. Since a time-varying gravitational coupling is beyond the scope of this study, matter can only be conserved independently if $\nabla^\mu \Lambda(\tilde{t}) = 0$ – in other words, only if $\Lambda(\tilde{t})$ goes back to being a cosmological *constant*, which is not what we want here. Consequently, the models considered in the rest of the chapter are characterised by an exchange of energy between matter and dark energy.

We proceed by taking the time derivative of Eq. (3.21) and using Eq. (3.22) to substitute for $\dot{\rho}_\mathrm{m} + \dot{\Lambda}(\tilde{t})/8\pi G$. The resulting equation reads:

$$8\pi G \tilde{a}^2 (p_\mathrm{m} + \rho_\mathrm{m}) - 2(\tilde{\kappa} + \dot{\tilde{a}}^2) + 2\tilde{a}\ddot{\tilde{a}} = 0 \ . \tag{3.24}$$

The next step consists in choosing a proper model for the matter distribution and an expression for $\Lambda(\tilde{t})$.

[48] $\rho_\Lambda = \Lambda(\tilde{t})/8\pi G$.

[49] $T^\mathrm{m}_{\mu\nu}$ is the matter part of the energy–momentum tensor.

Λ proportional to $\tilde{a}^{-q}$

In the first model with a dynamical Λ, we retain the VdW EoS [Eq. (3.5)] for the matter part of the mixture, and represent the time-dependent vacuum term by [198]:

$$\Lambda(\tilde{t}) = \frac{\Lambda_{\rm I}}{\tilde{a}^q} \ , \tag{3.25}$$

where the parameter q lies in the range $[0, 2]$ and $\Lambda_{\rm I}$ is the value of $\Lambda(\tilde{t})$ at $\tilde{t} = 0$.

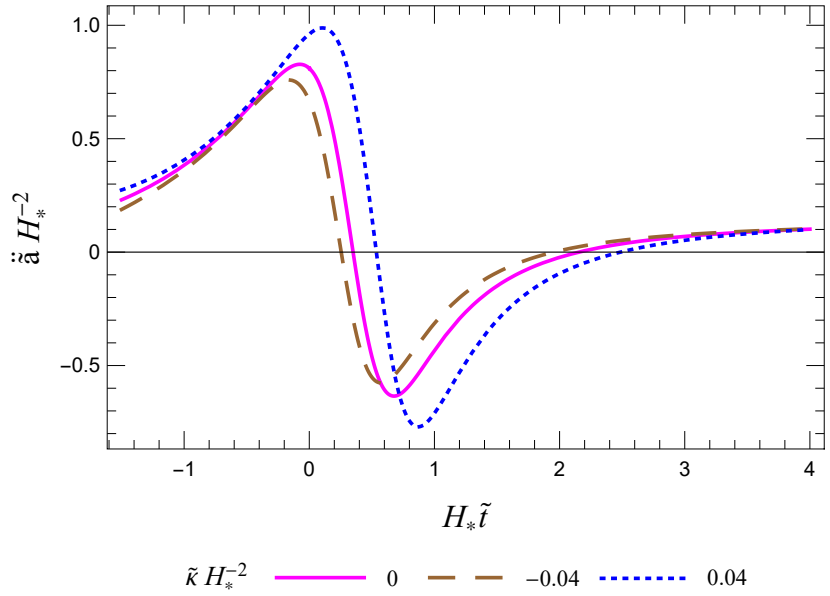

FIGURE 3.16: The variation of acceleration with time for a universe composed of a VdW matter distribution and a dynamical $\Lambda \propto \tilde{a}^{-1/2}$.

The fundamental equation is obtained from (3.24) by making use of Eq. (3.5) to write $p_{\rm m}$ in terms of $\rho_{\rm m}$, then replacing the latter with the corresponding expression from Eq. (3.21). When $\Lambda(\tilde{t})$ is substituted by the right-hand side of Eq. (3.25), we get:

$$\begin{aligned} &\tilde{\kappa} + \dot{\tilde{a}}^2 - \frac{\Lambda_{\rm I}}{\tilde{a}^{q-2}} - \frac{3}{8\pi G}\left[\frac{s(\tilde{t},\tilde{\kappa})}{\tilde{a}}\right]^2 - \frac{64\pi G w_{\rm m}\tilde{a}^2 s(\tilde{t},\tilde{\kappa})}{24\pi G\tilde{a}^2 + s(\tilde{t},\tilde{\kappa})} + 2\tilde{a}\ddot{\tilde{a}} = 0 \ ; \\ &s(\tilde{t},\tilde{\kappa}) = \frac{\Lambda_{\rm I}}{\tilde{a}^{q-2}} - 3(\tilde{\kappa} + \dot{\tilde{a}}^2) \ . \end{aligned} \tag{3.26}$$

The parameters $w_{\rm m}$, q, $\Lambda_{\rm I}$ and $|\tilde{\kappa}|$ are assigned the values 0.5, 0.5, 0.2 and 0.04 (or 0), respectively. With the initial conditions set once more to $\tilde{a}(0) = \dot{\tilde{a}}(0) = 1$, Eq. (3.26) yields the cosmic history shown in Figs. 3.16–3.19. It can be seen that the effects of curvature tally with what was observed for the previous models. As before, slight

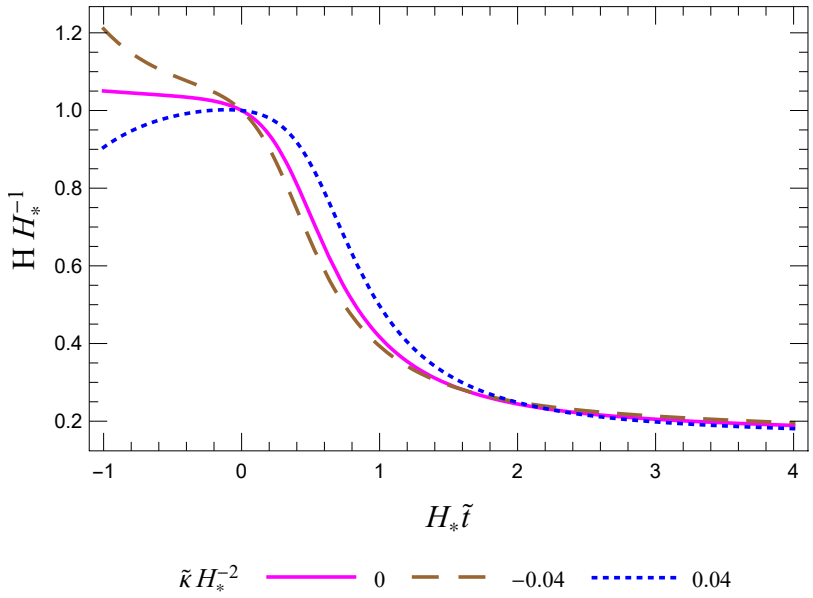

FIGURE 3.17: The variation of the Hubble parameter with time for a universe composed of a VdW matter distribution and a dynamical $\Lambda \propto \tilde{a}^{-1/2}$.

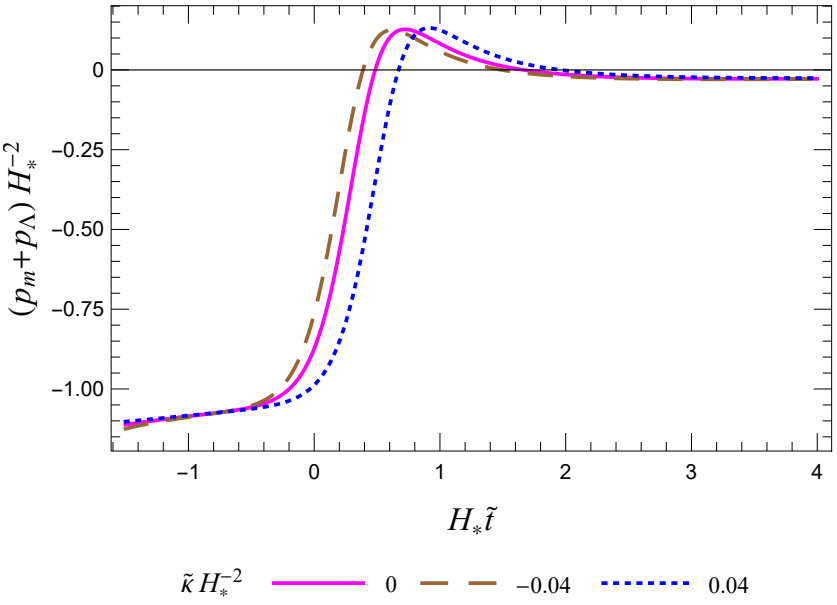

FIGURE 3.18: The variation of total pressure with time for a universe composed of a VdW matter distribution and a dynamical $\Lambda \propto \tilde{a}^{-1/2}$.

variations in the initial conditions or the parameters only modify the magnitude of the said effects, although this is subject to the condition that the evolution of $p_{\rm m}$ remains smooth.

We are now in a position to carry out an analysis similar to the one for the VdW–

Quintessence model. The questions that most merit attention are two, namely: why is it that deceleration and inflationary acceleration are largest for the closed universe? And why does positive curvature delay the onset of deceleration and late-time acceleration?

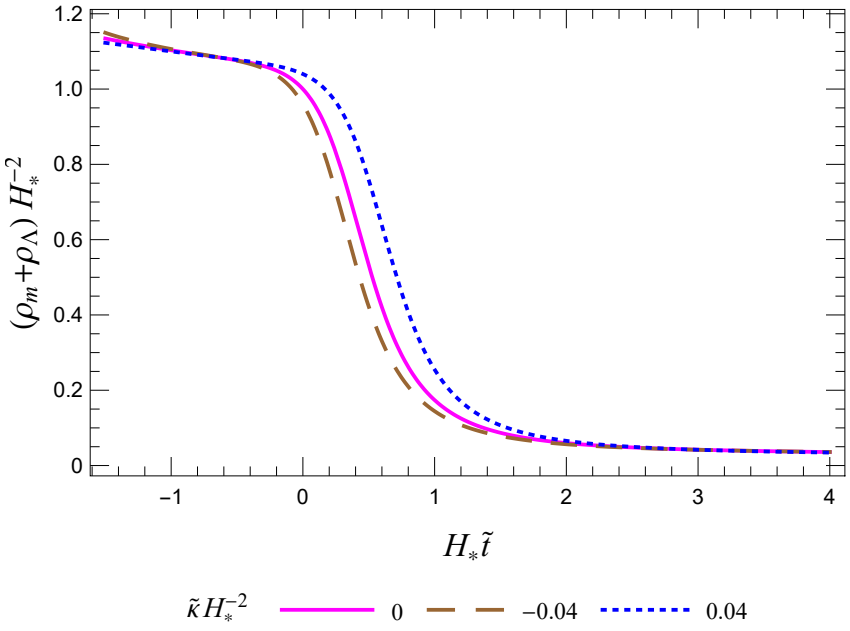

FIGURE 3.19: The variation of total energy density with time for a universe composed of a VdW matter distribution and a dynamical $\Lambda \propto \tilde{a}^{-1/2}$.

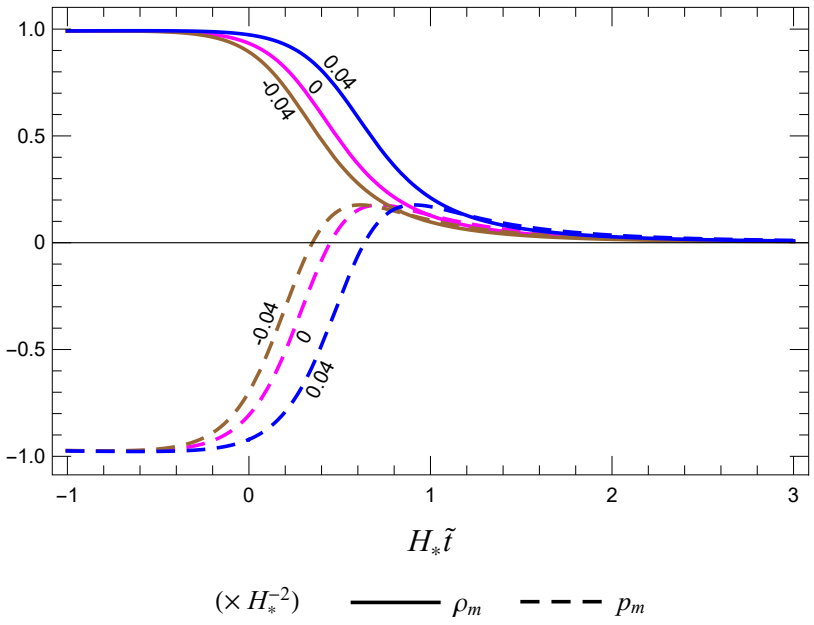

FIGURE 3.20: The temporal variation of the energy density and pressure of matter, in a universe comprising a VdW fluid and a dynamical $\Lambda \propto \tilde{a}^{-1/2}$. The labels denote the respective values of $\tilde{\kappa}$.

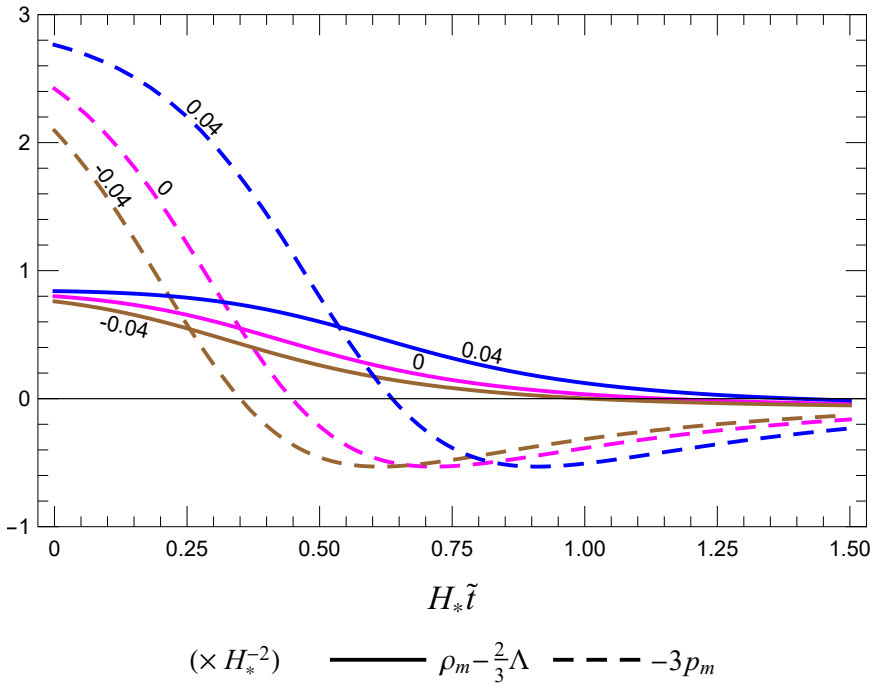

FIGURE 3.21: The evolution of $4\pi G\rho_{\rm m} - \Lambda(\tilde{t})$ and $-4\pi G\,(3p_{\rm m})$ for a universe composed of a VdW fluid and a dynamical $\Lambda \propto \tilde{a}^{-1/2}$. When these two quantities are equal, $\ddot{\tilde{a}}$ evaluates to zero [Eq. (3.27)]. Hence, the point of intersection between curves with the same value of $\tilde{\kappa}$ (as indicated by the label on each curve) denotes the onset of deceleration for the corresponding universe.

Initially, the second term on the right-hand side of Eq. (3.5) dominates the dynamics of the VdW matter distribution, causing it to exert negative pressure. Eq. (3.21) implies that at $\tilde{t} = 0$, $\rho_{\rm m}$ is greatest in the closed universe, for which $\tilde{\kappa} > 0$. Consequently, this is also where the pressure of the VdW fluid is strongest (Fig. 3.20), and hence where the resulting repulsive effect is most significant. In fact, it is the closed universe that experiences the greatest acceleration during inflation.

Eq. (3.22) allows us to deduce that the larger matter density associated with positive curvature at $\tilde{t} = 0$ also means a smaller $|\dot{\rho}_{\rm m}|$. Together, these two factors (larger $\rho_{\rm m}$, smaller $|\dot{\rho}_{\rm m}|$) imply that the first term in Eq. (3.5) takes longer to dominate over the second, and hence more time passes before $p_{\rm m}$ becomes positive. This explains why the transition to the epoch of deceleration happens last for the closed universe (Fig. 3.21). As for the difference in the maximum deceleration each universe undergoes, Fig. 3.22 demonstrates that the main cause is the variation of the scale factor with $\tilde{\kappa}$. Finally, the delay in the onset of late-time acceleration when $\tilde{\kappa} > 0$ may be attributed to the fact that the evolution of $p_{\rm m}$ lags behind that in the open and flat scenarios. The result is that the decay of $p_{\rm m}$ begins at a later time in the closed universe. As may

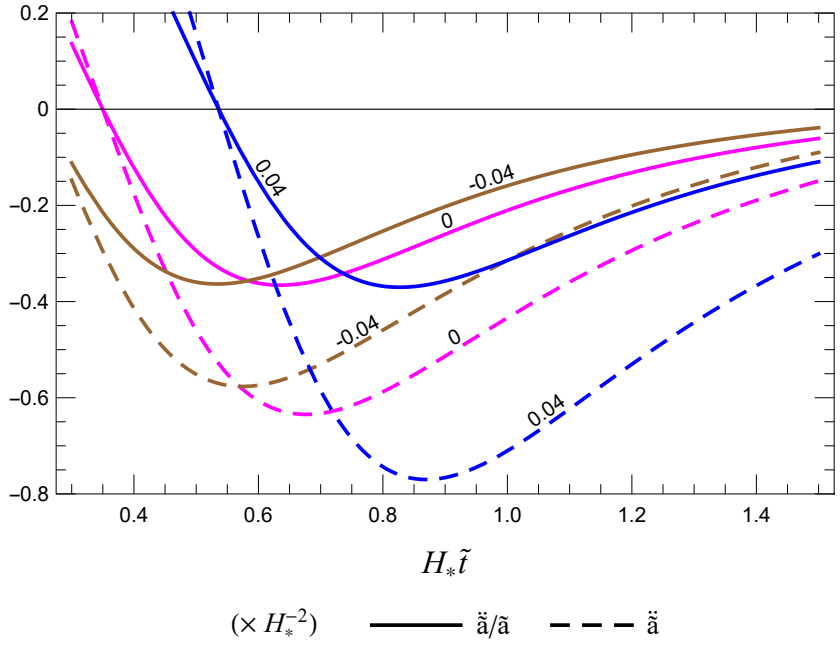

FIGURE 3.22: The temporal variation of $\ddot{\tilde{a}}/\tilde{a}$ and $\ddot{\tilde{a}}$ for a universe comprising a VdW fluid and a dynamical $\Lambda \propto \tilde{a}^{-1/2}$. Curves are labelled with the respective values of $\tilde{\kappa}$.

be concluded from the equation:

$$\ddot{\tilde{a}} = -\frac{\tilde{a}}{3}\left[4\pi G\left(\rho_{\rm m} + 3p_{\rm m}\right) - \Lambda(\tilde{t})\right] \ , \tag{3.27}$$

acceleration sets in when $\Lambda(\tilde{t})$ equates to $4\pi G\left(\rho_{\rm m} + 3p_{\rm m}\right)$. The longer $p_{\rm m}$ takes to start decaying, the longer it is before this equality is realised.

3.3 Modelling Matter with EoS $p_{\rm m} = w_{\rm m}\rho_{\rm m}$

Let us again use t to represent ordinary cosmic time. In this section, we also revert to the usual definitions of a and κ, so that the former is now equal to the ratio of the scale factor $\mathcal{R}$ to its present-day value, $\mathcal{R}_0$, and the spatial curvature $\kappa = k/\mathcal{R}_0^2$ (with $k = 0$ or ± 1). The matter distribution is described by the EoS:

$$p_{\rm m} = w_{\rm m}\rho_{\rm m} \ . \tag{3.28}$$

As before, $p_{\rm m}$ and $\rho_{\rm m}$ stand for the pressure and energy density, respectively. The parameter $w_{\rm m} \in [0, 1]$ acts as a constant of proportionality and characterises the fluid, taking the value $1/3$ for radiation, 1 for a stiff fluid, and zero in the case of dust.

We combine matter with a dark energy component that evolves according to the equation [199]:

$$\Lambda(t) = \Lambda_\infty + 3\left(\frac{H}{H_{\rm I}}\right)^n \left(\frac{\kappa}{a^2} + H^2\right) \ . \tag{3.29}$$

Here, Λ_∞ is the value of $\Lambda(t)$ as $a \to \infty$, $H_{\rm I}$ stands for the Hubble parameter associated with the primordial de Sitter stages,[50] and $n \geq 1$ is an integer. At very early times, $H \sim H_{\rm I}$ and the vacuum dynamics are driven by the second term on the right-hand side of Eq. (3.29). When $H \ll H_{\rm I}$, however, this term becomes negligible, rendering $\Lambda(t)$ approximately equal to Λ_∞. Consequently, the resulting cosmology converges to ΛCDM at late times [199].

The governing equation may be obtained by inserting (3.28) into Eq. (3.24) and using Eq. (3.21) to eliminate $\rho_{\rm m}$. The final result reads:

$$(\kappa + \dot{a}^2)\left\{3(1+w_{\rm m})\left[1 - \left(\frac{\dot{a}}{H_{\rm I}a}\right)^n\right] - 2\right\} - \Lambda_\infty(1+w_{\rm m})a^2 + 2a\ddot{a} = 0 \ , \tag{3.30}$$

where $\Lambda(t)$ has been expressed according to Eq. (3.29). With a few modifications, Eq. (3.30) is seen to be equivalent to Eq. (22) in Ref. [199].[51] The authors of [199] point out that $\Lambda(t)$ attains its final value (Λ_∞) at the start of the adiabatic radiation phase, and so Λ_∞ shall be identified with Λ_0, the cosmological constant.

We consider the inflationary epoch first and redefine the time coordinate as $\hat{t} = H_{\rm I}t - 1$. With this definition, the Hubble parameter is automatically rescaled to $\hat{H} = H/H_{\rm I}$, so that when $H = H_{\rm I}$, $\hat{H} = 1$ and, assuming the relation $t \sim 1/H$, one gets that $\hat{t} \approx 0$. The reference time $\hat{t} = 0$ is thus specified as the point at which the Hubble parameter $\hat{H}$ is (approximately) equal to unity, in line with the procedure adopted in the previous section. Additionally, the rescaled time coordinate implies that Eq. (3.30) can be rewritten in the form:

$$\left[\hat{\kappa} + a'(\hat{t})^2\right]\left\{3(1+w_{\rm m})\left[1 - \left(\frac{a'(\hat{t})}{a}\right)^n\right] - 2\right\} - 3(1+w_{\rm m})\hat{H}_0^2\Omega_\Lambda^0 a^2 + 2aa''(\hat{t}) = 0, \tag{3.31}$$

where $\hat{\kappa} = \kappa/H_{\rm I}^2$, $a'(\hat{t}) = \dot{a}/H_{\rm I}$, $a''(\hat{t}) = \ddot{a}/H_{\rm I}^2$ and $\hat{H}_0 = H_0/H_{\rm I}$ (H_0 being the

[50] $H_{\rm I}$ can be treated as an arbitrary parameter and its value inferred from CMB constraints [199]. Here we assume that deflation begins at around the time of grand unification, which means that $H_{\rm I} \sim 10^{35}$ s [200].

[51] Care should be taken when comparing the two equations. In (3.30), a represents the normalised scale factor (rather than the *non-normalised* version, as in Ref. [199]), while κ stands for the ratio $k/\mathcal{R}_0^2$. The authors of Ref. [199] use κ to represent the *normalised* curvature parameter (which is denoted by k here).

current value of H). The relation $\Lambda_0 = 3H_0^2\Omega_\Lambda^0$ has been used to express Λ_0 in terms of the corresponding density parameter.

Eq. (3.31) is solved subject to the initial conditions $a(0) = 1.03\,\hat{H}_0$ and $a'(\hat{t} = 0) = \hat{H}_0$. The slight difference between the values of $a(0)$ and $a'(\hat{t} = 0)$ – while being small enough to ensure that $\hat{H}(0)$ is still sufficiently close to unity – improves the performance of the numerical simulator, because it ensures that the first term enclosed in curly brackets in Eq. (3.31) does not drop out of the equation at $\hat{t} = 0$.

The matter distribution for our model shall be assumed to consist of dust. In cosmology, *dust* is understood to be a pressureless perfect fluid [18] – in other words, a fluid made up of non-relativistic, non-interacting particles [8]. The cold dark matter that is thought to dominate the matter sector falls into this category, and so we shall model the matter component in the same fashion. This is achieved by assigning $w_{\rm m}$ a null value. Next, we set $|\hat{\kappa}|$ to $0.08\,\hat{H}_0^2$ (or 0) and fix n at 2, the latter being in accordance with the proposal that n should be even in flat space, as indicated by the covariance of the effective action of Quantum Field Theory in curved spacetimes [201, 202]. The parameter $\hat{H}_0$ is estimated at[52] 10^{-}[53]. Finally, we put Ω_Λ^0 equal to 0.692, the value reported by the *Planck* collaboration in Ref. [22]. Although the *Planck* constraints are obtained in the context of a ΛCDM cosmology, this poses no serious issue, since our model converges to ΛCDM at late times.

Figs. 3.23 and 3.24 show the evolution of $a''(\hat{t})$ and $\hat{H}$ during the inflationary epoch and the first stages of cosmic deceleration. At early times, the behaviour of $\Lambda(\hat{t})$ is determined by the second term on the right-hand side of Eq. (3.29) – and in turn, $\Lambda(\hat{t})$ controls the cosmic evolution, as evidenced by Fig. 3.25. Since the term in question is a function of $\hat{\kappa}$, the dynamics of the early Universe depend significantly on the spatial geometry. It can be seen that the effects of curvature match those observed for all the other models. But how does the cosmic history compare to ΛCDM?

According to the flat ΛCDM cosmology, the expansion of the Universe is governed by the equation:

$$2aa''(\hat{t}) + a'(\hat{t})^2 + \hat{H}_0^2(\Omega_{\rm r}^0 a^{-2} - 3\Omega_\Lambda^0 a^2) = 0\ , \tag{3.32}$$

where $\Omega_{\rm r}^0$ is the present-day value of the radiation density parameter, equivalent to[53]

[52] To a good approximation, this would mean that the beginning of the deflationary epoch coincides with grand unification. More information is available in Ref. [200]. One should note, however, that due to updated constraints on H_0 [22], the above value for $\hat{H}_0$ differs slightly from the one in [200], but is nonetheless compatible with typical estimates for the Hubble parameter at the end of inflation [203].

[53] This can be calculated from the current value of the matter density parameter ($\Omega_{\rm m}^0 = 0.308$ [22]) and the redshift at which matter and radiation were equally dense, $z_{\rm eq} = 3365$ [22].

9.15×10^{-5}. Its smallness implies that we may safely leave out the term in $\Omega_{\rm r}^0$ at late times. The initial conditions and parameter values used are as for the dynamical vacuum case.

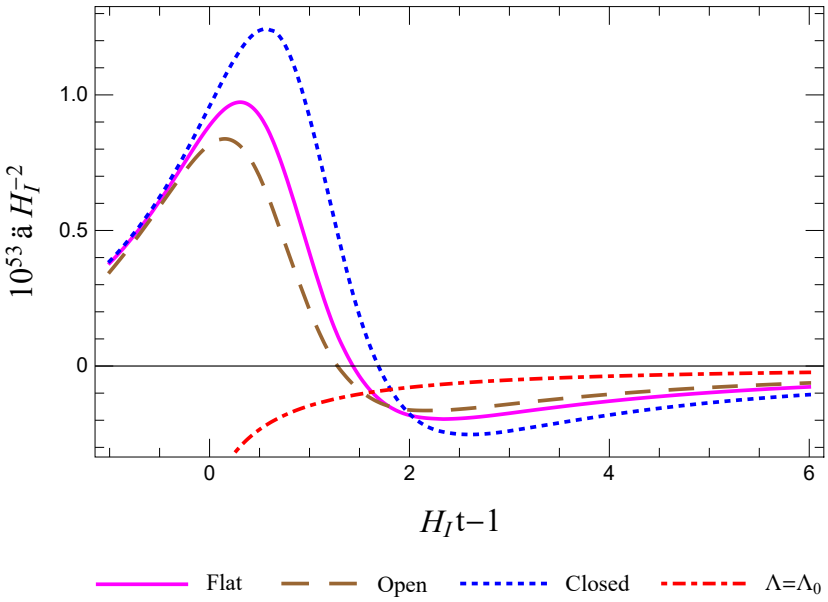

FIGURE 3.23: The evolution of the acceleration at early times. The Universe is assumed to consist of dust and a dynamical Λ that is given by Eq. (3.29). The acceleration of a *flat* universe containing dust and a cosmological constant is represented by the red dot-dashed curve. In this case, there is no mechanism that can give rise to an inflationary epoch.

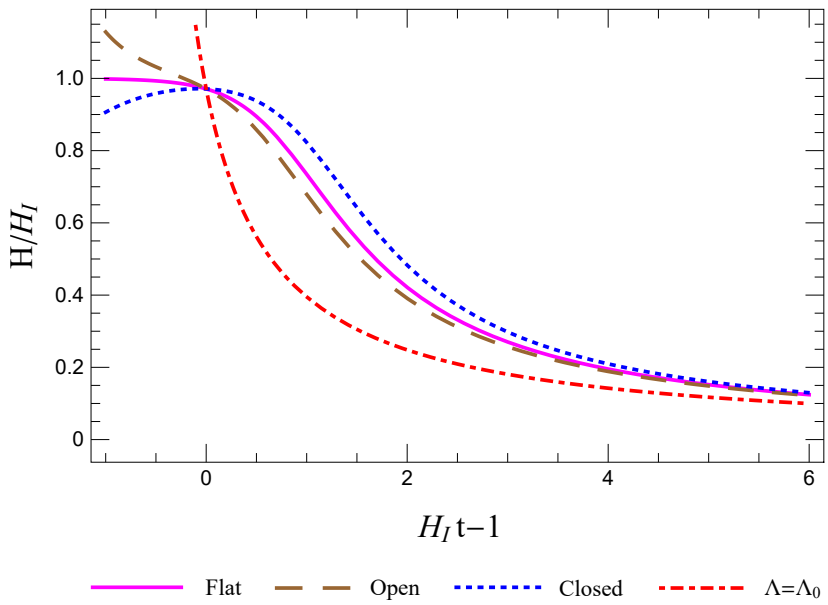

FIGURE 3.24: The evolution of the Hubble parameter at early times. The Universe is assumed to consist of dust and a dynamical Λ that is given by Eq. (3.29). The Hubble parameter for a *flat* universe containing dust and a cosmological constant is represented by the red dot-dashed curve.

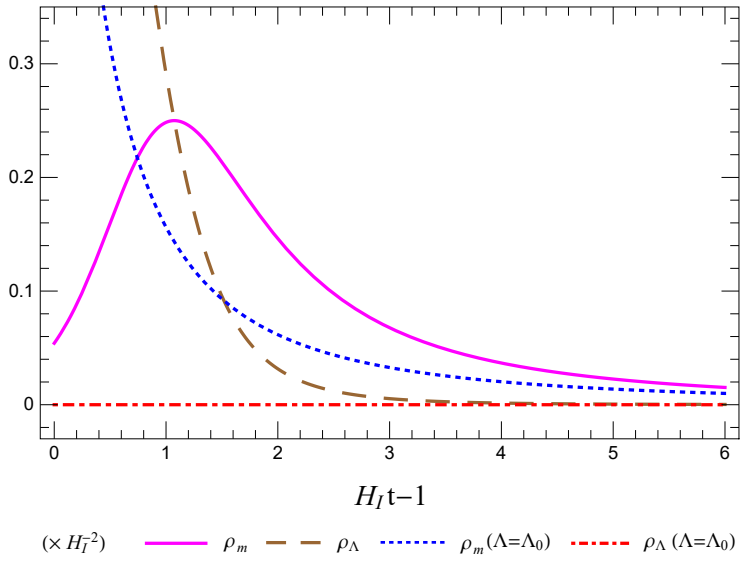

FIGURE 3.25: The evolution of $\rho_{\rm m}$ and ρ_Λ at early times. The Universe is assumed to consist of dust and a dynamical Λ that is given by Eq. (3.29). Only the case of spatial flatness is considered. The blue dotted curve depicts the evolution of $\rho_{\rm m}$ in the presence of a cosmological constant, whose associated energy density is represented by the red dot-dashed curve.

In the ΛCDM cosmology, the Universe is modelled as a mixture of dust, radiation, and a dark energy component that takes the form of a cosmological constant Λ. The dust distribution consists of both baryonic and dark matter and its density varies as a^{-3}. Meanwhile, radiation density is proportional to a^{-4}, meaning that radiation gets diluted faster as the Universe expands. On the other hand, the density of dark energy is not affected by cosmic dynamics and remains constant throughout the entire evolution. Cosmological observations put the present-day values of the matter and dark energy density parameters $\left(\Omega_{\rm m}^0 \text{ and } \Omega_\Lambda^0\right)$ at around 0.3 and 0.7 [20], respectively, which implies that the current epoch is dominated by dark energy. In contrast, as we have just seen, $\Omega_{\rm r}^0$ is negligibly small. However, radiation would have been very significant at early times, and indeed it is thought that the matter-dominated epoch was preceded by a period of time during which radiation was the dominant component of the cosmic fluid. Nonetheless, our model is compared with a ΛCDM cosmology consisting solely of dust and the cosmological constant. We are thus better able to investigate the effects of a dynamical Λ, this being the only difference between the two models. Strictly speaking, therefore, our results are compared with the ones predicted by a constant-Λ model rather than by ΛCDM – a distinction that is especially pronounced at early times.

Fig. 3.23 shows that the maximum deceleration attained during the matter-

dominated epoch is smaller for the constant-Λ model. We may attribute this to the fact that when Λ is allowed to evolve according to Eq. (3.29), the vacuum transfers energy to the matter component as it decays [refer to Eq. (3.22) and Fig. 3.25], causing the energy density of the latter to grow. Consequently, the deceleration resulting from the attractive pressure of matter is larger than in the constant-Λ scenario, where such a mechanism is absent.[54]

As pointed out in Ref. [199] and shown in Fig. 3.24, only a flat universe would initially have a constant Hubble parameter. The effect of positive curvature would be to decrease the initial $\hat{H}$ below that in the flat case, while for negative $\hat{\kappa}$ the plot of $H/H_{\rm I}$ $(= \hat{H})$ against $\hat{t}$ should be truncated at $H/H_{\rm I} = 1$ to prevent the weak energy condition from being violated. We note that these characteristics are consistent with the properties of the primordial de Sitter solutions as outlined in Ref. [199].

It is now time to turn our attention to the evolution of the Universe at late times. For this purpose, the time parameter is redefined as $\bar{t} = H_0 t - 1$, so that if one assumes the relation $t \sim 1/H$, the current time corresponds to $\bar{t} = 0$. The Hubble parameter is automatically rescaled to $\bar{H} = H/H_0$ and becomes equal to unity at present. Using this notation, Eq. (3.30) can be rewritten as:

$$\left[\bar{\kappa} + a'(\bar{t})^2\right]\left\{3(1+w_{\rm m})\left[1 - \left(\frac{a'(\bar{t})}{a}\hat{H}_0\right)^n\right] - 2\right\} - 3(1+w_{\rm m})\Omega_\Lambda^0 a^2 + 2aa''(\bar{t}) = 0, \tag{3.33}$$

while Eq. (3.32) takes the form:

$$2aa''(\bar{t}) + a'(\bar{t})^2 + \Omega_{\rm r}^0 a^{-2} - 3\Omega_\Lambda^0 a^2 = 0\ , \tag{3.34}$$

where $\bar{\kappa} = \kappa/H_0^2$, $a'(\bar{t}) = \dot{a}/H_0$ and $a''(\bar{t}) = \ddot{a}/H_0^2$. The initial conditions are set to $a(0) = a'(\bar{t} = 0) = 1$. The first is required by the definition of the normalised scale factor, and the second follows from the fact that $\bar{H}(0) = 1$. The parameters $\bar{\kappa}$, n and $w_{\rm m}$ are assigned the same values as for the early evolution. Since $\bar{\kappa} = \hat{H}_0^{-2}\hat{\kappa}$, however, $|\bar{\kappa}|$ is equal to 0.08 (or 0 if the Universe is flat).

The resulting curves of acceleration vs time are depicted in Fig. 3.26. As expected, the open universe would be the first to exit the matter-dominated epoch, and the evolution according to the constant-Λ cosmology (which is essentially equivalent to

[54] It could be argued that the dot-dashed curve in Fig. 3.23 is directed downwards for decreasing t, so at face value a constant Λ appears to allow for a greater deceleration than its dynamical counterpart. However, it is important to remember that this behaviour is due to the failure of the constant-Λ model to account for the inflationary epoch.

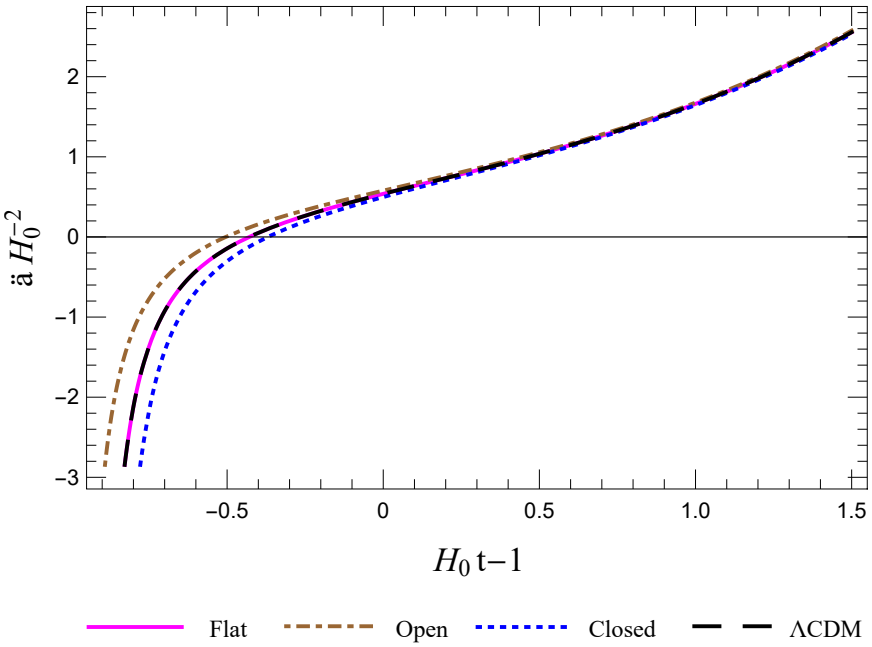

FIGURE 3.26: The variation of acceleration with time during the current period of cosmic acceleration and the latter part of the preceding matter-dominated epoch. The Universe is modelled as a composition of dust and a dynamical Λ that evolves according to Eq. (3.29). At this stage, the dynamics of the flat universe are indistinguishable from those predicted by flat ΛCDM.

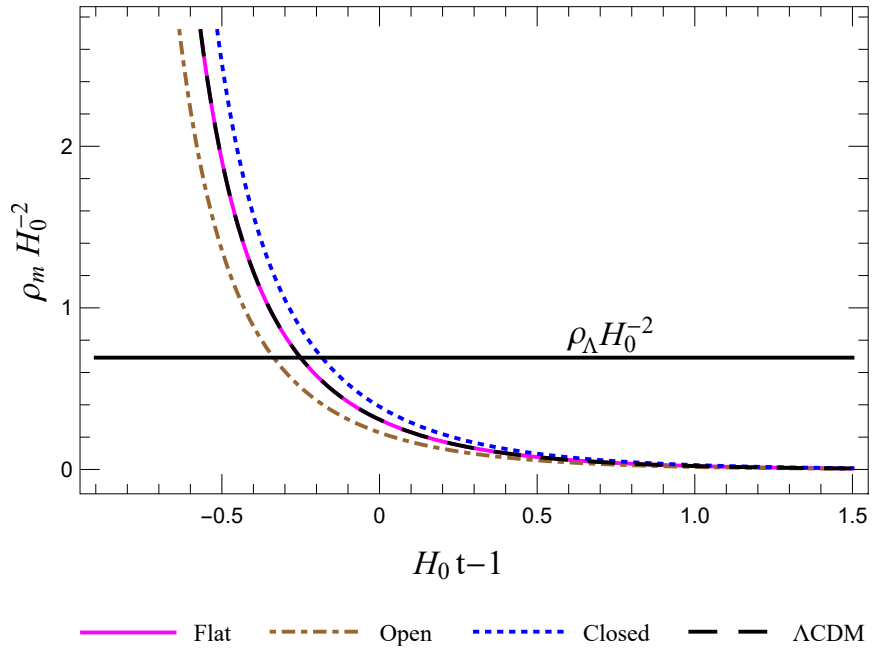

FIGURE 3.27: The variation of $\rho_{\rm m}$ with time during the transition from the matter-dominated epoch to the current period of cosmic acceleration. The dashed black curve indicates how $\rho_{\rm m}$ would evolve in a flat ΛCDM cosmology, while the straight horizontal line corresponds to the energy density associated with the cosmological constant.

flat ΛCDM at this stage) becomes indistinguishable from that of the flat, dynamical-Λ scenario at late times. Additionally, the presence of curvature no longer affects the evolution significantly after the transition to the current epoch of acceleration (Fig. 3.27).

3.4 In Brief...

This chapter investigates whether the presence of spatial curvature could influence the evolution of the Universe – and if so, in what way. We have seen that for a closed universe, the transition to the epoch of decelerated expansion would be delayed with respect to the flat case. So would the start of the current dark energy-dominated era; additionally, inflationary acceleration and the subsequent deceleration would both be larger. The opposite was noted for an open universe. The fact that these features are common to the different scenarios we consider has an important implication: it suggests that the effects of curvature are independent of the way we model matter and dark energy.

This work shows that it is possible to reproduce the main characteristics of the expansion history using only a few simple fluids. In the first model, the matter/energy content of the Universe is represented by a VdW fluid. It is found that the current period of acceleration requires the presence of a dark energy component, and thus in the remaining four models dark energy is introduced as Quintessence, a Chaplygin gas or a dynamical cosmological 'constant'; the desired late-time acceleration is indeed obtained. The VdW EoS is retained in the first four models but changed to the customary $p_{\rm m} = w_{\rm m}\rho_{\rm m}$ for the last one. Another unique feature of the last model is a time-dependent vacuum energy (density) that functions as an inflaton at early times, and mimics a cosmological constant during the present epoch [199].

In conclusion, a non-zero Ω_k^0 would have left definite signatures on the past dynamics of the Universe. Although these might in reality be too small to be probed by current cosmological experiments, the study presented here highlights the possibility that spatial curvature could have played a role in the early universe, and not – as is often asserted – just at late times. It turns out, in fact, that the evolution is only mildly dependent on curvature at low redshifts.

CHAPTER 4

Endowing Λ with a Dynamic Nature: Constraints in a Spatially Curved Universe

4.1 Introduction

Despite the many dark energy models that have been proposed, the available evidence is not sufficient for ΛCDM to be discarded in favour of one of the alternatives [204,205]. And for good reason: theoretically, its framework is appealingly simple, and when it comes to observations, ΛCDM is compatible with local gravity constraints [206, 207] and has successfully predicted the baryon acoustic oscillation (BAO) imprint on galaxy clustering [208]. It also provides a good description of the cosmology at redshifts probed by cosmic microwave background (CMB) data [19, 20, 22]. This list is by no means complete, but it serves to illustrate why ΛCDM is considered the standard model of cosmology. On the other hand, it has a number of shortcomings that cannot be overlooked, prominent among which are the cosmic coincidence and smallness problems [209].

A sound alternative model of dark energy, therefore, is expected to emulate the successes of ΛCDM while overcoming its drawbacks (or some of them, at least). Consequently, such models should mimic ΛCDM at the high redshifts where it is well-tested by CMB data, and give a comparable expansion history at low redshifts, albeit without invoking a true cosmological constant [210]. Furthermore, on Solar-System scales their behaviour must be in accordance with experimentally-supported General Relativistic predictions [140]. One way of achieving this is by means of screening mechanisms, which depend on the density contrast between the local environment and the cosmic fluid to suppress small-scale deviations from the standard model (see, for instance, Ref. [211] and works cited therein).

In view of the above, and keeping in mind that the successes of ΛCDM have not been

eclipsed, the simplest – and perhaps most natural – extension of the standard model is a scenario characterised by a mildly-evolving cosmological 'constant'. We shall therefore consider three dynamical-Λ models: the Running Vacuum Model (RVM), in which Λ varies with the Hubble parameter H according to the relation $\Lambda(H) = A + BH^2$ (A and B being constants), a generalisation of the RVM (GRVM) with $\Lambda(H) = A + BH^2 + C(\mathrm{d}H/\mathrm{d}t)$, where t is cosmic time and C another constant, and a second sub-case of the GRVM: $\Lambda(H) = A + C(\mathrm{d}H/\mathrm{d}t)$. We shall refer to the last as the 'Generalised Running Vacuum Sub-case', or GRVS. The GRVM and RVM were introduced in Refs. [212] and [213], respectively, and have been analysed in works such as Refs. [212, 214–217] and [218], while the GRVS was investigated in Ref. [219] as a model with a variable dark energy equation-of-state parameter.

These models are especially appealing due to the fact that they are motivated by Quantum Field Theory (QFT) considerations [220–223]. Additionally, the RVM can properly account for cosmic dynamics at both the linear perturbation and background levels [218] – and in certain cases has been shown to outperform ΛCDM [215,224–226]. Likewise, the GRVM is compatible with observations [212, 214, 219], and it, too, has been reported to receive greater support from cosmological data than ΛCDM [226]. A prominent advantage of both the RVM and GRVM is their ability to ease the σ_8 tension that emerges in the standard model [215, 224, 226].

Although they feature in numerous studies, the GRVM, RVM and GRVS [with $\Lambda(H)$ taking the exact forms specified above] have not been analysed in the context of a spatially curved space-time (but extended versions have, as discussed in section 4.4). Indeed, a great number of works in the literature are based on the premise of spatial flatness. This practice is rather concerning, because although it is true that observational data appears to favour a flat geometry, the evidence comes mainly from studies which assume a flat ΛCDM cosmology [19, 20, 106, 107]. Our primary aim, therefore, will be to investigate whether the GRVM, RVM and GRVS can accommodate spatial curvature while remaining compatible with the data available.

4.2 Dynamical-Λ Models

The literature contains many examples of models in which dynamical dark energy takes the form of a varying Λ. In most cases, Λ is allowed to have a large value at early times, and this then decays to the much smaller one observed at present. Therefore,

such models go some way in addressing the smallness problem [201, 227, 228], which refers to the fact that in ΛCDM, the observed value of ρ_Λ (where ρ_Λ is the vacuum energy density) happens to be around a factor of 10^{120} smaller than the theoretical estimate [209].

Endowing Λ with a dynamic nature may be achieved in two ways. One can either model Λ as an explicit function of time, or else take an implicit approach and express it in terms of appropriate cosmic parameters. In the former case, the most popular choice is undoubtedly the inverse power relation given by[55] $\Lambda(t) \propto t^{-n}$. The inverse power-law model features in works such as Refs. [229–233] – the list is by no means exhaustive – and has additionally been investigated in differing scenarios, including a Bianchi Type-I cosmology with variable gravitational coupling [234] and the Brans-Dicke theory [235,236]. Albeit less popular, exponential decay has also been proposed [228, 237].

In the category of implicit time dependence, one finds studies in which Λ is a function of the scale factor a, with expressions such as $\Lambda(a) = Aa^n + Ba^m$ [238–241] and $\Lambda(a) = A + Ba^{-n}, A \neq 0$ [242]. Models having $\Lambda(a) \propto a^{-n}$ are very popular – the reader is referred to Refs. [243–247] – and under certain conditions may be seen as equivalent to standard cosmology with matter, radiation and an additional component: an exotic fluid characterised by an equation of state parameter $w = n/3 - 1$ [248]. The case $n = 2$ is of particular interest. It may not only have its foundations in quantum cosmology [249], but has also been shown – in the framework of a closed geometry – to result from the assumption that the matter/radiation density of the Universe is equal to the critical density at all times, not just at present [250]. This assumption would ensure that the current epoch is not special in any way.

Another notable study is Ref. [251]. Here, the authors present a model in which the vacuum couples with radiation (during the radiation-dominated epoch), and has an associated energy density that scales as $a^{-4(1-x)}$, where x depends on the balance between the energy densities of radiation and dark energy. Meanwhile, the innovative approach detailed in Ref. [252] is based on the ansatz that the energy density of cold dark matter (CDM) varies as a^{-3+y}, rather than the customary a^{-3}. The small positive constant y results from the interaction with dark energy and quantifies the decrease in the rate at which CDM gets diluted. It is interesting to note that provided $\Omega_{\mathrm{m}}^0 \geq 0.2$ and $n \geq 1.6$, spatially flat cosmologies having $\Lambda(a) \propto a^{-n}$ show consistency with lensing data [248].

[55] The parameters n, m, A and B shall henceforth represent constants.

A third popular class of expressions for Λ is based on the Hubble parameter H and functions thereof. Prominent among these is again the power law: $\Lambda(H) \propto H^n$ [241, 243, 253–256]. Other interesting possibilities include combinations of H or H^n with either a^m [240, 244] or $\mathrm{d}H/\mathrm{d}t$, or even the total energy density [253]. A case in point is the entropic acceleration model [257]. This model is characterised by an entropic force which acts at the apparent horizon of the Universe,[56] and which behaves essentially like a dark energy component whose density varies as $A(\mathrm{d}H/\mathrm{d}t) + BH^2$ ($B \neq 0$) in flat space. According to the authors of Ref. [258], however, the entropic model is problematic in that the sign of its deceleration parameter never changes. Additionally, the possibility that it describes the late-time behaviour of a more complete model is ruled out by its failure to reconcile recent cosmic growth data with an accelerated expansion [258]. An alternative entropic model in which $\Lambda(H) = AH + BH^2$ also has this shortcoming, while putting $\Lambda(H) \propto H$ results in a scenario that is disqualified by CMB data [258]. It has in fact been proposed that when $\Lambda(H)$ is a simple function of terms from the set $\{H, \mathrm{d}H/\mathrm{d}t, H^2\}$, the addition of a constant to the said function is crucial to get a valid model [258].

4.3 Analytical Solutions with a Dynamical Λ

4.3.1 The equations in an FLRW cosmology

Let us go back to Eq. (3.24). It is reproduced below for ease of reference:

$$8\pi G a^2(p_\mathrm{m} + \rho_\mathrm{m}) - 2(\kappa + \dot{a}^2) + 2a\ddot{a} = 0 \ . \tag{4.1}$$

In this chapter, a and κ take their usual definitions ($a = \mathcal{R}/\mathcal{R}_0, \kappa = k/\mathcal{R}_0^2$), and an overdot denotes differentiation with respect to t.

The energy density (ρ_m) of the matter distribution may be expressed in terms of a and $\dot{a}$ via the first Friedmann equation [Chapter 1, Eq. (1.38)]. Using the customary barotropic equation of state, $p_\mathrm{m} = w_\mathrm{m}\rho_\mathrm{m}$, to write the pressure p_m as a function of ρ_m (and hence of a and $\dot{a}$), we get that

$$2\ddot{a}a - (1 + w_\mathrm{m})a^2\Lambda(t) + (1 + 3w_\mathrm{m})(\kappa + \dot{a}^2) = 0 \ . \tag{4.2}$$

[56] The apparent horizon is determined by the quantity $\left(H^2 + k/a^2\right)^{-1/2}$, where k is the spatial curvature parameter and a the scale factor, both in normalised form [257]. In the absence of spatial curvature, the apparent and Hubble horizons are equivalent.

Any solutions to the above equation should meet the following conditions:

- $\ddot{a} > 0$, implying an accelerated cosmic expansion (since the focus is on late times);
- $a > 0$ and $\dot{a} > 0$ – the scale factor is positive and increases with time;
- $H > 0$ and decreases with time;
- $\rho_{\rm m} \geq 0$ at all times, in line with the stipulations of the weak energy condition (the requirement that $\rho_{\rm m} + p_{\rm m} \geq 0$ is then satisfied automatically);
- $\Lambda(t) > 0$ and decreases with time.[57] The latter is a necessary prerequisite if the smallness problem of the cosmological constant is to be alleviated.

The analytical models constructed on the basis of these criteria are presented below. The work was carried out using WOLFRAM MATHEMATICA® 12.0.

4.3.2 The models

Model 1

Let us start from a candidate function for $\Lambda(t)$ that depends on the Hubble parameter and has three constants (D, E and m):

$$\Lambda(H) = D + EH^m = D + E\left(\frac{\dot{a}}{a}\right)^m \ . \tag{4.3}$$

Upon inserting it into Eq. (4.2), we get that:

$$2\ddot{a}a - (1 + w_{\rm m})a^2(D + E\dot{a}^m a^{-m}) + (1 + 3w_{\rm m})(\kappa + \dot{a}^2) = 0 \ , \tag{4.4}$$

but this cannot be solved analytically. However, there is always the possibility that a less generalised version can. Indeed, it is found that setting

$$m = 2 \quad \text{and} \quad E = \frac{2 + 3w_{\rm m}}{1 + w_{\rm m}} \tag{4.5}$$

[57] The notation $\Lambda(t)$ is meant to stress the dynamical nature of Λ. It should not be taken to indicate an explicit dependence on t.

reduces Eq. (4.4) to

$$2\ddot{a}a - D(1+w_{\rm m})a^2 - \dot{a}^2 + \kappa(1+3w_{\rm m}) = 0 \ , \tag{4.6}$$

which admits two solutions. We shall pick the one whose dependence on κ is not exponentially suppressed:

$$a(t) = \frac{{\rm e}^{-\sqrt{\epsilon}(t+c_2)}}{4H_0^2\epsilon}\left[H_0^4\left(-1+c_1{\rm e}^{\sqrt{\epsilon}(t+c_2)}\right)^2 - 4D{\rm e}^{2\sqrt{\epsilon}(t+c_2)}\left(1+4w_{\rm m}+3w_{\rm m}^2\right)\kappa\right] \ . \tag{4.7}$$

Here, the parameter ϵ stands for the quantity $D(1+w_{\rm m})$ and each c_i $(i=\{1,2\})$ is a constant of integration.

An easy way in which to construct graphical representations of the evolution is by taking the approach outlined in subsection 2.3.2. This is based on the introduction of a dimensionless time coordinate $\bar{t}$ that is defined as a scaled version of t : $\bar{t} = H_0 t$. We again set $\bar{t}_0$ to 0.95, and fix the value of D by requiring that $\Lambda(H)$ is currently equal to the cosmological constant ($D = 0.1H_0^2$). Additionally, given that this is a late-time solution, the matter component is best modelled as dust, with $w_{\rm m} = 0$. The

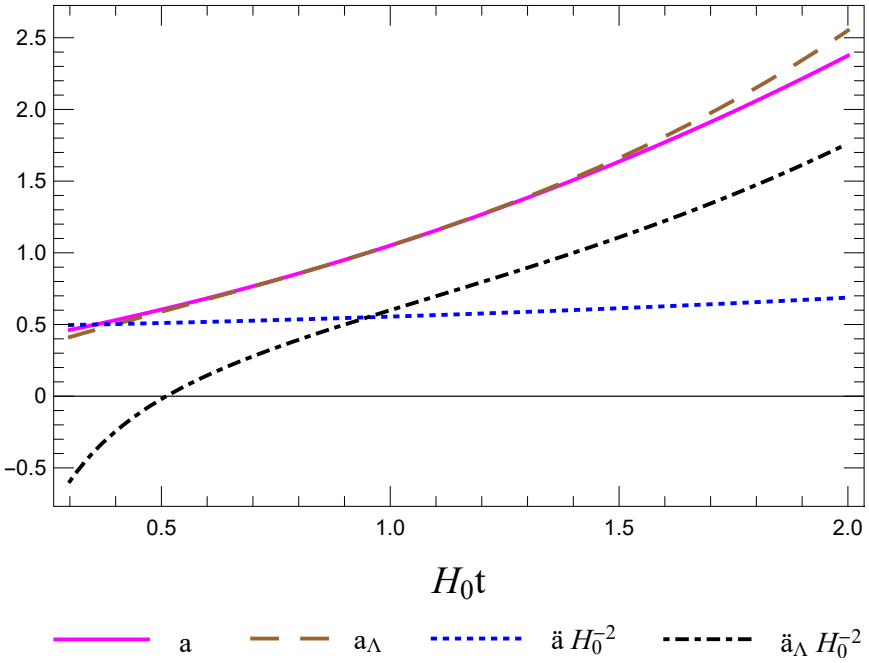

FIGURE 4.1: The variation of the scale factor and acceleration with time. The Universe is assumed to have flat spatial sections, a dust-like matter distribution, and a dynamical Λ given by $D+EH^2$, where D and E are constants. The evolution in a flat ΛCDM cosmology with $\Omega_{\rm m}^0 = 0.3$ and $\Omega_\Lambda^0 = 0.7$ [20] is shown for comparison (the associated quantities are indicated by a subscript Λ).

constants of integration are treated as functions of spatial curvature. Once κ has been assigned a value, c_1 and c_2 may be determined by applying the boundary conditions derived in Chapter 2: $a(\bar{t}_0) = a'(\bar{t}_0) = 1$.

The resulting dynamics are compared to the standard model predictions in Figs. 4.1, 4.2 and 4.3. It may be noted that the acceleration of the Universe according to ΛCDM is significantly steeper. Furthermore, our model is only valid at late times and cannot account for the matter-dominated deceleration that preceded the current epoch. This feature also emerges in Fig. 4.2. Here, we observe that while the matter density in a ΛCDM cosmology increases appreciably as we go back in time, finally exceeding the energy density of the vacuum, the same cannot be said for the dynamical-Λ model. Nor should such behaviour be expected: these analytical solutions were constructed as potential models of the Universe for the period of dark energy-dominated expansion.

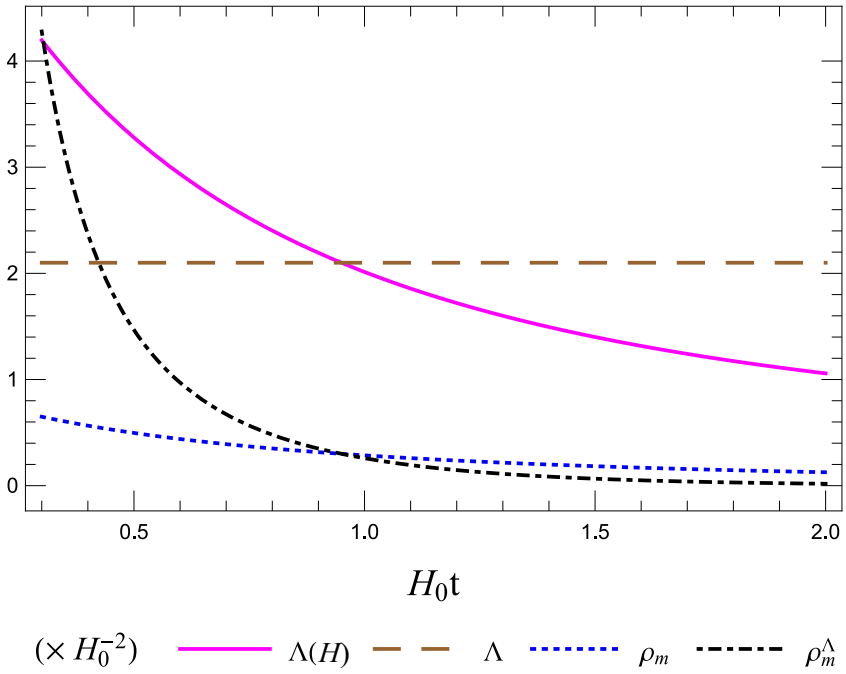

FIGURE 4.2: The variation of $\Lambda(H)$ and $\rho_{\rm m}$ with time. The evolution of the matter density in a flat ΛCDM cosmology ($\rho_{\rm m}^{\Lambda}$) is shown for comparison, while the horizontal dashed line represents the cosmological constant.

The decaying nature of $\Lambda(H)$ shows up clearly in Fig. 4.2. It gives $\Lambda(H)$ the ability to interpolate between a large value at early times and a small one at present, meaning that the model may naturally evade the smallness problem associated with the cosmological constant. Meanwhile, Fig. 4.3 deals with the effect of spatial curvature on the acceleration of the Universe. We note that negative curvature appears to enhance the acceleration at late times.

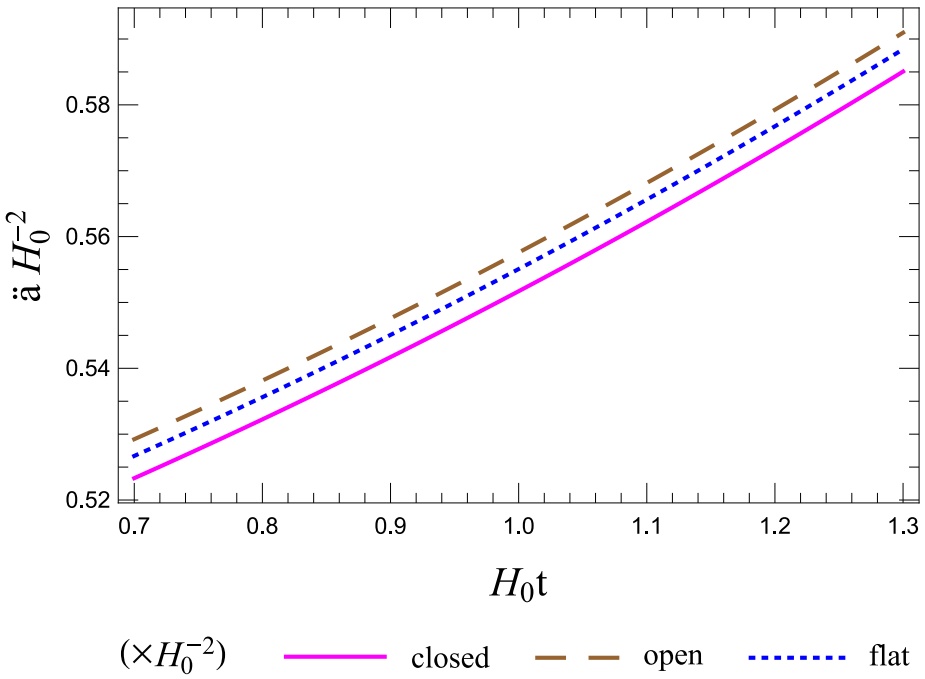

FIGURE 4.3: The variation of acceleration with time in a universe filled with dust-like matter and dark energy. The latter takes the form of a dynamical Λ given by $D + EH^2$. The spatially non-flat models have $|\kappa| = 0.0067H_0^2$, and the parameters c_1 and c_2 are curvature dependent: $c_1 = 0.9$, $c_2 = 1.454/H_0$ ($\kappa = 0$), $c_1 = 0.893$, $c_2 = 1.5/H_0$ ($\kappa > 0$), $c_1 = 0.905$, $c_2 = 1.418/H_0$ ($\kappa < 0$).

Model 2

This time, we model $\Lambda(t)$ as a function of a and H having four constants (I, J, n and m):

$$\Lambda(a, H) = IH^n + Ja^m = I\left(\frac{\dot{a}}{a}\right)^n + Ja^m \ . \tag{4.8}$$

For our choice of $\Lambda(t)$, Eq. (4.2) reads:

$$2\ddot{a}a - (1 + w_\mathrm{m})a^{2-n}\left(Ja^{m+n} + I\dot{a}^n\right) + (1 + 3w_\mathrm{m})\left(\kappa + \dot{a}^2\right) = 0 \ , \tag{4.9}$$

which needs to be simplified if we hope to find an analytical solution. The most intuitive option is to put n equal to 2 and m to -2, whence Eq. (4.9) becomes

$$2\ddot{a}a - (1 + w_\mathrm{m})\left(J + I\dot{a}^2\right) + (1 + 3w_\mathrm{m})\left(\kappa + \dot{a}^2\right) = 0 \ . \tag{4.10}$$

Setting I to $(3w_\mathrm{m} - 1)/(1 + w_\mathrm{m})$ further reduces this to

$$2\ddot{a}a + 2\dot{a}^2 + \kappa(1 + 3w_\mathrm{m}) - J(1 + w_\mathrm{m}) = 0 \ . \tag{4.11}$$

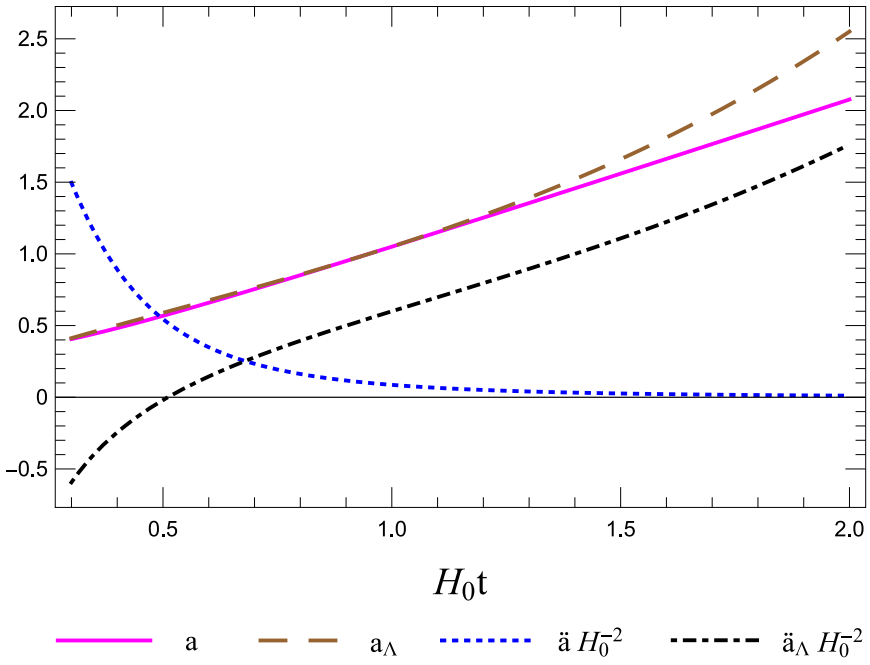

FIGURE 4.4: The variation of the scale factor and acceleration with time. The Universe is assumed to have flat spatial sections, a matter distribution with $w_{\rm m} = 1$, and a dynamical Λ given by $IH^2 + Ja^{-2}$, where I is a function of $w_{\rm m}$ and J represents an arbitrary constant, here set to $1.1H_0^2$. The evolution in a flat ΛCDM cosmology having $\Omega_{\rm m}^0 = 0.3$ and $\Omega_\Lambda^0 = 0.7$ [20] is shown for comparison (the associated quantities are indicated by a subscript Λ).

It is now fairly straightforward to solve for a. We find that the scale factor varies with t according to the relation[58]

$$a(t) = \sqrt{\frac{c_2 + \gamma^2 t^2 + \gamma^2 c_1 (2t + c_1)}{\gamma}} \ . \tag{4.12}$$

Here, c_1 and c_2 are constants of integration, and the dependence on κ is via the parameter γ:

$$\gamma = \frac{1}{2}\left[J(1 + w_{\rm m}) - \kappa(1 + 3w_{\rm m})\right] \ .$$

The main features of the resulting cosmic dynamics are shown in Figs. 4.4, 4.5 and 4.6. It can be seen (Fig. 4.4) that the acceleration asymptotes to zero, in stark contrast to what happens in ΛCDM. On the other hand, Fig. 4.5 demonstrates that the evolution of the matter densities is very similar at late times. This despite the fact that the matter distribution is modelled as a stiff fluid (with $w_{\rm m} = 1$) in the presence of a dynamical Λ (putting $w_{\rm m} = 0$ makes it difficult to meet the requirements listed in subsection 4.3.1), whereas for ΛCDM $w_{\rm m}$ is fixed at zero.

[58] Setting $\Lambda(t) = Ua^{-2} + Wa^{-4}$ (where U and W are constants) yields a similar expression for a.

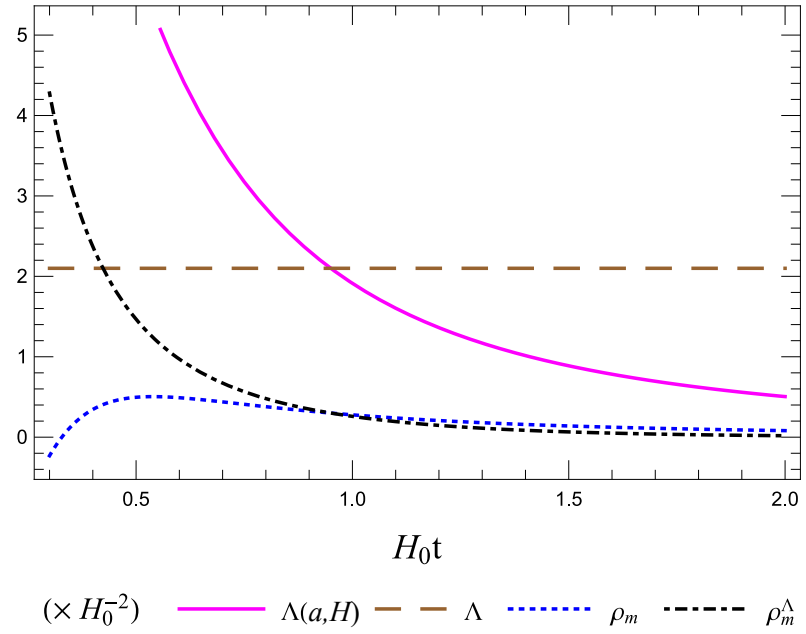

FIGURE 4.5: The variation of $\Lambda(a, H)$ and $\rho_{\rm m}$ with time. The evolution of the matter density in a flat ΛCDM cosmology ($\rho_{\rm m}^{\Lambda}$) is shown for comparison, while the horizontal dashed line represents the cosmological constant.

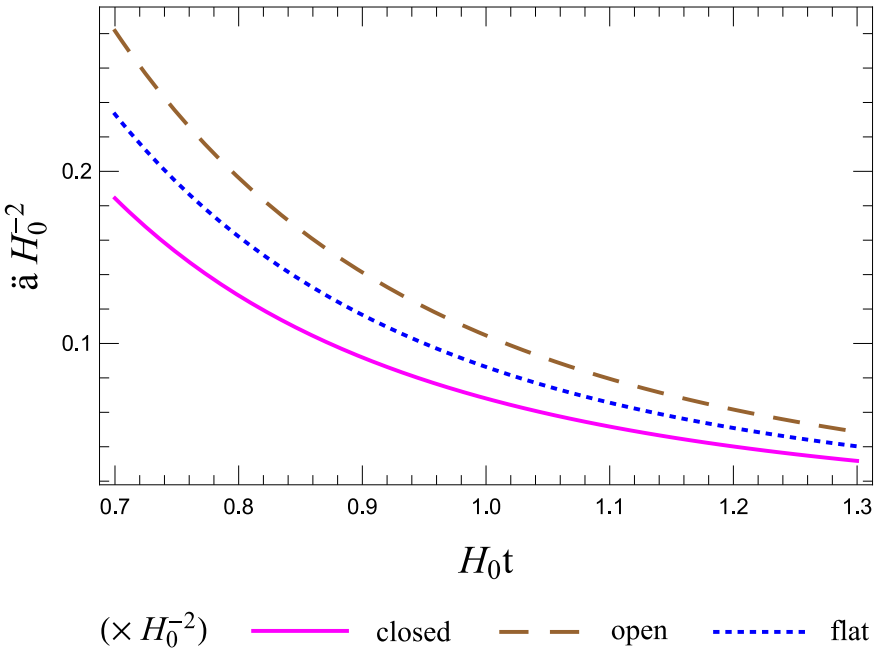

FIGURE 4.6: The variation of acceleration with time in a universe filled with a stiff fluid and dark energy. The latter takes the form of a dynamical Λ given by $IH^2 + Ja^{-2}$. The spatially non-flat models have $|\kappa| = 0.0106H_0^2$ [20], and the parameters c_1 and c_2 are curvature-dependent: $c_1 = -0.041/H_0$, $c_2 = 0.1H_0^2$ ($\kappa = 0$), $c_1 = -0.023/H_0$, $c_2 = 0.079H_0^2$ ($\kappa > 0$), $c_1 = -0.058/H_0$, $c_2 = 0.121H_0^2$ ($\kappa < 0$).

As done in the case of model 1, the integration constants are treated as functions of spatial curvature. The reason is that the conditions $a(\bar{t}_0) = a'(\bar{t}_0) = 1$ cannot otherwise be satisfied for $\kappa = 0$, $\kappa > 0$ and $\kappa < 0$ simultaneously. We again note (Fig. 4.6) that the cosmic acceleration is largest for the open universe and smallest for the closed one.

4.4 The Generalised Running Vacuum Model

The inspiration for the GRVM comes from the interpretation of Λ as a running parameter in the curved space-time version of QFT. The associated energy density, ρ_Λ, is thus expected to evolve according to a renormalisation group equation of the form [259]

$$\frac{\mathrm{d}\rho_\Lambda}{\mathrm{d}\ln\beta} = \frac{1}{(4\pi)^2}\sum_{n=1}^{\infty} S_n \beta^{2n} \ , \tag{4.13}$$

where the dynamical variable β represents some characteristic infrared-cutoff scale. In a cosmological context, the role of β may be played by the Hubble parameter H, since the latter is of the order of the energy scale associated with the Friedmann-Lemaître-Robertson-Walker (FLRW) cosmology [214]. We furthermore note that the coefficients S_n result from loop contributions of fields having different masses and spins [259]. Meanwhile, the absence of odd powers of β reflects the general covariance of the effective action [214, 260].

Given that $\beta \sim H$, the small present-day value of H ($\sim 10^{-27}\,\mathrm{m}^{-1}$) implies that terms in Eq. (4.13) with $n \geq 2$ would be suppressed in the current epoch. An expression for ρ_Λ $\left(\text{henceforth } \rho_{\Lambda(H)}\right)$ may hence be obtained by integrating the remaining term on the right-hand side. One gets the relation $(4\pi)^2\rho_{\Lambda(H)} = S_0 + S_1\beta^2/2$, with S_0 denoting the constant of integration. Consequently, if β^2 is identified with a linear combination of[59] H^2 and $\mathrm{d}H/\mathrm{d}t$, the expression for $\rho_{\Lambda(H)}$ becomes $(4\pi)^2\rho_{\Lambda(H)} = S_0 + \tilde{S}_2 H^2 + \tilde{S}_3(\mathrm{d}H/\mathrm{d}t)$, where $\tilde{S}_2$ and $\tilde{S}_3$ are constants [214].

In conclusion, we shall be investigating a model in which the cosmological constant is replaced with

$$\Lambda(H) = A + BH^2 + C\dot{H} \ . \tag{4.14}$$

The leading constant and the coefficients of H^2 and $\dot{H}$ have been written as A, B and C for the sake of simplicity, B and C being dimensionless and A having units of

[59] These two quantities represent independent degrees of freedom [212].

length^{-2}. The model specified by Eq. (4.14) is none other than the GRVM, introduced in section 4.1 – the RVM and GRVS follow as special cases by setting $C = 0$ and $B = 0$, respectively. One notes that $\Lambda(H)$ is not an *explicit* function of time (the dependence on t is established implicitly, via H), and it is this property that the name 'running vacuum model' is meant to reflect [214].

The dynamic nature of $\Lambda(H)$ means that the Bianchi identity may be satisfied in one of two ways [226, 261, 262]. Let us see how such a possibility comes about. If $\Lambda(H)$ is not incorporated into $T_{\mu\nu}$, Einstein's field equations read

$$G_{\mu\nu} = 8\pi G T_{\mu\nu} - \Lambda(H) g_{\mu\nu} \ , \tag{4.15}$$

so that the twice-contracted Bianchi identity, $\nabla^\mu G_{\mu\nu} = 0$ [8], implies that

$$\nabla^\mu (8\pi G T_{\mu\nu}) = g_{\mu\nu} \nabla^\mu \Lambda(H) \ . \tag{4.16}$$

The above makes use of the fact that ∇_μ is constructed from a metric-compatible connection (i.e. $\nabla^\rho g_{\mu\nu} = 0$ at all points) [8]. In the presence of a time-varying G, $T_{\mu\nu}$ may be conserved separately, in which case Eq. (4.16) becomes $8\pi T_{\mu\nu} \nabla^\mu G(t) = g_{\mu\nu} \nabla^\mu \Lambda(H)$. If G is constant, however, the Bianchi identity requires that $8\pi G \nabla^\mu T_{\mu\nu} = g_{\mu\nu} \nabla^\mu \Lambda(H)$. In other words, we have the option of either a 'running' gravitational coupling $G(t)$ or of energy transfer between the vacuum and any other component/s of the cosmic fluid.[60] We shall take the constant-G approach. Assuming that the densities of baryonic matter and radiation evolve as in the standard model, it may be deduced that dark energy interacts with cold dark matter (whose energy density is denoted by $\rho_{\rm cdm}$) according to the equation

$$\dot{\rho}_{\rm cdm} + 3H\rho_{\rm cdm} = -\dot{\rho}_{\Lambda(H)} \ . \tag{4.17}$$

The relation $\rho_{\Lambda(H)} = \Lambda(H)/(8\pi G)$ and Eq. (4.14) can be combined to give

$$\rho_{\Lambda(H)} = \frac{1}{8\pi G} \left(A + BH^2 + C\dot{H} \right) \ , \tag{4.18}$$

so that Eq. (4.17) becomes

$$\dot{\rho}_{\rm cdm} = -3H\rho_{\rm cdm} - \frac{1}{8\pi G} \left(2BH\dot{H} + C\ddot{H} \right) \ . \tag{4.19}$$

[60] It is also possible to combine the two options.

To obtain an expression for $\dot{H}$, one uses (4.14) in conjunction with the second Friedmann equation [refer to Chapter 1, Eq. (1.37)], which reads:

$$\dot{H} + H^2 = -\frac{4\pi G}{3}(\rho + 3p) + \frac{\Lambda(H)}{3} \ . \tag{4.20}$$

Here, ρ denotes the sum of the energy densities of cold dark matter ($\rho_{\rm cdm}$), baryons ($\rho_{\rm b}$) and radiation[61] ($\rho_{\rm r}$), while p represents the total of the corresponding pressures. Dark energy is modelled with an equation of state parameter $w_{\Lambda(H)}$ fixed at -1, as in ΛCDM. If $w_{\Lambda(H)}$ is instead allowed to vary, it would be possible for dark energy to be conserved independently of the other cosmic components. Such a scenario has been investigated in Ref. [219].

As stated previously, it is assumed that neither radiation nor baryons interact with dark energy. Consequently, cosmic expansion dilutes the respective energy densities in accordance with the familiar ΛCDM relations:

$$\rho_{\rm b} = \rho_{\rm b}^0 a^{-3} \ , \qquad \rho_{\rm r} = \rho_{\rm r}^0 a^{-4} \ . \tag{4.21}$$

A 0-superscript indicates present-day quantities.

Let us now return to Eq. (4.20). It provides us with an expression for $\dot{H}$, and we proceed by differentiating it with respect to t to find $\ddot{H}$. We are then able to eliminate the first and second time derivatives of H from Eq. (4.19), getting that

$$4\pi G\Big\{(C-2)(C-3)\rho'_{\rm cdm}(a)a + 2\left[9 - B + C(C-5)\right]\rho_{\rm cdm} - \left[2B + (C-5)C\right]\rho_{\rm b}^0 a^{-3}$$
$$-\frac{4}{3}[3B + C(2C-9)]\rho_{\rm r}^0 a^{-4}\Big\} + 2(B-C)\left[A + (B-3)H^2\right] = 0 \ , \tag{4.22}$$

where a prime denotes differentiation with respect to the argument and $\mathrm{d}/\mathrm{d}t$ has been replaced with $aH(\mathrm{d}/\mathrm{d}a)$. The next step is to solve the differential equation (4.22), but before attempting to do so, the Hubble parameter must be expressed in terms of a. To this end, one makes use of the first Friedmann equation [Chapter 1, Eq. (1.38)]:

$$H^2 = \frac{8\pi G}{3}\left(\rho_{\rm cdm} + \rho_{\rm b} + \rho_{\rm r} + \rho_{\Lambda(H)}\right) - \kappa a^{-2} \ . \tag{4.23}$$

The energy densities in Eq. (4.23) may be replaced with the corresponding relations

[61] *Radiation* refers to photons and massless neutrinos.

given by Eqs. (4.18) and (4.21). This allows us to determine H as a function of a:

$$H = \frac{\left[24\pi G a(C-2)\left(\rho_{\rm cdm}a^3+\rho_{\rm b}^0\right)+16\pi G(2C-3)\rho_{\rm r}^0-6(C-3)\kappa a^2-6Aa^4\right]^{1/2}}{\sqrt{6(B-3)}\,a^2}\,. \tag{4.24}$$

Inserting the above into Eq. (4.22) yields the final version of Eq. (4.17):

$$8\pi G\left[(C-2)\rho'_{\rm cdm}(a)a+2(B-3)\rho_{\rm cdm}+(2B-3C)\rho_{\rm b}^0a^{-3}+\frac{8}{3}(B-2C)\rho_{\rm r}^0a^{-4}\right]- 4(B-C)\kappa a^{-2}=0\,, \tag{4.25}$$

which can readily be solved for $\rho_{\rm cdm}$. It is found that

$$\rho_{\rm cdm}=\left[a^{\frac{2(3-B)}{C-2}}\Omega_{\rm cdm}^0-\left(a^{-3}-a^{\frac{2(3-B)}{C-2}}\right)\Omega_{\rm b}^0-\frac{4(B-2C)}{3(B-2C+1)}\left(a^{-4}-a^{\frac{2(3-B)}{C-2}}\right)\Omega_{\rm r}^0 - \frac{2(B-C)}{3(B-C-1)}\left(a^{-2}-a^{\frac{2(3-B)}{C-2}}\right)\Omega_k^0\right]\frac{3H_0^2}{8\pi G}\,. \tag{4.26}$$

Now we require a similar expression for $\rho_{\Lambda(H)}$. Equipped with Eq. (4.26), one first eliminates $\rho_{\rm cdm}$ from Eq. (4.24). Next, Eq. (4.26) is used in conjunction with Eq. (4.21), the updated version of Eq. (4.24), and Eq. (4.14); they are inserted into Eq. (4.20) and $\dot{H}$ is solved for. In all cases, the energy densities are written in terms of the current values of the density parameters. Finally, one replaces $\dot{H}$ in Eq. (4.18) with the newly-found solution, and substitutes Eq. (4.24) for H. Eq. (4.18) consequently takes the form

$$\rho_{\Lambda(H)}=\frac{3H_0^2}{8\pi G}\left\{\frac{(2B-3C)}{2(B-3)}\left(1-a^{\frac{2(3-B)}{C-2}}\right)\Omega_{\rm m}^0+\frac{B-2C}{3(B-3)(B-2C+1)}\left[(B-3)a^{-4} +2(3C-2B)a^{\frac{2(3-B)}{C-2}}+3(B-2C+1)\right]\Omega_{\rm r}^0-\frac{(B-C)}{3(B-3)(B-C-1)}\left[(B-3)a^{-2} +(2B-3C)a^{\frac{2(3-B)}{C-2}}-3(B-C-1)\right]\Omega_k^0+\Omega_{\Lambda(H)}^0\right\}\,, \tag{4.27}$$

with $\Omega_{\rm m}^0 = \Omega_{\rm cdm}^0+\Omega_{\rm b}^0$. The requirement that $\rho_{\Lambda(H)}$ is currently equal to $3H_0^2\Omega_{\Lambda(H)}^0/(8\pi G)$ has been used to fix the value of A at $H_0^2(3\Omega_{\Lambda(H)}^0-B)$.

A few comments about the role of spatial curvature are in order before we proceed. In Ref. [201], the RVM is represented as the late-time limit of a model that can describe the complete cosmic history. Its generalised version takes spatial curvature

into account [199], and is based on the following expression for Λ:

$$\Lambda(H,a) = \Lambda_\infty + 3\nu\left(H^2 - H_\mathrm{F}^2 + \frac{\kappa}{a^2}\right) + 3\zeta\left(\frac{H}{H_\mathrm{I}}\right)^n\left(H^2 + \frac{\kappa}{a^2}\right) \ , \tag{4.28}$$

where the integer n satisfies $n \geq 1$ [201] and Λ_∞ is the limit of $\Lambda(H,a)$ as $a \to \infty$. H_I and H_F stand for the Hubble parameter in two different epochs. The former characterises inflation, while the latter denotes the 'final' value of H (or the limit of H as $a \to \infty$) [199]. Lastly, ν and ζ correspond to dimensionless constants [199]. The quantity 3ν is the counterpart of the model parameter B introduced in Eq. (4.14).

The reason why we shall limit ourselves to the RVM, instead of analysing the extended version just described, is twofold. Firstly, H is expected to be already much smaller than H_I at the start of the adiabatic radiation phase [199]. Since we are not concerned with inflation, but rather with the late-time behaviour of dark energy models, the term in $(H/H_\mathrm{I})^n$ may be dropped. Secondly, the explicit inclusion of κ in Eq. (4.28) is motivated by phenomenological considerations [199]. It would therefore be interesting to study how the RVM – in its original simple form – behaves if Ω_κ^0 is allowed to vary.

4.5 Likelihoods and Observational Data

If a dark energy model is to be considered a viable alternative to ΛCDM, one must firstly determine whether it is compatible with observational data. To this end, we shall employ Bayesian statistics, and perform a Markov Chain Monte Carlo (MCMC) analysis using the Cosmic Linear Anisotropy Solving System (CLASS) v.2.6.3 [263] in conjunction with MONTE PYTHON v.2.2.2 [264].

This section is a brief introduction to the likelihoods with which cosmological and model-specific parameters shall be constrained.

4.5.1 The JLA likelihood for SNeIa

Type-Ia supernovae (SNeIa) make it possible to probe the expansion history of the Universe by looking at how the luminosity distance to an object varies with redshift z. Whenever this relation departs from a pure Hubble law [2], the difference (to lowest order in z) depends on just the deceleration parameter, and can thus yield important information about the rate of cosmic expansion. SNeIa are ideal in this

regard because they act as standard candles – in the sense that their homogeneity as a group means their intrinsic luminosity (or absolute magnitude) can be calibrated [7], and hence astronomers may readily find how distant they are by measuring their observed luminosity (called the apparent magnitude) [10].

The Joint Light-Curve Analysis (JLA) data set is based on a sample of 740 SNeIa [265]. The observable relevant to us is the distance modulus $\mu_{\rm obs}$, which has a theoretical counterpart given by:

$$\mu_{\rm th} = 5\log_{10}\left(\frac{d_{\rm L}}{\rm Mpc}\right) + 25 \ , \tag{4.29}$$

where the luminosity distance $d_{\rm L}$ should be quoted in Mpc, and is in turn determined from the equation

$$d_{\rm L} = \frac{1+z}{H_0\sqrt{|\Omega_k^0|}}\ \bar{\mathcal{F}}\left(\sqrt{|\Omega_k^0|}\int_0^z \frac{H_0 {\rm d}\bar{z}}{H(\bar{z})}\right) \ . \tag{4.30}$$

The above was derived in Chapter 1 [refer to Eq. (1.78)].

We are now in a position to construct the associated χ^2. This may be expressed as

$$\chi^2_{\rm JLA} = \Delta\mu^{\rm T} C^{-1}_{\rm JLA} \Delta\mu \ , \tag{4.31}$$

where $\Delta\mu$ is a vector whose $i^{\rm th}$ entry is the quantity $(\mu^i_{\rm obs} - \mu^i_{\rm th})$ – the difference between the observed and theoretical distance moduli of the $i^{\rm th}$ supernova. $\Delta\mu^{\rm T}$ represents its transpose [266].

The inverted covariance matrix for the observational values of μ is denoted in Eq. (4.31) by $C^{-1}_{\rm JLA}$. The reader is directed to Ref. [265] for more details about its construction.

4.5.2 The cosmic chronometer (clocks) likelihood

The Hubble parameter is defined in terms of the scale factor as the ratio $\dot{a}/a$, and the relation $a = 1/(1+z)$ allows us to express it as a function of the redshift z:

$$H(z) = -\frac{1}{1+z}\frac{{\rm d}z}{{\rm d}t} \ . \tag{4.32}$$

The differential age (or cosmic chronometer/clocks) method entails measuring ${\rm d}z/{\rm d}t$ to directly arrive at $H(z)$. This approach, first put forward in Ref. [274], effectively involves determining the age difference between two cosmic 'chronometers' [274] located in a given redshift interval. The best chronometers are massive early-type

TABLE 4.1: Cosmic chronometer data. Each value of $H(z)$ in the third column is measured at an effective redshift z given in the second column, and has a corresponding error σ (fourth column).

Ref.	z	$H(z)$ $\left(\mathrm{km\,s^{-1}\,Mpc^{-1}}\right)$	σ	Ref.	z	$H(z)$ $\left(\mathrm{km\,s^{-1}\,Mpc^{-1}}\right)$	σ
[267]	0.0700	69.0	19.6	[268]	0.4783	80.9	9.0
[267]	0.1200	68.6	26.2	[269]	0.4800	97.0	62.0
[270]	0.1700	83.0	8.0	[271]	0.5929	104.0	13.0
[271]	0.1791	75.0	4.0	[271]	0.6797	92.0	8.0
[271]	0.1993	75.0	5.0	[271]	0.7812	105.0	12.0
[267]	0.2000	72.9	29.6	[271]	0.8754	125.0	17.0
[270]	0.2700	77.0	14.0	[269]	0.8800	90.0	40.0
[267]	0.2800	88.8	36.6	[270]	0.9000	117.0	23.0
[271]	0.3519	83.0	14.0	[271]	1.0370	154.0	20.0
[268]	0.3802	83.0	13.6	[270]	1.3000	168.0	17.0
[270]	0.4000	95.0	17.0	[272]	1.3630	160.0	33.6
[268]	0.4004	77.0	10.2	[270]	1.4300	177.0	18.0
[268]	0.4247	87.1	11.2	[270]	1.5300	140.0	14.0
[268]	0.4497	92.8	12.9	[270]	1.7500	202.0	40.0
[273]	0.4700	89.0	49.6	[272]	1.9650	186.5	50.4

galaxies which acquired more than 90 percent of their stellar mass very rapidly at high redshifts, and have been evolving passively since then, without major episodes of star formation [271] that would otherwise dominate the emission spectrum [274]. The age of such a galaxy can consequently be inferred from the differential dating of its stellar population [271].

Table 4.1 lists the cosmic chronometer data employed in this chapter.[62] Where possible, constraints on $H(z)$ obtained using the Bruzual and Charlot 2003 (BC03) stellar population synthesis (SPS) model [275] were given preference. It should be pointed out, however, that the values of the Hubble parameter at different redshifts are expected to be largely unaffected by the choice of SPS [269, 271].

The χ^2 for the cosmic chronometer likelihood reads:

$$\chi^2_{H(z)} = \sum_i \left(\frac{H_i^{\mathrm{obs}} - H^{\mathrm{th}}\left(z_i\right)}{\sigma_{H(z),i}} \right)^2 . \tag{4.33}$$

[62] In the case of the Ratsimbazafy et al. data point [273], σ was calculated by summing the systematic and statistical errors in quadrature.

Here, each $H_i^{\rm obs}$ is the observed value from Table 4.1 corresponding to $z = z_i$, σ_i represents the associated error, and $H^{\rm th}(z_i)$ stands for the theoretical prediction at the same redshift.

4.5.3 The CMB likelihood

Anisotropies present in the temperature and polarization power spectra of the CMB can yield a wealth of information when used as cosmological probes. We shall work with two main distance priors: the shift parameter $\mathscr{R}$ and the acoustic scale $l_{\rm A}$. These are related to the amplitude and distribution of the temperature anisotropy peaks. The shift parameter $\mathscr{R}$ characterises the temperature power spectrum in the line-of-sight direction and is defined as follows [276]:

$$\mathscr{R}(z_*) = \sqrt{\Omega_{\rm m}^0}\, H_0(1+z_*)d_{\rm A}(z_*) \ , \tag{4.34}$$

where z_* denotes the redshift of the photon decoupling epoch. The angular diameter distance $d_{\rm A}$ may be expressed via the distance-duality relation as $d_{\rm L}/(1+z)^2$, $d_{\rm L}$ being the luminosity distance from Eq. (4.30).

The acoustic scale $l_{\rm A}$, on the other hand, relates to attributes of the CMB temperature power spectrum in the transverse direction [277]. It, too, depends on $d_{\rm A}$ [276]:

$$l_{\rm A}(z_*) = (1+z_*)\frac{\pi d_{\rm A}(z_*)}{r_{\rm s}(z_*)} \ . \tag{4.35}$$

Here, $r_{\rm s}(z_*)$ is the comoving sound horizon evaluated at z_*. In our case, it shall be determined numerically by CLASS, although it is worth noting that in general, the function $r_{\rm s}(z)$ takes the form

$$r_{\rm s}(z) = \int_z^\infty \frac{c_{\rm s}(\bar{z})}{H(\bar{z})}{\rm d}\bar{z} \ , \tag{4.36}$$

where $c_{\rm s}(z)$ is the sound speed in the photon-baryon fluid and equates to $1/\sqrt{3[1+\eta(z)]}$. The function $\eta(z)$ is given by $0.75\rho_{\rm b}/\rho_\gamma$ in the standard scenario [276–278] (ρ_γ stands for the energy density of photons), but should be modified when considering cosmological models in which $\rho_{\rm b}$ and ρ_γ scale differently with z. More details may be found in Ref. [214].

It is interesting to note that while $l_{\rm A}$ determines the acoustic peak structure, changes

TABLE 4.2: Mean values and corresponding errors for the CMB distance priors [277].

$\mathscr{R}$	$l_{\rm A}$	$\Omega_{\rm b}^0 h^2$
1.7448 ± 0.0054	301.460 ± 0.094	0.02240 ± 0.00017

in $\mathscr{R}$ are mainly responsible for modifying the amplitude of the peaks [116, 277].

The data used to constrain our model parameters is taken from Ref. [277] and shown in Table 4.2. It was obtained in the context of a flat ΛCDM cosmology with $A_{\rm L}$ as a free parameter ($A_{\rm L}$ being the amplitude of the lensing power spectrum). The fact that a particular cosmological model had to be assumed is, however, only a minor disadvantage, since $\mathscr{R}(z_*)$ and $l_{\rm A}(z_*)$ are effective observables, while the quantity $\Omega_{\rm b}^0 h^2$ – which serves as a third distance prior[63] –is virtually unaffected by the choice of cosmology [277].

The χ^2 associated with this likelihood reads:

$$\chi^2_{\rm CMB} = \Delta x^{\rm T} C^{-1}_{\rm CMB} \Delta x \ . \tag{4.37}$$

In the above, Δx is the vector $\{\mathscr{R}_{\rm obs}(z_*) - \mathscr{R}_{\rm th}(z_*), l_{\rm A}^{\rm obs}(z_*) - l_{\rm A}^{\rm th}(z_*), (\Omega_{\rm b}^0 h^2)_{\rm obs} - (\Omega_{\rm b}^0 h^2)_{\rm th}\}$. The notation 'obs' is used to indicate the observed values listed in Table 4.2, while 'th' denotes theoretical quantities. The covariance matrix $C_{\rm CMB}$ may be obtained in normalised form from Ref. [277]. It is reproduced below for ease of reference:

$$C^{\rm norm}_{\rm CMB} = \begin{array}{c} \\ \mathscr{R} \\ l_{\rm A} \\ \Omega_{\rm b}^0 h^2 \end{array} \begin{array}{c} \begin{array}{ccc} \mathscr{R} & l_{\rm A} & \Omega_{\rm b}^0 h^2 \end{array} \\ \begin{bmatrix} 1.00 & 0.53 & -0.73 \\ 0.53 & 1.00 & -0.42 \\ -0.73 & -0.42 & 1.00 \end{bmatrix} \end{array} . \tag{4.38}$$

4.5.4 The BAO likelihood

The physics of BAOs is centred around the imprint left by pre-recombination acoustic waves on large-scale structure [283]. Simply put, galaxies clustered with a preferred comoving separation equal to $r_{\rm s}(z_{\rm d})$, the sound horizon at the drag epoch.[64] A prominent signature of BAOs is the presence of a localised peak in the galaxy correlation function. Another characteristic feature consists of a damped series of oscillations in

[63] The dimensionless constant h is equivalent to $H_0/(100\,{\rm km\,s^{-1}\,Mpc^{-1}})$.

[64] $r_{\rm s}(z)$ is given by Eq. (4.36), and $z_{\rm d}$ denotes the redshift of the drag epoch.

TABLE 4.3: Uncorrelated BAO data measured at different effective redshifts, $z_{\rm eff}$. Column 4 gives the error in each quantity.

Ref.	$z_{\rm eff}$	Quantity	σ	Type
[279]	0.106	0.323	0.014	1
[280]	0.150	4.490	0.170	2
[281]	1.520	26.005	0.995	2
[282]	2.330	1.031	0.026	3
1: $r_s(z_{\rm d})/d_{\rm v}$; 2: $d_{\rm v}/r_s(z_{\rm d})$;				
3: $\alpha_{\parallel}^{0.7}\alpha_{\perp}^{0.3}$;				
$r_{\rm s,\ fid}(z_{\rm d}) = 147.78\,{\rm Mpc}$ [283].				

TABLE 4.4: BAO data. In the case of the first six data points, the associated errors – displayed in column 4 – were derived from the corresponding covariance matrix. The value of σ for the last two entries was estimated by constructing the covariance matrix for the quantities numbered 4 and 5.

Ref.	$z_{\rm eff}$	Quantity	σ	Type
[283]	0.380	1512.390	24.994	4
[283]	0.380	81.209	2.368	5
[283]	0.510	1975.220	30.096	4
[283]	0.510	90.903	2.329	5
[283]	0.610	2306.680	37.083	4
[283]	0.610	98.965	2.502	5
[284]	2.400	5277.480	246.091	4
[284]	2.400	225.067	8.750	5
4: $D_{\rm A} \times r_{\rm s,\ fid}(z_{\rm d})/r_{\rm s}(z_{\rm d})({\rm Mpc})$;				
5: $H \times r_{\rm s}(z_{\rm d})/r_{\rm s,\ fid}(z_{\rm d})({\rm km\,s^{-1}\,Mpc^{-1}})$;				
$r_{\rm s,\ fid}(z_{\rm d}) = 147.78\,{\rm Mpc}$ [283].				

the CMB power spectrum (see Ref. [283] and works cited therein), and so $r_{\rm s}(z_{\rm d})$ may be inferred from CMB data. Once the comoving separation between clusters is known, it may be combined with measurements of the angular and redshift separations, and utilised to calculate both the local expansion rate $H(z)$ and the angular diameter distance to the clusters [285]. However, it is common practice to adopt a distance measure that depends on H and $d_{\rm A}$ simultaneously – and this is where the volume distance (or dilation scale) $d_{\rm v}$ comes in [208]:

$$d_{\rm v} = \left(D_{\rm A}^2 \frac{z}{H} \right)^{1/3} \ . \tag{4.39}$$

In the above, $D_{\rm A}$ stands for the comoving angular diameter distance and is equivalent to $(1+z)d_{\rm A}$.

The data employed in our analysis is summarised in Tables 4.3 and 4.4. We shall be using $r_{\rm s,\,fid}(z_{\rm d})$ to represent the sound horizon as evaluated at the drag epoch in the fiducial cosmology (quantities pertaining to this cosmology shall henceforth be indicated by a sub/superscript 'fid'). As for the dimensionless parameters $\alpha_\perp$ and $\alpha_\parallel$, these describe how the BAO peak is displaced with respect to its position in the fiducial model, and correspond to shifts perpendicular and parallel to the line of sight, respectively [283]:

$$\alpha_\perp = \frac{D_{\rm A} r_{\rm s,\,fid}\,(z_{\rm d})}{D_{\rm A}^{\rm fid}\, r_{\rm s}\,(z_{\rm d})} \ , \qquad \alpha_\parallel = \frac{H^{\rm fid}\, r_{\rm s,fid}\,(z_{\rm d})}{H\, r_{\rm s}\,(z_{\rm d})} \ . \tag{4.40}$$

The choice of a fiducial cosmology is necessary to convert redshifts into comoving distances. The problem is that this may inadvertently distort the data. In Ref. [283], therefore, constraints on distances are scaled by the ratio $r_{\rm s,\,fid}(z_{\rm d})/r_{\rm s}(z_{\rm d})$, the aim being to make a conversion of length scales and thus erase any bias potentially resulting from the fiducial model [283]. The same fiducial value of $r_{\rm s}(z_{\rm d})$ has been used to scale any data points obtained from other studies. Accordingly, the values listed under 'Quantity' in Table 4.3 and in the last two rows of Table 4.4 are scaled versions of the original.

The χ^2 for the BAO likelihood may be expressed in the usual way:

$$\chi^2_{\rm BAO} = \Delta x^{\rm T} C^{-1}_{\rm BAO} \Delta x \ . \tag{4.41}$$

Here, the vector Δx gives the difference between the observed quantities from Tables 4.3 and 4.4 (in that order) and their theoretical counterparts, while $C_{\rm BAO}$ is the covariance matrix and takes the form indicated below:

$$C_{\rm BAO} = \begin{pmatrix} \sigma_1^2 & 0 & 0 & 0 & 0 & 0 \\ 0 & \sigma_2^2 & 0 & 0 & 0 & 0 \\ 0 & 0 & \sigma_3^2 & 0 & 0 & 0 \\ 0 & 0 & 0 & \sigma_4^2 & 0 & 0 \\ 0 & 0 & 0 & 0 & C_{\rm A} & 0 \\ 0 & 0 & 0 & 0 & 0 & C_{\rm B} \end{pmatrix} \ , \tag{4.42}$$

σ_1 to σ_4 being the standard deviations listed in column 4 of Table 4.3.[65] As for the submatrices, $C_{\rm A}$ is the covariance matrix for the Alam et al. observations (the first six data points in Table 4.4), and $C_{\rm B}$ corresponds to the quantities reported by des Bourboux et al. (the last two entries in Table 4.4). These matrices may be constructed from the data available in Refs. [283] and [284], respectively.

4.5.5 The LSS likelihood

The redshift of a galaxy depends on its velocity relative to us, and is hence affected by any peculiar velocity the galaxy might have. If only the Hubble recession is taken into account when converting redshifts into distances, therefore, the recovered over-density field is characterised by redshift space distortions (RSDs) [286] along the line of sight. The anisotropies that RSDs introduce into the galaxy power spectrum encode information about the growth of large-scale structure (LSS) [287].

In this work we shall be using LSS data in the form of $f\sigma_8$ measurements. The growth rate f and the quantity σ_8 are defined as follows [288]:

$$f = \frac{\mathrm{d}(\ln \delta_{\rm m})}{\mathrm{d}\ln a} \ , \quad \sigma_8 = \sigma_{8,0}\,\frac{\delta_{\rm m}(a)}{\delta_{\rm m}(1)} \ , \tag{4.44}$$

where $\delta_{\rm m}$ denotes the matter density contrast function, $\delta_{\rm m}(1) = \delta_{\rm m}(a=1)$ and $\sigma^2_{8,0}$ is the variance of the density field in spheres of radius $R_8 = 8\,h^{-1}$ Mpc. It is important to note that $\sigma_{8,0}$ is calculated by linearly evolving the initial power spectrum to the present time, so the square of its value is not necessarily equal to the variance of the current distribution [289].

Let us consider $\delta_{\rm m}$ and σ_8 one by one. In both cases, the derivations are closely based on the work presented in Refs. [215] and [290].

[65] Data points from different studies can be put together into one set as long as one knows how they are correlated. The associated covariance matrix is formulated as follows:

$$C \;=\; \begin{array}{c} \\ \text{data pt. 1} \\ \text{data pt. 2} \\ \vdots \\ \text{data pt. } n \end{array} \begin{array}{c} \begin{array}{cccc} \text{data pt. 1} & \text{data pt. 2} & \ldots & \text{data pt. } n \end{array} \\ \begin{bmatrix} \sigma_1^2 & c_{12}\sigma_1\sigma_2 & \ldots & c_{1n}\sigma_1\sigma_n \\ c_{21}\sigma_2\sigma_1 & \sigma_2^2 & \ldots & c_{2n}\sigma_2\sigma_n \\ \vdots & \vdots & \ddots & \vdots \\ c_{n1}\sigma_n\sigma_1 & c_{n2}\sigma_n\sigma_2 & \ldots & \sigma_n^2 \end{bmatrix} \end{array} . \tag{4.43}$$

In the above, σ_i is the uncertainty in the $i^{\rm th}$ data point and c_{ij} reflects the degree of correlation between the $i^{\rm th}$ and $j^{\rm th}$ data points: it takes the value 0 if they are uncorrelated, and 1 if $i = j$ (i.e. if there is maximal correlation). When two experiments A and B are independent, the data produced by A is not correlated with the data from B.

The matter density contrast function ($\delta_{\rm m}$)

The linear perturbation analysis is carried out as detailed in Appendix A. One starts by considering Eq. A.14, the time-time component of the perturbed Einstein equation, but replaces $\rho_{\rm m}\delta_{\rm m}$ $(= \delta\rho_{\rm m})$ with a sum over baryon, cold dark matter and dark energy perturbations:[66]

$$\Phi(k_\dagger^2 - 3\kappa) + 3\mathcal{H}\left[\Phi'(\tau) + \Phi\mathcal{H}\right] + 4\pi G a^2 \sum_i \delta\rho_i = 0 \ ;$$
$$i = \{\mathrm{b}, \mathrm{cdm}, \Lambda(H)\} \ . \tag{4.45}$$

The presence of vacuum energy perturbations reflects the dynamic nature of Λ in the models under study – they are, in fact, absent from ΛCDM. Radiation need not be taken into account for the late times we are interested in.

We proceed by considering the conservation of the energy-momentum tensor. Let us recall that cold dark matter and dark energy interact with each other, and hence are conserved jointly: $\nabla_\mu(T^{\mu\nu}_{\rm cdm} + T^{\mu\nu}_{\Lambda(H)}) = 0$ [290]. This condition still holds when perturbations are introduced. Therefore, the equivalents of Eqs. (A.20) and (A.21) read, respectively:[67]

$$\sum_{i=\mathrm{cdm},\Lambda(H)} \left\{\delta\rho_i'(\tau) + (\rho_i + p_i)\left[k_\dagger v_{(i)} - 3\Phi'(\tau)\right] + 3\mathcal{H}\left(\delta\rho_i + \delta p_i\right)\right\} = 0 \ ; \tag{4.46}$$

$$\sum_{i=\mathrm{cdm},\Lambda(H)} \left\{-\frac{\mathrm{d}}{\mathrm{d}\tau}\left[(\rho_i + p_i)\, v_{(i)}\right] + (\rho_i + p_i)\left(k_\dagger\Phi - 4\mathcal{H}v_{(i)}\right) + k_\dagger\delta p_i\right\} = 0 \ , \tag{4.47}$$

although the above equations also hold when baryons are considered on their own (that is, when the sum is over baryons only, so to speak).

Our next task is to simplify Eqs. (4.46) and (4.47). One starts by assuming that $\delta p_i/\delta\rho_i = p_i/\rho_i = w_i$ (w_i being the equation-of-state parameter for the $i^{\rm th}$ distribution of matter/energy) [291], and then uses the conformal analogue of Eq. (4.17) to substitute for $\rho'_{\rm cdm}(\tau)$ (since $\delta\rho_{\rm cdm} = \rho_{\rm cdm}\delta_{\rm cdm}$). As for the perturbations in dark energy, it can be shown that $\delta\rho_{\Lambda(H)} \ll \delta\rho_{\rm cdm}$ for modes that are deep inside the

[66] $\delta\rho_i$ denotes the perturbation in the density ρ_i of the $i^{\rm th}$ fluid, while δp_i is the perturbation in the corresponding pressure (p_i). Additionally, $\delta_i = \delta\rho_i/\rho_i$. The symbols τ, Φ, $k_\dagger$ and $\mathcal{H}$ stand for conformal time, the metric perturbation, the comoving wave number, and the conformal (or comoving) Hubble parameter, respectively.

[67] $v_{(i)}$ is the velocity potential of the $i^{\rm th}$ fluid, and should not be confused with v_i, the $i^{\rm th}$ component (in covariant form) of the spatial velocity (itself a perturbation).

horizon [290]. The sub-horizon and quasi-static approximations are also introduced at this point.

Once all of the above considerations have been taken into account, Eqs. (4.46) and (4.47) become

$$\delta'_{\rm cdm}(\tau) + \psi\delta_{\rm cdm} = -k_\dagger v_{\rm cdm} + 3\Phi'(\tau) \ ; \tag{4.48}$$

$$v'_{\rm cdm}(\tau) + v_{\rm cdm}(\mathcal{H} + \psi) - k_\dagger\Phi + k_\dagger\frac{\delta\rho_{\Lambda(H)}}{\rho_{\rm cdm}} = 0 \ , \tag{4.49}$$

where $\psi = -\rho'_{\Lambda(H)}(\tau)/\rho_{\rm cdm}$, while $w = 0$ for cold dark matter and -1 for $\Lambda(H)$. The terms $v_{\rm cdm}\psi$ and $k_\dagger\delta\rho_{\Lambda(H)}/\rho_{\rm cdm}$ in Eq. (4.49) reflect the rate of change in $v_{\rm cdm}$ attributable to the decay of dark energy. If this decay is solely due to an increase in the mass of cold dark matter particles – and provided the weak equivalence principle (i.e. the universality of free fall) holds [292] – Eq. (4.49) should reduce to its ΛCDM counterpart. With this in mind, one imposes the relation

$$\delta\rho_{\Lambda(H)} = -\frac{\psi}{k_\dagger}v_{\rm cdm}\,\rho_{\rm cdm} = \frac{\rho'_{\Lambda(H)}(\tau)}{k_\dagger}v_{\rm cdm} \ , \tag{4.50}$$

which is also valid if vacuum decay occurs via the only other alternative – particle production. Eq. (4.49) may hence be replaced with its ΛCDM equivalent:

$$v'_{\rm cdm}(\tau) + \mathcal{H}v_{\rm cdm} - k_\dagger\Phi = 0 \ . \tag{4.51}$$

Thus far, we have been considering the conservation of energy-momentum for cold dark matter and dark energy. As previously mentioned, baryons are conserved separately, so in their case Eqs. (4.46) and (4.47) become

$$\delta'_{\rm b}(\tau) = -k_\dagger v_{\rm b} + 3\Phi'(\tau) \ ; \tag{4.52}$$

$$v'_{\rm b}(\tau) + \mathcal{H}v_{\rm b} - k_\dagger\Phi = 0 \ . \tag{4.53}$$

The contrast function and velocity potential may be cast in a form that accounts for baryons and cold dark matter jointly (the subscript 'm' simply stands for 'matter'):

$$\delta_{\rm m} = \frac{\rho_{\rm cdm}\delta_{\rm cdm} + \rho_{\rm b}\delta_{\rm b}}{\rho_{\rm cdm} + \rho_{\rm b}} \ ; \quad v_{\rm m} = \frac{v_{\rm cdm}\rho_{\rm cdm} + v_{\rm b}\rho_{\rm b}}{\rho_{\rm cdm} + \rho_{\rm b}} \ . \tag{4.54}$$

The above definitions make it possible to combine Eqs. (4.51) and (4.53) into one

equation that reads:

$$v'_{\rm m}(\tau) + \mathcal{H} v_{\rm m} - k_\dagger \Phi = 0 \ . \tag{4.55}$$

The details are given in Appendix A. Similarly, Eqs. (4.48) and (4.52) may be conjointly expressed as:

$$\delta'_{\rm m}(\tau) + \psi \delta_{\rm m} = -k_\dagger v_{\rm m} + 3\Phi'(\tau) \ . \tag{4.56}$$

Differentiating this with respect to τ and inserting Eq. (4.55) into the result yields

$$\delta''_{\rm m}(\tau) + \psi \delta'_{\rm m}(\tau) + \psi'(\tau)\delta_{\rm m} + k_\dagger^2 \Phi - k_\dagger \mathcal{H} v_{\rm m} - 3\Phi''(\tau) = 0 \ . \tag{4.57}$$

Next, we apply the sub-horizon and quasi-static approximations to Eq. (4.45), and find that

$$\Phi(k_\dagger^2 - 3\kappa) + 4\pi G a^2 \left(\rho_{\rm cdm}\delta_{\rm cdm} + \rho_{\rm b}\delta_{\rm b} + \delta\rho_{\Lambda(H)} \right) = 0 \ . \tag{4.58}$$

The above equation can be further simplified by recalling that $\delta\rho_{\Lambda(H)} \ll \delta\rho_{\rm cdm}$ on sub-horizon scales. Moreover, values of the comoving wave number $k_\dagger$ in the relevant range – that is, the range that most contributes to the integral in Eq. (4.72) [290] – can be shown to satisfy $k_\dagger^2 \gg |\kappa|$. Therefore, the final version of Eq. (4.45) is simply:

$$k_\dagger^2 \Phi + 4\pi G a^2 \rho_{\rm m} \delta_{\rm m} = 0 \ , \tag{4.59}$$

where $\rho_{\rm m}\delta_{\rm m} = (\rho_{\rm cdm} + \rho_{\rm b})\,\delta_{\rm m} = \rho_{\rm cdm}\delta_{\rm cdm} + \rho_{\rm b}\delta_{\rm b}$ [refer to Eq. (4.54)]. Finally, Eq. (4.59) is inserted into Eq. (4.57) along with Eq. (4.56). The result is a second-order differential equation that stipulates how matter density perturbations evolve:

$$\delta''_{\rm m}(\tau) + \delta'_{\rm m}(\tau)(\psi + \mathcal{H}) + \delta_{\rm m}\left[\psi'(\tau) + \psi\mathcal{H} - 4\pi G a^2 \rho_{\rm m} \right] = 0 \ . \tag{4.60}$$

The absence of any terms in $\Phi'(\tau)$ or $\Phi''(\tau)$ is a consequence of employing the sub-Hubble and quasi-static approximations, as explained in Appendix A. In terms of the scale factor a, the above equation reads:

$$\delta''_{\rm m}(a) + \frac{F_1(a)}{a}\delta'_{\rm m}(a) + \frac{F_2(a)}{a^2}\delta_{\rm m}(a) = 0 \ , \tag{4.61}$$

with

$$\begin{aligned} F_1(a) &= 2 + \frac{a\mathcal{H}'(a) + \psi}{\mathcal{H}} \ ; \\ F_2(a) &= \frac{a\psi'(a) + \psi}{\mathcal{H}} - \frac{4\pi G a^2 \rho_{\rm m}}{\mathcal{H}^2} \ . \end{aligned} \tag{4.62}$$

We are now in a position to derive initial conditions for $\delta_{\rm m}$ and $\delta'_{\rm m}(a)$. Let us start by finding the approximate form that $\rho_{\rm cdm}$ and $\rho_{\Lambda(H)}$ take deep in the matter-dominated epoch. We return to Eqs. (4.26) and (4.27) and look for the dominant terms by taking a number of factors into account, such as the order of magnitude of the ratios $\Omega^0_{\rm m}/\Omega^0_{\rm r}$ and $\Omega^0_{\rm m}/\Omega^0_k$, the value of a at which the initial conditions will be applied ($a = 0.01$), and the fact that B and C are expected to be much less than unity – which makes it possible to expand algebraic functions of B and/or C via the binomial theorem. To first order in B and C, the final expressions read:

$$\rho_{\rm m} \approx \frac{3H_0^2}{8\pi G}\Omega^0_{\rm m} a^{B-3-3C/2} \ , \quad \Omega^0_{\rm m} = \Omega^0_{\rm b} + \Omega^0_{\rm cdm} \ , \tag{4.63}$$

$$\rho_{\Lambda(H)} \approx \frac{3H_0^2}{8\pi G}\left[\Omega^0_{\Lambda(H)} + \frac{1}{6}(2B-3C)\Omega^0_{\rm m} a^{B-3-3C/2}\right] \ . \tag{4.64}$$

These are used in conjunction with Eq. (4.24) to obtain an approximation for $\mathcal{H}$:

$$\mathcal{H} \approx H_0\sqrt{\Omega^0_{\rm m}}\left[1 + \frac{1}{12}(2B-3C)\right] a^{(2B-3C-2)/4} \ , \tag{4.65}$$

while combining Eqs. (4.63)–(4.65) allows us to write ψ as:

$$\begin{aligned}\psi &= -\frac{\rho'_{\Lambda(H)}(\tau)}{\rho_{\rm m}} = -\frac{\rho'_{\Lambda(H)}(a)\mathcal{H}a}{\rho_{\rm m}} \ , \\ &\approx \frac{1}{2}(2B-3C)H_0\sqrt{\Omega^0_{\rm m}}\, a^{(2B-3C-2)/4} \ .\end{aligned} \tag{4.66}$$

Next, the above results are inserted into Eq. (4.62) to estimate F_1 and F_2, and it is found that:

$$F_1 \approx \frac{1}{4}(6 + 6B - 9C) \ , \ F_2 \approx \frac{1}{2}(-3 + 2B - 3C) \ . \tag{4.67}$$

Eq. (4.61) may finally be solved analytically. The expression obtained for the density contrast function is a sum of two modes:

$$\delta_{\rm m} = A_1 a^{1-B+3C/2} + A_2 a^{(-6-2B+3C)/4} \ , \tag{4.68}$$

a growing mode and a decaying one. The latter is expected to be subdominant at the redshifts of interest ($z \lesssim 100$), and so only the former is retained:

$$\delta_{\rm m} = A_1 a^{1-B+3C/2} \ . \tag{4.69}$$

This is the 'initial' condition that is assigned to $\delta_{\rm m}$ at $a = 0.01$. Taking its derivative

with respect to a yields the corresponding initial value for $\delta'_{\mathrm{m}}(a)$. We shall deal with the constant of integration (A_1) below.

The standard deviation of density perturbations (σ_8)

The variance of the perturbation density field in spheres of radius $R_8 = 8\,h^{-1}$ Mpc may be calculated as follows [288, 293]:

$$\sigma^2_{8,0} = \frac{1}{2\pi^2} \int\limits_0^\infty P(k_\dagger) W^2(k_\dagger) k_\dagger^2 \, \mathrm{d}k_\dagger \ . \tag{4.70}$$

Here, $P(k_\dagger)$ is the present-day power spectrum, and the function $W(k_\dagger)$ represents the Fourier transform of a spherical top-hat window function having radius R_8:

$$W(k_\dagger) = \frac{3}{k_\dagger^2 R_8^2} \left[\frac{\sin\left(k_\dagger R_8\right)}{k_\dagger R_8} - \cos\left(k_\dagger R_8\right) \right] \ . \tag{4.71}$$

An expression for $P(k_\dagger)$ is constructed as outlined in Refs. [215] and [290]. The result is inserted into Eq. (4.70), and we get that

$$\sigma^2_8(a) = \delta^2_{\mathrm{m}}(a) \int\limits_0^\infty k_\dagger^{2+n_s} \left[\frac{4}{25} \frac{A_s \, k_*^{1-n_s}}{H_0^4 \left(\Omega^0_{\mathrm{m}}\right)^2} \right] T^2(k_\dagger) W^2(k_\dagger) \, \mathrm{d}k_\dagger \ , \tag{4.72}$$

where use has been made of Eq. (4.44). The absence of the normalising factor $[\delta_{\mathrm{m}}(1)]$ is due to the fact that we account for it indirectly by putting the integration factor of Eq. (4.69) equal to unity.

The quantities n_s and A_s that appear in Eq. (4.72) are the index and amplitude of the primordial scalar power spectrum, respectively, defined at a pivot scale k_* of $0.05\,\mathrm{Mpc}^{-1}$ [294]. A_s is either fixed by setting $\ln\left(10^{10} A_s\right)$ equal to the *Planck* 2015 TT+lowP+lensing mean value of 3.062 [22] or treated as a free parameter. In the latter case, a likelihood is constructed for A_s by assuming that it is sampled from a Gaussian distribution whose mean and standard deviation are given by $(2.139 \pm 0.063) \times 10^{-9}$ [22]. The primordial spectral index n_s is allowed to vary subject to the CMB constraint of Ref. [277] ($n_s = 0.9680 \pm 0.0051$), while the matrix of Eq. (4.38) is updated to include the correlation between n_s and the parameters $\mathscr{R}$, l_{A} and $\Omega^0_{\mathrm{b}} h^2$ (which is also provided in Ref. [277]). Finally, the transfer function $T(k_\dagger)$ is modelled as specified in the work of Eisenstein and Hu [295]. $T(k_\dagger)$ describes how

perturbations evolve as they cross the horizon and as matter begins to dominate [296], and computing it requires that we estimate the wave number ($k_\dagger^{\rm eq}$) of the mode that crosses the horizon at matter-radiation equality.

An approximation for $k_\dagger^{\rm eq}$ is arrived at by following the method of Ref. [290]. Terms whose order in B and C is higher than linear are discarded, and the fact that the scale factor at equality satisfies $a \sim \mathcal{O}(10^{-3})$ is used to remove subdominant terms. The resulting expression reads:

$$k_\dagger^{\rm eq} \approx \sqrt{2}\, H_0 \frac{\Omega_{\rm m}^0}{\sqrt{\Omega_{\rm r}^0}} \left[1 - \frac{7B}{6} + \frac{19C}{8} + \frac{2\Omega_k^0}{3\Omega_{\rm m}^0}(C-B) + \left(B - \frac{3C}{2} \right) \ln\left(\frac{\Omega_{\rm r}^0}{\Omega_{\rm m}^0} \right) \right] . \quad (4.73)$$

TABLE 4.5: LSS data from the compilation presented in Ref. [288]. Each $f\sigma_8$ measurement is listed together with the corresponding redshift z and error σ. Column 5 shows the values of $\Omega_{\rm m}^0$ for the respective fiducial cosmologies.

Ref.	z	$f\sigma_8(z)$	σ	$\Omega_{\rm m,0}^{\rm fid}$
[21, 297]	0.02	0.3140	0.0480	0.266
[298]	0.17	0.5100	0.0600	0.300
[299]	0.18	0.3600	0.0900	0.270
[299]	0.38	0.4400	0.0600	0.270
[300]	0.25	0.3512	0.0583	0.250
[300]	0.37	0.4602	0.0378	0.250
[301]	0.44	0.4130	0.0800	0.270
[301]	0.60	0.3900	0.0630	0.270
[301]	0.73	0.4370	0.0720	0.270
[302]	0.60	0.5500	0.1200	0.300
[302]	0.86	0.4000	0.1100	0.300
[303]	1.40	0.4820	0.1160	0.270

Constructing χ^2

The data employed (Table 4.5) is a subset of the updated Gold-2017 compilation of Nesseris et al. [288, 304]. Apart from the $f\sigma_8$ values from Ref. [301] – which are correlated with each other – all data points are independent. Moreover, measurements derived from the same survey data as any of the observables associated with previ-

ous likelihoods (especially the BAO likelihood) are excluded. This is done to avoid potential correlations.

At a given redshift z_i, the theoretical prediction $f\sigma_8^{\rm th}$ is computed by combining $\sigma_8(z_i)$ with the growth rate $f(z_i)$ returned by CLASS. The quantity $\sigma_8(z_i)$ itself is obtained from Eq. 4.72.

The χ^2 to be minimised is constructed as follows [305]:

$$\chi^2 = V^i C_{ij}^{-1} V^j \ . \tag{4.74}$$

In the above, C is the covariance matrix, assembled as described in Refs. [288] and [304], and the vector V contains elements of the form[68] [305]

$$V^i = f\sigma_8^{\rm obs}(z_i) - f\sigma_8^{\rm th}(z_i)/r^i_{\rm AP} \ , \tag{4.75}$$

$f\sigma_8^{\rm obs}(z_i)$ being the $i^{\rm th}$ data point from Table 4.5. The factor $1/r^i_{\rm AP}$ is designed to correct for the Alcock-Paczynski (AP) effect. As was also the case with BAO data, each of the studies from which the values in Table 4.5 are quoted makes use of a different fiducial cosmology to convert redshifts to distances. If the fiducial cosmology is not the same as the true one, the data incorporates an additional anisotropy that is degenerate with RSDs [305]. This is the above-mentioned AP effect [306]. One way of correcting for it involves multiplying the observational value of $f\sigma_8(z_i)$ and its associated error by the ratio [307]

$$r^i_{\rm AP} = \frac{H(z_i) d_{\rm A}(z_i)}{H^{\rm fid}(z_i) d^{\rm fid}_{\rm A}(z_i)} \ . \tag{4.76}$$

A superscript 'fid' indicates quantities calculated in the framework of the respective fiducial cosmologies (flat ΛCDM).

Alternatively, one may simply rescale $f\sigma_8^{\rm th}(z_i)$ by $1/r^i_{\rm AP}$ [305], as done in Eq. (4.75).

[68] There is no summation over i in Eq. (4.75); z_i is simply the redshift of the $i^{\rm th}$ data point from Table 4.5.

4.6 Results

4.6.1 Preliminaries

The joint likelihood on which our analysis is based is specified by the function

$$\mathscr{L}_{\text{tot}} \propto \exp\left[-\frac{1}{2}\left(\chi^2_{\text{JLA}} + \chi^2_{H(z)} + \chi^2_{\text{CMB}} + \chi^2_{\text{BAO}} + \chi^2_{\text{LSS}}\right)\right], \tag{4.77}$$

where the relation $\mathscr{L}_i \propto \exp\left(-\chi_i^2/2\right)$ has been used for each likelihood considered in section 4.5. The full data set – consisting of the JLA + $H(z)$ + CMB + BAO + LSS measurements – shall be referred to as All + LSS, and as the All data set when LSS observations are excluded.

In order to investigate how results are affected by the value of the Hubble constant, the parameters of each model are constrained six times, first using the All data set, then extending this to JLA + $H(z)$ + CMB + BAO + H_0^{R} $\left(\text{All} + H_0^{\text{R}}\right)$ and to JLA + $H(z)$ + CMB + BAO + H_0^{E} $\left(\text{All} + H_0^{\text{E}}\right)$, and finally repeating the whole procedure with the All+LSS data set replacing All. H_0^{R} is the value of H_0 reported by Riess et al. [26] and equates to 73.48 ± 1.66 km s^{-1} Mpc^{-1}. As for H_0^{E}, this stands for the Hubble constant as determined by Efstathiou [308] and amounts to 70.6 ± 3.3 km s^{-1} Mpc^{-1}. We shall not include the *Planck* result [20], opting instead for values of H_0 which were derived independently of any cosmological model.

One of the topics currently at the forefront of cosmological research is the growing discrepancy between – on the one hand – the value of H_0 determined locally from Cepheid parallax measurements [26], and on the other, that obtained in a ΛCDM framework using measurements of CMB observables. It turns out that H_0^{R} is in a 3.5σ tension with the *Planck* 2018 value ($H_0 = 67.27 \pm 0.60$ km s^{-1}Mpc^{-1}) [20]. One reason for the said tension could be the presence of systematic errors in the data used by either group. However, despite the investigative studies carried out, no obvious problem has been identified so far (refer to [20] and works cited therein). The other possibility is that this discrepancy provides compelling evidence for new physics [309–311].

In conclusion, the lack of consensus about the value of the Hubble constant makes it imperative to consider different options for H_0, especially since, as we later find out from the posterior probability plots, there is significant correlation between H_0 and

TABLE 4.6: The flat priors for the baseline parameters.

Parameter	Min	Max
H_0 $\left(\text{km s}^{-1}\text{Mpc}^{-1}\right)$	50	95
$\Omega_{\text{b}}^0 h^2$	0.005	0.100
$\Omega_{\text{cdm}}^0 h^2$	0.01	0.99
Ω_k^0	-0.3	0.3
B	-1.0	1.0
C	-1.0	1.0
n_s	0.75	1.25

the model parameters B and C.

The likelihood combinations just described are used to run MCMC chains and place constraints on the parameters of the GRVM, RVM and GRVS. The general baseline set Θ is given by[69] $\{H_0, \Omega_{\text{b}}^0 h^2, \Omega_{\text{cdm}}^0 h^2, \Omega_k^0, B, C, n_s\}$, although Ω_k^0 is set to zero for a flat space-time, and so is C (B) when the RVM (GRVS) is studied. Furthermore, the primordial spectral index is only considered a free parameter if LSS observations are included in the data sets. The reason is that n_s features explicitly in the LSS likelihood but is of minimal importance otherwise. We shall also differentiate between two scenarios in relation to the amplitude of the primordial power spectrum: the case with a fixed value of A_s, and that in which A_s is incorporated into Θ and allowed to vary freely. However, the two approaches yield very similar results, and consequently one need not distinguish between them when discussing the effects of introducing growth data.

The flat priors for the main baseline parameters are listed in Table 4.6. With the exception of the reionization redshift z_{reio} (which is set to 8.8 [22]), all other parameters take the CLASS default values.[70] In particular, this implies that the effective number of relativistic neutrino species (N_{eff}) is fixed at 3.046 [312], and the current CMB temperature (T_{CMB}) at 2.7255 K [313].

The plots presented in the next subsections were constructed using the MCMC analysis package GETDIST v.0.2.8 [314].

[69] The four nuisance parameters associated with the JLA likelihood (α, β, M and ΔM) also form part of Θ.

[70] The exception is A_s, and only when LSS data is included in the analysis. More details are provided in subsection 4.5.5.

4.6.2 The GRVM

The GRVM is characterised by two highly-correlated parameters, B and C. The constraints we get in the flat case are nonetheless tight enough to be informative (Fig. 4.7), but when Ω_k^0 is allowed to vary, the data used proves insufficient to break the degeneracy between B and C or between Ω_k^0 and the model parameters (Fig. 4.8).

TABLE 4.7: Mean values and 1σ confidence limits obtained with each data set combination in the context of a flat GRVM scenario. LSS observations were excluded from the analysis. Results for the baseline parameters are presented in the top block, whereas the last row is reserved for the derived parameter, $\Omega^0_{\Lambda(H)}$. H_0 is quoted in units of km s^{-1} Mpc^{-1}.

Parameter	ALL	ALL+$H_0^{\rm R}$	ALL+$H_0^{\rm E}$
H_0	$68.8330^{+1.6845}_{-1.6725}$	$71.1120^{+1.2073}_{-1.1912}$	$69.1850^{+1.4937}_{-1.4954}$
$10^3\,\Omega_{\rm b}^0 h^2$	$22.4090^{+0.1755}_{-0.1744}$	$22.4190^{+0.1747}_{-0.1726}$	$22.4110^{+0.1735}_{-0.1732}$
$\Omega^0_{\rm cdm} h^2$	$0.1217^{+0.0070}_{-0.0073}$	$0.1305^{+0.0056}_{-0.0059}$	$0.1230^{+0.0064}_{-0.0066}$
B	$0.0555^{+0.1660}_{-0.1430}$	$0.2341^{+0.1186}_{-0.1069}$	$0.0845^{+0.1491}_{-0.1306}$
C	$0.0365^{+0.1096}_{-0.0940}$	$0.1553^{+0.0776}_{-0.0701}$	$0.0558^{+0.0980}_{-0.0858}$
$\Omega^0_{\Lambda(H)}$	$0.6958^{+0.0070}_{-0.0067}$	$0.6976^{+0.0069}_{-0.0065}$	$0.6961^{+0.0069}_{-0.0066}$

TABLE 4.8: Mean values and 1σ confidence limits obtained with each data set combination in the context of a flat GRVM scenario. Double dashes indicate cases in which $\ln(10^{10}A_s)$ was assigned a fixed value.

Parameter	ALL+LSS	ALL+LSS+$H_0^{\rm R}$	ALL+LSS+$H_0^{\rm E}$	ALL+LSS	ALL+LSS+$H_0^{\rm R}$	ALL+LSS+$H_0^{\rm E}$
H_0	$67.5240^{+0.8710}_{-0.8880}$	$68.8020^{+0.7935}_{-0.8142}$	$67.7140^{+0.8367}_{-0.8635}$	$67.5440^{+0.8705}_{-0.8936}$	$68.8580^{+0.8092}_{-0.8326}$	$67.7460^{+0.8515}_{-0.8706}$
$10^3\Omega_{\rm b}^0 h^2$	$22.4140^{+0.1750}_{-0.1732}$	$22.4470^{+0.1729}_{-0.1742}$	$22.4210^{+0.1737}_{-0.1743}$	$22.4160^{+0.1732}_{-0.1734}$	$22.4460^{+0.1754}_{-0.1740}$	$22.4200^{+0.1728}_{-0.1724}$
$\Omega^0_{\rm cdm} h^2$	$0.1151^{+0.0024}_{-0.0025}$	$0.1170^{+0.0024}_{-0.0024}$	$0.1154^{+0.0024}_{-0.0025}$	$0.1152^{+0.0025}_{-0.0026}$	$0.1173^{+0.0025}_{-0.0026}$	$0.1155^{+0.0025}_{-0.0026}$
B	$-0.0491^{+0.1118}_{-0.1014}$	$0.0571^{+0.1022}_{-0.0933}$	$-0.0338^{+0.1088}_{-0.0996}$	$-0.0483^{+0.1114}_{-0.1027}$	$0.0619^{+0.1026}_{-0.0937}$	$-0.0301^{+0.1093}_{-0.1000}$
C	$-0.0340^{+0.0719}_{-0.0655}$	$0.0353^{+0.0657}_{-0.0602}$	$-0.0240^{+0.0700}_{-0.0644}$	$-0.0334^{+0.0718}_{-0.0662}$	$0.0385^{+0.0661}_{-0.0604}$	$-0.0215^{+0.0704}_{-0.0644}$
n_s	$0.9683^{+0.0052}_{-0.0052}$	$0.9688^{+0.0053}_{-0.0052}$	$0.9684^{+0.0053}_{-0.0052}$	$0.9683^{+0.0052}_{-0.0052}$	$0.9688^{+0.0052}_{-0.0052}$	$0.9683^{+0.0052}_{-0.0052}$
$\ln\left(10^{10}A_s\right)$	$--$	$--$	$--$	$3.0580^{+0.0310}_{-0.0294}$	$3.0503^{+0.0314}_{-0.0298}$	$3.0571^{+0.0309}_{-0.0296}$
$\Omega^0_{\Lambda(H)}$	$0.6983^{+0.0067}_{-0.0065}$	$0.7052^{+0.0062}_{-0.0059}$	$0.6993^{+0.0066}_{-0.0064}$	$0.6982^{+0.0068}_{-0.0064}$	$0.7051^{+0.0062}_{-0.0060}$	$0.6993^{+0.0066}_{-0.0063}$

The challenges posed by the fact that B is correlated with C are also highlighted in Ref. [214]. In this work, the authors find a way around the problem by defining a particular combination of $\nu\,(=B/3)$ and $\alpha\,(=C/2)$ as another effective parameter – labeled $\nu_{\rm eff}$ – that is then constrained instead of the original two. They do this by

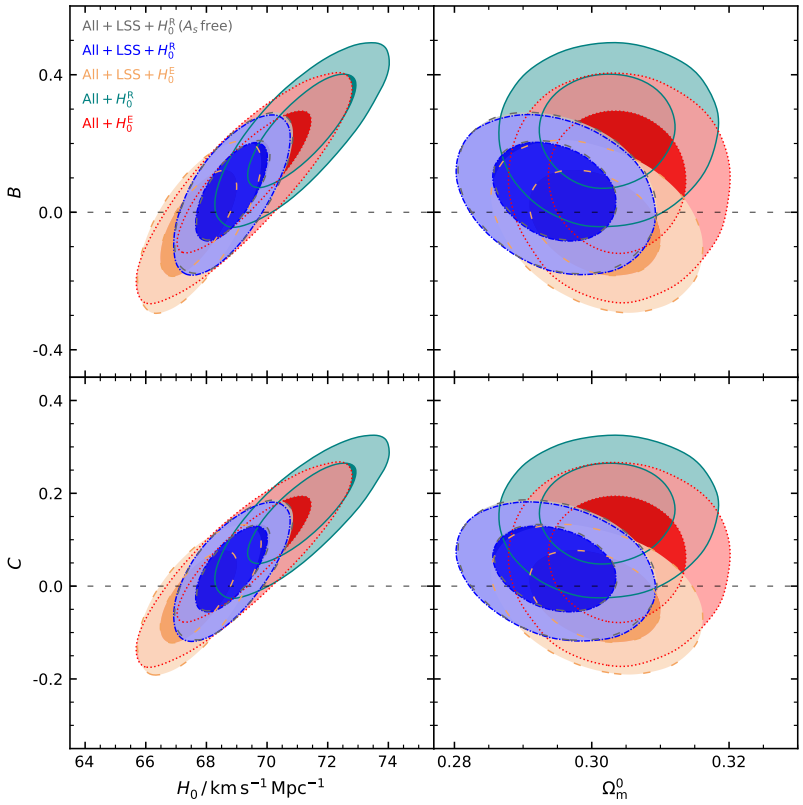

FIGURE 4.7: *(top panel)* Marginalised posterior probability distributions for the GRVM parameter B vs *(left)* H_0, *(right)* $\Omega_{\rm m}^0$. The bottom panel shows analogous plots for the second GRVM parameter, C. Darker (lighter) shades denote 1σ (2σ) confidence intervals (the first two data sets listed in the legend produce contours that overlap almost exactly). Space-time is assumed to be spatially flat.

TABLE 4.9: Mean values and 1σ confidence limits obtained with each data set combination in the context of a GRVM scenario. LSS observations were excluded from the analysis, and the condition of spatial flatness was not imposed.

Parameter	ALL	ALL+$H_0^{\rm R}$	ALL+$H_0^{\rm E}$
H_0	$68.8780^{+1.6279}_{-1.6844}$	$71.0800^{+1.1760}_{-1.1827}$	$69.2380^{+1.4922}_{-1.5051}$
$10^3\,\Omega_{\rm b}^0 h^2$	$22.4050^{+0.1754}_{-0.1715}$	$22.4180^{+0.1698}_{-0.1739}$	$22.4060^{+0.1719}_{-0.1725}$
$\Omega_{\rm cdm}^0 h^2$	$0.1219^{+0.0069}_{-0.0072}$	$0.1303^{+0.0055}_{-0.0058}$	$0.1232^{+0.0063}_{-0.0067}$
Ω_k^0	$-0.0019^{+0.0121}_{-0.0110}$	$-0.0020^{+0.0067}_{-0.0150}$	$-0.0023^{+0.0109}_{-0.0124}$
B	$0.1068^{+0.7911}_{-0.3660}$	$0.2685^{+0.7313}_{-0.1610}$	$0.1587^{+0.8389}_{-0.2599}$
C	$0.0688^{+0.5045}_{-0.2378}$	$0.1765^{+0.4745}_{-0.1036}$	$0.1027^{+0.5202}_{-0.1861}$
$\Omega_{\Lambda(H)}^0$	$0.6978^{+0.0143}_{-0.0144}$	$0.6998^{+0.0173}_{-0.0110}$	$0.6986^{+0.0145}_{-0.0140}$

TABLE 4.10: Mean values and 1σ confidence limits obtained with each data set combination in the context of a GRVM scenario. Ω_k^0 was treated as a free parameter.

Parameter	ALL+LSS	ALL+LSS+$H_0^{\rm R}$	ALL+LSS+$H_0^{\rm E}$	ALL+LSS	ALL+LSS+$H_0^{\rm R}$	ALL+LSS+$H_0^{\rm E}$
H_0	$67.7460^{+0.8958}_{-0.9245}$	$69.0740^{+0.7971}_{-0.8411}$	$67.8870^{+0.8656}_{-0.8824}$	$67.7420^{+0.9102}_{-0.9459}$	$69.1410^{+0.8361}_{-0.8330}$	$67.9370^{+0.8750}_{-0.8964}$
$10^3\Omega_{\rm b}^0h^2$	$22.4070^{+0.1716}_{-0.1729}$	$22.4430^{+0.1723}_{-0.1756}$	$22.4140^{+0.1743}_{-0.1733}$	$22.4090^{+0.1716}_{-0.1730}$	$22.4400^{+0.1664}_{-0.1741}$	$22.4180^{+0.1739}_{-0.1709}$
$\Omega_{\rm cdm}^0h^2$	$0.1157^{+0.0026}_{-0.0028}$	$0.1180^{+0.0026}_{-0.0027}$	$0.1160^{+0.0026}_{-0.0028}$	$0.1159^{+0.0027}_{-0.0028}$	$0.1183^{+0.0027}_{-0.0026}$	$0.1162^{+0.0027}_{-0.0028}$
Ω_k^0	$-0.0050^{+0.0106}_{-0.0141}$	$-0.0073^{+0.0064}_{-0.0155}$	$-0.0029^{+0.0105}_{-0.0124}$	$-0.0035^{+0.0111}_{-0.0129}$	$-0.0062^{+0.0071}_{-0.0160}$	$-0.0040^{+0.0108}_{-0.0149}$
B	$0.1637^{+0.8362}_{-0.2790}$	$0.3591^{+0.6489}_{-0.2050}$	$0.0834^{+0.6882}_{-0.4039}$	$0.0979^{+0.7169}_{-0.4212}$	$0.3148^{+0.6953}_{-0.3449}$	$0.1248^{+0.8194}_{-0.3556}$
C	$0.1019^{+0.5339}_{-0.1816}$	$0.2282^{+0.4148}_{-0.1312}$	$0.0508^{+0.4411}_{-0.2577}$	$0.0599^{+0.4592}_{-0.2687}$	$0.2000^{+0.4444}_{-0.2230}$	$0.0773^{+0.5241}_{-0.2270}$
n_s	$0.9680^{+0.0052}_{-0.0051}$	$0.9687^{+0.0050}_{-0.0052}$	$0.9682^{+0.0053}_{-0.0052}$	$0.9681^{+0.0051}_{-0.0052}$	$0.9686^{+0.0051}_{-0.0052}$	$0.9682^{+0.0049}_{-0.0053}$
$\ln\left(10^{10}A_s\right)$	$--$	$--$	$--$	$3.0584^{+0.0311}_{-0.0293}$	$3.0514^{+0.0309}_{-0.0275}$	$3.0578^{+0.0302}_{-0.0293}$
$\Omega_{\Lambda(H)}^0$	$0.7038^{+0.0170}_{-0.0132}$	$0.7128^{+0.0193}_{-0.0091}$	$0.7024^{+0.0154}_{-0.0130}$	$0.7021^{+0.0152}_{-0.0144}$	$0.7116^{+0.0198}_{-0.0102}$	$0.7034^{+0.0176}_{-0.0141}$

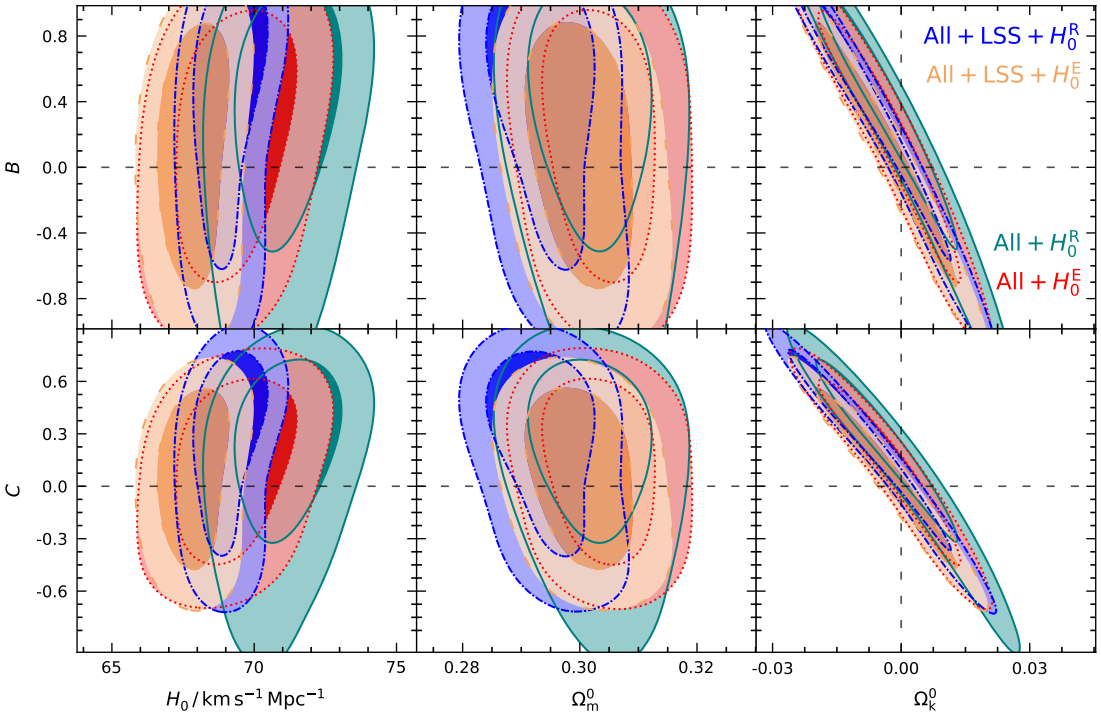

FIGURE 4.8: *(top panel)* Marginalised posterior probability distributions for the GRVM parameter B vs *(left)* H_0, *(centre)* $\Omega_{\rm m}^0$, *(right)* Ω_k^0. The bottom panel shows analogous plots for the second GRVM parameter, C.

making the approximation

$$\xi = \frac{1-\nu}{1-\alpha} \sim 1-(\nu-\alpha) \equiv 1-\nu_{\rm eff}\ , \tag{4.78}$$

which is justified on the basis that $|\nu|$ and $|\alpha|$ must both be much smaller than unity if the deviation from ΛCDM is to be mild. The parameter ξ controls the way the

matter energy density ($\rho_{\rm m}$) scales with a, and for the purposes of data fitting the authors assume that $\rho_{\rm r}$ evolves as in the standard model.

There are several reasons, however, why the approach outlined in Ref. [214] cannot be taken here. To begin with, the authors determine $\rho_{\rm m}$ and $\rho_{\rm r}$ in terms of a by considering the cosmic fluid to have only two components at any given time – dynamical dark energy and either matter or radiation, depending on which of the two dominates. The expressions thus obtained are then used to formulate $\rho_{\Lambda(H)}$ as a function of $\rho_{\rm m}$ and $\rho_{\rm r}$. The fact that we do not simplify our analysis likewise introduces more terms into the relevant equations, as does the decision to treat Ω_k^0 as a free parameter for part of the study. In conclusion, the relations we get for $\rho_{\rm cdm}$ and $\rho_{\Lambda(H)}$ – Eqs. (4.26) and (4.27), respectively – include several different combinations of B and C, so that it is not possible to reduce the number of degrees of freedom as detailed in Ref. [214].

The constraints one gets in the context of a flat geometry are nonetheless instructive. The most prominent feature of Fig. 4.7 is the shift in the marginalised 2D posteriors that is brought about by the addition of LSS data. Table 4.8 shows that (in the absence of the $H_0^{\rm R}$ likelihood) this shift results in negative mean values for B and C – rather than the positive ones obtained otherwise (Table 4.7). A second characteristic which emerges in Fig. 4.7 is the correlation between B (or C) and H_0. In the case of B, this behaviour is in stark contrast with the negative correlation observed in the RVM scenario (Figs. 4.9 and 4.10). The fact that a larger value of H_0 favours a larger B explains why, in the top panel of Fig. 4.7 , the contours corresponding to the $\textsc{All} + H_0^{\rm R}$ and $\textsc{All} + \textsc{LSS} + H_0^{\rm R}$ data sets have a marked shift in the direction of increasing B relative to their $H_0^{\rm E}$ counterparts. The same holds true for C (Fig. 4.7, bottom panel). Consequently, in the context of a flat geometry, the $\textsc{All} + H_0^{\rm R}$ mean values of B and C are inconsistent with zero within a 1σ confidence interval. However, Fig. 4.7 plainly demonstrates that the introduction of growth data causes the contours to close around the ΛCDM limit. Additionally, the 2D posteriors for B (or C) vs H_0 make it clear that LSS data lends support to the Hubble constant as established by *Planck* $\left(H_0 = 67.27 \pm 0.60\,{\rm km\,s^{-1}Mpc^{-1}}\right)$ [20], rather than to $H_0^{\rm R}$. This may be observed in both the flat and non-flat cases (results for the latter are shown in Tables 4.9 and 4.10). We find that even the $\textsc{All} + H_0^{\rm R}$ mean values for H_0 become more compatible with the *Planck* constraints when the LSS likelihood is added. Moreover, the Hubble constant from *Planck* is endorsed irrespectively of whether A_s is allowed to vary, which makes it less likely that this is an indirect consequence of using the ΛCDM value for A_s. Before the possibility can be ruled out, however, one would need

to repeat the procedure with a wider Gaussian likelihood for A_s.[71]

4.6.3 The RVM

The results for the RVM are summarised in Tables 4.11–4.14. As can be deduced from Figs. 4.9 and 4.10 (left panel), there is significant negative correlation between the model parameter B and the Hubble constant H_0, although in the flat case the use of LSS data makes this much less pronounced. The said correlation explains why including $H_0^{\rm R}$ with the observational data – rather than the lower value of $H_0^{\rm E}$ – shifts the corresponding contours in all the plots of Figs. 4.9 and 4.10 downwards, in the direction of decreasing B.

TABLE 4.11: Mean values and 1σ confidence limits obtained with each data set combination in the context of a flat RVM scenario. LSS observations were excluded from the analysis. Results for the baseline parameters are presented in the top block, whereas the last row is reserved for the derived parameter, $\Omega^0_{\Lambda(H)}$. H_0 is quoted in units of km s^{-1} Mpc^{-1}.

Parameter	ALL	ALL+$H_0^{\rm R}$	ALL+$H_0^{\rm E}$
H_0	$67.4240^{+0.4759}_{-0.4944}$	$67.8950^{+0.4785}_{-0.4939}$	$67.4900^{+0.4723}_{-0.4939}$
$10^3\,\Omega^0_{\rm b}h^2$	$22.3030^{+0.1380}_{-0.1387}$	$22.3830^{+0.1378}_{-0.1373}$	$22.3140^{+0.1393}_{-0.1383}$
$\Omega^0_{\rm cdm}h^2$	$0.1175^{+0.0032}_{-0.0035}$	$0.1190^{+0.0033}_{-0.0036}$	$0.1177^{+0.0032}_{-0.0035}$
10^3B	$3.0279^{+3.1358}_{-3.1698}$	$1.0225^{+3.1603}_{-3.1745}$	$2.7498^{+3.1121}_{-3.1691}$
$\Omega^0_{\Lambda(H)}$	$0.6925^{+0.0066}_{-0.0064}$	$0.6932^{+0.0067}_{-0.0064}$	$0.6926^{+0.0066}_{-0.0064}$

TABLE 4.12: Mean values and 1σ confidence limits obtained with each data set combination in the context of a flat RVM scenario. Double dashes indicate cases in which $\ln(10^{10}A_s)$ was assigned a fixed value.

Parameter	ALL+LSS	ALL+LSS+$H_0^{\rm R}$	ALL+LSS+$H_0^{\rm E}$	ALL+LSS	ALL+LSS+$H_0^{\rm R}$	ALL+LSS+$H_0^{\rm E}$
H_0	$67.8130^{+0.6130}_{-0.6275}$	$68.4770^{+0.5816}_{-0.5896}$	$67.9030^{+0.6059}_{-0.6135}$	$67.8270^{+0.6179}_{-0.6319}$	$68.5050^{+0.5812}_{-0.6036}$	$67.9160^{+0.6059}_{-0.6155}$
$10^3\Omega^0_{\rm b}h^2$	$22.3780^{+0.1568}_{-0.1561}$	$22.4970^{+0.1517}_{-0.1497}$	$22.3940^{+0.1551}_{-0.1551}$	$22.3800^{+0.1550}_{-0.1560}$	$22.4990^{+0.1512}_{-0.1509}$	$22.3960^{+0.1548}_{-0.1547}$
$\Omega^0_{\rm cdm}h^2$	$0.1158^{+0.0019}_{-0.0019}$	$0.1161^{+0.0019}_{-0.0019}$	$0.1159^{+0.0019}_{-0.0019}$	$0.1159^{+0.0019}_{-0.0020}$	$0.1163^{+0.0019}_{-0.0020}$	$0.1160^{+0.0019}_{-0.0020}$
10^3B	$3.6665^{+1.9661}_{-2.0391}$	$2.3309^{+1.8986}_{-1.9689}$	$3.4801^{+1.9351}_{-2.0277}$	$3.5647^{+2.0408}_{-2.1165}$	$2.1456^{+1.9740}_{-2.0357}$	$3.3725^{+2.0146}_{-2.0964}$
n_s	$0.9670^{+0.0045}_{-0.0046}$	$0.9705^{+0.0044}_{-0.0044}$	$0.9675^{+0.0045}_{-0.0045}$	$0.9671^{+0.0046}_{-0.0045}$	$0.9706^{+0.0044}_{-0.0044}$	$0.9675^{+0.0045}_{-0.0045}$
$\ln\left(10^{10}A_s\right)$	$--$	$--$	$--$	$3.0564^{+0.0307}_{-0.0294}$	$3.0525^{+0.0311}_{-0.0294}$	$3.0559^{+0.0308}_{-0.0293}$
$\Omega^0_{\Lambda(H)}$	$0.6994^{+0.0063}_{-0.0061}$	$0.7043^{+0.0060}_{-0.0058}$	$0.7000^{+0.0062}_{-0.0060}$	$0.6993^{+0.0063}_{-0.0060}$	$0.7042^{+0.0060}_{-0.0058}$	$0.6999^{+0.0062}_{-0.0060}$

[71] A flat prior would not work well, as it would result in the LSS likelihood 'picking' values of A_s well outside the established range.

The introduction of LSS data is a game-changer. In the flat scenario, it reduces or even neutralizes the positive/negative correlation between B and the parameters H_0, $\Omega^0_{\rm m}$ and $\Omega^0_{\Lambda(H)}$ (Fig. 4.9). This makes the constraints on B less compatible with the ΛCDM limit, and indeed the new 1D posteriors for B exclude a null value at a little over 1σ. Similar behaviour is noted when Ω^0_k is allowed to vary. A few differences are worth mentioning, however: in the presence of spatial curvature, the effect of the LSS likelihood on the negative correlation between B and H_0 is less significant (Fig. 4.10). Furthermore, comparison of the average values of B in Tables 4.13 and 4.14 reveals that the addition of growth data changes their sign from negative to positive (which results from the tightening of contours around positive values of B; see Fig. 4.10). Another point of interest is the fact that while the ALL + $H_0^{\rm R}$ posteriors favour an open universe at more than 2σ, the inclusion of LSS data causes them to close up around $\Omega_k = 0$. Moreover, we note that the tendency of the LSS likelihood to select smaller values for the Hubble constant emerges again in the non-flat case. It may easily be deduced that the resulting mean values of H_0 resonate with the *Planck* constraint rather than with $H_0^{\rm R}$.

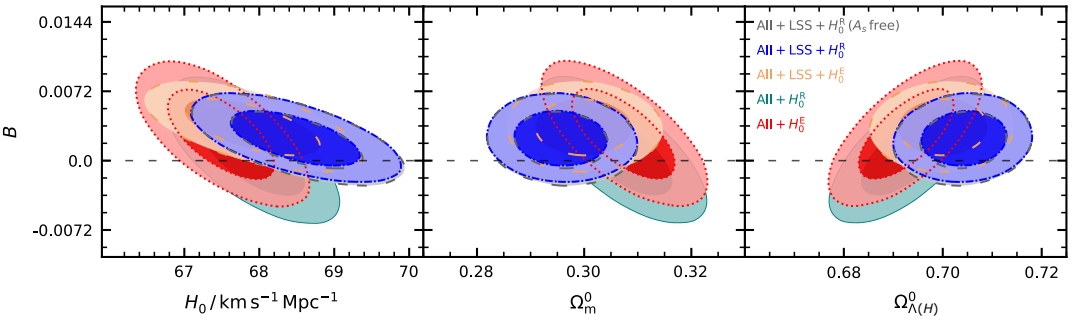

FIGURE 4.9: Marginalised posterior probability distributions for the RVM parameter B vs *(left)* H_0, *(centre)* $\Omega^0_{\rm m}$, *(right)* $\Omega^0_{\Lambda(H)}$. Space-time is assumed to be spatially flat.

Let us now take a look at the literature and see how our findings for the flat scenario fare in comparison.[72] The authors of Ref. [224] report that the RVM appears to be more consistent with observations than ΛCDM, and furthermore remark that the inclusion of an LSS likelihood tips the balance in favour of the *Planck* value for H_0. Our results paint a somewhat different picture. We find no statistically significant evidence that the RVM is preferred over ΛCDM (more details are provided in subsection 4.6.5). Secondly, the addition of LSS data increases the mean values of H_0 slightly when $\Omega^0_k = 0$, although one cannot say that it spoils the consistency

[72]The studies considered here are based on the assumption of spatial flatness.

with the *Planck* constraints. Nonetheless, once the conversion from ν to B $(= 3\nu)$ is made, the mean values of B and the corresponding uncertainties (Tables 4.11 and 4.12) are found to be of the same order of magnitude[73] as those obtained in Ref. [224] with the full data set.

TABLE 4.13: Mean values and 1σ confidence limits obtained with each data set combination in the context of an RVM scenario. LSS observations were excluded from the analysis, and the condition of spatial flatness was not imposed.

Parameter	ALL	ALL+$H_0^{\rm R}$	ALL+$H_0^{\rm E}$
H_0	$68.5350^{+1.5435}_{-1.5236}$	$70.7750^{+1.1456}_{-1.1488}$	$68.8920^{+1.4166}_{-1.3974}$
$10^3\,\Omega_{\rm b}^0 h^2$	$22.2870^{+0.1420}_{-0.1399}$	$22.2940^{+0.1409}_{-0.1396}$	$22.2870^{+0.1394}_{-0.1404}$
$\Omega_{\rm cdm}^0 h^2$	$0.1220^{+0.0066}_{-0.0069}$	$0.1309^{+0.0055}_{-0.0057}$	$0.1234^{+0.0062}_{-0.0065}$
$10^3\Omega_k^0$	$2.1474^{+2.9676}_{-2.6744}$	$5.9320^{+2.1120}_{-2.0502}$	$2.7793^{+2.6796}_{-2.5027}$
$10^3 B$	$-0.3265^{+4.9193}_{-5.8219}$	$-7.1221^{+3.6466}_{-4.1096}$	$-1.5054^{+4.6128}_{-5.2781}$
$\Omega_{\Lambda(H)}^0$	$0.6908^{+0.0069}_{-0.0068}$	$0.6883^{+0.0067}_{-0.0065}$	$0.6903^{+0.0068}_{-0.0067}$

TABLE 4.14: Mean values and 1σ confidence limits obtained with each data set combination in the context of an RVM scenario. Ω_k^0 was treated as a free parameter.

Parameter	ALL+LSS	ALL+LSS+$H_0^{\rm R}$	ALL+LSS+$H_0^{\rm E}$	ALL+LSS	ALL+LSS+$H_0^{\rm R}$	ALL+LSS+$H_0^{\rm E}$
H_0	$67.5010^{+0.8679}_{-0.8693}$	$68.7760^{+0.7858}_{-0.7956}$	$67.7000^{+0.8428}_{-0.8546}$	$67.5280^{+0.8876}_{-0.8918}$	$68.8250^{+0.8011}_{-0.8075}$	$67.7310^{+0.8496}_{-0.8716}$
$10^3\Omega_{\rm b}^0 h^2$	$22.4130^{+0.1730}_{-0.1696}$	$22.4500^{+0.1730}_{-0.1714}$	$22.4180^{+0.1728}_{-0.1723}$	$22.4120^{+0.1723}_{-0.1725}$	$22.4490^{+0.1724}_{-0.1725}$	$22.4190^{+0.1717}_{-0.1733}$
$\Omega_{\rm cdm}^0 h^2$	$0.1150^{+0.0026}_{-0.0026}$	$0.1170^{+0.0025}_{-0.0025}$	$0.1153^{+0.0025}_{-0.0026}$	$0.1151^{+0.0026}_{-0.0027}$	$0.1173^{+0.0026}_{-0.0027}$	$0.1154^{+0.0026}_{-0.0027}$
$10^3\Omega_k^0$	$-1.0358^{+2.1119}_{-2.0708}$	$1.0969^{+1.9576}_{-1.9154}$	$-0.6868^{+2.0555}_{-2.0362}$	$-0.9842^{+2.1179}_{-2.0898}$	$1.1876^{+1.9680}_{-1.9402}$	$-0.6480^{+2.0761}_{-2.0397}$
$10^3 B$	$4.0567^{+2.1064}_{-2.2043}$	$2.0203^{+1.9293}_{-2.0197}$	$3.7450^{+2.0332}_{-2.1945}$	$3.9637^{+2.1855}_{-2.3301}$	$1.7766^{+2.0335}_{-2.1403}$	$3.6112^{+2.1647}_{-2.2666}$
n_s	$0.9682^{+0.0052}_{-0.0051}$	$0.9689^{+0.0051}_{-0.0051}$	$0.9683^{+0.0052}_{-0.0052}$	$0.9682^{+0.0051}_{-0.0052}$	$0.9689^{+0.0052}_{-0.0052}$	$0.9683^{+0.0052}_{-0.0052}$
$\ln\left(10^{10}A_s\right)$	$--$	$--$	$--$	$3.0581^{+0.0311}_{-0.0292}$	$3.0504^{+0.0315}_{-0.0302}$	$3.0572^{+0.0312}_{-0.0294}$
$\Omega_{\Lambda(H)}^0$	$0.6994^{+0.0063}_{-0.0059}$	$0.7039^{+0.0060}_{-0.0057}$	$0.7001^{+0.0062}_{-0.0060}$	$0.6993^{+0.0063}_{-0.0061}$	$0.7036^{+0.0060}_{-0.0058}$	$0.7000^{+0.0063}_{-0.0060}$

The tendency of the RVM to lend support to the *Planck* bounds for H_0 is also pointed out in Ref. [225]. The authors find that $\nu = 0$ is excluded at more than 3σ when they include LSS data, and although our results do not corroborate this conclusion, the mean and uncertainty for ν again translate into values for B that match ours in order of magnitude. The same can be said of the constraints placed on ν in Ref. [226] by means of a fit to SNeIa+BAO+$H(z)$+LSS+BBN+CMB data. This despite the fact

[73] Two values ($a \times 10^p$ and $b \times 10^p$, where $1 \leq a, b < 10$ and p is an integer) shall be deemed to have the same magnitude if $|a - b| < 5$.
Given the quantity $M_{-\ell}^{+n}$, $n + \ell$ shall be referred to as the *uncertainty* in M.

that the study in question considers radiation to interact with dark energy, which is not the case here. We note that our mean values for B (excluding the ones obtained with the $\text{All} + H_0^{\text{R}}$ and $\text{All} + \text{LSS} + H_0^{\text{R}}$ data sets) have ν equivalents that lie within 1σ of the value found in Ref. [226] using the full dataset.

On the contrary, our results are in some tension with that of Ref. [218] [$\nu = B/3 = (1.37^{+0.72}_{-0.95}) \times 10^{-4}$]. The authors attribute their strong constraints on ν to the effectiveness of CMB temperature fluctuations as cosmological probes [218]. One should keep in mind, however, that the approach taken in Ref. [218] differs from ours in a number of ways, the most prominent being the assumption that dark energy decays into both radiation and matter, and the incorporation of massive neutrinos into the model.

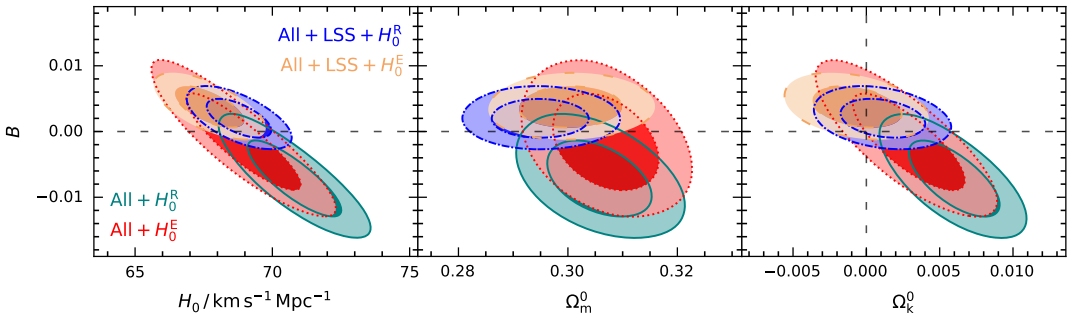

FIGURE 4.10: Marginalised posterior probability distributions for the RVM parameter B vs *(left)* H_0, *(centre)* Ω_{m}^0, *(right)* Ω_k^0.

We turn our attention to the study presented in Ref. [215] next. Here, the joint analysis is based on measurements of observables associated with SNeIa, BAOs, cosmic chronometers, LSS and the CMB, and again it transpires that the mean value of ν and associated standard deviation have the same order of magnitude as the ones we get (for $B/3$). The authors also investigate the impact of the individual likelihoods on the results, and observe that using both LSS and CMB data tightens constraints on ν, consequently endowing it with a definite sign. They go on to show that the absence of either makes ν compatible with the ΛCDM limit ($\nu = 0$). The authors conclude that the BAO+LSS+CMB combination excludes the standard model at more than 3σ.

Although some of the studies we've just reviewed allow radiation to couple with vacuum energy, we shall not do likewise. There is an important reason for this: namely, any interaction between radiation and dark energy would cause the CMB temperature (T_{CMB}) to scale differently with redshift than it does in ΛCDM. Additionally, any net changes in photon number would alter the relation between the angular diameter and

luminosity distances [315]. The literature contains many examples of studies that have constrained departures from the standard-model prediction for $T_{\rm CMB}$ [$T_{\rm CMB} \propto (1+z)$] [315–318], or placed bounds on violations of the distance-duality relation [319–322]. As yet, however, no compelling evidence of deviations from ΛCDM has been found. In other words, there is currently little observational justification for energy exchange between radiation and the vacuum to be incorporated into a cosmological model.

In the same vein, since $\Omega_{\rm b}^0$ is subject to very tight constraints, it is best to refrain from coupling the baryon component with dark energy, as this would alter the way in which $\rho_{\rm b}$ scales with redshift. The reader is referred to Refs. [323] and [324] (and the works cited therein) for a review of the said constraints.

4.6.4 The GRVS

Results are presented in Tables 4.15–4.18. The inclusion of LSS data again proves to be important. In the flat case, it tightens constraints on C and endows it with a definite (negative) sign, while also reducing (or even neutralizing) the correlation between C and the parameters H_0, $\Omega_{\rm m}^0$ and $\Omega_{\Lambda(H)}^0$ (Fig. 4.11). As a result, the 1D posteriors for C exclude the ΛCDM limit at a little over 1σ. The situation is in many ways analogous to the RVM scenario. When the assumption of spatial flatness is relaxed, we again find that LSS data shows mild preference for a closed (rather than open) geometry, and tends to decrease the mean values of H_0 (Fig. 4.12). Contrary to what was observed for the RVM, the latter effect is also noted in the flat case.

TABLE 4.15: Mean values and 1σ confidence limits obtained with each data set combination in the context of a flat GRVS scenario. LSS observations were excluded from the analysis. Results for the baseline parameters are presented in the top block, whereas the last row is reserved for the derived parameter, $\Omega_{\Lambda(H)}^0$. H_0 is quoted in units of km s^{-1} Mpc^{-1}.

Parameter	ALL	ALL+$H_0^{\rm R}$	ALL+$H_0^{\rm E}$
H_0	$68.2640^{+0.7812}_{-0.8232}$	$69.2520^{+0.7381}_{-0.7772}$	$68.3850^{+0.7663}_{-0.8033}$
$10^3\,\Omega_{\rm b}^0 h^2$	$22.4300^{+0.1647}_{-0.1640}$	$22.5740^{+0.1559}_{-0.1563}$	$22.4490^{+0.1627}_{-0.1617}$
$\Omega_{\rm cdm}^0 h^2$	$0.1193^{+0.0036}_{-0.0040}$	$0.1222^{+0.0037}_{-0.0041}$	$0.1197^{+0.0036}_{-0.0040}$
$10^3 C$	$-0.1050^{+2.4635}_{-2.4237}$	$2.2458^{+2.3401}_{-2.2670}$	$0.1792^{+2.4189}_{-2.3773}$
$\Omega_{\Lambda(H)}^0$	$0.6957^{+0.0069}_{-0.0066}$	$0.6980^{+0.0069}_{-0.0066}$	$0.6960^{+0.0069}_{-0.0066}$

TABLE 4.16: Mean values and 1σ confidence limits obtained with each data set combination in the context of a flat GRVS scenario. Double dashes indicate cases in which $\ln(10^{10}A_s)$ was assigned a fixed value.

Parameter	ALL+LSS	ALL+LSS+$H_0^{\rm R}$	ALL+LSS+$H_0^{\rm E}$	ALL+LSS	ALL+LSS+$H_0^{\rm R}$	ALL+LSS+$H_0^{\rm E}$
H_0	$67.7840^{+0.6186}_{-0.6298}$	$68.4770^{+0.5943}_{-0.5972}$	$67.8800^{+0.6095}_{-0.6200}$	$67.8000^{+0.6284}_{-0.6370}$	$68.4960^{+0.5958}_{-0.5968}$	$67.8990^{+0.6132}_{-0.6292}$
$10^3\Omega_{\rm b}^0h^2$	$22.3790^{+0.1543}_{-0.1565}$	$22.5010^{+0.1519}_{-0.1500}$	$22.3960^{+0.1540}_{-0.1539}$	$22.3820^{+0.1549}_{-0.1567}$	$22.5020^{+0.1501}_{-0.1493}$	$22.3980^{+0.1547}_{-0.1540}$
$\Omega_{\rm cdm}^0h^2$	$0.1157^{+0.0019}_{-0.0019}$	$0.1161^{+0.0019}_{-0.0019}$	$0.1158^{+0.0019}_{-0.0019}$	$0.1158^{+0.0019}_{-0.0020}$	$0.1163^{+0.0019}_{-0.0020}$	$0.1159^{+0.0020}_{-0.0020}$
10^3C	$-2.3810^{+1.3190}_{-1.2607}$	$-1.4761^{+1.2662}_{-1.2102}$	$-2.2558^{+1.2957}_{-1.2541}$	$-2.3120^{+1.3602}_{-1.3179}$	$-1.3684^{+1.3103}_{-1.2737}$	$-2.1795^{+1.3530}_{-1.3042}$
n_s	$0.9671^{+0.0045}_{-0.0045}$	$0.9706^{+0.0044}_{-0.0044}$	$0.9675^{+0.0044}_{-0.0044}$	$0.9671^{+0.0045}_{-0.0045}$	$0.9707^{+0.0044}_{-0.0044}$	$0.9676^{+0.0045}_{-0.0045}$
$\ln\left(10^{10}A_s\right)$	$--$	$--$	$--$	$3.0565^{+0.0309}_{-0.0295}$	$3.0522^{+0.0309}_{-0.0294}$	$3.0560^{+0.0310}_{-0.0292}$
$\Omega_{\Lambda(H)}^0$	$0.6993^{+0.0063}_{-0.0061}$	$0.7043^{+0.0060}_{-0.0057}$	$0.7000^{+0.0062}_{-0.0060}$	$0.6992^{+0.0063}_{-0.0061}$	$0.7041^{+0.0060}_{-0.0057}$	$0.6999^{+0.0062}_{-0.0060}$

The correlation between C and H_0 explains why the $H_0^{\rm R}$ likelihood shifts the contours in Figs. 4.11 and 4.12 in the direction of increasing C. The introduction of growth data makes this displacement much less pronounced.

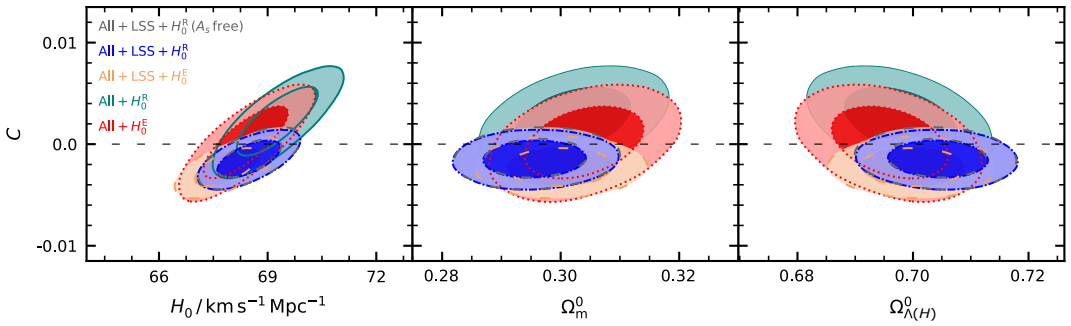

FIGURE 4.11: Marginalised posterior probability distributions for the GRVS parameter C vs *(left)* H_0, *(centre)* $\Omega_{\rm m}^0$, *(right)* $\Omega_{\Lambda(H)}^0$. Space-time is assumed to be spatially flat.

TABLE 4.17: Mean values and 1σ confidence limits obtained with each data set combination in the context of a GRVS scenario. LSS observations were excluded from the analysis, and the condition of spatial flatness was not imposed.

Parameter	ALL	ALL+$H_0^{\rm R}$	ALL+$H_0^{\rm E}$
H_0	$68.7530^{+1.5454}_{-1.5507}$	$70.9130^{+1.1628}_{-1.1578}$	$69.0730^{+1.4051}_{-1.4109}$
$10^3\,\Omega_{\rm b}^0h^2$	$22.4090^{+0.1726}_{-0.1718}$	$22.4320^{+0.1720}_{-0.1700}$	$22.4120^{+0.1716}_{-0.1715}$
$\Omega_{\rm cdm}^0h^2$	$0.1214^{+0.0066}_{-0.0070}$	$0.1298^{+0.0056}_{-0.0058}$	$0.1227^{+0.0062}_{-0.0064}$
$10^3\,\Omega_k^0$	$1.0452^{+2.9292}_{-2.7865}$	$4.3585^{+2.3047}_{-2.2526}$	$1.5638^{+2.7015}_{-2.6167}$
10^3C	$0.7443^{+3.7198}_{-3.2210}$	$4.9508^{+2.6763}_{-2.3946}$	$1.4163^{+3.3940}_{-2.9272}$
$\Omega_{\Lambda(H)}^0$	$0.6946^{+0.0074}_{-0.0073}$	$0.6928^{+0.0074}_{-0.0072}$	$0.6943^{+0.0074}_{-0.0072}$

TABLE 4.18: Mean values and 1σ confidence limits obtained with each data set combination in the context of a GRVS scenario. Ω_k^0 was treated as a free parameter.

Parameter	ALL+LSS	ALL+LSS+$H_0^{\rm R}$	ALL+LSS+$H_0^{\rm E}$	ALL+LSS	ALL+LSS+$H_0^{\rm R}$	ALL+LSS+$H_0^{\rm E}$
H_0	$67.5080^{+0.8646}_{-0.8940}$	$68.7710^{+0.7891}_{-0.7891}$	$67.7040^{+0.8326}_{-0.8632}$	$67.5270^{+0.8799}_{-0.9011}$	$68.8250^{+0.7975}_{-0.8066}$	$67.7270^{+0.8537}_{-0.8650}$
$10^3\Omega_{\rm b}^0h^2$	$22.4130^{+0.1718}_{-0.1742}$	$22.4490^{+0.1719}_{-0.1728}$	$22.4190^{+0.1739}_{-0.1709}$	$22.4140^{+0.1734}_{-0.1718}$	$22.4500^{+0.1720}_{-0.1716}$	$22.4170^{+0.1707}_{-0.1723}$
$\Omega_{\rm cdm}^0h^2$	$0.1150^{+0.0025}_{-0.0026}$	$0.1170^{+0.0025}_{-0.0025}$	$0.1153^{+0.0025}_{-0.0026}$	$0.1151^{+0.0026}_{-0.0027}$	$0.1173^{+0.0026}_{-0.0026}$	$0.1154^{+0.0026}_{-0.0027}$
$10^3\Omega_k^0$	$-0.9464^{+2.0824}_{-2.0889}$	$1.1408^{+1.9543}_{-1.9133}$	$-0.6118^{+2.0552}_{-2.0364}$	$-0.9229^{+2.1097}_{-2.0864}$	$1.2022^{+1.9458}_{-1.9261}$	$-0.5637^{+2.0727}_{-2.0289}$
10^3C	$-2.5839^{+1.4209}_{-1.3420}$	$-1.2927^{+1.2993}_{-1.2392}$	$-2.3797^{+1.3910}_{-1.3091}$	$-2.5323^{+1.4719}_{-1.4069}$	$-1.1341^{+1.3627}_{-1.2930}$	$-2.3232^{+1.4490}_{-1.3732}$
n_s	$0.9682^{+0.0052}_{-0.0052}$	$0.9689^{+0.0051}_{-0.0052}$	$0.9683^{+0.0052}_{-0.0051}$	$0.9682^{+0.0051}_{-0.0052}$	$0.9690^{+0.0051}_{-0.0052}$	$0.9683^{+0.0052}_{-0.0052}$
$\ln\left(10^{10}A_s\right)$	$--$	$--$	$--$	$3.0584^{+0.0309}_{-0.0297}$	$3.0504^{+0.0313}_{-0.0299}$	$3.0571^{+0.0312}_{-0.0296}$
$\Omega_{\Lambda(H)}^0$	$0.6993^{+0.0063}_{-0.0061}$	$0.7038^{+0.0060}_{-0.0059}$	$0.7000^{+0.0062}_{-0.0060}$	$0.6993^{+0.0063}_{-0.0061}$	$0.7036^{+0.0061}_{-0.0058}$	$0.6999^{+0.0062}_{-0.0061}$

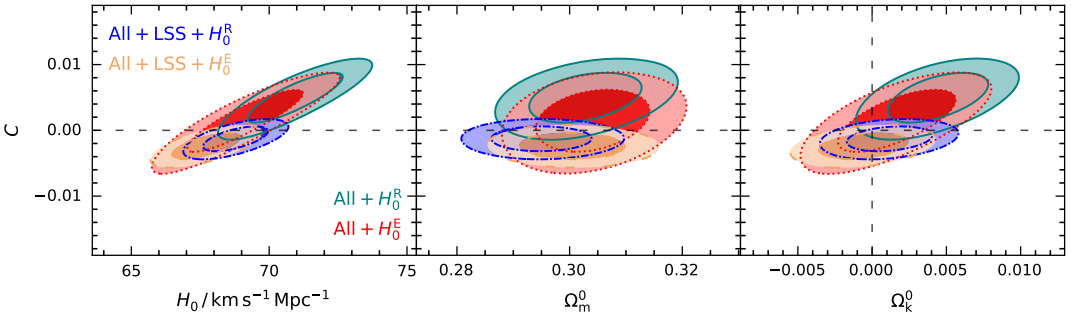

FIGURE 4.12: Marginalised posterior probability distributions for the GRVS parameter C vs *(left)* H_0, *(centre)* $\Omega_{\rm m}^0$, *(right)* Ω_k^0.

Before we move on, let us consider how well the GRVM, RVM and GRVS account for RSD measurements. The values of $f\sigma_8(z)$ inferred from CMB data (for a ΛCDM cosmology) seem to be in excess of what observations related to structure growth suggest. This is a result of the fact that the constraints on $\Omega_{\rm m}^0$ and $\sigma_{8,0}$ obtained from weak lensing, Sunyaev-Zel'dovich cluster counts, and RSDs appear to be in some tension with the Planck analysis of primary fluctuations [305]. However, the cause of the discrepancy is as yet a subject of debate. According to a recent study, the lower value for the reionisation optical depth reported in more recent *Planck* papers has partially solved the problem [325]. Whether or not any tension is detected also depends on the choice of data set. In particular, RSD measurements published in the last few years tend to probe higher redshifts, at which degeneracies can set in between different models. Such measurements are therefore more likely to be consistent with the ΛCDM values for $f\sigma_8$ [305].

Figs. 4.13 and 4.14 show the variation of $f\sigma_8$ with z for the dynamical-Λ models and ΛCDM. The greater majority of the data points are located below the ΛCDM curve,

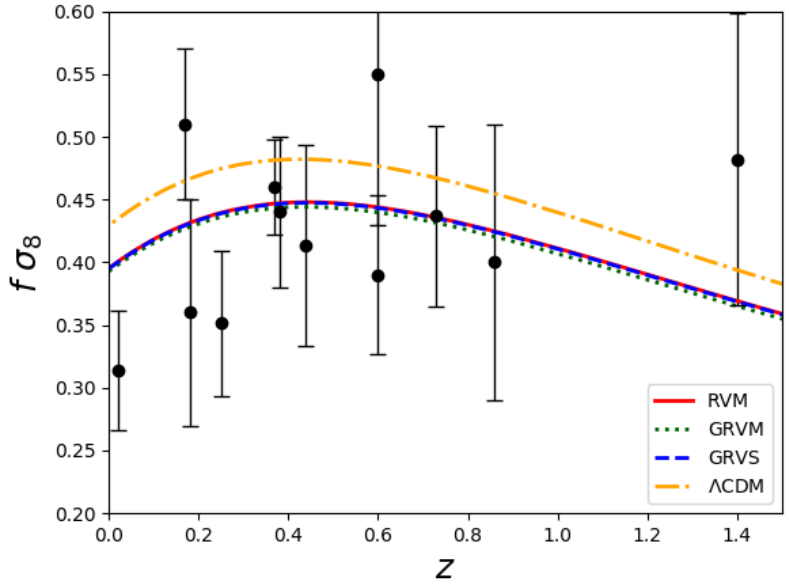

FIGURE 4.13: The variation of $f\sigma_8$ with z in a flat scenario. The data points of Table 4.5 are shown as black circles with 1σ error bars, and it can be seen that they mainly probe redshifts less than unity, at which different models are less likely to be degenerate [305]. The dynamical-Λ curves are based on the ALL+LSS (+ fixed A_s) mean values. In the greater majority of cases, these curves are closer to the observed values than their ΛCDM counterpart, which was obtained using the *Planck* 2015 (TT+lowP+lensing) results.

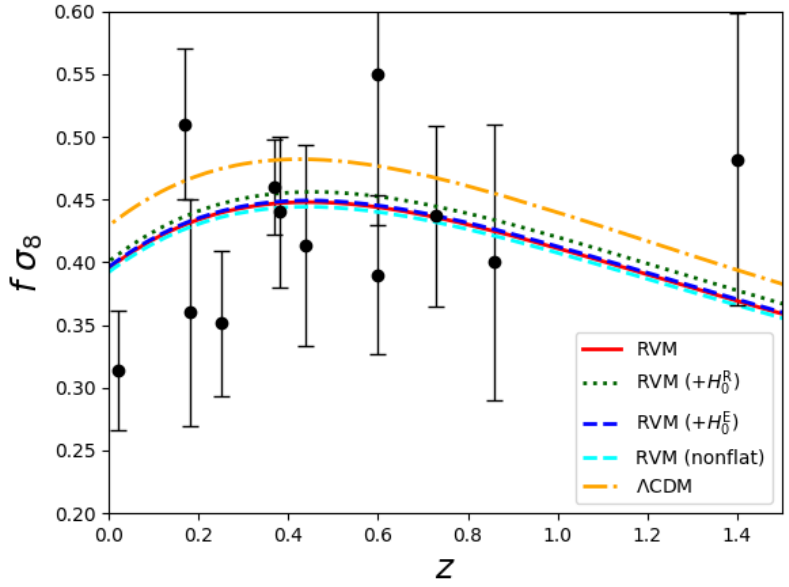

FIGURE 4.14: The variation of $f\sigma_8$ with z. The dynamical-Λ curves are based on the ALL+LSS (+ H_0^R/H_0^E) data set, with the H_0^R/H_0^E likelihood included if specified in the legend. All curves but one were obtained in the context of a flat geometry. The sole exception is labelled accordingly.

so the fact that the GRVM, RVM and GRVS yield smaller values for $f\sigma_8(z)$ augurs well. Indeed, both figures show that the dynamical-Λ set of curves is closer to the mean values of the observations. It can be noted that the performance of the running vacuum models is almost identical in this regard, although the GRVM and the non-flat RVM produce slightly lower curves – a feature that in all probability is due to their having an extra parameter (and hence an extra degree of freedom). Finally, it appears that the addition of $H_0^{\rm R}$ to the data set results in a slightly higher value of $f\sigma_8$ at a given z. This observation is perfectly in accord with our conclusion that LSS data lends support to the *Planck* constraints on H_0.

4.6.5 Comparison with ΛCDM

In this subsection, we consider the cosmological parameter constraints obtained by using the ALL + LSS, ALL + LSS + $H_0^{\rm R}$ and ALL + LSS + $H_0^{\rm E}$ data sets in the framework of a ΛCDM cosmology with freely-varying Ω_k^0. The mean values and 1σ confidence limits are presented in Table 4.19.

TABLE 4.19: Mean values and 1σ confidence limits for the baseline cosmological parameters *(top block)* and the derived quantity Ω_Λ^0 *(bottom row)* in the context of a ΛCDM cosmology. The condition $\Omega_k^0 = 0$ was not imposed.

Parameter	ALL+LSS	ALL+LSS+$H_0^{\rm R}$	ALL+LSS+$H_0^{\rm E}$	ALL+LSS	ALL+LSS+$H_0^{\rm R}$	ALL+LSS+$H_0^{\rm E}$
H_0	$68.6250^{+0.6557}_{-0.6720}$	$69.2690^{+0.6243}_{-0.6256}$	$68.7000^{+0.6456}_{-0.6569}$	$68.6080^{+0.6579}_{-0.6631}$	$69.2560^{+0.6229}_{-0.6348}$	$68.6790^{+0.6499}_{-0.6644}$
$10^3\Omega_{\rm b}^0 h^2$	$22.4650^{+0.1700}_{-0.1697}$	$22.4740^{+0.1697}_{-0.1707}$	$22.4640^{+0.1711}_{-0.1705}$	$22.4570^{+0.1707}_{-0.1696}$	$22.4680^{+0.1706}_{-0.1694}$	$22.4600^{+0.1703}_{-0.1711}$
$\Omega_{\rm cdm}^0 h^2$	$0.1190^{+0.0015}_{-0.0015}$	$0.1191^{+0.0015}_{-0.0015}$	$0.1190^{+0.0015}_{-0.0015}$	$0.1191^{+0.0015}_{-0.0015}$	$0.1191^{+0.0015}_{-0.0015}$	$0.1191^{+0.0015}_{-0.0015}$
$10^3\Omega_k^0$	$0.3456^{+1.9551}_{-1.9447}$	$1.6406^{+1.8794}_{-1.8476}$	$0.5135^{+1.9412}_{-1.9091}$	$0.4033^{+1.9647}_{-1.9491}$	$1.6730^{+1.8754}_{-1.8582}$	$0.5333^{+1.9657}_{-1.9232}$
n_s	$0.9698^{+0.0051}_{-0.0051}$	$0.9697^{+0.0051}_{-0.0051}$	$0.9698^{+0.0051}_{-0.0051}$	$0.9696^{+0.0051}_{-0.0051}$	$0.9696^{+0.0051}_{-0.0051}$	$0.9696^{+0.0051}_{-0.0051}$
$\ln\left(10^{10}A_s\right)$	$--$	$--$	$--$	$3.0417^{+0.0300}_{-0.0287}$	$3.0425^{+0.0300}_{-0.0286}$	$3.0418^{+0.0303}_{-0.0282}$
Ω_Λ^0	$0.6991^{+0.0063}_{-0.0060}$	$0.7032^{+0.0060}_{-0.0057}$	$0.6995^{+0.0063}_{-0.0060}$	$0.6987^{+0.0063}_{-0.0060}$	$0.7029^{+0.0060}_{-0.0058}$	$0.6992^{+0.0062}_{-0.0060}$

How may the results obtained for ΛCDM be compared with those for the GRVM, RVM and GRVS? The number of baseline parameters differs from model to model (11 for the GRVM, 10 for the RVM and GRVS, and 9 in the case of ΛCDM), so one cannot simply assess performance by looking at the minimum χ^2. Instead, we employ the Akaike Information Criterion (AIC) [326]. This takes into account both the number of free parameters (p) and the value of the maximum likelihood ($\mathscr{L}_{\rm max}$):

$$\mathrm{AIC} = 2p - 2\ln\left(\mathscr{L}_{\rm max}\right) . \tag{4.79}$$

Additionally, since the theoretical quantities associated with each likelihood are treated as samples from a multivariate Gaussian distribution, the AIC may equivalently be expressed in terms of the minimum χ^2:

$$\mathrm{AIC} = 2p + \chi^2_{\mathrm{min}} \ . \tag{4.80}$$

Another tool for model selection is the Bayesian Information Criterion (BIC) [327]:

$$\mathrm{BIC} = p \ln N - 2 \ln \left(\mathscr{L}_{\mathrm{max}} \right) \ . \tag{4.81}$$

Here, N is the number of observations, which in this work amounts to 798 or 799,[74] depending on whether H_0^{R} or H_0^{E} are included. Provided the assumption of sampling from a multivariate Gaussian distribution holds, Eq. (4.81) may alternatively take the form

$$\mathrm{BIC} = p \ln N + \chi^2_{\mathrm{min}} \ . \tag{4.82}$$

The AIC and BIC for the RVM and GRVS can be found in Tables 4.20 and 4.21. The GRVM is not included, since some of its parameters are not well-constrained in the non-flat case.

TABLE 4.20: The AIC and BIC statistics for the RVM, GRVS and ΛCDM. The values in the top, middle and bottom sections were obtained using the ALL + LSS, ALL + LSS + H_0^{R} and ALL + LSS + H_0^{E} data sets, respectively. Ω_k^0 was treated as a free parameter in all cases, while A_s was set to a fixed value.

Model	$\chi^2_{\mathrm{min.}}$	AIC	ΔAIC	BIC	ΔBIC
RVM	722.9	742.9	−1.8	789.7	2.9
GRVS	722.9	742.9	−1.8	789.7	2.9
ΛCDM	726.7	744.7	0.0	786.8	0.0
RVM ($+H_0^{\mathrm{R}}$)	733.2	753.2	1.1	800.0	5.8
GRVS ($+H_0^{\mathrm{R}}$)	733.1	753.1	1.0	799.9	5.7
ΛCDM ($+H_0^{\mathrm{R}}$)	734.1	752.1	0.0	794.3	0.0
RVM ($+H_0^{\mathrm{E}}$)	723.7	743.7	−1.4	790.5	3.3
GRVS ($+H_0^{\mathrm{E}}$)	723.7	743.7	−1.4	790.5	3.3
ΛCDM ($+H_0^{\mathrm{E}}$)	727.1	745.1	0.0	787.3	0.0

[74] JLA: 740, $H(z)$: 30, CMB: 4, BAO: 12, LSS: 12 .

TABLE 4.21: The AIC and BIC statistics for the RVM, GRVS and ΛCDM. Ω_k^0 and A_s were treated as free parameters in all cases.

Model	$\chi^2_{\text{min.}}$	AIC	ΔAIC	BIC	ΔBIC
RVM	723.1	745.1	−1.2	796.6	3.5
GRVS	722.7	744.7	−1.6	796.2	3.1
ΛCDM	726.3	746.3	0.0	793.1	0.0
RVM ($+H_0^{\text{R}}$)	733.2	755.2	1.5	806.7	6.2
GRVS ($+H_0^{\text{R}}$)	733.1	755.1	1.4	806.6	6.1
ΛCDM ($+H_0^{\text{R}}$)	733.7	753.7	0.0	800.5	0.0
RVM ($+H_0^{\text{E}}$)	724.0	746.0	−0.6	797.5	4.1
GRVS ($+H_0^{\text{E}}$)	723.7	745.7	−0.9	797.2	3.8
ΛCDM ($+H_0^{\text{E}}$)	726.6	746.6	0.0	793.4	0.0

Tables 4.20 and 4.21 demonstrate that the minimum χ^2 for the RVM and GRVS is smaller than its ΛCDM counterpart. What is more, this holds for all three data set combinations. One must however determine whether the difference in χ^2_{min} is enough to justify the extra free parameter of the RVM and GRVS. The reason is that although the addition of parameters introduces more degrees of freedom – and hence allows the model to better approximate the data – it does not necessarily yield a model of greater merit, because when the information supplied by the data has to be 'shared' among more parameters the resulting estimates tend to be less precise [328]. In such cases, information criteria like the AIC and BIC become indispensable to find a trade-off.[75] As can be deduced from Eqs. (4.79) and (4.81), the AIC and BIC statistics do not only penalise for a smaller value of $\mathscr{L}_{\text{max}}$, but also for a larger number of free parameters. In general, a smaller AIC/BIC indicates better performance.

Let us consider this in more detail. We start by noting that ΔAIC indicates the level of support the data provides for the model with the smaller AIC. An absolute value between 0 and 2 is usually not deemed enough to draw conclusions. If |ΔAIC| lies in the range from 2 to 4, the model with the larger AIC is considerably disfavoured, while a value of $|\Delta\text{AIC}| > 10$ renders it practically irrelevant. In the same vein, a difference of magnitude 2 in the BIC is considered as evidence against the model with the larger

[75] There is nonetheless a caveat: the AIC and BIC should, strictly speaking, only be applied if certain conditions are satisfied [329, 330]. For instance, they are both meant to be used with independent observations [331, 332].

BIC, while a difference of magnitude 6 or more constitutes strong evidence [333]. It may thus be concluded that the models perform similarly when assessed by the AIC. However, the BIC penalises for extra parameters more harshly than the AIC [334], and consequently provides a considerable level of support for ΛCDM.

4.7 In Brief...

This chapter focuses on three models from the literature that feature a dynamical Λ: the GRVM, whose characteristic $\Lambda(H)$ takes the form $A + BH^2 + C\dot{H}$, and two sub-cases: the RVM, obtained by setting C to zero, and the model we have called the GRVS, which has $B = 0$ instead. It is assumed that the vacuum only interacts with cold dark matter. The parameters B and/or C are constrained by fitting the models to cosmological observations using MCMC techniques.

In the case of the GRVM, we find that the addition of the LSS likelihood lowers the average values of H_0 when $\Omega_k^0 = 0$, enhancing compatibility with the results reported by the *Planck* collaboration [20]. This was also noted for the RVM (in the non-flat scenario) and the GRVS.

Another consequence of including LSS observations when constraining the GRVM – again under the assumption of flatness – is the tightening of the posterior distributions for B and C around the ΛCDM limit. On the other hand, we have seen that for both the RVM and GRVS, the introduction of growth data results in a dynamical Λ being preferred to a cosmological constant at a little over 1σ.[76] Additionally, it makes constraints on Ω_k^0 consistent with a flat geometry.

We may conclude that a running vacuum (modelled as in the RVM or GRVS) is only marginally favoured over a cosmological constant. Moreover, this mild preference comes at the cost of an extra parameter which – while not given much weight by the AIC – has a negative impact on the BIC score. Another point of interest is the fact that merging the RVM and GRVS expressions for Λ into a two-parameter combination (the GRVM) appears to weaken support for dynamical vacuum energy. Furthermore, the addition of LSS data reduces the ability of the models to accommodate a non-zero Ω_k^0.

[76] In the majority of cases, this holds whether or not we assume that the Universe is spatially flat.

CHAPTER 5

Spatial Curvature in Metric $f(R)$ Gravity

5.1 Introduction

Fourth-order metric theories of gravitation can be said to have originated from Weyl's 1918 non-integrable relativity theory. This theory (or variants of it) was further investigated by scientists such as W. Pauli, R. Weitzenböck and F. Jüttner, and served to introduce or promulgate key concepts such as conformal invariance, gravitational theories based on a geometrical approach, and the unification of the forces of nature [335][77]. However, the popularity of Weyl's theory soon declined, namely due to the ambiguity of the Lagrangian and the problems posed by the higher order of the field equations. Additionally, there did not seem to be any experimental evidence against General Relativity that would favour the introduction of a more complicated theory [335]. It was not until the 1970s that interest was revived. This happened as a result of factors such as the one-loop renormalizability of fourth-order metric theories, and the natural way in which inflation can be incorporated into them [335]. Moreover, given a classical gravitational field arising from the energy-momentum tensor ($T_{\mu\nu}$) of quantised matter/radiation, the Lagrangian of fourth-order theories helps to erase any singularities that the gravitational interaction induces in $T_{\mu\nu}$ [336].

The general class of *Fourth-Order Gravity* is governed by an action whose gravitational part reads [337, 338]

$$S = \int \frac{\sqrt{-g}}{16\pi G}\, f\left(R, R_{\alpha\beta}R^{\alpha\beta}, R_{\alpha\beta\gamma\delta}R^{\alpha\beta\gamma\delta}\right) \mathrm{d}^4x \ , \tag{5.1}$$

where R, $R_{\alpha\beta}$ and $R_{\alpha\beta\gamma\delta}$ are the Ricci scalar and the Ricci and Riemann tensors, respectively, and f represents an unspecified analytical function. In the metric approach, the field equations are derived by varying the action with respect to $g_{\mu\nu}$ [338].

[77] Also refer to works cited therein.

Among the theories obtained in such a way is Conformal Weyl Gravity [77]. This is based on the principle of conformal invariance, and has been the subject of significant interest in the last thirty years.

Another popular example is metric $f(R)$ gravity. Formulated by replacing the Ricci scalar in the GR action with a function thereof, $f(R)$ theory can be seen as a natural extension of General Relativity (GR) [339]. Despite its simplicity, however, it incorporates some of the basic characteristics of higher-order theories of gravity (i.e. theories constructed from actions in which R is generalised to some function of higher-order curvature invariants), and is furthermore advantageous in that it appears to be the only higher-order theory that does not suffer from the Ostrogradski instability [56]. The prototype of $f(R)$ gravity has $f(R) = R - \alpha^4/R$ (where $\alpha \sim H_0$). It was adopted in an attempt to explain late-time cosmic acceleration [57, 340, 341], but has been ruled out on the basis of the Dolgov-Kawasaki instability [57, 342] and the fact that it does not have a viable weak-field limit [57, 343]. In general, the class of models with $f(R) = R + \alpha R^{-n}$ cannot give rise to an acceptable cosmological expansion history for any $n > 0$ and $n < -1$ [344].

The function associated with Starobinsky's inflationary model [$f(R) = R + \alpha R^2$] [345] was also one of the first to be proposed. Since then, $f(R)$ gravity has been the subject of numerous studies. One of its apparent benefits is the ability of certain models to reproduce both the early period of inflation and the current acceleration [346]. That said, due to the stringent constraints that a candidate model must satisfy – for example, it has to predict a matter-dominated era – only a few are still considered valid [339]. These are best tested on cosmological scales. It is here that deviations from GR show up, so measurements of observables such as those related to galaxy clustering, the CMB or weak lensing make excellent probes [347].

5.2 Metric $f(R)$ Gravity: Preliminaries

5.2.1 The field equations

$f(R)$ theory is a *modified gravity* model. In other words, it adjusts the General Relativistic description of space-time geometry in a way that precludes the need for a mysterious dark energy component. At the basis of $f(R)$ theory is a generalisation

of the Einstein-Hilbert action of GR [Chapter 1, Eq. (1.5)]:

$$S = \int \frac{\sqrt{-g}}{16\pi G} f(R)\, \mathrm{d}^4x \ . \tag{5.2}$$

Here, $f(R)$ is a generic function of the Ricci curvature scalar. The field equations are obtained by varying the action with respect to the inverse metric tensor $g^{\mu\nu}$ [57], and collectively read

$$\left(G_{\mu\nu} + \frac{1}{2}Rg_{\mu\nu} - \nabla_\mu\nabla_\nu + g_{\mu\nu}\Box\right) f_R - \frac{1}{2}f(R)g_{\mu\nu} = 8\pi G\, T_{\mu\nu} \ , \tag{5.3}$$

where $f_R = \mathrm{d}f/\mathrm{d}R$, the quantity ∇_μ represents the covariant derivative operator constructed from the metric connection, and $\Box \equiv g_{\mu\nu}\nabla^\mu\nabla^\nu$. We shall model the matter/energy content of the Universe as a perfect fluid with proper density[78] ρ, corresponding isotropic pressure p and four-velocity u^μ, and hence

$$T_{\mu\nu} = (\rho + p)u_\mu u_\nu + pg_{\mu\nu} \ . \tag{5.4}$$

In an FLRW cosmology, the field equations [(5.3) above] can be cast in the same form as their General Relativistic counterparts[79] [348]. We may therefore write:[80]

$$H^2 = \frac{8\pi G}{3}\rho_{\mathrm{tot}} - \frac{\kappa}{a^2} \ ; \tag{5.5}$$

$$\frac{\ddot{a}}{a} = -\frac{4\pi G}{3}\left(\rho_{\mathrm{tot}} + 3p_{\mathrm{tot}}\right) \ , \tag{5.6}$$

with $\rho_{\mathrm{tot}} = \rho + \rho_{\mathrm{de}}$ and $p_{\mathrm{tot}} = p + p_{\mathrm{de}}$, ρ and p being the energy density and pressure from Eq. 5.4. However, while in General Relativity ρ_{de} and p_{de} are attributes of a physical dark energy component – namely, the vacuum energy we denote by Λ – in $f(R)$ theory they refer to a collection of terms which result from the modification to the geometry of space-time:

$$\rho_{\mathrm{de}} = \frac{1}{8\pi G}\left[\frac{1}{2}(f_R R - f) - 3H\dot{f}_R + 3(1 - f_R)H^2 + \frac{3\kappa}{a^2}(1 - f_R)\right] \ ; \tag{5.7}$$

$$p_{\mathrm{de}} = \frac{1}{8\pi G}\left[-\frac{1}{2}(f_R R - f) + \ddot{f}_R + 2H\dot{f}_R - (1 - f_R)(2\dot{H} + 3H^2) + \frac{\kappa}{a^2}(f_R - 1)\right] \ . \tag{5.8}$$

[78] The proper density is the density as measured by an observer comoving with the fluid [18].
[79] Refer to Chapter 1, Eqs. (1.38) and (1.37).
[80] An overdot again indicates differentiation with respect to t, the cosmic time.

Simply put, the occurrence of these geometric terms mimics the presence of dark energy [348] and is hence able to drive the late-time cosmic acceleration. Eq. (5.6) implies that the expansion of the Universe accelerates if $\rho_{\rm tot} < -3p_{\rm tot}$, or equivalently if

$$\rho + 3p < -\left(\rho_{\rm de} + 3p_{\rm de}\right) \ . \tag{5.9}$$

In other words, acceleration sets in when matter and radiation have become too dilute to offset the effect of dark energy. For theories in which dark energy is a physical component of the cosmic fluid, such as a scalar field, the said effect is a repulsion arising from its negative pressure. Here, however, the acceleration is due to the geometry of the spacetime manifold itself (although, as shown in subsection 5.2.3, $f(R)$ gravity may be interpreted as a type of Brans-Dicke theory by treating f_R as a scalar field). We additionally note that this effective dark energy does not interact with matter or radiation. Consequently, conservation of energy and momentum implies that:

$$\dot{\rho} + 3H(\rho + p) = 0 \ , \tag{5.10}$$

where $\rho = \rho_{\rm m} + \rho_{\rm r}$ and $p = p_{\rm m} + p_{\rm r}$. The subscripts 'm' and 'r' denote matter (cold dark matter and baryons) and radiation (photons and massless neutrinos), respectively.

A valid $f(R)$ theory must satisfy a number of constraints [56, 57, 349]. Firstly, since the quantity $G_{\rm eff} \equiv G/f_R$ acts as an effective gravitational coupling, the requirement that the graviton carries positive kinetic energy implies that $G_{\rm eff} > 0$, which in turn imposes the condition $f_R > 0$. Secondly, avoiding instabilities of the Dolgov-Kawasaki type [342] necessitates that $f''(R) \geq 0$. As for the cosmological dynamics, the theory should behave like ΛCDM at high redshifts, because the standard model is well-supported by CMB data in this regime. We therefore stipulate that $\lim_{R\to\infty} f(R) = R + \text{constant}$. A late-time expansion history similar to the one in a ΛCDM cosmology is also desirable, albeit in the absence of a cosmological constant; that is to say, one expects that $\lim_{R\to 0} f(R) = R + 0$ [210].

The successes of ΛCDM on Solar-System scales suggest that its phenomenology should be included as a limiting case [210] of any viable alternative theory. In metric $f(R)$, however, the Ricci curvature introduces a scalar degree of freedom, which could cause post-Newtonian constraints obtained from Solar System experiments to be violated. The model only remains valid if the scalar field can somehow be 'shielded' from such experiments. This may be achieved via the so-called *chameleon mechanism*, whereby

the effective mass M of the scalar varies according to the energy density of the local environment. In high-density regions like the Solar System, a large M would shorten the range of the scalar field to scales that cannot currently be probed by weak-field experiments. On the other hand, M would have to be small at cosmological densities, so as to allow the scalar field to act over a long range and drive the acceleration of the Universe [56, 350, 351]. One important thing to note about chameleon behaviour is that it cannot be described as a fine-tuning mechanism. Rather, it is a natural and intrinsic property of those $f(R)$ models whose weak-field limit satisfies observational constraints.

Phase space analysis can also yield a wealth of information. In a particularly noteworthy study that takes this approach [344], the authors consider the quantities $m = [Rf_{RR}/f_R](r)$ (f_{RR} stands for $\mathrm{d}^2 f/\mathrm{d}R^2$) and $r = -Rf_R/f$ and investigate the behaviour of the $m(r)$ curve on the (r, m) plane. It is found that for an $f(R)$ model to admit a viable matter-dominated epoch, the curve should satisfy the conditions $m(r) \approx +0$ and $\mathrm{d}m/\mathrm{d}r > -1$ at $r \approx -1$. Additionally, a valid period of late-time acceleration requires that $m = -r - 1$ while $(\sqrt{3} - 1)/2 < m \leq 1$ and $\mathrm{d}m/\mathrm{d}r < -1$, or that m lies in the range $(0, 1]$ at $r = -2$ [344].

5.2.2 The cosmological equations as a set of first-order differential equations

To avoid instabilities when solving Eqs. (5.5) and (5.6) numerically, we rewrite them as a set of first order ordinary differential equations. To this end, we follow the study of de la Cruz-Dombriz et al. [352], generalising their equations to the case of a non-flat geometry and also including a radiation component. The starting-point is the following change of variables:

$$
\begin{aligned}
s &= \frac{R}{6\left(H_0^{\Lambda}\,\eta\right)^2}\ ; & x &= -R'(z)(1+z)\ ; \\
y &= \frac{f(R)}{6 f_R\left(H_0^{\Lambda}\,\eta\right)^2}\ ; & \omega_{\mathrm{m}} &= \frac{\Omega_{\mathrm{m},0}^{\Lambda}(1+z)^3}{\eta^2 f_R}\ ; \\
\omega_{\mathrm{r}} &= \frac{\Omega_{\mathrm{r},0}^{\Lambda}(1+z)^4}{\eta^2 f_R}\ ; & K &= \frac{\kappa(1+z)^2}{\left(H_0^{\Lambda}\,\eta\right)^2}\ .
\end{aligned}
\tag{5.11}
$$

Here, a prime denotes differentiation with respect to the argument, $\eta = H/H_0^{\Lambda}$, $\Omega_{\mathrm{m},0}$ and $\Omega_{\mathrm{r},0}$ are the present-day values of the matter and radiation density parameters, respectively, and a superscript Λ indicates quantities as measured/inferred in the framework of a ΛCDM cosmology.

We have already seen that a candidate $f(R)$ model ideally satisfies the condition $\lim_{R\to\infty} f(R) = R + \text{constant}$. The constant should be equal to -2Λ (Λ stands for the cosmological constant), so that Eq. (5.2) becomes indistinguishable from the Einstein-Hilbert action at high redshifts. At late times, though, an $f(R)$ cosmology diverges from ΛCDM. As a result, the values that parameters like Ω_{m} and H currently attain are expected to differ in the two models, and we can write [353]

$$H_0^{f(R)} \neq H_0^{\Lambda} \; ; \quad \Omega_{\mathrm{m},0}^{f(R)} \neq \Omega_{\mathrm{m},0}^{\Lambda} \; , \tag{5.12}$$

where a 0 subscript labels present-day quantities and a superscript is used to indicate the corresponding model.

The matter density ρ_{m} in $f(R)$ gravity takes the same form as in ΛCDM:

$$\rho_{\mathrm{m}} = \frac{3H_0^2\Omega_{\mathrm{m},0}}{8\pi G}(1+z)^3 \; . \tag{5.13}$$

This follows from the fact that in both cases, matter is conserved independently of any other cosmic fluid component. We may thus infer that there must be some redshift z_{bound} at which

$$\Omega_{\mathrm{m},0}^{\Lambda}\left(H_0^{\Lambda}\right)^2(1+z_{\mathrm{bound}})^3 \to \Omega_{\mathrm{m},0}^{f(R)}\left(H_0^{f(R)}\right)^2(1+z_{\mathrm{bound}})^3 \; , \tag{5.14}$$

because the $f(R)$ models we consider reduce to ΛCDM at high redshifts. Consequently,

$$\Omega_{\mathrm{m},0}^{\Lambda}\left(H_0^{\Lambda}\right)^2 = \Omega_{\mathrm{m},0}^{f(R)}\left(H_0^{f(R)}\right)^2 \; . \tag{5.15}$$

This is another way of saying that the matter density (as expressed in physical units) is not model-dependent [210]. Similarly, for radiation density we have that:

$$\Omega_{\mathrm{r},0}^{\Lambda}\left(H_0^{\Lambda}\right)^2 = \Omega_{\mathrm{r},0}^{f(R)}\left(H_0^{f(R)}\right)^2 \; . \tag{5.16}$$

The curvature parameter κ does not change with time and hence must satisfy

$$\kappa^{\Lambda} = -\Omega_{k,0}^{\Lambda}\left(H_0^{\Lambda}\right)^2 = -\Omega_{k,0}^{f(R)}\left(H_0^{f(R)}\right)^2 = \kappa^{f(R)} \ , \tag{5.17}$$

since the relevant $f(R)$ models evolve into ΛCDM as we go back in time. We recall (from Chapter 1, section 1.3) that κ is defined as the ratio $k/\mathcal{R}_0^2$, k being the normalised curvature parameter (equal to ± 1 or 0) and $\mathcal{R}_0$ the present-day value of the non-normalised scale factor. So if $\kappa^{\Lambda} = \kappa^{f(R)}$, it must mean that at high redshifts, an $f(R)$ model with current scale factor $\hat{\mathcal{R}}_0$ behaves as a ΛCDM model that also has $\mathcal{R}_0 = \hat{\mathcal{R}}_0$.

Eqs. (5.15)–(5.17) make it possible to rewrite the parameters $H_0^{f(R)}$, $\Omega_{\mathrm{m},0}^{f(R)}$, $\Omega_{\mathrm{r},0}^{f(R)}$ and $\Omega_{k,0}^{f(R)}$ in terms of their ΛCDM counterparts. This was already done for the expressions in Eq. (5.11). Additionally, the fact that Λ represents the cosmological constant in both models implies that

$$3\left(H_0^{\Lambda}\right)^2\Omega_{\Lambda,0}^{\Lambda} = 3\left(H_0^{f(R)}\right)^2\Omega_{\Lambda,0}^{f(R)} \ . \tag{5.18}$$

The equivalence between the spatial curvature and energy densities (in physical units) of ΛCDM and $f(R)$ gravity becomes especially useful when we carry out the fitting analysis, because it enables us to construct priors for the cosmological parameters from the *Planck* mean values and 1σ confidence intervals [20] (which were obtained in the context of a ΛCDM cosmology).

Let us now return to Eq. (5.11). In terms of the new variables (η, s, x, y, ω_{m}, ω_{r} and K), the system of cosmological equations to be solved becomes:

$$\eta'(z) = \frac{\eta}{z+1}(2 - s + K) \ ; \tag{5.19}$$

$$s'(z) = -\frac{s}{z+1}\left(\frac{x}{R} + 4 - 2s + 2K\right) \ ; \tag{5.20}$$

$$\begin{aligned} x'(z) = {} & \frac{1}{\Gamma(z+1)}\left[(x\Gamma)^2 + s(x\Gamma - 1) + 3y - 1 - K(1 + x\Gamma) + \omega_{\mathrm{r}}\right] \\ & - x\Gamma'(z)\Gamma^{-1} \ ; \end{aligned} \tag{5.21}$$

$$y'(z) = -\frac{1}{z+1}\left[s\frac{x}{R} + y(4 - x\Gamma - 2s + 2K)\right] \ ; \tag{5.22}$$

$$\omega_{\mathrm{m}}'(z) = \frac{\omega_{\mathrm{m}}}{z+1}(x\Gamma + 2s - 2K - 1) \ ; \tag{5.23}$$

$$\omega_{\mathrm{r}}'(z) = \frac{\omega_{\mathrm{r}}}{z+1}(x\Gamma + 2s - 2K) \ ; \tag{5.24}$$

$$K'(z) = -\frac{2K}{z+1}(K-s+1) \ , \tag{5.25}$$

where Γ is equal to f_{RR}/f_R and serves to identify the model. The majority of the above differential equations result directly from the change of variables specified in Eq. (5.11). In other words, they would automatically be satisfied if the new variables were rewritten in terms of the original ones. The sole exceptions are Eq. (5.21) – which incorporates (5.5) and (5.6) – and Eq. (5.19); the latter is simply the expression for R in an FLRW Universe:

$$R = 6\left(\dot{H} + 2H^2 + \frac{\kappa}{a^2}\right) \ , \tag{5.26}$$

as rendered by the new choice of variables. Since Eqs. (5.24) and (5.25) do not in themselves contain any information about cosmological dynamics, we replace them with the relations for $\omega_{\rm r}$ and K from Eq. (5.11) to simplify the numerical analysis.

5.2.3 The Einstein and Jordan frames

The action of metric $f(R)$ [Eq. (5.2)] may be recast in a form suggestive of scalar-tensor theory. More specifically, it turns out to be the same as the action for a Brans-Dicke theory with characteristic parameter $\omega = 0$ [56]. An outline of the main points is provided below.

To begin with, let us introduce a new field χ and consider the action [56]

$$S = \int \frac{\sqrt{-g}}{16\pi G}\left[f(\chi) + f'(\chi)(R-\chi)\right] \mathrm{d}^4x \ . \tag{5.27}$$

Variation with respect to χ yields

$$f''(\chi)(R-\chi) = 0 \ , \tag{5.28}$$

from which if follows that if $f''(\chi) \neq 0$, χ must necessarily be equal to R, and the original action [Eq. (5.2)] is recovered. Provided $f''(\chi) \neq 0$, therefore, the actions in Eqs. (5.2) and (5.27) are equivalent.

Next, we model $f'(\chi)$ as a scalar field that we denote by ϕ. This implies that $f(\chi) + f'(\chi)(R-\chi) = f(\chi) + \phi R - \phi\chi = \phi R - [\phi\chi - f(\chi)]$ [56], and consequently Eq. (5.27) becomes [56]

$$S = \int \frac{\sqrt{-g}}{16\pi G} \left[\phi R - V(\phi)\right] \mathrm{d}^4x \ , \tag{5.29}$$

with the quantity $\phi\chi - f(\chi)$ playing the role of the field potential $V(\phi)$. Eq. (5.29) is the Jordan frame representation of the action for an $\omega = 0$ Brans-Dicke theory [56]. However, Solar System data constrains $|\omega|$ to be greater than 40 000 [152], so metric $f(R)$ gravity would be invalidated were it not for the chameleon mechanism.

$f(R)$ theory may be formulated in the Einstein frame via a conformal transformation [56]:

$$g_{\mu\nu} \to \bar{g}_{\mu\nu} = \Theta^2 g_{\mu\nu} \ . \tag{5.30}$$

Here,[81] $\Theta^2 = f_R = \phi$, and a bar has been introduced to indicate Einstein-frame quantities. The field ϕ is related to its Einstein-frame counterpart, $\bar{\phi}$, as specified below [56]:

$$\phi \equiv f_R = \exp\left(\bar{\phi}\sqrt{16\pi G/3}\right) \ . \tag{5.31}$$

The potential associated with $\bar{\phi}$ takes the form [56]

$$\bar{V}(\bar{\phi}) = \frac{R f_R - f(R)}{16\pi G f_R^2} \ , \tag{5.32}$$

while the conformally-transformed gravitational action reads [56]

$$\bar{S} = \int \sqrt{-\bar{g}} \left[\frac{\bar{R}}{16\pi G} - \frac{1}{2}\partial^\alpha\bar{\phi}\partial_\alpha\bar{\phi} - \bar{V}\left(\bar{\phi}\right)\right] \mathrm{d}^4x \ . \tag{5.33}$$

5.2.4 Specific $f(R)$ models

Among the viable $f(R)$ models are the ones put forward by Hu and Sawicki [210], Starobinsky [354], Tsujikawa [355] and Cognola *et al.* [346]. The said models are the subject of numerous works in the literature [339, 348, 356], but almost always in the context of a spatially flat Universe. In contrast, we will use observational data to constrain cosmological and model-specific parameters without setting Ω_k^0 to zero. First, however, let us take a closer look at each of these models in turn.

[81] We have already seen that $\phi = f'(\chi)$ and $\chi = R$, which means that $\phi = f_R$.

The Hu-Sawicki model

Hu and Sawicki proposed a class of 'broken power-law' models [210]:

$$f(R)_{\rm HS} = R - \mu^2 \frac{c_1 \left(R/\mu^2\right)^{n_{\rm HS}}}{1 + c_2 \left(R/\mu^2\right)^{n_{\rm HS}}} \ . \tag{5.34}$$

Here, c_1 and c_2 are dimensionless parameters, $n_{\rm HS}$ represents a positive constant that is usually assumed to be an integer, and $\mu^2 \approx H_0^2 \Omega_{\rm m}^0$.

It may be shown that the Hu-Sawicki model includes ΛCDM as a limiting case and can, in fact, be seen as a late-time modification of the latter [356]. Moreover, it is possible to explicitly incorporate the cosmological constant Λ into Eq. (5.34) by making the substitutions [357]

$$\Lambda = \frac{\mu^2 c_1}{2c_2} \ ; \quad b = \frac{2c_2^{1-n_{\rm HS}^{-1}}}{c_1} \ , \tag{5.35}$$

which cast $f(R)_{\rm HS}$ into the form [357, 358]:

$$f(R)_{\rm HS} = R - 2\Lambda \left(1 - \frac{1}{1 + [R/(b\Lambda)]^{n_{\rm HS}}}\right) \ . \tag{5.36}$$

Eq. (5.36) makes it apparent that at high redshifts, when $R \gg \Lambda$, $f(R)_{\rm HS}$ reduces to $R - 2\Lambda$ and ΛCDM is consequently recovered [358]. The differences that emerge at smaller redshifts are quantified by the *deviation parameter* b [357] ($b = 0$ corresponds to ΛCDM). Constraints placed on b by means of cosmological data, therefore, translate into bounds on the allowed variation from the standard model. Additionally, the time at which these variations set in is controlled by $n_{\rm HS}$: the larger its value, the longer it takes for the Hu-Sawicki model to diverge from ΛCDM [210].

Now that we have clarified what effect any changes in $n_{\rm HS}$ would have, we may (without loss of generality) simplify the analysis by fixing this parameter at some specified value. We shall follow other works in the literature and set $n_{\rm HS}$ to unity [348, 356, 357]. Furthermore, only non-negative values of b will be considered. The reason is that when $n_{\rm HS} = 1$, $f_{RR} = 4b\Lambda^2/(R + b\Lambda)^3$, and so having $b < 0$ would mean that f_{RR} becomes negative as soon as $R > -b\Lambda$. We have already seen that f_{RR} is required to be positive (or zero) for an $f(R)$ theory to be viable.

Before proceeding to the next model, it would be interesting – and extremely useful for

the fitting analysis performed later – to determine at what redshift the Hu-Sawicki model becomes effectively indistinguishable from ΛCDM. To this end, we adopt a procedure similar to the one proposed in Ref. [353] for exponential $f(R)$. Eq. (5.36) allows us to deduce that if $f(R)_{\rm HS}$ is to approach $R - 2\Lambda$ at high redshifts, the magnitude of $1/\{1 + [R^{f(R)}/(b\Lambda)]^{n_{\rm HS}}\}$ must decrease asymptotically to zero as we go back in time. This may be expressed as the requirement that at some redshift $z_{\rm bound}$, the quantity $1/|1 + [R^{f(R)}/(b\Lambda)]^{n_{\rm HS}}|$ is equal to ϵ (with $\epsilon \ll 1$), at which point any differences between the $f(R)$ model and ΛCDM are negligible. Additionally, at $z = z_{\rm bound}$ one expects $R^{f(R)}$ to take the form $R^\Lambda + \xi$ (for some $|\xi| \ll |R^\Lambda|$). With these considerations in mind, we may write

$$
\begin{aligned}
& 1 + \left(\frac{R^\Lambda + \xi}{b\Lambda}\right)^{n_{\rm HS}} \approx 1 + \left(\frac{R^{f(R)}}{b\Lambda}\right)^{n_{\rm HS}} = \frac{1}{\epsilon} \ ; \\
\implies & \left(\frac{b\Lambda}{R^\Lambda + \xi}\right)^{n_{\rm HS}} \approx \frac{\epsilon}{1-\epsilon} \ ; \\
\implies & \frac{b\Lambda}{R^\Lambda + \xi} \approx \left(\frac{\epsilon}{1-\epsilon}\right)^{n_{\rm HS}^{-1}} = \nu \ ; \\
\implies & \frac{b\Lambda}{R^\Lambda} \approx \nu \left(1 + \frac{\xi}{R^\Lambda}\right) \ ,
\end{aligned}
$$

and if terms higher than first order in ϵ and ξ/R^Λ are discarded, it follows that

$$
\begin{aligned}
& \nu = \left(\frac{\epsilon}{1-\epsilon}\right)^{n_{\rm HS}^{-1}} = \epsilon^{n_{\rm HS}^{-1}} (1-\epsilon)^{-n_{\rm HS}^{-1}} \approx \epsilon^{n_{\rm HS}^{-1}} \left(1 + \frac{\epsilon}{n_{\rm HS}}\right) \approx \epsilon^{n_{\rm HS}^{-1}} \ ; \\
\implies & \frac{b\Lambda}{R^\Lambda} \approx \nu \left(1 + \frac{\xi}{R^\Lambda}\right) \approx \epsilon^{n_{\rm HS}^{-1}} \left(1 + \frac{\xi}{R^\Lambda}\right) \approx \epsilon^{n_{\rm HS}^{-1}} \approx \nu \ . \qquad (5.37)
\end{aligned}
$$

Therefore, $b\Lambda/R^\Lambda \approx \nu$ at $z = z_{\rm bound}$. Using the relation[82] $R^\Lambda = 3H_0^2[\Omega_{\rm m}^0(1+z)^3 + 4\Omega_\Lambda^0]$, we solve for $z_{\rm bound}$ and find that

$$
z_{\rm bound} = \left[\frac{\Omega_\Lambda^0}{\Omega_{\rm m}^0}\left(\frac{b}{\nu} - 4\right)\right]^{1/3} - 1 \ . \qquad (5.38)
$$

[82] This may be obtained from Eq. (5.26) by writing H^2 as $H_0^2(\Omega_{\rm m}^0 a^{-3} + \Omega_{\rm r}^0 a^{-4} + \Omega_\Lambda^0 + \Omega_k^0 a^{-2})$, which is simply Eq. (1.38) with $\rho = \rho_{\rm m} + \rho_{\rm r}$ and $\rho_{\rm m}$, $\rho_{\rm r}$, Λ and κ expressed in terms of the respective density parameters.

The Starobinsky model

Starobinsky proposed the function [354]:

$$f(R)_{\rm S} = R + \lambda R_{\rm S}\left[\left(1+\frac{R^2}{R_{\rm S}^2}\right)^{-n_{\rm S}} - 1\right] \ , \tag{5.39}$$

where $n_{\rm S}$ and λ denote positive constants, and the third constant ($R_{\rm S}$) is of the order of the present-day Ricci scalar [355]. As was done for the Hu-Sawicki model, we cast $f(R)_{\rm S}$ in the form of a perturbed ΛCDM Lagrangian [348]:

$$f(R)_{\rm S} = R - 2\Lambda\left[1 - \left(1+\frac{R^2}{(b\Lambda)^2}\right)^{-n_{\rm S}}\right] \ , \tag{5.40}$$

which clearly shows that $f(R)_{\rm S} \to R - 2\Lambda$ when $R \gg \Lambda$ or when $b \to 0$. Λ and b may be expressed in terms of the original parameters as $\lambda R_{\rm S}/2$ and $2/\lambda$, respectively [348].

The redshift $z_{\rm bound}$ is again given by Eq. (5.38). This time, though, we have that

$$\epsilon = \left(1+\frac{R^2}{(b\Lambda)^2}\right)^{-n_{\rm S}} \ ; \qquad \nu = \sqrt{\frac{\epsilon^{1/n_{\rm S}}}{1-\epsilon^{1/n_{\rm S}}}} \ . \tag{5.41}$$

The Exponential model

In this case, the $f(R)$ function reads [346]

$$f(R)_{\rm E} = R + \beta\left[\exp(-\gamma R) - 1\right] \ , \tag{5.42}$$

or equivalently [348]

$$f(R)_{\rm E} = R - 2\Lambda\left[1 - \exp\left(-\frac{R}{b\Lambda}\right)\right] \ , \tag{5.43}$$

with $\Lambda = \beta/2$ and $b = 2/(\gamma\beta)$. The parameter γ must be non-negative so that at high redshifts, when $R \gg \Lambda$, the exponential function becomes negligible and ΛCDM is recovered [353]. This also happens for $b = 0$.

The redshift $z_{\rm bound}$ may be estimated from Eq. (5.38) by making use of the relations

$$\epsilon = \exp\left(-\frac{R}{b\Lambda}\right) \ ; \qquad \nu = \frac{1}{\ln\left(1/\epsilon\right)} \ . \tag{5.44}$$

The Tsujikawa model

The model proposed by Tsujikawa is based on the function [355]

$$f(R)_{\rm T} = R - \zeta R_{\rm T} \tanh\left(\frac{R}{R_{\rm T}}\right) , \tag{5.45}$$

where ζ and $R_{\rm T}$ are positive constants. We may alternatively write

$$f(R)_{\rm T} = R - 2\Lambda \tanh\left(\frac{R}{b\Lambda}\right) . \tag{5.46}$$

Here, $b = 2/\zeta$ and $\Lambda = \zeta R_{\rm T}/2$ [348], and the model becomes equivalent to ΛCDM either when $R \gg \Lambda$ or when $b = 0$ (since $\tanh\left[R/(b\Lambda)\right] \to 1$ in both cases). The quantities ϵ and ν required to calculate $z_{\rm bound}$ [Eq. (5.38)] are given by

$$\epsilon = 1 - \tanh\left(\frac{R}{b\Lambda}\right) ; \quad \nu = \frac{1}{\operatorname{arctanh}(1-\epsilon)} \quad . \tag{5.47}$$

5.3 Perturbations in $f(R)$ Gravity

The perturbation equations are derived as outlined in Appendix A. The $f(R)$ analogue of Eq. (A.3) is given by:

$$\begin{aligned} &\delta G^{\mu}_{\nu} f_R + \left(R^{\mu}_{\nu} - \nabla^{\mu}\nabla_{\nu} + \delta^{\mu}_{\nu}\Box\right) f_{RR}\delta R + \left(\delta g^{\mu\alpha}\nabla_{\nu}\nabla_{\alpha} - \delta^{\mu}_{\nu}\delta g^{\alpha\beta}\nabla_{\alpha}\nabla_{\beta}\right) f_R + \\ &\left(g^{\alpha\mu}\delta\Gamma^{\gamma}_{\alpha\nu} - \delta^{\mu}_{\nu} g^{\alpha\beta}\delta\Gamma^{\gamma}_{\beta\alpha}\right)\partial_{\gamma} f_R = 8\pi G\, \delta T^{\mu}_{\nu} , \end{aligned} \tag{5.48}$$

where R^{μ}_{ν} is the Ricci tensor, and the quantities δR, $\delta g_{\mu\nu}$ and $\delta\Gamma^{\mu}_{\sigma\nu}$ denote perturbations in the Ricci scalar, the metric tensor and the metric connection, respectively. The perturbations in the energy-momentum tensor are as specified in Eq. (A.4).

To first order in the metric perturbations Φ and Ψ, and expressed in terms of momentum-space variables, the time-time component of Eq. (5.48) reads:

$$\begin{aligned} &2f_R\left\{\Psi\left(k_{\dagger}^2 - 3\kappa\right) + 3\mathcal{H}\left[\Psi'(\tau) + \Phi\mathcal{H}\right]\right\} + f_{RR}\left[3\mathcal{H}'(\tau)\delta R - k_{\dagger}^2\delta R - 3\mathcal{H}\,\delta R'(\tau)\right] - \\ &3\mathcal{H}\,\delta R\, f'_{RR}(\tau) + 3f'_R(\tau)\left[2\mathcal{H}\Phi + \Psi'(\tau)\right] + 8\pi G a^2 \rho_{\rm m}\delta_{\rm m} = 0 , \end{aligned} \tag{5.49}$$

with all symbols having the same meaning as in Appendix A, and

$$\delta R = \frac{2}{a^2}\left\{k_\dagger^2(\Phi - 2\Psi) - 3\left[2\Phi\mathcal{H}'(\tau) + 3\mathcal{H}\Psi'(\tau) + \mathcal{H}\Phi'(\tau) - 2\kappa\Psi + \Psi''(\tau) + 2\Phi\mathcal{H}^2\right]\right\} . \tag{5.50}$$

Φ and Ψ are not equal in $f(R)$ gravity. Instead, they satisfy:

$$\Psi - \Phi = \frac{f_{RR}\delta R}{f_R} . \tag{5.51}$$

This relation follows from the i-j component ($i \neq j$) of Eq. (5.48).

Eqs. (5.49) and (5.50) are quite involved but may be simplified using the sub-Hubble and quasi-static approximations, whence they become:[83]

$$2f_R\Psi(k_\dagger^2 - 3\kappa) - f_{RR}k_\dagger^2\delta R + 8\pi G a^2\rho_{\rm m}\delta_{\rm m} = 0 ; \tag{5.52}$$

$$\delta R = \frac{2}{a^2}\left[k_\dagger^2(\Phi - 2\Psi) + 6\kappa\Psi\right] . \tag{5.53}$$

Meanwhile, the conservation equations retain the same form as in GR:[84]

$$\delta'_{\rm m}(\tau) = (1 + w_{\rm m})\left[-k_\dagger v + 3\Psi'(\tau)\right] ; \tag{5.54}$$

$$v'(\tau) = \mathcal{H}v(3w_{\rm m} - 1) + k_\dagger\left(\Phi + \frac{w_{\rm m}\delta_{\rm m}}{1 + w_{\rm m}}\right) . \tag{5.55}$$

and may readily be combined to give:

$$\delta''_{\rm m}(\tau) + \mathcal{H}\delta'_{\rm m}(\tau) + k_\dagger^2\Phi - 3\Psi''(\tau) - 3\mathcal{H}\Psi'(\tau) = 0 , \tag{5.56}$$

where we have utilised the fact that a dust distribution (which provides a good description of the matter in the Universe) has $w_{\rm m} = 0$. Under the sub-Hubble and quasi-static approximations, Eq. (5.56) further simplifies to

$$\delta''_{\rm m}(\tau) + \mathcal{H}\delta'_{\rm m}(\tau) + k_\dagger^2\Phi = 0 . \tag{5.57}$$

To obtain an expression for Φ, we insert Eq. (5.53) into Eqs. (5.51) and (5.52) and

[83] More details about the way in which Eqs. (5.49), (5.50) and (5.56) are reduced to Eqs. (5.52), (5.53) and (5.57), respectively, may be found at the end of Appendix A.

[84] Refer to Appendix A, Eqs. A.20 and A.21.

solve the last two for Φ (and Ψ), then use the solution to substitute for Φ in Eq. (5.57), getting that

$$\delta_{\rm m}''(\tau)+\mathcal{H}\delta_{\rm m}'(\tau)-4\pi G\rho_{\rm m}a^2\frac{k_\dagger^2\left[a^2f_R+4f_{RR}(k_\dagger^2-3\kappa)\right]}{f_R\left[3f_{RR}k_\dagger^2\left(k_\dagger^2-4\kappa\right)+a^2f_R\left(k_\dagger^2-3\kappa\right)\right]}\delta_{\rm m}=0\ , \tag{5.58}$$

which may also be written as

$$\delta_{\rm m}''(\tau)+\mathcal{H}\delta_{\rm m}'(\tau)-4\pi\rho_{\rm m}\delta_{\rm m}a^2G_{\rm eff}=0\ , \tag{5.59}$$

with

$$\frac{G_{\rm eff}}{G}=\frac{k_\dagger^2\left[a^2f_R+4f_{RR}(k_\dagger^2-3\kappa)\right]}{f_R\left[3f_{RR}k_\dagger^2\left(k_\dagger^2-4\kappa\right)+a^2f_R\left(k_\dagger^2-3\kappa\right)\right]}\ . \tag{5.60}$$

In terms of our new variables [Eq. (5.11)], $G_{\rm eff}/G$ reads:

$$\frac{G_{\rm eff}}{G}=\frac{k_\dagger^2\omega_{\rm m}a^3\eta^2\left[a^2+4\Gamma(k_\dagger^2-3\kappa)\right]}{\Omega_{\rm m,0}^\Lambda\left[a^2(k_\dagger^2-3\kappa)+3k_\dagger^2\Gamma(k_\dagger^2-4\kappa)\right]}\ . \tag{5.61}$$

5.4 Numerical Analysis

5.4.1 Preliminaries

The parameter values that best allow the models to describe what we observe are those that maximise the joint likelihood function:

$$\mathscr{L}_{\rm total}\propto\exp\left[-\frac{1}{2}\left(\chi^2_{\rm SNeIa}+\chi^2_{H(z)}+\chi^2_{\rm CMB}+\chi^2_{\rm BAO}+\chi^2_{\rm LSS}\right)\right]\ . \tag{5.62}$$

We shall use the same observables and likelihoods presented in Chapter 4, section 4.5. The few modifications made are listed below.

- The JLA likelihood is exchanged for a more recent version available with MONTE PYTHON v.3.0.1 – the Pantheon likelihood, based on a sample of 1048 SNeIa in the redshift range $0.01<z<2.3$ [359].
- The index of the primordial scalar power spectrum, n_s, is added to Table 4.2 (as was done in Chapter 4 when we included LSS measurements with the data). The new set of CMB distance priors is shown below:

TABLE 5.1: Mean values and corresponding errors for the CMB distance priors [277].

$\mathscr{R}$	l_A	$\Omega_\mathrm{b}^0 h^2$	n_s
1.7448 ± 0.0054	301.460 ± 0.094	0.02240 ± 0.00017	0.9680 ± 0.0051

The normalised covariance matrix of Eq. (4.38) is updated accordingly:

$$C_\mathrm{CMB} = \begin{array}{c} \\ \mathscr{R} \\ l_\mathrm{A} \\ \Omega_\mathrm{b}^0 h^2 \\ n_s \end{array} \begin{array}{c} \begin{array}{cccc} \mathscr{R} & l_\mathrm{A} & \Omega_\mathrm{b}^0 h^2 & n_s \end{array} \\ \begin{bmatrix} 1.00 & 0.53 & -0.73 & -0.80 \\ 0.53 & 1.00 & -0.42 & -0.43 \\ -0.73 & -0.42 & 1.00 & 0.59 \\ -0.80 & -0.43 & 0.59 & 1.00 \end{bmatrix} \end{array} . \tag{5.63}$$

- For the BAO likelihood, we shall be using Table 4.4 in conjunction with the following selection from Table 4.3:

TABLE 5.2: Uncorrelated BAO data measured at different effective redshifts, z_eff. Column 4 gives the error in each quantity.

Ref.	z_eff	Quantity	σ	Type
[279]	0.106	0.323	0.014	1
[280]	0.150	4.490	0.170	2
[282]	2.330	1.031	0.026	3
1: $r_s(z_\mathrm{d})/d_\mathrm{v}$; 2: $d_\mathrm{v}/r_s(z_\mathrm{d})$; 3: $\alpha_\parallel^{0.7}\alpha_\perp^{0.3}$; $r_{\mathrm{s,\,fid}}(z_\mathrm{d}) = 147.78\,\mathrm{Mpc}$ [283].				

The remaining entries are excluded so as to remove potential correlations between BAO and $f\sigma_8$ data.

- The compilation of $f\sigma_8$ measurements is taken from Ref. [288] and presented in Table 5.3. The covariance matrices for the data points from Ref. [301] and those from Ref. [360] may be found in Ref. [288].

To calculate $f\sigma_8(z)$ for a given model, we need two quantities: the growth rate f,

TABLE 5.3: LSS data. Each $f\sigma_8$ measurement is listed together with the corresponding redshift z and error $\sigma_{f\sigma_8}$. Column 5 shows the values of $\Omega_{\rm m}^0$ in the respective fiducial cosmologies.

Ref.	z	$f\sigma_8(z)$	$\sigma_{f\sigma_8}$	$\Omega_{\rm m,0}^{\rm fid}$
[21, 297]	0.02	0.314	0.048	0.266
[301]	0.44	0.413	0.080	0.27
[301]	0.60	0.390	0.063	0.27
[301]	0.73	0.437	0.072	0.27
[302]	0.60	0.550	0.120	0.30
[302]	0.86	0.400	0.110	0.30
[303]	1.40	0.482	0.116	0.27
[360]	0.978	0.379	0.176	0.31
[360]	1.230	0.385	0.099	0.31
[360]	1.526	0.342	0.070	0.31
[360]	1.944	0.364	0.106	0.31

and the standard deviation of density perturbations in spheres of radius $8\,h^{-1}\,\mathrm{Mpc}$, $\sigma_8(z)$. The former is a function of $\delta_{\rm m}$, the matter density contrast:

$$f = \frac{\mathrm{d}(\ln \delta_{\rm m})}{\mathrm{d}\ln a}\ , \tag{5.64}$$

which may in turn be obtained from Eq. (5.58) by solving it as part of the system of differential equations given by (5.19)–(5.23) [$\omega_{\rm r}$ and K are directly inputted as defined in Eq. (5.11)].

Since Eq. (5.58) is dependent on $k_\dagger$, it is necessary to choose an appropriate comoving wave number at which f is evaluated. We shall focus exclusively on values of $k_\dagger$ lying in the range $0.02\,h\,\mathrm{Mpc}^{-1} \leq k_\dagger \leq 0.2\,h\,\mathrm{Mpc}^{-1}$. The choice of bounds is based on two considerations: firstly, modes with $k_\dagger \lesssim 0.2\,h\,\mathrm{Mpc}^{-1}$ represent perturbations which may safely be considered linear [296], and secondly, the mode that crosses the horizon at matter-radiation equality has[85] $k_\dagger \sim 0.015\,h\,\mathrm{Mpc}^{-1}$. The latter implies that smaller scales – corresponding to a larger $k_\dagger$ – would be well within the horizon deep in the matter era and during the subsequent period of acceleration (these being the epochs of interest). We shall therefore determine f at two different wave numbers:

[85]This estimate is obtained from Eq. (4.73) by putting $B = C = 0$ (i.e. assuming a ΛCDM cosmology) and assigning the *Planck* TT,TE,EE+lowE+lensing mean values to H_0, $\Omega_{\rm m}^0$ and $z_{\rm eq}$ [20]. The quantity $z_{\rm eq}$ is the redshift at which matter and radiation densities were equal, and may be used to calculate $\Omega_{\rm r}^0$ [since $\Omega_{\rm r}^0 = \Omega_{\rm m}^0/(1+z_{\rm eq})$].

$k_\dagger = 0.1\,h\,\mathrm{Mpc}^{-1}$ and $k_\dagger = 0.05\,h\,\mathrm{Mpc}^{-1}$. These values of $k_\dagger$ satisfy the relation[86] $k_\dagger^2 \gg |\kappa|$, and so Eq. (5.60) may be simplified to:

$$\frac{G_{\mathrm{eff}}}{G} = \frac{a^2 f_R + 4 f_{RR} k_\dagger^2}{f_R\left(3 f_{RR} k_\dagger^2 + a^2 f_R\right)} \,. \tag{5.65}$$

Finally, solving Eq. (5.58) requires a pair of initial conditions. The simplest choice is putting $\delta_{\mathrm{m}}(a_{\mathrm{ini}}) = a_{\mathrm{ini}}$ and $\delta'_{\mathrm{m}}(a = a_{\mathrm{ini}}) = 1$ [or equivalently, $\delta_{\mathrm{m}}(\tau_{\mathrm{ini}}) = a_{\mathrm{ini}}$ and $\delta'_{\mathrm{m}}(\tau = \tau_{\mathrm{ini}}) = H(a_{\mathrm{ini}})a_{\mathrm{ini}}^2$], a_{ini} and τ_{ini} being the scale factor and conformal time at which the initial conditions are applied, respectively. However, this is only an option if two requirements are met: firstly, a_{ini} must be deep in the matter-dominated epoch, when dark energy and any spatial curvature are still very sub-dominant and need not be taken into account. Secondly, the given initial conditions are only valid in a ΛCDM cosmology [296]. This is where the quantity z_{bound} derived in subsection 5.2.4 comes in. Let us recall that when $z = z_{\mathrm{bound}}$, $f(R) = R - 2\Lambda(1-\epsilon)$ for some $\epsilon \ll 1$. Therefore, by calculating z_{bound} for the expected range of values of b, we may estimate the maximum redshift at which a model becomes effectively indistinguishable from ΛCDM, and we can also ensure that this happens in the matter-dominated era by choosing an adequate ϵ. Consequently, we know where to apply the initial conditions in question. The specific value of ϵ is thus dependent upon the dynamics of the model being considered (Table 5.4). For instance, in the case of the Hu-Sawicki model, it suffices to have $\epsilon \sim 10^{-5}$. On the other hand, the Exponential model converges to ΛCDM extremely rapidly and hence a smaller ϵ works better, although it is still necessary to fix $z_{\mathrm{ini}}\,(= a_{\mathrm{ini}}^{-1} - 1)$ at a value larger than the maximum z_{bound}. The same can be said for the Tsujikawa model. It should be noted that the final results are *not* dependent on the exact value of ϵ (provided ϵ is chosen properly). This was verified for both the Exponential and Tsujikawa models.

The initial conditions for Eqs. (5.19)–(5.23) are essentially the ΛCDM limits of the quantities in Eq. (5.11). Once we have an approximate upper bound for z_{bound}, we are able to identify a range of redshifts at which these conditions are best specified. The exact value we pick is not important.

The second quantity we need is $\sigma_8(z)$. This is defined as in Eq. (4.72), but with one

[86] For the given range of wave numbers, we have that $4 \times 10^{-4}\,h^2\,\mathrm{Mpc}^{-2} \leq k_\dagger^2 \leq 4 \times 10^{-2}\,h^2\,\mathrm{Mpc}^{-2}$. In contrast, Eq. (1.51) implies that the spatial curvature $\kappa\,(= -\Omega_k^0 H_0^2)$ is constrained to lie in the interval $-H_0^2 \leq \kappa \leq H_0^2$, otherwise expressed as $-1.11 \times 10^{-7}\,h^2\,\mathrm{Mpc}^{-2} \leq \kappa \leq 1.11 \times 10^{-7}\,h^2\,\mathrm{Mpc}^{-2}$ – although in reality $|\Omega_k^0|$ is not expected to exceed 0.1 [20], let alone approach unity.

TABLE 5.4: The value of ϵ adopted for each model.

Model	ϵ
Hu-Sawicki	10^{-5}
Starobinsky	10^{-10}
Exponential	10^{-50}
Tsujikawa	10^{-15}

exception: the contrast function $\delta_{\rm m}$ is $k_\dagger$-dependent in $f(R)$ gravity, and so must be included as part of the integrand when we integrate over $k_\dagger$:

$$\sigma_8^2(z) = \int_0^\infty \delta_{\rm m}^2(z, k_\dagger)\, k_\dagger^{2+n_s} \left[\frac{4A_s\, k_*^{1-n_s}}{25 H_0^4 \left(\Omega_{\rm m}^0\right)^2}\right] T^2(k_\dagger) W^2(k_\dagger)\, {\rm d}k_\dagger \ . \tag{5.66}$$

That one modification, however, means much in terms of code complexity and run time. Every different value of $k_\dagger$ we consider entails that we solve Eq. (5.58) numerically for $\delta_{\rm m}$ over the relevant redshift range. The results are stored in a table, and at a given redshift z and comoving wave number $k_\dagger$, $\delta_{\rm m}(z, k_\dagger)$ is extracted from the table by interpolation and used to calculate the integrand in Eq. (5.66). This way, the numerical integrator is supplied with the value of the integrand at any $k_\dagger$ and z. To cut down on running time, it is best to solve equations (5.19)–(5.23) first. These do not contain $\delta_{\rm m}$ or any of its derivatives. Hence, solving them separately from Eq. (5.58) is perfectly feasible. The results can then be made accessible to the numerical integrator, enabling it to read in (or acquire by interpolation) the value of the relevant parameters at any redshift while solving Eq. (5.58) for $\delta_{\rm m}$.

The approach detailed above makes it necessary to truncate the range of wave numbers over which integration is performed. The best way to achieve this is by plotting the integrand as a function of $k_\dagger$ for various values of z, then inferring the cut-off point from the outcome. Fig. 5.1 shows a sample of such plots. The intuitive choice is $k_\dagger = 0.5\, h\,{\rm Mpc}^{-1}$, but one must keep in mind that perturbations evolve non-linearly on scales smaller than around $0.2\, h\,{\rm Mpc}^{-1}$. Consequently, the linear perturbation equations we work with do not give an accurate description of structure growth beyond this limit. $k_\dagger = 0.5\, h\,{\rm Mpc}^{-1}$ is nonetheless a good starting point. We refine it further by calculating $\sigma_{8,0}$ for a ΛCDM cosmology and comparing it with the value returned by the default CLASS code. The two are closest when the upper integration limit is $\approx 0.4\, h\,{\rm Mpc}^{-1}$.

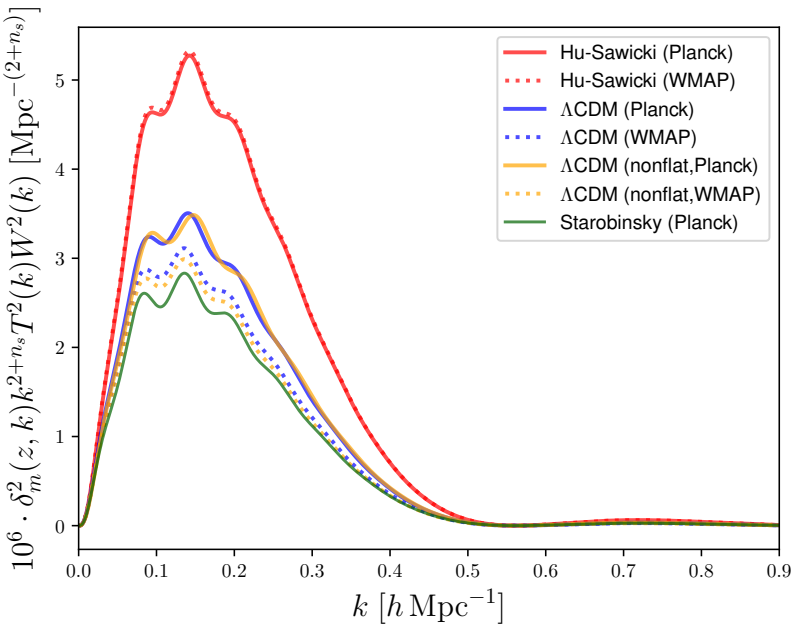

FIGURE 5.1: The variation of the integrand in Eq. (5.66) with comoving wave number (only the $k_\dagger$-dependent part is plotted). The curves labelled 'Hu-Sawicki' are based on the mean parameter values presented in Table V of Ref. [356], while the remaining parameters were fixed in accordance with either the *Planck* 2018 [20] or the WMAP 9-year [19] results. The label 'ΛCDM' indicates that only *Planck* or WMAP values were used. The curve for the Starobinsky model was obtained by combining the results of Ref. [339] with Planck values.

TABLE 5.5: The flat priors for the baseline parameters.

Parameter	Min	Max
$H_0\ \left(\mathrm{km\ s^{-1}Mpc^{-1}}\right)$	50	90
$\Omega_\mathrm{b}^0 h^2$	0.005	0.040
$\Omega_\mathrm{cdm}^0 h^2$	0.05	0.20
Ω_k^0	-0.3	0.3
b	0.0	1.0
n_s	0.75	1.25
$\ln\left(10^{10}A_s\right)$	2.8	3.2

The study was performed using the Cosmic Linear Anisotropy Solving System (CLASS) v.2.6.3 [263] (with the necessary modifications to the background module) to simulate the cosmological evolution. Markov Chain Monte Carlo (MCMC) sampling of parameter probability distributions was done with MONTE PYTHON v.3.0.1 [264, 361], and the plots presented in the next section were constructed with the MCMC anal-

ysis package GetDist v.1.0.3 [314]. The priors required for the MCMC part of the analysis are listed in Table 5.5. Any parameters not included in the baseline set were allowed to take their CLASS default values, the only exception being the reionization optical depth, which was set to 0.0544 [20]. Moreover, $\ln(10^{10}A_s)$ was varied subject to a likelihood constructed from the *Planck* 2018 TT,TE,EE+lowE+lensing mean value and 1σ confidence interval $\{A_s = (2.10 \pm 0.03) \times 10^{-9}$ [20]$\}$. This is necessary because otherwise, the LSS likelihood attempts to make model predictions compatible with LSS data by 'picking' values of A_s well outside the established range.

5.5 Results

5.5.1 The Hu-Sawicki model

As shown in Figs. 5.2 and 5.3, as well as in the triangle plots provided in Appendix B, the 2D posteriors for b are not Gaussian. Therefore, the mean and standard deviation tell us very little, and for this reason Table 5.6 includes the 68^{th} and 95^{th} percentiles i.e. the values of b below which 68% or 95% of sampled points (approximately equivalent to 68% or 95% of the one-dimensional posterior) may be found. Here it is important to note that not all sampled points are distinct: whenever a proposal is rejected by the algorithm, the previous sample (in other words, the last point to be incorporated into the chain) is repeated. A concise review of Markov Chain Monte-Carlo sampling is provided in Appendix D.

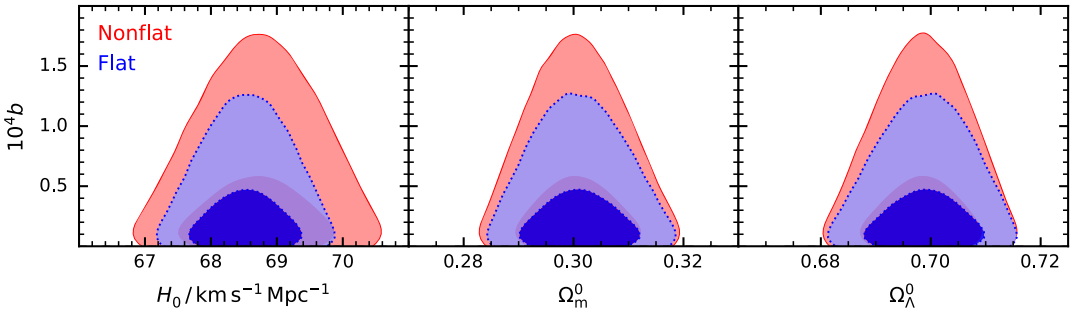

Figure 5.2: Marginalised posterior probability distributions for the deviation parameter b vs *(left)* H_0, *(centre)* Ω_{m}^0, *(right)* Ω_Λ^0, in the context of the Hu-Sawicki model. The label 'Flat' denotes constraints obtained with Ω_k^0 fixed at zero, while 'Nonflat' means that Ω_k^0 was treated as a free parameter. Dark and light shades represent 1σ and 2σ confidence intervals, respectively.

TABLE 5.6: Mean values and 1σ confidence limits for the Hu-Sawicki model.

Parameter	Flat	Nonflat	Nonflat
	$k_\dagger = 0.1\,h\,\mathrm{Mpc}^{-1}$	$k_\dagger = 0.1\,h\,\mathrm{Mpc}^{-1}$	$k_\dagger = 0.05\,h\,\mathrm{Mpc}^{-1}$
H_0	$68.5280^{+0.4797}_{-0.4851}$	$68.6820^{+0.6489}_{-0.6655}$	$68.6880^{+0.6491}_{-0.6628}$
$10^3\Omega_\mathrm{b}^0 h^2$	$22.4790^{+0.1441}_{-0.1460}$	$22.4310^{+0.1722}_{-0.1711}$	$22.4310^{+0.1731}_{-0.1725}$
$\Omega_\mathrm{cdm}^0 h^2$	$0.1188^{+0.0010}_{-0.0010}$	$0.1194^{+0.0015}_{-0.0016}$	$0.1194^{+0.0015}_{-0.0016}$
$10^3\Omega_k^0$	$--$	$0.8612^{+1.9846}_{-1.9610}$	$0.8798^{+1.9762}_{-1.9557}$
$10^4 b$	$0.2739^{+0.1789}_{-0.2739}$	$0.3819^{+0.0438}_{-0.3819}$	$1.8695^{+1.5232}_{-1.8695}$
$10^4 b\,(68\%)$	< 0.2721	< 0.3316	< 1.3738
$10^4 b\,(95\%)$	< 0.9357	< 1.2139	< 5.3355
n_s	$0.9705^{+0.0041}_{-0.0041}$	$0.9689^{+0.0051}_{-0.0051}$	$0.9689^{+0.0051}_{-0.0051}$
$\ln\left(10^{10} A_s\right)$	$3.0442^{+0.0148}_{-0.0144}$	$3.0442^{+0.0148}_{-0.0145}$	$3.0442^{+0.0150}_{-0.0143}$
$\Omega_\Lambda^0 h^2$	$0.6989^{+0.0062}_{-0.0061}$	$0.6982^{+0.0063}_{-0.0061}$	$0.6982^{+0.0063}_{-0.0061}$

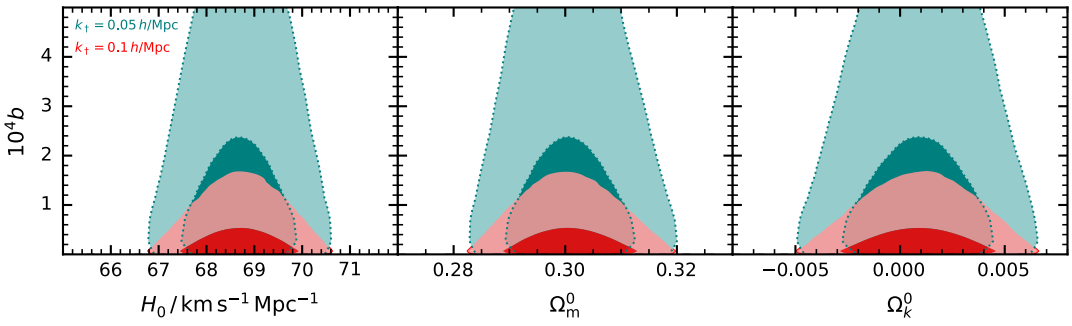

FIGURE 5.3: Marginalised posterior probability distributions for the deviation parameter b vs *(left)* H_0, *(centre)* Ω_m^0, *(right)* Ω_k^0, in the context of the Hu-Sawicki model. The contours are labelled according to the comoving wave number at which the growth rate f was calculated.

From the information presented in Table 5.6, we conclude that the constraints placed on b when $k_\dagger = 0.05\,h\,\mathrm{Mpc}^{-1}$ are considerably weaker than those corresponding to $k_\dagger = 0.1\,h\,\mathrm{Mpc}^{-1}$. This feature also emerges clearly in Fig. 5.2. As for spatial curvature, the role it plays is hardly significant: the 2D posteriors for b vs Ω_k^0 are compatible with a flat geometry within a 1σ confidence interval (as are the results of Table 5.6 for Ω_k^0), and Fig. 5.2 demonstrates that apart from slightly loosening constraints, the presence of curvature has minimal effect on b. We shall note much the same behaviour for the Starobinsky, Exponential and Tsujikawa models.

5.5.2 The Starobinsky model

As is immediately apparent from Fig. 5.5, constraints on b are again appreciably tighter for the larger wave number. It would be interesting to extend the analysis and investigate whether this is a general trend; in other words, whether smaller scales allow for less deviation from ΛCDM.

Here, too, spatial curvature has little impact on the mean values and percentiles we get for b.

TABLE 5.7: Mean values and 1σ confidence limits for the Starobinsky model.

Parameter	Flat	Nonflat	Nonflat
	$k_\dagger = 0.1\,h\,\mathrm{Mpc}^{-1}$	$k_\dagger = 0.1\,h\,\mathrm{Mpc}^{-1}$	$k_\dagger = 0.05\,h\,\mathrm{Mpc}^{-1}$
H_0	$68.4300^{+0.4808}_{-0.4885}$	$68.6080^{+0.6570}_{-0.6666}$	$68.5910^{+0.6512}_{-0.6586}$
$10^3\Omega_\mathrm{b}^0 h^2$	$22.4620^{+0.1461}_{-0.1457}$	$22.4250^{+0.1723}_{-0.1711}$	$22.4250^{+0.1703}_{-0.1729}$
$\Omega_\mathrm{cdm}^0 h^2$	$0.1190^{+0.0010}_{-0.0010}$	$0.1195^{+0.0015}_{-0.0016}$	$0.1195^{+0.0015}_{-0.0015}$
$10^3\Omega_k^0$	$--$	$0.7888^{+2.0068}_{-1.9766}$	$0.7448^{+2.0605}_{-1.8984}$
b	$0.0074^{+0.0256}_{-0.0074}$	$0.0087^{+0.0246}_{-0.0087}$	$0.0132^{+0.0021}_{-0.0132}$
$b\,(68\%)$	< 0.0067	< 0.0068	< 0.0137
$b\,(95\%)$	< 0.0178	< 0.0189	< 0.0382
n_s	$0.9699^{+0.0041}_{-0.0042}$	$0.9687^{+0.0051}_{-0.0051}$	$0.9687^{+0.0050}_{-0.0051}$
$\ln\left(10^{10}A_s\right)$	$3.0442^{+0.0148}_{-0.0146}$	$3.0442^{+0.0150}_{-0.0146}$	$3.0442^{+0.0152}_{-0.0144}$
$\Omega_\Lambda^0 h^2$	$0.6976^{+0.0063}_{-0.0061}$	$0.6975^{+0.0063}_{-0.0061}$	$0.6974^{+0.0064}_{-0.0058}$

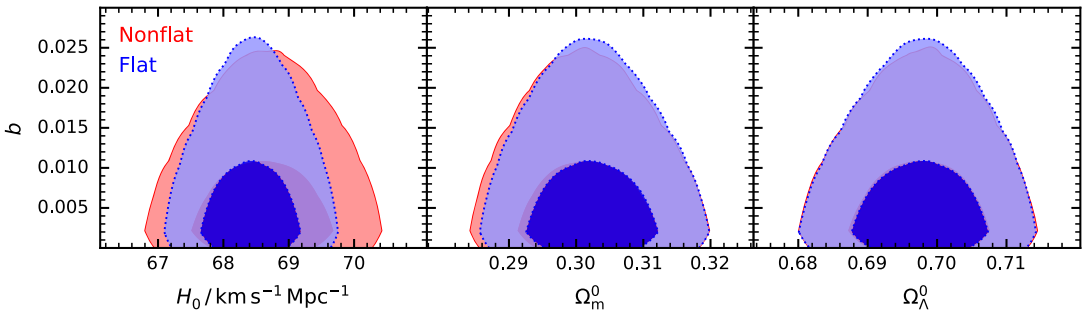

FIGURE 5.4: Marginalised posterior probability distributions for the deviation parameter b vs *(left)* H_0, *(centre)* Ω_m^0, *(right)* Ω_Λ^0, in the context of the Starobinsky model.

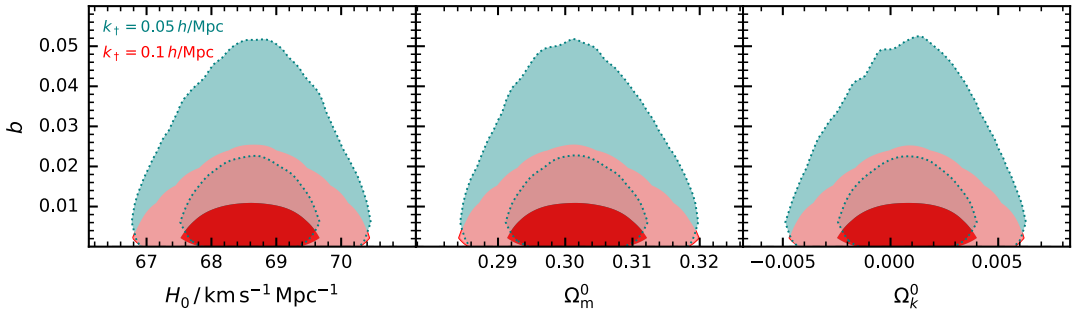

FIGURE 5.5: Marginalised posterior probability distributions for the deviation parameter b vs *(left)* H_0, *(centre)* Ω_m^0, *(right)* Ω_k^0, in the context of the Starobinsky model. The contours are labelled according to the comoving wave number at which the growth rate f was calculated.

5.5.3 The Exponential model

Results are presented in Table 5.8, in Figs. 5.6 and 5.7, and in Appendix B. As was the case for the Hu-Sawicki and Starobinsky models, the constraints obtained for the cosmological parameters[87] with $k_\dagger = 0.1\,h\,\mathrm{Mpc}^{-1}$ and $k_\dagger = 0.05\,h\,\mathrm{Mpc}^{-1}$ are very similar; this conclusion is especially reinforced by the triangle plot in Appendix B. The same plot shows that there is a high degree of anti-correlation between the age of the Universe and Ω_k^0. Accordingly, a universe with positive curvature (negative Ω_k^0) would be older than one having $\kappa < 0$. This feature is common to all $f(R)$ models we study. Contrary to what was noted for the previous two models, however, we find that a change in wave number does not have significant consequences for b.

The 2D marginalised posteriors for the flat and non-flat scenarios (included in Appendix B) demonstrate that fixing Ω_k^0 at zero tends to tighten contours, especially

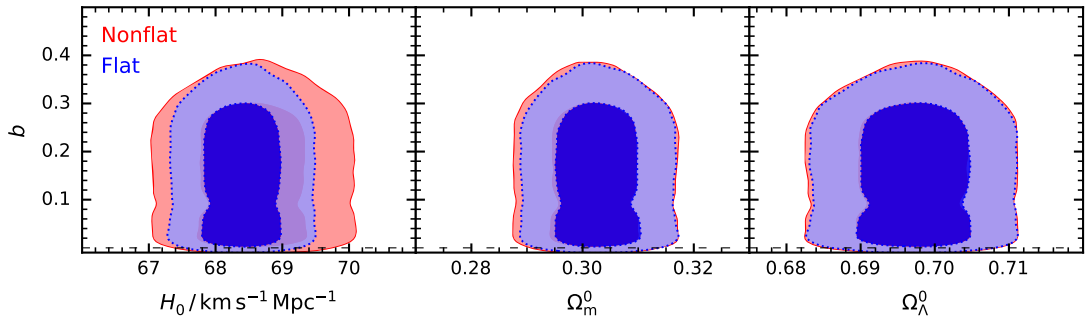

FIGURE 5.6: Marginalised posterior probability distributions for the deviation parameter b vs *(left)* H_0, *(centre)* Ω_m^0, *(right)* Ω_Λ^0, in the context of the Exponential model.

[87] b is classified as a *model* parameter, not a cosmological one.

TABLE 5.8: Mean values and 1σ confidence limits for the Exponential model.

Parameter	Flat $k_\dagger = 0.1\,h\,\mathrm{Mpc}^{-1}$	Nonflat $k_\dagger = 0.1\,h\,\mathrm{Mpc}^{-1}$	Nonflat $k_\dagger = 0.05\,h\,\mathrm{Mpc}^{-1}$
H_0	$68.3990^{+0.4800}_{-0.4810}$	$68.5510^{+0.6598}_{-0.6648}$	$68.5650^{+0.6520}_{-0.6657}$
$10^3\Omega_\mathrm{b}^0 h^2$	$22.4560^{+0.1457}_{-0.1448}$	$22.4210^{+0.1701}_{-0.1719}$	$22.4220^{+0.1719}_{-0.1715}$
$\Omega_\mathrm{cdm}^0 h^2$	$0.1191^{+0.0010}_{-0.0010}$	$0.1195^{+0.0016}_{-0.0016}$	$0.1195^{+0.0015}_{-0.0016}$
$10^3\Omega_k^0$	$--$	$0.7000^{+2.0506}_{-1.9734}$	$0.7216^{+1.9878}_{-1.9544}$
b	0.1601 ± 0.1029	0.1641 ± 0.1135	0.1769 ± 0.1124
n_s	$0.9697^{+0.0041}_{-0.0041}$	$0.9686^{+0.0051}_{-0.0052}$	$0.9686^{+0.0051}_{-0.0052}$
$\ln\left(10^{10}A_s\right)$	$3.0443^{+0.0147}_{-0.0146}$	$3.0441^{+0.0149}_{-0.0144}$	$3.0442^{+0.0149}_{-0.0144}$
Ω_Λ^0	$0.6972^{+0.0063}_{-0.0061}$	$0.6971^{+0.0063}_{-0.0061}$	$0.6971^{+0.0063}_{-0.0061}$

those that involve the age of the Universe. Such behaviour is in line with our previous observation that spatial curvature and cosmic age are strongly (anti-) correlated.

Another curious feature that emerges in Figs. 5.6 and 5.7 is the bi-modality of the 2D posteriors for b. In this regard, some important points to consider are the following:

- Bi-modality also appears in the plots presented in Fig. 4 of Ref. [348], especially the ones obtained with the combination of JLA, BAO, CC (cosmic clocks), and H_0 data sets. Let us focus on what the two studies have in common: the JLA, BAO and CC likelihoods (there are some differences – to begin with, we use the Pantheon rather than the JLA likelihood, and the BAO and CC data does not exactly match ours, either).

- Removing these likelihoods one at a time from the set specified in Eq. (5.62), and running a few chains, quickly allows us to deduce that the observed bi-modality cannot be attributed to the JLA, BAO or CC likelihoods. Whether or not it is an intrinsic property of the model is hard to tell, however, since it is not easy to test if any features of the posteriors are due to the LSS or CMB likelihoods. In the absence of the former, constraints on b become extremely weak, whereas removing the latter makes it very difficult to get good convergence.

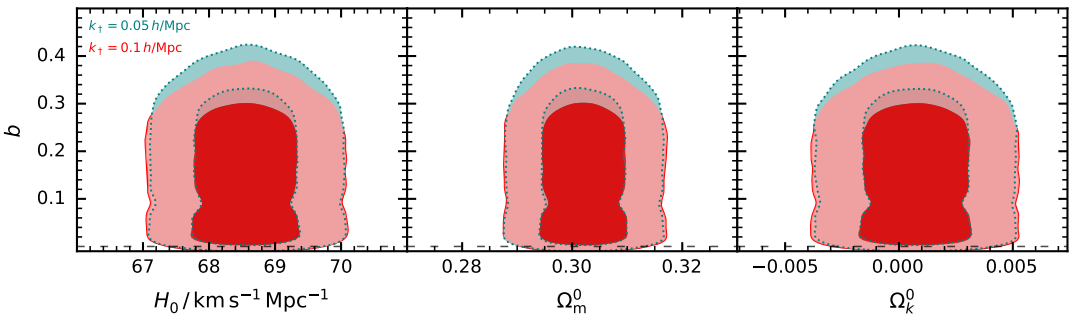

FIGURE 5.7: Marginalised posterior probability distributions for the deviation parameter b vs *(left)* H_0, *(centre)* Ω_m^0, *(right)* Ω_k^0, in the context of the Exponential model. The contours are labelled according to the comoving wave number at which the growth rate f was calculated.

5.5.4 The Tsujikawa model

In this case, the 2D marginalised posteriors for b (Figs. 5.8 and 5.9) also turn out to be bimodal. We again note (from Table 5.9 and the triangle plots in Appendix B) that changing $k_\dagger$ from $0.1\,h\,\mathrm{Mpc}^{-1}$ to $0.05\,h\,\mathrm{Mpc}^{-1}$ has very little effect on the results, and that parameter constraints are, on the whole, more stringent when the Universe is assumed to be flat.

TABLE 5.9: Mean values and 1σ confidence limits for the Tsujikawa model.

Parameter	Flat $k_\dagger = 0.1\,h\,\mathrm{Mpc}^{-1}$	Nonflat $k_\dagger = 0.1\,h\,\mathrm{Mpc}^{-1}$	Nonflat $k_\dagger = 0.05\,h\,\mathrm{Mpc}^{-1}$
H_0	$68.3970^{+0.4811}_{-0.4815}$	$68.5620^{+0.6480}_{-0.6591}$	$68.5540^{+0.6552}_{-0.6608}$
$10^3\Omega_\mathrm{b}^0 h^2$	$22.4550^{+0.1448}_{-0.1450}$	$22.4220^{+0.1713}_{-0.1712}$	$22.4210^{+0.1706}_{-0.1706}$
$\Omega_\mathrm{cdm}^0 h^2$	$0.1191^{+0.0010}_{-0.0010}$	$0.1195^{+0.0015}_{-0.0016}$	$0.1196^{+0.0015}_{-0.0016}$
$10^3\Omega_k^0$	$--$	$0.7180^{+1.9853}_{-1.9563}$	$0.7129^{+1.9839}_{-1.9624}$
b	0.3028 ± 0.1858	0.2999 ± 0.1843	0.3312 ± 0.2031
n_s	$0.9697^{+0.0041}_{-0.0041}$	$0.9686^{+0.0052}_{-0.0051}$	$0.9686^{+0.0051}_{-0.0051}$
$\ln\left(10^{10} A_s\right)$	$3.0443^{+0.0148}_{-0.0144}$	$3.0442^{+0.0149}_{-0.0145}$	$3.0442^{+0.0149}_{-0.0145}$
Ω_Λ^0	$0.6972^{+0.0063}_{-0.0061}$	$0.6971^{+0.0063}_{-0.0061}$	$0.6970^{+0.0063}_{-0.0061}$

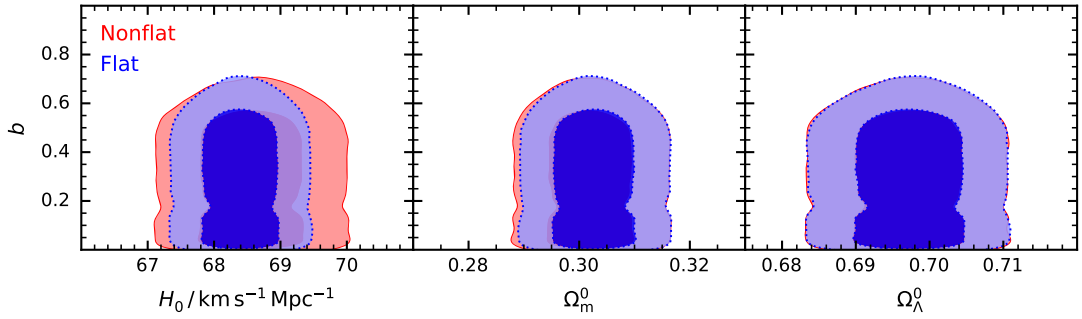

FIGURE 5.8: Marginalised posterior probability distributions for the deviation parameter b vs *(left)* H_0, *(centre)* Ω_m^0, *(right)* Ω_Λ^0, in the context of the Tsujikawa model.

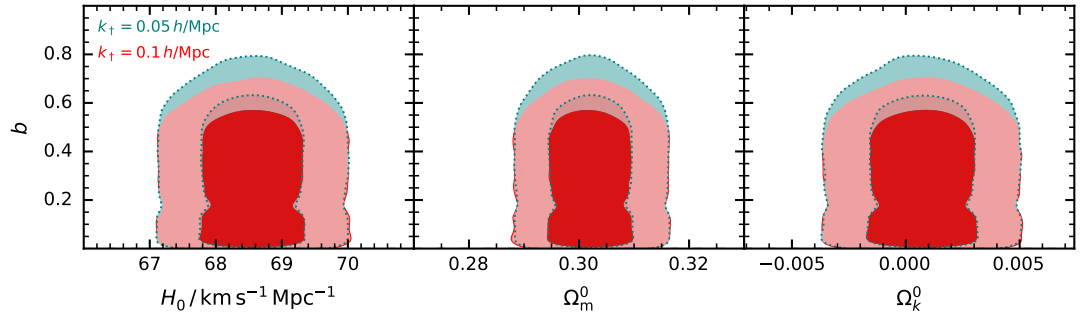

FIGURE 5.9: Marginalised posterior probability distributions for the deviation parameter b vs *(left)* H_0, *(centre)* Ω_m^0, *(right)* Ω_k^0, in the context of the Tsujikawa model. The contours are labelled according to the comoving wave number at which the growth rate f was calculated.

5.6 In Brief...

This chapter analyses the role of spatial curvature in the framework of $f(R)$ gravity: more specifically, in the context of the Hu-Sawicki, Starobinsky, Exponential and Tsujikawa models. The deviation from ΛCDM is quantified by a parameter b, which was found to exclude the ΛCDM limit ($b = 0$) at 1σ in the Exponential and Tsujikawa models.

We have seen that treating Ω_k^0 as a free parameter has little impact on the results in comparison to fixing it at zero. Moreover, the constraints obtained for Ω_k^0 are all compatible with a flat geometry within a 1σ confidence interval. This appears to be independent of the value we choose for the comoving wave number $k_\dagger$. In general, the constraints placed on cosmological parameters when $k_\dagger = 0.1\,h\,\mathrm{Mpc}^{-1}$ are essentially the same as those resulting from $k_\dagger = 0.05\,h\,\mathrm{Mpc}^{-1}$, but may change significantly in

the case of the model parameter b. The latter effect was mainly noted for the Hu-Sawicki and Starobinsky models, which yielded considerably tighter constraints for b when $k_\dagger$ was set to $0.1\,h\,\mathrm{Mpc}^{-1}$.

Conclusion

A successful cosmological model must incorporate the observed accelerated expansion of the Universe. This can mainly be done in two ways: by adding *dark energy* (i.e. a component with negative pressure) to the cosmic fluid, or by modifying gravity i.e. altering the General Relativistic description of the geometry of space-time. The most popular cosmological model is undoubtedly ΛCDM, in which the negative pressure is provided by a cosmological constant Λ that is identified with the energy of the vacuum itself. Unlike matter and radiation, this energy does not get diluted as the Universe expands. It eventually comes to dominate and causes the cosmic expansion to accelerate. ΛCDM has proven to be successful on many fronts, but its various shortcomings have prompted the scientific community to propose other models of dark energy. Chapter 1 provides an overview of the most well-known among these. The greater majority are characterised by some form of dark energy whose density varies with time (contrary to what happens in ΛCDM), and are hence called *dynamical dark energy models*. Theories which modify the gravitational sector directly are also included in this category, because they usually give rise to the same effects as a dynamical dark energy component.

Chapter 1 additionally introduces the issue of spatial curvature. The Universe is often assumed to be spatially flat, as evidenced by a great number of works in the literature. Many times, this is based on the fact that a flat geometry appears to be consistent with observations. For the most part, however, the studies which present evidence for such consistency do so in a ΛCDM context [19, 20, 106, 107]. It appears that the compatibility of observational data with non-zero spatial curvature depends on the model considered and even on the selected data sets. Indeed, some dynamical dark energy models seem to accommodate a non-flat geometry more readily than ΛCDM [112–114]. The crux of the matter is that spatial curvature is correlated with a good number of cosmological or model-dependent parameters, so a wrong assumption about it can greatly distort our conclusions regarding the nature and evolution of dark energy [115, 117]. It is therefore of utmost importance that the possibility of a curved geometry is not treated lightly. This brings us to the aim of the work presented here: the investigation of whether different dynamical dark energy models also support the

hypothesis of spatial flatness, or whether they fit the data best in the presence of curvature. In all cases, the space-time manifold is equipped with the Friedmann-Lemaître-Robertson-Walker (FLRW) metric. Chapter 1 outlines the main features of an FLRW cosmology.

In Chapter 2, dark energy is modelled as a scalar field that can either be minimally or non-minimally coupled to the Ricci scalar. Several analytical late-time solutions to the Friedmann equations are constructed – three are valid in the absence of spatial curvature, two hold in a closed universe, and another two in an open one. These solutions all give rise to an accelerated expansion and satisfy the weak energy condition. However, a good proportion of them have some unpalatable characteristic, such as the failure to account for a matter distribution, or the prediction of a cosmic age that is not in line with current constraints. The most promising is a model in which the scale factor increases exponentially with time, the matter content is dust-like, the minimally-coupled scalar field ϕ is given by $C(D_1 - D_2\mathrm{e}^{-Bt})^{3/2}$ (C, D_1 and D_2 being constants), and the spatial curvature is positive. The energy density of the scalar field gradually loses its dynamic nature, indicating that ϕ begins to behave like a cosmological constant as time goes by.

The work presented in Chapter 2 illustrates an important point: it is often necessary to combine analytical methods with numerical techniques when trying to solve the field equations for a particular model. The introduction of spatial curvature tends to increase the complexity of the equations. This makes it very difficult to find exact analytical solutions that can be reconciled with cosmological observations.

Chapter 3 attempts to answer the question: if three models are identical in all aspects except for curvature at some fixed point in time, how would they evolve? The role of curvature is thus investigated in the context of five models from the literature [176, 199]. The first model is constructed by using the Van der Waals (VdW) equation of state (EoS) to describe the cosmic fluid. This way, it is confirmed that a dark energy component is needed to correctly reproduce the current period of acceleration, and so in the remaining four models, dark energy is introduced as Quintessence, a Chaplygin gas or a dynamical Λ. Meanwhile, the matter distribution takes the form of a VdW fluid in the first four models but is dust-like in the last one. What is especially interesting about the fifth model is the fact that, since there is no VdW fluid which can give rise to inflation, the time-dependent vacuum must be the factor responsible for the accelerated expansion during both early and late times [199].

The effects due to curvature turn out to be quite significant. It is found that the

transition to the epoch of decelerated expansion would be delayed for the closed universe (with respect to the flat one); so would the start of the current dark energy-dominated era. Moreover, positive curvature appears to enhance both the inflationary acceleration and also the subsequent deceleration. On the other hand, the opposite is noted for an open universe. The commonality of these features among all five models[88] suggests that they are independent of the form that matter and dark energy take. Furthermore, small variations in the initial conditions or in any of the parameters only alter the magnitude of the effects due to curvature. Another interesting characteristic is the fact that the evolution appears to be much less dependent on spatial curvature at late times.

The work presented in Chapter 3 may be extended in a number of ways. In Ref. [362], the authors show that it actually *is* possible to attribute the current acceleration to a VdW fluid. It does not appear likely, however, that the EoS parameter values which reproduce the inflationary and matter-dominated epochs might, at the same time, also account for late-time acceleration. Hence, one could generalise the constant-value parameters in the VdW EoS to functions of time, and attempt to do this in such a way that the resulting EoS describes the whole cosmic evolution. Another option would be to cast the first four models in a form that enables comparison with ΛCDM. This promises to be quite challenging, because in their current state the models are mainly phenomenological, in the sense that they are meant to highlight the fact that a simple combination of fluids – a VdW matter distribution and a dark energy component – can provide an explanation for the basic features of the complete cosmic history. Choosing values for the EoS parameters solely on the basis of theoretical or observational considerations is another thing altogether. Indeed, with reference to $\log\left[\rho_{\mathrm{m}}(z=0)/\rho_{\mathrm{m}}^{\mathrm{c}}\right]$, Capozziello et al. report that 'there are no physical motivations to select a plausible range' of values [362].

Chapter 4 deals with three models from the literature that feature a dynamical Λ. The first is the General Running Vacuum Model (GRVM) – whose characteristic $\Lambda(H)$ takes the form $A + BH^2 + C\dot{H}$ [212] – and it is followed by two sub-cases: the Running Vacuum Model (RVM), obtained by setting C to zero [213], and the model we call the General Running Vacuum Sub-case (GRVS), which has a null value for B instead [219]. It is assumed that the vacuum only exchanges energy with cold dark matter as it decays. The parameters B and/or C are constrained by employing Markov Chain Monte Carlo techniques, initially using data for observables associated

[88] Or the last four, in the case of late-time acceleration.

with Type Ia supernovae, cosmic chronometers, the cosmic microwave background, and baryon acoustic oscillations. Each model is first investigated in the context of a flat space-time. Then Ω_k^0 is allowed to vary and any significant differences are analysed. The effects of introducing a measurement of the Hubble constant as a fifth likelihood are also considered. This is done for two different values of H_0: $H_0^{\mathrm{R}} = 73.48 \pm 1.66\ \mathrm{km\,s^{-1}\,Mpc^{-1}}$ [26] and $H_0^{\mathrm{E}} = 70.6 \pm 3.3\ \mathrm{km\,s^{-1}\,Mpc^{-1}}$ [308]. Finally, observations related to the growth of large-scale structure (LSS) are included in the collection of data sets, and the whole procedure is repeated. The amplitude of the primordial scalar power spectrum is either assigned a fixed value or treated as a freely-varying parameter.

In the case of the GRVM, the data employed is insufficient to break parameter degeneracies when the assumption of flatness is relaxed. The constraints obtained in the flat scenario are, however, informative: it is found that the addition of the LSS likelihood makes the 2D posteriors for B versus H_0 or Ω_{m}^0 close around the ΛCDM limit (and likewise for C). It also changes the mean values of B and C from positive to negative – although only if H_0^{R} is absent from the combination of data sets, because the correlation between B (or C) and the Hubble constant causes the H_0^{R} likelihood to shift the posteriors in the direction of increasing B (or C). It is furthermore noted that the inclusion of growth data lowers the averages for H_0, enhancing compatibility with the range of values established by *Planck* [20].

Next, we turn our attention to the RVM. This time, the use of LSS data excludes the ΛCDM limit at a little over 1σ (in both the flat and non-flat cases, with one exception in the latter). When spatial flatness is not imposed, the mean values of B change from negative to positive, and again it is found that growth data lends support to values of H_0 which resonate with the *Planck* result. Of particular relevance is the fact that all the constraints on Ω_k^0 become consistent with a flat geometry (within a 1σ confidence interval) once LSS observations are taken into account.

The GRVS parallels the RVM in many ways. Here, too, growth data is responsible for a dynamical Λ being preferred to a cosmological constant at a little over 1σ, and once more this turns out to hold (for the most part) whether or not the Universe is assumed to be flat. The LSS likelihood establishes a definite (negative) sign for C and increases compatibility between the average values of H_0 and the *Planck* constraints. Its effect on the 1D posterior distributions for Ω_k^0 is similar to what was noted for the RVM. In all cases, the addition of LSS observations puts $\Omega_k^0 = 0$ at less than 1σ from the resulting mean, but in its absence both the RVM and GRVS show some

preference for an open universe, and indeed the level of support provided by the RVM for a positive Ω_k^0 is over 2σ when $H_0^{\rm R}$ is included with the data.

To sum up, Chapter 4 indicates that a mildly-evolving Λ (modelled as in the RVM or GRVS) is only marginally favoured over the cosmological constant. Moreover, this comes at the cost of an extra parameter which – while not given much weight by the Akaike Information Criterion – has a negative impact on the BIC score (where BIC stands for 'Bayesian Information Criterion'). Another point of interest is the fact that merging the RVM and GRVS expressions for Λ into a two-parameter combination (the GRVM) appears to weaken the support for dynamical vacuum energy. Additionally, it seems that the addition of LSS data reduces the ability of the models to accommodate a non-zero Ω_k^0.

Chapter 4 opens up the possibility for further research in several ways. The study makes use of perturbation equations as approximated in the sub-Hubble, quasi-static regime. To begin with, therefore, one could compute the full set of linear perturbations, as this would increase the reliability of parameter constraints obtained with the LSS likelihood. A second advantage would be a much wider choice of data sets. There is also room for improvement with respect to the behaviour of the models deep in the radiation epoch. The exchange of energy between dark matter and the running vacuum means that at very early times, the high energy density of the dynamical-Λ component causes dark matter to have a negative energy density, which is not physically viable. In Ref. [218], the authors suggest that such problems could be avoided by allowing dark energy to interact with radiation as well, so this is something that could be looked into. One should however tread with caution here: if radiation is no longer conserved separately, the distance-duality relation would deviate from the form established by the standard model, as would the dependence of the CMB temperature on redshift. These modifications are constrained very tightly by numerous works in the literature [315–322].

In Chapter 5, we consider the $f(R)$ theory of gravitation and focus especially on four models: the Hu-Sawicki, Starobinsky, Exponential and Tsujikawa models. All of these become indistinguishable from ΛCDM at high redshifts, and are characterised by a *deviation parameter* b that quantifies the departure from ΛCDM. First, we generalise the differential equation for the contrast function and include spatial curvature. Then, using a collection of data sets very similar to the ones described above, an MCMC analysis is carried out. It turns out that the constraints placed on b are largely independent of curvature. Furthermore, the 2D posterior distributions for b vs Ω_k^0

appear to be compatible with a flat geometry (within a 1σ confidence interval) in all cases. However, we must not forget that it is the LSS likelihood which puts the strongest bounds on $b\ldots$ and in the study presented here, we limit the perturbation analysis to the sub-Hubble, quasi-static regime. It remains to be seen if using the full set of perturbations would reinforce our results. Non-linear growth could also be taken into account.

In conclusion, it appears that whether spatial curvature is ruled out or not is determined by a combination of factors. The properties of the particular model definitely play an important part, and for this reason, some authors have proposed ways in which to obtain model-independent constraints. Additionally, we might ask what happens if the FLRW metric is replaced [363].

The influence that the choice of data set has on curvature constraints emerges clearly in Chapter 4. We note that LSS data tends to favour a flat geometry (at least in the context of the dynamical-Λ models we consider), while in its absence, the H_0^{R} likelihood provides support for a spatially curved universe (this might partly explain why the results obtained for $f(R)$ gravity are so consistent with spatial flatness – the combined data set we use includes LSS data). We need to ask why it is that certain cosmological observables tend to rule out spatial curvature. For instance, in Fig. 29 of Ref. [20], the addition of BAO data causes the 2D posterior for Ω_{m}^0 vs Ω_k^0 to close up around $\Omega_k^0 = 0$. Could the dependence of BAO measurements on a fiducial cosmology be causing this?

One thing is certain. The possibility of a non-flat geometry should not be treated lightly. After all, Chapter 3 demonstrates that the presence of curvature could affect the whole expansion history in more ways than one.

Appendices

APPENDIX A

Perturbations in General Relativity

The background cosmology is assumed to be homogeneous and isotropic, but galaxy clusters and super-clusters are evidence to the fact that these assumptions break down on smaller scales. The formation of cosmic structure is attributed to the presence of over-densities in the early Universe. Although initially small, the said over-densities (thought to have been seeded by quantum fluctuations during inflation [364]) would have drawn in more matter by gravitational attraction, and this would in turn have strengthened the gravitational pull of the region. Provided gravity could outbalance the repulsive pressure arising from the random thermal motion of particles, matter accretion would have been sustained, ultimately leading to the formation of stars, galaxies, galaxy clusters and filaments. In short, cosmic growth can be attributed to *gravitational instability* [296].

Nowadays the literature contains a wealth of data relating to large-scale structure.[89] If we are to use it to test our models, however, it is imperative to move beyond the background analysis and incorporate matter perturbations into our equations. Furthermore, Einstein's equations tell us that there is an intrinsic connection between the matter content of the Universe and its geometry; as John A. Wheeler aptly puts it, 'space-time tells matter how to move; matter tells space-time how to curve' [366]. The feedback mechanism between the two means that perturbations in the matter sector must be accompanied by fluctuations in the metric tensor, since this provides the basis for any geometrical construct.

We shall be using quasi-Cartesian coordinates when dealing with perturbations. In this coordinate system, the Friedmann-Lemaître-Robertson-Walker (FLRW) metric takes the form:

$$\mathrm{d}s^2 = -\mathrm{d}t^2 + a^2(t)\gamma_{ij}\mathrm{d}x^i\mathrm{d}x^j \ , \tag{A.1}$$

[89] *Large-scale structure* usually refers to inhomogeneities on scales larger than that of a galaxy [365].

where $\gamma_{ij} = \delta_{ij}\left[1 + \frac{1}{4}\kappa\left(x^2 + y^2 + z^2\right)\right]^{-2}$ and δ_{ij} is the Kronecker delta [367]. The cosmic time t shall henceforth be replaced with its conformal analogue τ (the two quantities are related via the scale factor: $\mathrm{d}\tau = \mathrm{d}t/a$).

The analysis of cosmological perturbations requires a gauge to be selected. Given a physical, perturbed space-time $\mathcal{S}$, one may think of the background cosmology as a separate, fictitious space-time $\tilde{\mathcal{S}}$ whose coordinate system $\tilde{x}^\mu$ is extended to $\mathcal{S}$ by way of a one-to-one correspondence between points in $\mathcal{S}$ and $\tilde{\mathcal{S}}$. There are usually a number of candidate points in $\mathcal{S}$ to which a given point $\tilde{P}$ in $\tilde{\mathcal{S}}$ may be mapped, and so a specific correspondence is said to define a choice of *gauge*. Changing the correspondence (without altering the background coordinates) is equivalent to making a gauge transformation [368].

We shall be working exclusively in the *conformal Newtonian* gauge. This is sometimes also referred to as the longitudinal gauge, and is particularly simple due to the fact that it renders the metric diagonal [367, 369]:

$$\mathrm{d}s^2 = a^2(\tau)\left[-(1+2\Phi)\mathrm{d}\tau^2 + \gamma_{ij}(1-2\Psi)\mathrm{d}x^i\mathrm{d}x^j\right] \ , \tag{A.2}$$

although the simplicity comes at a price: the metric is only valid to study the scalar modes of perturbations [369]. Nonetheless, a generalised version that also incorporates vector and tensor modes is not difficult to obtain [370].

Eq. (A.2) introduces the scalar potentials $\Phi(\tau, \vec{x})$ and $\Psi(\tau, \vec{x})$. These constitute the metric perturbations in the conformal Newtonian gauge and are assumed to satisfy the condition $|\Phi|, |\Psi| \ll 1$. Moreover, up to a factor of ± 1, they are of the same form as Bardeen's gauge-invariant variables [368] (provided the latter are expressed in the longitudinal gauge). Another advantage is the fact that Φ plays the role of gravitational potential in the Newtonian limit [369], and so has a straightforward physical interpretation. Finally, the absence of residual gauge modes in the conformal Newtonian gauge [367] means that the meaning of physical modes cannot be obscured [369].

Metric perturbations appear on the left-hand side of the perturbed Einstein field equation:

$$\delta G^\mu_\nu = 8\pi G\, \delta T^\mu_\nu \ . \tag{A.3}$$

Meanwhile, the right-hand side constitutes the perturbed part δT^μ_ν of the energy-

momentum tensor, and may be expanded as follows [368]:

$$\delta T^0_0 = -\delta\rho_{\rm m} \ ; \quad \delta T^0_i = (\rho_{\rm m} + p_{\rm m}) v_i \ ; \quad \delta T^i_0 = -(\rho_{\rm m} + p_{\rm m}) v^i \ ; \quad \delta T^i_j = \delta p_{\rm m}\, \delta^i_j \ . \tag{A.4}$$

Here, $\rho_{\rm m}$ and $p_{\rm m}$ are the background values of the matter energy density and pressure, respectively, and $\delta\rho_{\rm m}$, $\delta p_{\rm m}$ the associated perturbations. The 3-vector v^i represents the perturbation in the spatial velocity.[90] Its covariant counterpart, v_i, may be obtained by using the spatial metric γ_{ij} from Eq. (A.1) ($v_i = \gamma_{ij} v^j$). We keep to the perfect-fluid form and hence do not consider anisotropic stresses (which explains why $\delta T^i_j = 0$ for $i \neq j$) [367]. Moreover, perturbations are included into the equations at linear order only, and are assumed to have adiabatic initial conditions.

The groundwork has now been laid to express the perturbed Einstein equations in physical space. The time-time component of Eq. (A.3) reads [367, 372]:

$$2\left\{-\Psi\left(\vec{\nabla}^2 + 3\kappa\right) + 3\mathcal{H}\left[\frac{{\rm d}\Psi}{{\rm d}\tau} + \Phi\mathcal{H}\right]\right\} + 8\pi G a^2 \rho_{\rm m}\delta_{\rm m} = 0 \ , \tag{A.5}$$

where the conformal Hubble parameter $\mathcal{H}$ is equivalent to the ratio $a'(\tau)/a$, while the matter density contrast $\delta_{\rm m}$ is defined as $\delta\rho_{\rm m}/\rho_{\rm m}$. Finally, $\vec{\nabla}_i$ is the covariant derivative constructed from the spatial metric γ_{ij} [refer to Eq. (A.1)], and $\vec{\nabla}^2 \equiv \vec{\nabla}_i \vec{\nabla}^i$.

The 0-i, i-i and i-j ($i \neq j$) components of Eq. (A.3) respectively take the form [367, 372]:

$$\mathcal{H}\Phi + \frac{{\rm d}\Psi}{{\rm d}\tau} = 4\pi G a^2 \left(\rho_{\rm m} + p_{\rm m}\right) v \ ; \tag{A.6}$$

$$\begin{aligned} &2\frac{{\rm d}\mathcal{H}}{{\rm d}\tau}\Phi + \mathcal{H}^2\Phi + \mathcal{H}\frac{{\rm d}\Phi}{{\rm d}\tau} + \frac{{\rm d}^2\Psi}{{\rm d}\tau^2} + 2\mathcal{H}\frac{{\rm d}\Psi}{{\rm d}\tau} - \kappa\Psi + \frac{1}{2}\left[\vec{\nabla}^2 - \vec{\nabla}^{i_0}\vec{\nabla}_{i_0}\right](\Phi - \Psi) \\ &= 4\pi G a^2 \delta p_{\rm m} \quad \text{(no summation over } i_0) \ ; \end{aligned} \tag{A.7}$$

$$\Psi - \Phi = 0 \ . \tag{A.8}$$

A few comments about the decomposition of the vector field v^i are in order before we proceed. The first thing to recall is that any vector may be expressed as the sum of two components, one corresponding to the gradient of a scalar field (and hence termed the scalar part) and the other with zero divergence (the vector part) [367, 371, 373]. In other words, a vector w^i may be written in the form $w^i_{\rm S} + w^i_{\rm V}$, where the subscripts S

[90] The isotropic nature of the FLRW geometry implies that the cosmic fluid is at rest in the background universe, so that its unperturbed 4-velocity u^μ is $a^{-1}(1, \vec{0})$ [371].

and V stand for 'scalar' and 'vector' and $w^i_{\rm S} = -\vec{\nabla}^i w$ [371]. Since we are dealing with first-order perturbation theory, the scalar and vector parts evolve independently of each other, and so we can focus exclusively on the scalar perturbations – these being the ones that lead to the formation of structure [367]. The component $w^i_{\rm V}$ may thus be safely excluded from our equations. The parameter v that appears in Eq. (A.6), meanwhile, is the velocity potential associated with v^i ($v^i_{\rm S} = -\vec{\nabla}^i v$).

The next thing to consider is how to model perturbations as wave functions in momentum space. If the spatial hypersurfaces are flat, the perturbation δf in a given quantity f may be expressed as an integral over Fourier modes:[91]

$$\delta f(\tau, \vec{x}) = \int \delta f_{k_\dagger}(\tau) \mathrm{e}^{i\vec{k}_\dagger \cdot \vec{x}} \, \mathrm{d}^3 k_\dagger \ . \tag{A.9}$$

Each of these modes has a characteristic comoving wave vector $\vec{k}_\dagger$ [374], and is an eigenfunction of the Laplace-Beltrami operator $\vec{\nabla}^2$ with eigenvalue $-k_\dagger^2$ ($k_\dagger = |\vec{k}_\dagger|$) [375]:

$$\left(\vec{\nabla}^2 + k_\dagger^2\right) \mathrm{e}^{i\vec{k}_\dagger \cdot \vec{x}} = 0 \ . \tag{A.10}$$

The form that the eigenfunctions take in the presence of spatial curvature will be dealt with later. At the moment, we shall simply replace $\mathrm{e}^{i\vec{k}_\dagger \cdot \vec{x}}$ with a generalised function $Q(\vec{k}_\dagger, \vec{x})$:

$$\left(\vec{\nabla}^2 + k_\dagger^2\right) Q(\vec{k}_\dagger, \vec{x}) = 0 \ . \tag{A.11}$$

Expanding the above equation in a quasi-Cartesian coordinate system yields:

$$\left\{ \frac{1}{16}(4 + \kappa X)^2 \left[-\frac{2\kappa}{4 + \kappa X} \left(x\partial_x + y\partial_y + z\partial_z \right) + \partial_x^2 + \partial_y^2 + \partial_z^2 \right] + k_\dagger^2 \right\} Q(\vec{k}_\dagger, \vec{x}) = 0 \ , \tag{A.12}$$

where $X = x^2 + y^2 + z^2 = |\vec{x}|^2$.

Eq. (A.9) indicates that a perturbation in physical space translates into a sum over $k_\dagger$-modes in momentum space (the sum becomes an integral if the spectrum of modes is continuous). Since our perturbation equations are linear, however, it follows that if $\delta f(\tau, \vec{x})$ satisfies a particular equation, then all of the individual eigenfunctions summed over in Eq. (A.9) also satisfy the equation in question, albeit for different values of $k_\dagger$. We may thus write our perturbations in terms of a generic mode Q

[91] π pre-factors are redundant in this context. Note also that $\vec{x}$ is the spatial vector (x, y, z).

[368, 375]:

$$\begin{aligned}
\Phi(\tau,\vec{x}) &= \Phi_{k_\dagger}(\tau)Q(\vec{k}_\dagger,\vec{x})\ ; & \Psi(\tau,\vec{x}) &= \Psi_{k_\dagger}(\tau)Q(\vec{k}_\dagger,\vec{x})\ ; \\
\delta\rho_{\rm m}(\tau,\vec{x}) &= \delta\rho_{\rm m}^{k_\dagger}(\tau)Q(\vec{k}_\dagger,\vec{x})\ ; & \delta p_{\rm m}(\tau,\vec{x}) &= \delta p_{\rm m}^{k_\dagger}(\tau)Q(\vec{k}_\dagger,\vec{x})\ ; \\
v^i(\tau,\vec{x}) &= v_{k_\dagger}(\tau)Q^i(\vec{k}_\dagger,\vec{x})\ ; & Q^i(\vec{k}_\dagger,\vec{x}) &= -k_\dagger^{-1}\vec{\nabla}^i Q(\vec{k}_\dagger,\vec{x})\ .
\end{aligned} \tag{A.13}$$

Quantities on the left-hand side denote perturbations in physical space, while the right-hand side is reserved for their momentum-space counterparts.

In view of the above, we can conclude that the conversion to momentum space requires us to make the following modifications:

- Expressing perturbations as in Eq. (A.13);

- Replacing $\vec{\nabla}^2$ with $-k_\dagger^2$. Let us take as example the quantity $\vec{\nabla}^2\Phi(\tau,\vec{x})$. In momentum space, this becomes $\vec{\nabla}^2[\Phi_{k_\dagger}(\tau)Q(\vec{k}_\dagger,\vec{x})]$, which is equal to $\Phi_{k_\dagger}(\tau)\vec{\nabla}^2 Q(\vec{k}_\dagger,\vec{x})$ and hence – via Eq. (A.11) – to $\Phi_{k_\dagger}(\tau)[-k_\dagger^2 Q(\vec{k}_\dagger,\vec{x})]$. We can thus infer that $\vec{\nabla}^2\Phi(\tau,\vec{x}) = -k_\dagger^2\Phi_{k_\dagger}(\tau)Q(\vec{k}_\dagger,\vec{x})$.

- Rewriting the velocity potential[92] v as $k_\dagger^{-1}v$. This follows from the last line of Eq. (A.13): $v^i(\tau,\vec{x}) = -v_{k_\dagger}(\tau)k_\dagger^{-1}\vec{\nabla}^i Q(\vec{k}_\dagger,\vec{x}) = -\vec{\nabla}^i[k_\dagger^{-1}v_{k_\dagger}(\tau)Q(\vec{k}_\dagger,\vec{x})]$. In physical space, $v^i(\tau,\vec{x}) = -\vec{\nabla}^i v(\tau,\vec{x})$.

- Putting $\vec{\nabla}^{i_0}\vec{\nabla}_{i_0}\Phi$ (where there is no summation over i_0) equal to $-k_\dagger^2\Phi/3$, the reason being that the relation $\vec{\nabla}^2\Phi = -k_\dagger^2\Phi$ can be expressed in quasi-Cartesian coordinates as $(\vec{\nabla}^x\vec{\nabla}_x + \vec{\nabla}^y\vec{\nabla}_y + \vec{\nabla}^z\vec{\nabla}_z)\Phi = -k_\dagger^2\Phi$, and so we may invoke the isotropy of the Universe to deduce that $\vec{\nabla}^{i_0}\vec{\nabla}_{i_0}\Phi = -k_\dagger^2\Phi/3$. In other words, $\vec{\nabla}^x\vec{\nabla}_x\Phi$, $\vec{\nabla}^y\vec{\nabla}_y\Phi$ and $\vec{\nabla}^z\vec{\nabla}_z\Phi$ all contribute the same amount to $-k_\dagger^2\Phi$.

Eq. (A.8) allows us to simplify our work significantly. It should be noted, however, that the absence of shear stresses does not necessarily imply the equivalence of Φ and Ψ in alternative theories of gravity.

[92] The introduction of $k_\dagger^{-1}$ and of a minus sign when writing Q^i as $-k_\dagger^{-1}\vec{\nabla}^i Q$ is mainly a convention. Variations exist in the literature, and consequently one must compare equations from different sources with caution.

The momentum-space equivalents of Eqs. (A.5)-(A.7) read:

$$2\left\{\Phi\left(k_\dagger^2-3\kappa\right)+3\mathcal{H}\left[\Phi'(\tau)+\Phi\mathcal{H}\right]\right\}+8\pi G a^2\rho_{\rm m}\delta_{\rm m}=0\ ; \tag{A.14}$$

$$k_\dagger\left[\mathcal{H}\Phi+\Phi'(\tau)\right]=4\pi G a^2\left(\rho_{\rm m}+p_{\rm m}\right)v\ ; \tag{A.15}$$

$$2\mathcal{H}'(\tau)\Phi+\mathcal{H}^2\Phi+\Phi''(\tau)+3\mathcal{H}\Phi'(\tau)-\kappa\Phi=4\pi G a^2\delta p_{\rm m}\ . \tag{A.16}$$

Here, a prime indicates differentiation with respect to the argument, $k_\dagger$ is the comoving wave number and the function $Q(\vec{k}_\dagger,\vec{x})$ has been factored out of the equations, while Φ takes the place of Ψ. Additionally, despite the fact that $k_\dagger$ is not included explicitly as a sub/super script, one should keep in mind that Φ, $\delta_{\rm m}$ and v correspond to $\Phi_{k_\dagger}(\tau)$, $\delta_{\rm m}^{k_\dagger}(\tau)$ and $v_{k_\dagger}(\tau)$, respectively.

Let us now take a look at the perturbed version of energy-momentum conservation. The condition $\nabla_\mu T^\mu_\nu=0$ still holds, but in this case $T^\mu_\nu=\tilde{T}^\mu_\nu+\delta T^\mu_\nu$ (the tilde denotes the unperturbed part) and the covariant derivative ∇_μ – not to be confused with the *spatial* covariant derivative, $\vec{\nabla}_i$ – must be constructed from the perturbed metric tensor of Eq. (A.2) [291]. The relation $\nabla_\mu T^\mu_\nu$ may consequently be expanded as follows:

$$\tilde{\nabla}_\mu\tilde{T}^\mu_\nu+\tilde{\nabla}_\mu\delta T^\mu_\nu+\delta\Gamma^\mu_{\sigma\mu}\tilde{T}^\sigma_\nu-\delta\Gamma^\sigma_{\nu\mu}\tilde{T}^\mu_\sigma=0\ , \tag{A.17}$$

where:

- $\tilde{\nabla}_\mu$ is the covariant derivative based on the metric of Eq. (A.1);
- $\tilde{T}^\mu_\nu$ is the unperturbed energy momentum tensor. We shall assume that it describes a perfect fluid (with energy density $\rho_{\rm m}$, pressure $p_{\rm m}$ and 4-velocity u^μ):

$$\tilde{T}^\mu_\nu=\left(\rho_{\rm m}+p_{\rm m}\right)u^\mu u_\nu+p_{\rm m}\delta^\mu_\nu\ . \tag{A.18}$$

- δT^μ_ν is its perturbed counterpart and has been specified in Eq. (A.4);
- $\delta\Gamma^\mu_{\nu\sigma}$ represents the perturbed Christoffel symbols and is given by:

$$\delta\Gamma^\mu_{\nu\sigma}=\frac{1}{2}\delta g^{\mu\alpha}\left(\partial_\sigma\tilde{g}_{\alpha\nu}+\partial_\nu\tilde{g}_{\alpha\sigma}-\partial_\alpha\tilde{g}_{\nu\sigma}\right)+\frac{1}{2}\tilde{g}^{\mu\alpha}\left(\partial_\sigma\delta g_{\alpha\nu}+\partial_\nu\delta g_{\alpha\sigma}-\partial_\alpha\delta g_{\nu\sigma}\right)\ . \tag{A.19}$$

  The quantities $\tilde{g}_{\mu\nu}$ and $\delta g_{\mu\nu}$ may be determined by writing the metric in Eq. (A.2) as the sum of an unperturbed part ($\tilde{g}_{\mu\nu}$) and a perturbed one ($\delta g_{\mu\nu}$): $g_{\mu\nu}=\tilde{g}_{\mu\nu}+\delta g_{\mu\nu}$.

We note that the first term in Eq. (A.17) has no perturbed components. It is therefore

conserved separately, giving rise to the familiar relation $\rho'_{\rm m}(\tau) = -3\mathcal{H}(\rho_{\rm m} + p_{\rm m})$. The remaining terms yield the equations:

$$\delta'_{\rm m}(\tau) = (1 + w_{\rm m}) \left[-k_\dagger v + 3\Phi'(\tau) \right] \ ; \tag{A.20}$$

$$v'(\tau) = \mathcal{H} v (3w_{\rm m} - 1) + k_\dagger \left(\Phi + \frac{w_{\rm m} \delta_{\rm m}}{1 + w_{\rm m}} \right) \ , \tag{A.21}$$

which correspond to the cases $\nu = 0$ and $\nu = i$, respectively. The above utilise the fact that $\Phi = \Psi$ and are based on the implicit assumption that $\delta p_{\rm m} / \delta \rho_{\rm m} = p_{\rm m} / \rho_{\rm m} = w_{\rm m}$ [291]. If matter is modelled as a pressureless perfect fluid (called 'dust') [18], $w_{\rm m}$ equates to zero, and the two equations are easily combined to give:

$$\delta''_{\rm m}(\tau) + \mathcal{H} \delta'_{\rm m}(\tau) + k_\dagger^2 \Phi - 3\Phi''(\tau) - 3\mathcal{H}\Phi'(\tau) = 0 \ . \tag{A.22}$$

Eqs. (A.5)–(A.7) and (A.22) may be simplified by applying the *sub-Hubble* and *quasi-static* approximations. The former holds if we limit our analysis to modes that are well within the horizon[93] during the time of interest – in other words, those with $k_\dagger \gg \mathcal{H}$. There is considerable advantage in working on scales that are significantly sub-horizon. In this regime, the dynamics of the metric potentials are effectively 'frozen out' [376],[94] and the quasi-static approximation comes into play as the condition that [380, 381]:

$$|Y'(\tau)| \lesssim \mathcal{H} |Y| \ , \quad \text{where } Y = \Phi,\ \mathcal{H} \text{ or } \Phi'(\tau) \ . \tag{A.23}$$

This means that the (conformal) time derivative of $\ln |Y|$ is at most of order $\mathcal{H}$. In short, we can conclude that the evolution of Y may essentially be attributed to the expansion of the Universe [382], and is thus negligible in comparison to its spatial derivatives. Interestingly, the quasi-static regime is the relevant stage for weak lensing/galaxy redshift surveys [383].

The sub-Hubble and quasi-static approximations reduce Eq. (A.22) to:

$$\delta''_{\rm m}(\tau) + \mathcal{H} \delta'_{\rm m}(\tau) + k_\dagger^2 \Phi = 0 \ . \tag{A.24}$$

The remaining terms are discarded on the basis that:

[93] In perturbation theory, the word 'horizon' generally refers to the Hubble distance $(1/H)$ or its comoving counterpart $(1/\mathcal{H})$.

[94] Explicit references to the 'quasi-static approximation' are usually found in the context of modified gravity models. The information presented here is mainly an adaptation of the concept for General Relativity [377–379].

- $|\Phi''(\tau)| \lesssim \mathcal{H}|\Phi'(\tau)|$;
- $\mathcal{H}|\Phi'(\tau)| \lesssim \mathcal{H}^2|\Phi| \ll k_\dagger^2|\Phi|$,

while similar considerations imply that Eq. (A.14) may be simplified to:

$$\Phi(k_\dagger^2 - 3\kappa) + 4\pi G a^2 \rho_{\rm m}\delta_{\rm m} = 0 \ . \tag{A.25}$$

In our analysis, we shall be focusing exclusively on values of $k_\dagger$ lying in the range $0.01\,h\,{\rm Mpc}^{-1} \leq k_\dagger \leq 0.2\,h\,{\rm Mpc}^{-1}$. The reason for this is twofold: firstly, modes with $k_\dagger \lesssim 0.2\,h\,{\rm Mpc}^{-1}$ represent perturbations which may safely be considered linear (in most models, at least) [296], and secondly, the mode that crosses the horizon at present has $k_\dagger = \mathcal{H} = aH = 1 \times 10^5\,c^{-1}\,h\,{\rm Mpc}^{-1} \sim 10^{-4}\,h\,{\rm Mpc}^{-1}$, but we require that $k_\dagger \gg \mathcal{H}$ for the sub-horizon approximation to hold and so fix the lower bound at $k_\dagger \sim 10^{-2}\,h\,{\rm Mpc}^{-1}$ [290, 374].

The range of values for $k_\dagger^2$ is therefore:

$$10^{-4}\,h^2\,{\rm Mpc}^{-2} \leq k_\dagger^2 \leq 4 \times 10^{-2}\,h^2\,{\rm Mpc}^{-2} \ . \tag{A.26}$$

In contrast, the spatial curvature κ ($= -\Omega_k^0 H_0^2$) is theoretically constrained to lie in the interval $-H_0^2 \leq \kappa \leq H_0^2$, otherwise expressed as

$$-\,10^{-7}\,h^2\,{\rm Mpc}^{-2} \leq \kappa \leq 10^{-7}\,h^2\,{\rm Mpc}^{-2} \ , \tag{A.27}$$

although in reality the low and high ends are out of bounds for any physically viable model. Indeed, we do not expect $|\Omega_k^0|$ to reach 0.1 in ΛCDM [20] – much less approach unity.

Comparing (A.26) and (A.27) makes it amply clear that $|\kappa| \ll k_\dagger^2$. In light of this, Eq. (A.25) is reduced to just two terms:

$$k_\dagger^2\Phi + 4\pi G a^2 \rho_{\rm m}\delta_{\rm m} = 0 \ . \tag{A.28}$$

The above relation can be used to substitute for Φ in Eq. (A.24). The result reads:

$$\delta_{\rm m}''(\tau) + \mathcal{H}\delta_{\rm m}'(\tau) - 4\pi G a^2 \rho_{\rm m}\delta_{\rm m} = 0 \ , \tag{A.29}$$

and the absence of $k_\dagger$ leads us to conclude that the evolution of $\delta_{\rm m}$ is scale-independent in the sub-horizon regime.

Momentum-space modes in the presence of spatial curvature

We know that when $\kappa = 0$, the eigenfunctions of the Laplace-Beltrami operator take the form $\mathrm{e}^{i\vec{k}_\dagger \cdot \vec{x}}$. To find how these eigenfunctions change in the presence of spatial curvature, let us start by noting that the exponential function can be expressed in terms of the spherical Bessel functions $j_\ell(k_\dagger r)$ and the spherical harmonics[95] $Y_{\ell m}$ [375]:

$$\mathrm{e}^{i\vec{k}_\dagger \cdot \vec{x}} = 4\pi \sum_{\ell,m} i^\ell j_\ell(k_\dagger r) Y^*_{\ell m}(\theta_{k_\dagger}, \phi_{k_\dagger}) Y_{\ell m}(\theta, \phi) \ . \tag{A.30}$$

The harmonics are in turn constructed from the associated Legendre functions P^m_ℓ:

$$Y_{\ell m}(\theta, \phi) = \left[\frac{(2\ell+1)(\ell-m)!}{4\pi(\ell+m)!}\right]^{1/2} P^m_\ell(\cos\theta)\mathrm{e}^{im\phi} \ . \tag{A.31}$$

Eq. (A.30) allows us to deduce that the spatial component of each mode is $Q(\vec{x}) = j_\ell(k_\dagger r)Y_{\ell m}(\theta, \phi)$. Since only the radial dependence of the metric in Eq. (A.1) is affected by a non-zero κ, we expect changes solely in that part of the eigenfunctions which is a function of r, and may hence generalise $Q(\vec{x})$ as indicated below [375]:

$$Q(\vec{x}) = \Theta^\ell_\beta(r) Y_{\ell m}(\theta, \phi) \ . \tag{A.32}$$

The function Θ^ℓ_β depends directly on the geometry of the Universe [375]:

- When $\kappa = 0$, $\Theta^\ell_\beta = j_\ell(k_\dagger r)$.
- When $\kappa > 0$,

$$\Theta^\ell_\beta = \left(\frac{\pi M^\ell_\beta}{2\beta^2 \sin\epsilon}\right)^{1/2} P^{-1/2-\ell}_{-1/2+\beta}(\cos\epsilon) \ , \tag{A.33}$$

  where $M^\ell_\beta = \prod_{n=0}^{\ell}(\beta^2 - n^2)$ and $k^2_\dagger = \kappa(\beta^2 - 1)$ $(\beta = 3, 4, 5 \ldots, \beta > \ell)$. P is an associated Legendre function, while $\sin\epsilon = 4r\sqrt{\kappa}/(4 + \kappa r^2)$.

- When $\kappa < 0$,

$$\Theta^\ell_\beta = \left(\frac{\pi N^\ell_\beta}{2\beta^2 \sinh\epsilon}\right)^{1/2} P^{-1/2-\ell}_{-1/2+i\beta}(\cosh\epsilon) \ , \tag{A.34}$$

  with $N^\ell_\beta = \prod_{n=0}^{\ell}(\beta^2 + n^2)$, $k^2_\dagger = -\kappa(\beta^2 + 1)$ $(\beta \geq 0)$ and $\sinh\epsilon = 4r\sqrt{-\kappa}/(4 + \kappa r^2)$.

[95] A superscript * stands for complex conjugation, while θ and ϕ give the direction of $\vec{x}$ [126] (similarly, $\theta_{k_\dagger}$ and $\phi_{k_\dagger}$ give the direction of $\vec{k}_\dagger$).

Now that we have determined what form the eigenfunctions take, we may proceed with the transformation from physical to momentum space by using them as the new modes. A given perturbation δf may then be expressed in the following way:

$$\delta f(\tau,\vec{x}) = \sum_{k_\dagger}\sum_{\ell,m} \delta f_{k_\dagger}(\tau) i^\ell \Theta^\ell_\beta(r) Y^*_{\ell m}(\theta_{k_\dagger},\phi_{k_\dagger}) Y_{\ell m}(\theta,\phi) \ , \tag{A.35}$$

or, in the case of a continuous spectrum of modes:

$$\delta f(\tau,\vec{x}) = \int \delta f_{k_\dagger}(\tau) \times \sum_{\ell,m} i^\ell \Theta^\ell_\beta(r) Y^*_{\ell m}(\theta_{k_\dagger},\phi_{k_\dagger}) Y_{\ell m}(\theta,\phi) \ \mathrm{d}^3 k_\dagger \ . \tag{A.36}$$

In the above, individual modes are labelled by β, ℓ and m [375] and π pre-factors have been dropped. The linearity of our perturbation equations means that different modes decouple, and so we may conclude that a perturbation $\delta f(\tau,\vec{x})$ in physical space has momentum-space counterpart $\delta f_{k_\dagger}(\tau)\Theta^\ell_\beta(r)Y_{\ell m}(\theta,\phi)$ [375], which we can write concisely as $f(\tau)Q(\vec{k}_\dagger,\vec{x})$ (having restored $\vec{k}_\dagger$ as an explicit argument of the generic function Q). The absence of the factors i^ℓ and $Y^*_{\ell m}(\theta_{k_\dagger},\phi_{k_\dagger})$ reflects the fact that the Laplace-Beltrami operator only acts on functions of the spatial coordinates. Any factors that are independent of these coordinates are therefore redundant.

Baryons: to include or not to include?

Thus far, the subscript 'm' (in ρ_m, δ_m etc.) has been used to indicate attributes of the matter component. We are now in a position to ask what exactly this component comprises. There is broad consensus in the scientific community that the greater proportion is cold dark matter (cdm) [20, 384, 385], a form of non-baryonic matter that interacts very weakly with electromagnetic radiation (hence why it is termed 'dark') and is furthermore non-relativistic or 'cold' [18]. Cdm is expected to make up some 26% of the cosmic fluid. On the other hand, only about 5% of this fluid consists of baryons [20]. If one is mainly interested in getting a simple approximation for the growth of matter perturbations, therefore, baryons may be left out of the picture.

How does the presence of baryons affect matter perturbations? Before recombination, baryons are tightly coupled to photons due to Thomson scattering. This induces damped acoustic oscillations in the modes that enter the horizon [369], a consequence of the competition between gravitational attraction on one hand and strong radiation pressure on the other. After recombination, the now-decoupled baryons quickly fall

into the potential wells of cdm, and as a result their density contrast function $\delta_{\rm b}$ experiences rapid growth, ultimately catching up with its cdm counterpart ($\delta_{\rm cdm}$). In fact, $\delta_{\rm b}$ and $\delta_{\rm cdm}$ are almost identical at low redshifts [369]. The velocity potentials $v_{\rm b}$ and $v_{\rm cdm}$ are also very similar at late times. The difference between them scales as $1+z$, and so one may write $v_{\rm b} \sim v_{\rm cdm}$ for sufficiently small values of z [290].

Let us introduce the density-weighted contrast function and velocity potential [290]:

$$\delta_{\rm m} = \frac{\rho_{\rm cdm}\delta_{\rm cdm} + \rho_{\rm b}\delta_{\rm b}}{\rho_{\rm cdm} + \rho_{\rm b}} \; ; \qquad v = \frac{v_{\rm cdm}\rho_{\rm cdm} + v_{\rm b}\rho_{\rm b}}{\rho_{\rm cdm} + \rho_{\rm b}} \; . \tag{A.37}$$

In the above, $\rho_{\rm cdm}$ and $\rho_{\rm b}$ denote the energy densities of cdm and baryons, respectively. The new definition of v makes it clear that having $v_{\rm b} \sim v_{\rm cdm}$ in turn implies that $v \sim v_{\rm b} \sim v_{\rm cdm}$. Consequently, Eq. (A.21) – with $w_{\rm m} = 0$ – holds both when matter is assumed to consist of cdm only (so that $v = v_{\rm cdm}$), and also when baryons are included and v is expressed as in Eq. (A.37) – provided we consider late times [290]. Similarly, the validity of Eq. (A.14) does not depend on whether we account for baryons or not. One recalls that any matter attributes appearing in this equation were introduced there via δT^0_0. In the cdm-only scenario, $-\delta T^0_0 = \delta\rho_{\rm cdm} = \rho_{\rm cdm}\delta_{\rm cdm} \equiv \rho_{\rm m}\delta_{\rm m}$, while the addition of baryons changes $\rho_{\rm m}\delta_{\rm m}$ to $(\rho_{\rm cdm} + \rho_{\rm b})\,\delta_{\rm m}$, with $\delta_{\rm m}$ defined as in Eq. (A.37). It follows that $\rho_{\rm m}\delta_{\rm m} = \rho_{\rm cdm}\delta_{\rm cdm} + \rho_{\rm b}\delta_{\rm b} = \delta\rho_{\rm cdm} + \delta\rho_{\rm b}$, which is indeed the form that $-\delta T^0_0$ takes in the presence of baryons and cdm.

Eq. (A.20) is not as straightforward to generalise. In the first place, let us note that it holds for baryons and cdm separately:

$$\delta'_{\rm cdm}(\tau) = -k_\dagger v_{\rm cdm} \; ; \tag{A.38}$$

$$\delta'_{\rm b}(\tau) = -k_\dagger v_{\rm b} \; . \tag{A.39}$$

Here, we have applied the sub-horizon and quasi-static approximations. The next step consists of taking the τ-derivative of $\delta_{\rm m}$ [with $\delta_{\rm m}$ as defined in Eq. (A.37)], then substituting for $\rho'_{\rm cdm}(\tau)$ and $\rho'_{\rm b}(\tau)$ using the conformal conservation equations [$\rho'_{\rm cdm}(\tau) + 3\mathcal{H}\rho_{\rm cdm} = 0$; $\rho'_{\rm b}(\tau) + 3\mathcal{H}\rho_{\rm b} = 0$], and for $\delta'_{\rm cdm}(\tau)$ and $\delta'_{\rm b}(\tau)$ by utilizing Eqs. (A.38) and (A.39), respectively. After replacing $v_{\rm cdm}$ and $v_{\rm b}$ with v, it becomes evident that Eq. (A.20) remains valid when $\delta_{\rm m}$ is given by Eq. (A.37) [290].

In short, at late times Eq. (A.29) holds whether the baryon component is included or not. One simply has to define v, $\delta_{\rm m}$ and $\rho_{\rm m}$ accordingly.

The sub-Hubble and quasi-static approximations in $f(R)$ gravity

Detailed explanations of the sub-Hubble and quasi-static approximations have been given in this same appendix. Here, we briefly summarise the two:

- Sub-Hubble approximation: $k_\dagger \gg \mathcal{H}$;
- Quasi-static approximation: $|Y'(\tau)| \lesssim \mathcal{H}|Y|$; $Y = \Phi$, Ψ, $\mathcal{H}$, $\Phi'(\tau)$, $\Psi'(\tau)$ or $\mathcal{H}'(\tau)$.

The presence of Ψ reflects the fact that Φ and Ψ are not equal in $f(R)$ gravity.

The equation for δR, the perturbation in the Ricci scalar

The full equation is:

$$\delta R = \frac{2}{a^2}\left\{k_\dagger^2(\Phi - 2\Psi) - 3\left[2\mathcal{H}'(\tau)\Phi + 3\mathcal{H}\Psi'(\tau) + \mathcal{H}\Phi'(\tau) - 2\kappa\Psi + \Psi''(\tau) + 2\mathcal{H}^2\Phi\right]\right\} , \tag{A.40}$$

but the quantity $2a^{-2}k_\dagger^2(\Phi - 2\Psi)$ dominates, since

- $|\mathcal{H}'(\tau)\Phi| \lesssim \mathcal{H}^2|\Phi| \ll k_\dagger^2|\Phi|$;
- $\mathcal{H}|\Psi'(\tau)| \lesssim \mathcal{H}^2|\Psi| \ll k_\dagger^2|\Psi|$;
- $\mathcal{H}|\Phi'(\tau)| \lesssim \mathcal{H}^2|\Phi| \ll k_\dagger^2|\Phi|$;
- $|\Psi''(\tau)| \lesssim \mathcal{H}|\Psi'(\tau)| \lesssim \mathcal{H}^2|\Psi| \ll k_\dagger^2|\Psi|$;
- $\mathcal{H}^2|\Phi| \ll k_\dagger^2|\Phi|$.

Whether or not the term in κ is negligible depends on how κ compares with the values $k_\dagger^2$ is allowed to take. The term in question shall therefore be retained for now, which means that Eq. (A.40) becomes

$$\delta R = \frac{2}{a^2}\left[k_\dagger^2(\Phi - 2\Psi) + 6\kappa\Psi\right] . \tag{A.41}$$

The time-time component of the field equations

Let us first rewrite the equation in its entirety:

$$2f_R\left\{\Psi\left(k_\dagger^2-3\kappa\right)+3\mathcal{H}\left[\Psi'(\tau)+\mathcal{H}\Phi\right]\right\}+f_{RR}\left[3\mathcal{H}'(\tau)\delta R-k_\dagger^2\delta R-3\mathcal{H}\,\delta R'(\tau)\right]-$$
$$3\mathcal{H}\,\delta R\,f'_{RR}(\tau)+3f'_R(\tau)\left[2\mathcal{H}\Phi+\Psi'(\tau)\right]+8\pi Ga^2\rho_{\rm m}\delta_{\rm m}=0\ . \qquad \text{(A.42)}$$

Next, we consider that

- $\mathcal{H}|\Psi'(\tau)|\lesssim\mathcal{H}^2|\Psi|\ll k_\dagger^2|\Psi|$;
- $\mathcal{H}^2|\Phi|\ll k_\dagger^2|\Phi|\sim k_\dagger^2|\Psi|$;[96]
- $|\mathcal{H}'(\tau)\delta R|\lesssim\mathcal{H}^2|\delta R|\ll k_\dagger^2|\delta R|$;
- $-3\mathcal{H}[f_{RR}\delta R'(\tau)+\delta R f'_{RR}(\tau)]=-3\mathcal{H}[\delta R\,f_{RR}]'(\tau)$. Using the $i-j$ component of the field equations, $\delta R\,f_{RR}$ may be expressed as $f_R(\Psi-\Phi)$, and hence we get that $-3\mathcal{H}[f_{RR}\delta R'(\tau)+\delta R f'_{RR}(\tau)]=-3\mathcal{H}\{f'_R(\tau)(\Psi-\Phi)+f_R[\Psi'(\tau)-\Phi'(\tau)]\}$. The second term on the right-hand side can be absorbed into the curly brackets of Eq. (A.42). We immediately note, however, that it is negligible in comparison to $2f_R\Psi(k_\dagger^2-3\kappa)$, so we turn our attention to the first term instead. This may be combined with the second-from-last term of Eq. (A.42):

$$\begin{aligned}
&-3\mathcal{H}f'_R(\tau)(\Psi-\Phi)+3f'_R(\tau)[2\mathcal{H}\Phi+\Psi'(\tau)]\ =\\
&3f_{RR}R'(\tau)[-\mathcal{H}(\Psi-\Phi)+2\mathcal{H}\Phi+\Psi'(\tau)]\ =\\
&3f_{RR}\{6a^{-2}[\mathcal{H}''(\tau)-2\mathcal{H}^3-2\mathcal{H}\kappa]\}[3\mathcal{H}\Phi-\mathcal{H}\Psi+\Psi'(\tau)]\ =\\
&18a^{-2}f_{RR}[3\mathcal{H}\mathcal{H}''(\tau)\Phi-\mathcal{H}\mathcal{H}''(\tau)\Psi+\mathcal{H}''(\tau)\Psi'(\tau)-6\mathcal{H}^4\Phi+2\mathcal{H}^4\Psi\\
&-2\mathcal{H}^3\Psi'(\tau)-6\mathcal{H}^2\kappa\Phi+2\mathcal{H}^2\kappa\Psi-2\mathcal{H}\kappa\Psi'(\tau)]\ . \qquad \text{(A.43)}
\end{aligned}$$

In the above, the function $f'_R(\tau)$ that appears in the first line is subsequently replaced by $f_{RR}R'(\tau)$, and the expression for $R'(\tau)$ follows from the conformal-time counterpart of Eq. (5.26). The terms of (A.43) are analysed one by one:

- $3|\mathcal{H}\mathcal{H}''(\tau)\Phi|\lesssim 3\mathcal{H}\times\mathcal{H}|\mathcal{H}'(\tau)|\times|\Phi|=3\mathcal{H}^2|\mathcal{H}'(\tau)\Phi|\lesssim 3\mathcal{H}^2\times\mathcal{H}^2|\Phi|=3\mathcal{H}^4|\Phi|\ll 3k_\dagger^4|\Phi|$. Similarly, $|\mathcal{H}\mathcal{H}''(\tau)\Psi|\ll k_\dagger^4|\Psi|$. Terms in $k_\dagger^4\Phi$ and $k_\dagger^4\Psi$ are present in $k_\dagger^2\delta R$.
- $|\mathcal{H}''(\tau)\Psi'(\tau)|\lesssim|\mathcal{H}''(\tau)|\mathcal{H}|\Psi|=|\mathcal{H}\mathcal{H}''(\tau)\Psi|\ll k_\dagger^4|\Psi|$;

[96] Φ and Ψ are assumed to be of the same order.

* $\mathcal{H}^4|\Phi| \ll k_\dagger^4|\Phi|$;
* $\mathcal{H}^4|\Psi| \ll k_\dagger^4|\Psi|$;
* $\mathcal{H}^3|\Psi'(\tau)| \lesssim \mathcal{H}^4|\Psi| \ll k_\dagger^4|\Psi|$;
* $6\mathcal{H}^2|\kappa\Phi| \ll 6k_\dagger^2|\kappa\Phi|$. Similarly, $2\mathcal{H}^2|\kappa\Psi| \ll 2k_\dagger^2|\kappa\Psi|$. The expression $18a^{-2}f_{RR}(-6\mathcal{H}^2\kappa\Phi + 2\mathcal{H}^2\kappa\Psi)$ is thus sub-dominant to $-f_{RR}k_\dagger^2\delta R$ [which forms part of Eq. (A.42)], since $k_\dagger^2\delta R$ contains a term in $k_\dagger^2\kappa\Psi$.
* $2\mathcal{H}|\kappa\Psi'(\tau)| \lesssim 2\mathcal{H}|\kappa| \times \mathcal{H}|\Psi| = 2\mathcal{H}^2|\kappa\Psi| \ll 2k_\dagger^2|\kappa\Psi|$.

In conclusion, the sub-Hubble and quasi-static approximations reduce Eq. (A.42) to:

$$2f_R\Psi(k_\dagger^2 - 3\kappa) - f_{RR}k_\dagger^2\delta R + 8\pi G a^2\rho_{\rm m}\delta_{\rm m} = 0 \ . \tag{A.44}$$

The evolution equation for the density contrast function, δ_m

This time, our starting point is Eq. (5.56):

$$\delta_{\rm m}''(\tau) + \mathcal{H}\delta_{\rm m}'(\tau) + k_\dagger^2\Phi - 3\Psi''(\tau) - 3\mathcal{H}\Psi'(\tau) = 0 \ . \tag{A.45}$$

Again we have that

- $|\Psi''(\tau)| \lesssim \mathcal{H}|\Psi'(\tau)| \lesssim \mathcal{H}^2|\Psi| \ll k_\dagger^2|\Psi|$;
- $\mathcal{H}|\Psi'(\tau)| \lesssim \mathcal{H}^2|\Psi| \ll k_\dagger^2|\Psi|$,

and so the evolution equation becomes

$$\delta_{\rm m}''(\tau) + \mathcal{H}\delta_{\rm m}'(\tau) + k_\dagger^2\Phi = 0 \ . \tag{A.46}$$

APPENDIX B

Marginalised Posteriors for $f(R)$ models

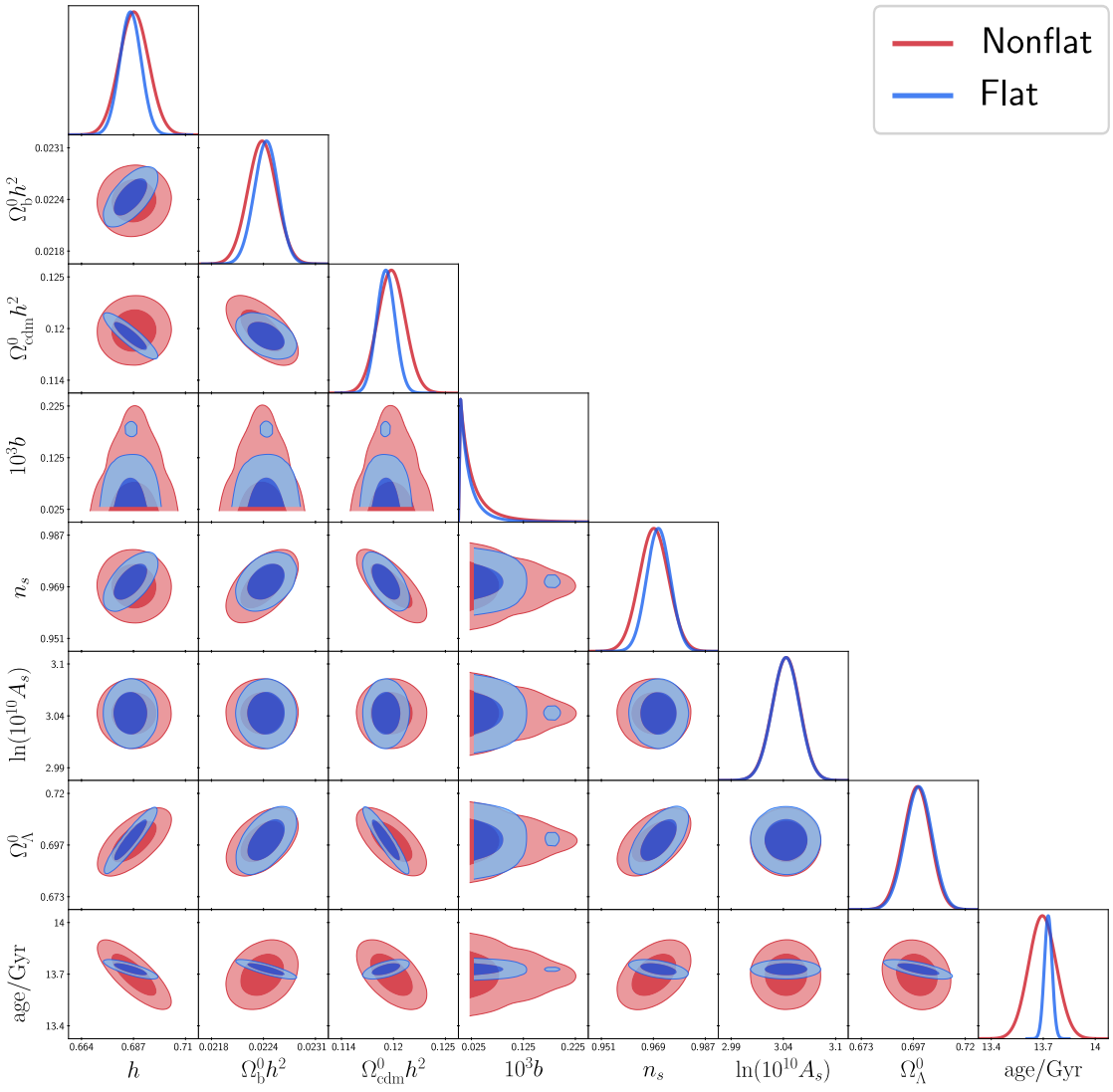

FIGURE B.1: Marginalised 2D and 1D posterior probability distributions for the Hu-Sawicki model. The label 'Flat' denotes constraints obtained with Ω_k^0 fixed at zero, while 'Nonflat' means that Ω_k^0 was treated as a free parameter. Dark and light shades represent 1σ and 2σ confidence intervals, respectively.

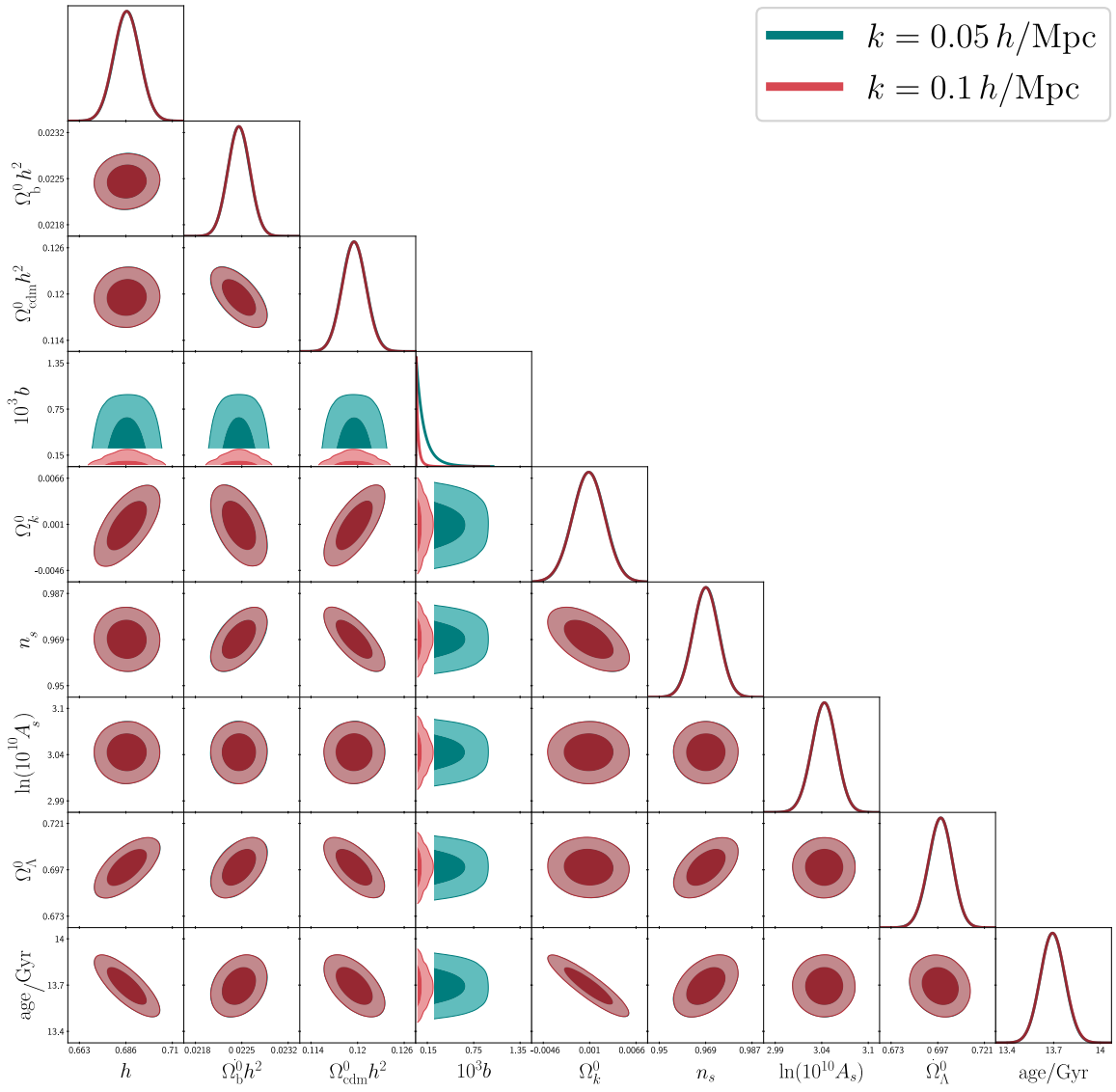

FIGURE B.2: Marginalised 2D and 1D posterior probability distributions for the Hu-Sawicki model. The legend refers to the comoving wave number at which the growth rate f was calculated.

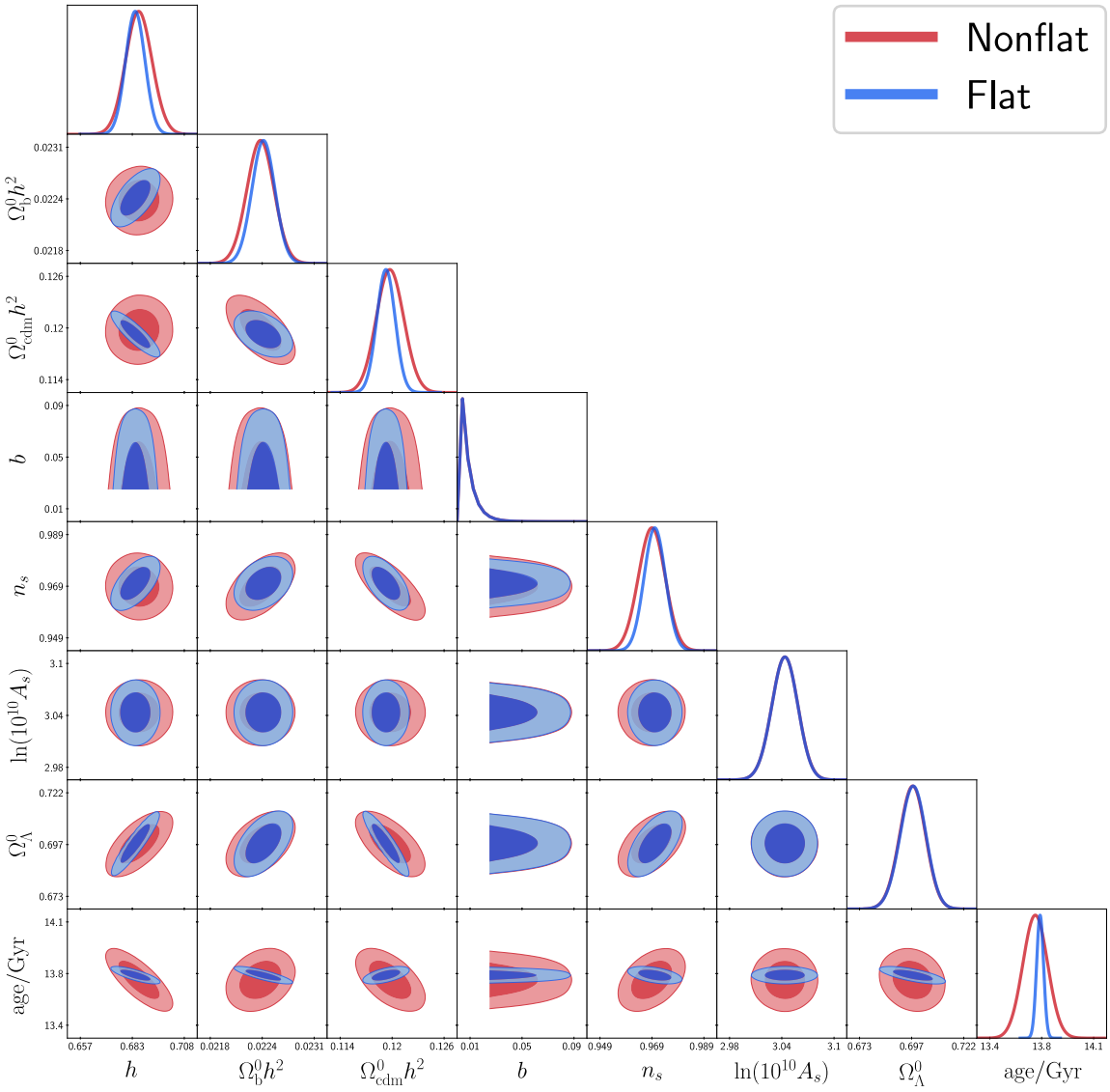

FIGURE B.3: Marginalised 2D and 1D posterior probability distributions for the Starobinsky model.

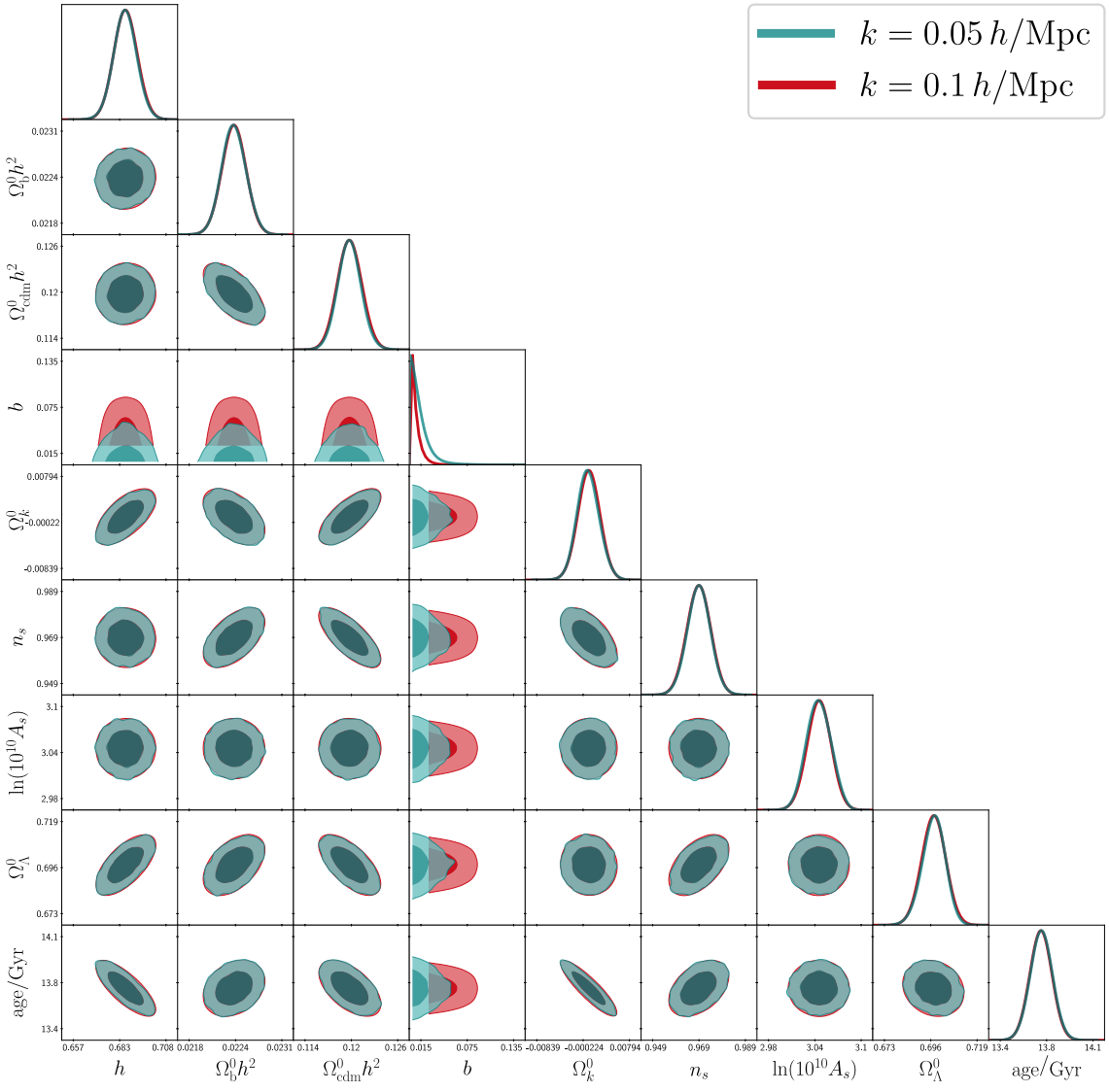

FIGURE B.4: Marginalised 2D and 1D posterior probability distributions for the Starobinsky model. The legend refers to the comoving wave number at which the growth rate f was calculated.

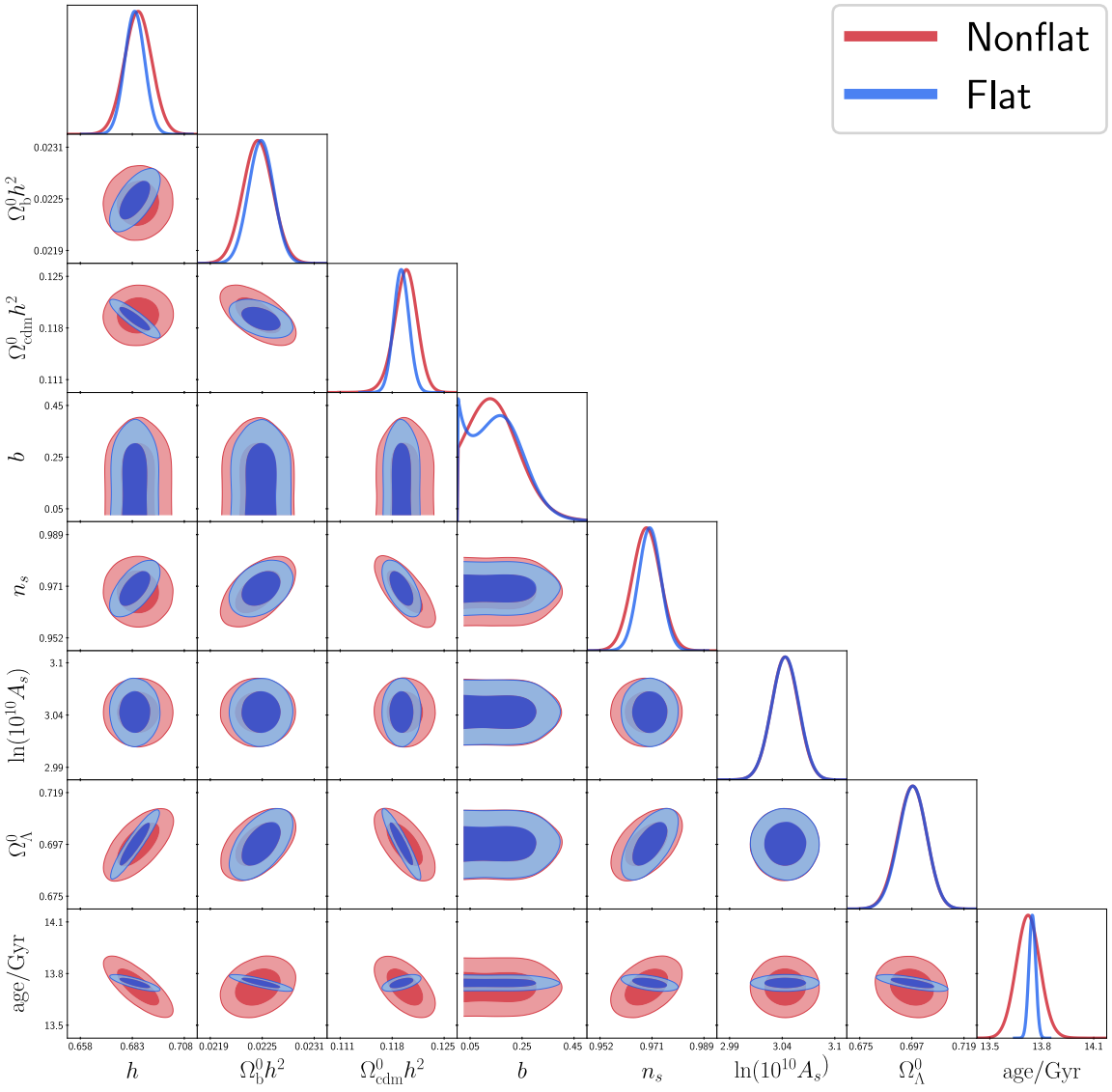

FIGURE B.5: Marginalised 2D and 1D posterior probability distributions for the Exponential model.

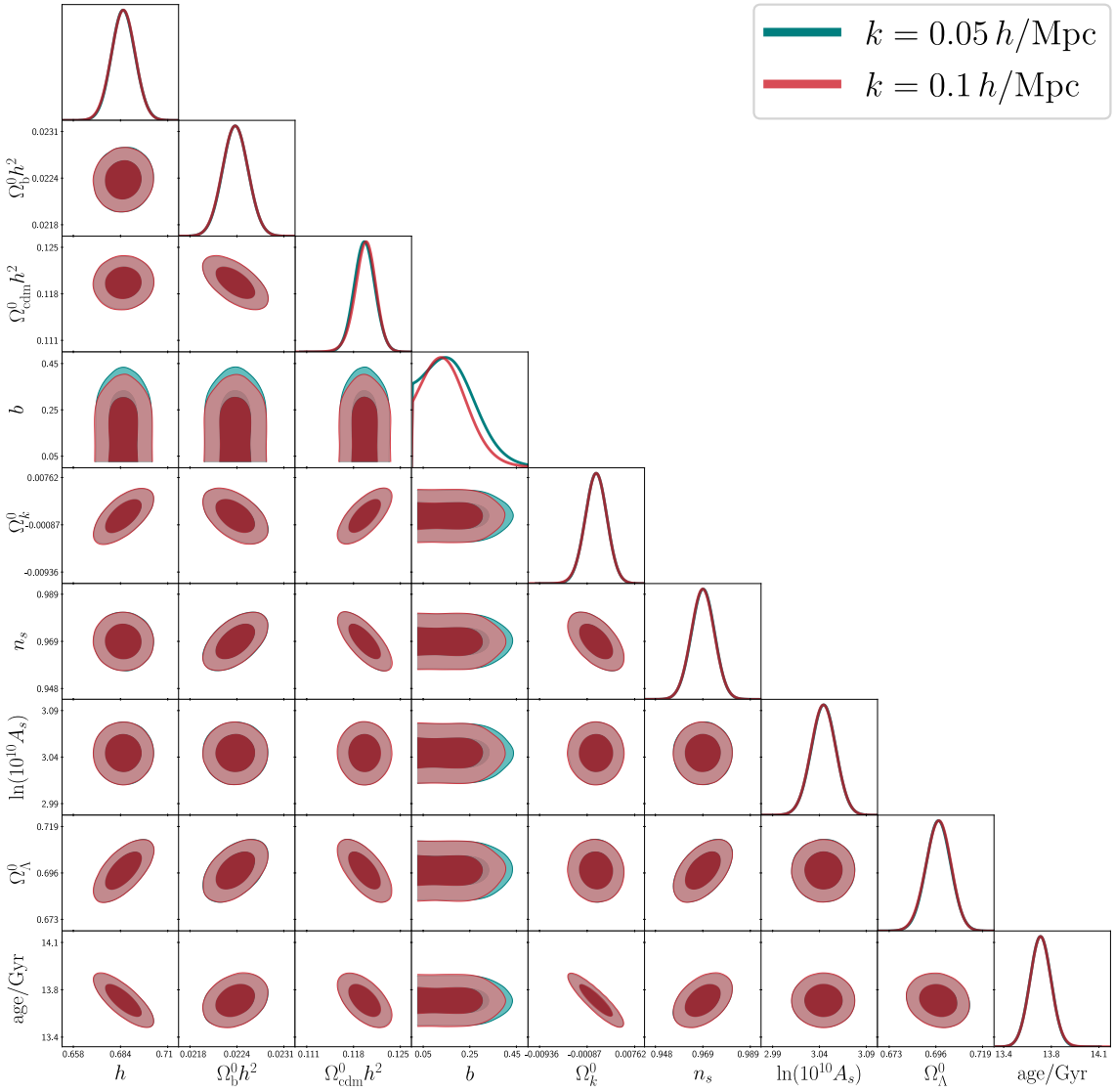

FIGURE B.6: Marginalised 2D and 1D posterior probability distributions for the Exponential model. The legend refers to the comoving wave number at which the growth rate f was calculated.

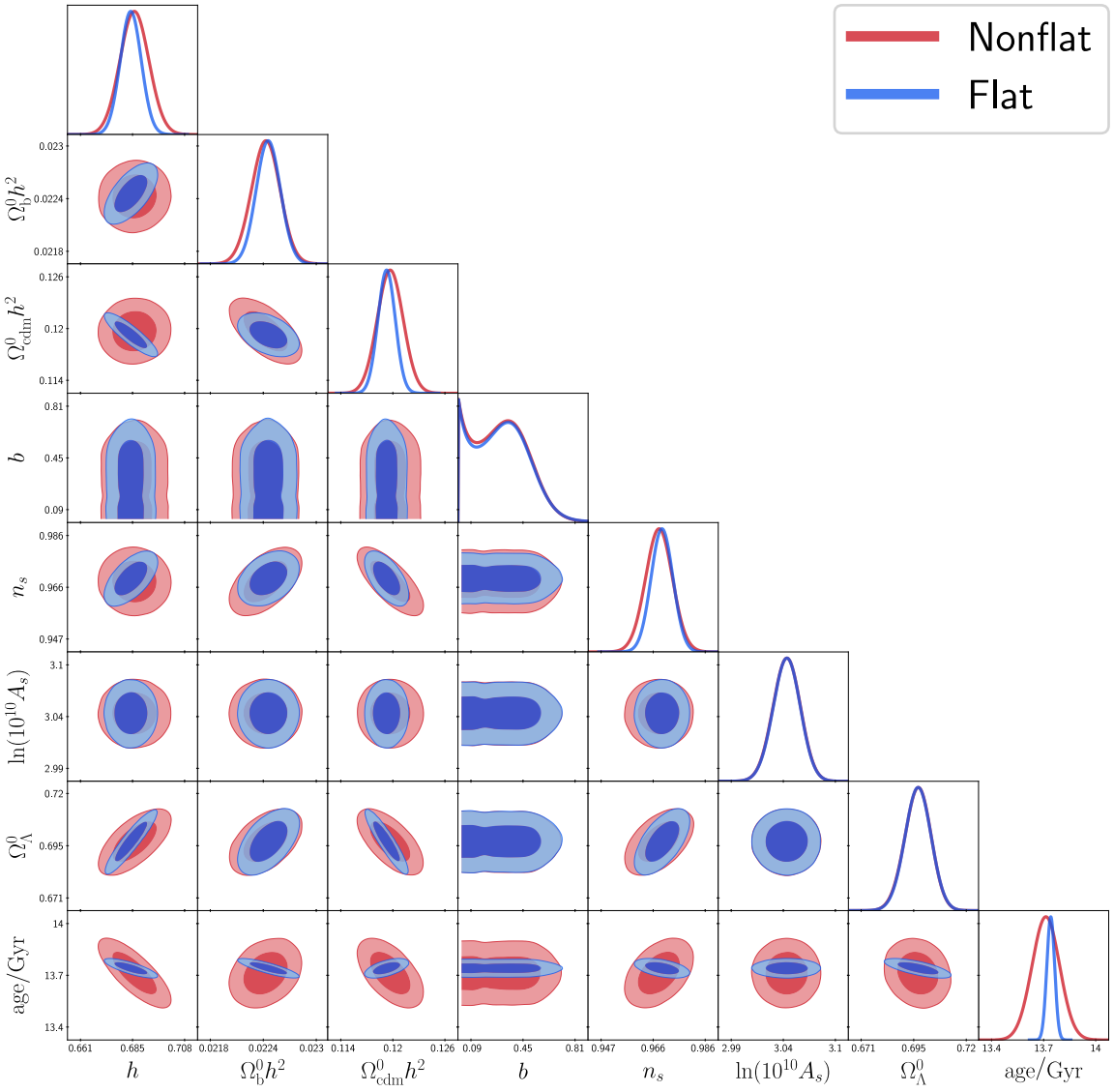

FIGURE B.7: Marginalised 2D and 1D posterior probability distributions for the Tsujikawa model.

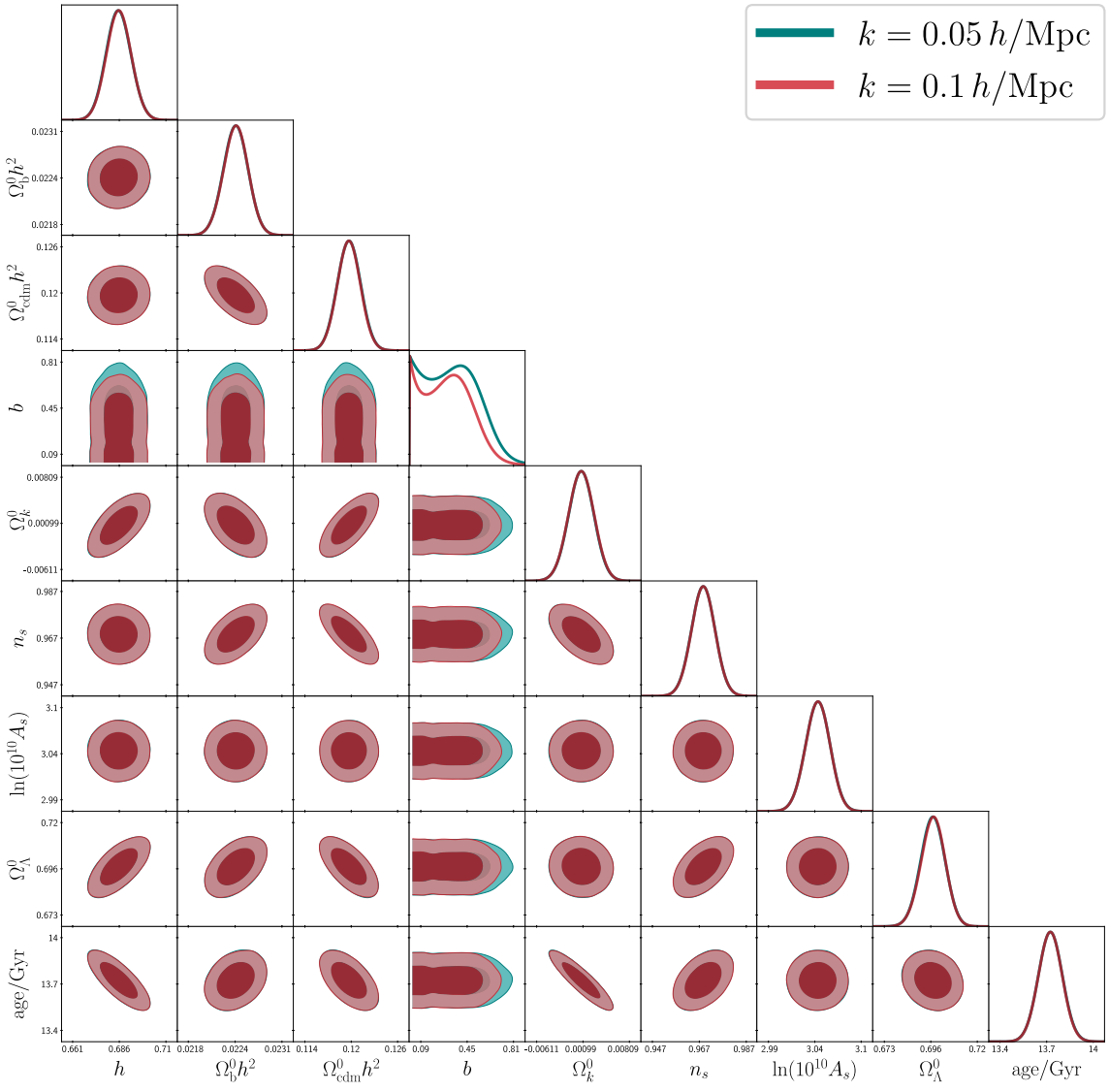

FIGURE B.8: Marginalised 2D and 1D posterior probability distributions for the Tsujikawa model. The legend refers to the comoving wave number at which the growth rate f was calculated.

APPENDIX C

Source Code

Listing C.1: Mathematica code for the principal STT equations.

```
(*First Friedmann equation*)
Eq1 := \[Kappa]/a[t]^2 + Derivative[1][a][t]^2/a[t]^2 - ((8*Pi*G)
   /(3*(1 - 8*Pi*G*\[Xi]*\[Phi][t]^2)))*(Derivative[1][\[Phi]][t
   ]^2/2 + V[t] + 6*\[Xi]*(Derivative[1][a][t]/a[t])*\[Phi][t]*
   Derivative[1][\[Phi]][t]+\[Rho]0/a[t]^(3*(1 + w)))

(*Klein-Gordon equation in curved space-time*)
Eq2 := Derivative[2][\[Phi]][t] + 3*(Derivative[1][a][t]/a[t])*
   Derivative[1][\[Phi]][t] + ((8*Pi*G*\[Xi]*\[Phi][t])/(1 - 8*Pi*G
   *\[Xi]*\[Phi][t]^2))*(-Derivative[1][\[Phi][t]^2 + 18*\[Xi]*(
   Derivative[1][a][t]/a[t])*\[Phi][t]*Derivative[1][\[Phi]][t] + 4*
   V[t] + (\[Rho]0*(1 - 3*w))/a[t]^(3*(1 + w))+6*\[Xi]*Derivative
   [1][\[Phi]][t]^2 + 6*\[Xi]*\[Phi][t]*Derivative[2][\[Phi]][t]) +
   D[V[t], t]/Derivative[1][\[Phi]][t]

(*Energy density of scalar field*)
\[Rho]\[Phi] := (1/(1 - 8*Pi*G*\[Xi]*\[Phi][t]^2))*((1/2)*Derivative
   [1][\[Phi]][t]^2 + V[t] + 6*\[Xi]*(Derivative[1][a][t]/a[t])*\[
   Phi][t]*Derivative[1][\[Phi]][t])

(*Pressure of scalar field*)
P\[Phi] := (1/(1 - 8*Pi*G*\[Xi]*\[Phi][t]^2))*((1/2 - 2*\[Xi])*
   Derivative[1][\[Phi]][t]^2 - V[t] - 2*\[Xi]*\[Phi][t]*Derivative
   [2][\[Phi]][t] - 4*\[Xi]*(Derivative[1][a][t]/a[t])*\[Phi][t]*
   Derivative[1][\[Phi]][t])

(*Potential of scalar field*)
V[t_] := (-(1/(8*G*Pi)))*a[t]^(-3 - 3*w)*(-4*G*Pi*\[Rho]0 - 12*G*Pi*w
   *\[Rho]0 + 24*G*Pi*\[Xi]*a[t]^(2 + 3*w)*\[Phi][t]*Derivative[1][a
   ][t]*Derivative[1][\[Phi]][t] - 8*G*Pi*a[t]^(3 + 3*w)*Derivative
   [1][\[Phi]][t]^2 + 24*G*Pi*\[Xi]*a[t]^(3 + 3*w)*Derivative[1][\[
```

```
   Phi]][t]^2 - 3*a[t]^(2 + 3*w)*Derivative[2][a][t] + 24*G*Pi*\[Xi
   ]*a[t]^(2 + 3*w)*\[Phi][t]^2*Derivative[2][a][t] + 24*G*Pi*\[Xi]*
   a[t]^(3 + 3*w)*\[Phi][t]*Derivative[2][\[Phi]][t])
```

LISTING C.2: Mathematica code for extracting coefficients from a polynomial equation.

```
Eq3 :=
(*Provide the relevant equation here, in expanded form. Exponents
   should not be factorised, and if they contain multiple terms,
   these should not be placed over a common denominator*)

\[Alpha]1 := Position[Eq3, t^_]
\[Alpha]2 := Position[Eq3, t]

\[Beta] := If[Length[\[Alpha]1] == Length[\[Alpha]2],
   DeleteDuplicates[Extract[Eq3, \[Alpha]1]], DeleteDuplicates[Join[
   Extract[Eq3, \[Alpha]1], {t}]]]
\[Beta]
(*Returns a list of all powers of t that appear in Eq3*)

list := Reap[Do[
  \[Gamma] := Collect[Eq3, \[Beta][[\[Iota]]]];
  \[Delta] := Position[\[Gamma], \[Beta][[\[Iota]]]];
  \[Epsilon]1 := Total[Flatten[DeleteCases[Reap[Do[Sow[Extract[\[
     Gamma], {\[Delta][[i,1]]}]], {i, 1, Length[\[Delta]]}]], Null
     ]]]*(1/\[Beta][[\[Iota]]]);
  \[Epsilon]2 := Position[\[Epsilon]1, t];
  \[Epsilon]3 := Total[Flatten[DeleteCases[Reap[Do[Sow[Extract[\[
     Epsilon]1, {\[Epsilon]2[[i,1]]}]], {i, 1, Length[\[Epsilon
     ]2]}]], Null]]]; Sow[Simplify[\[Epsilon]1 - \[Epsilon]3]],
    {\[Iota], 1, Length[\[Beta]]}]]
(*Extracts the coefficient of each element of \[Beta] from Eq3*)

\[Nu] := Flatten[DeleteCases[list, Null]]

\[Digamma] := Position[Eq3, t];
\[Lambda] := Total[Flatten[DeleteCases[Reap[Do[Sow[Extract[Eq3, {\[
   Digamma][[i,1]]}]], {i, 1, Length[\[Digamma]]}]], Null]]];
\[Omicron] := {Simplify[Eq3 - \[Lambda]]};
\[Omicron]
(*Returns any constant terms in Eq3*)

\[Upsilon] := Join[\[Nu], \[Omicron]]
```

```
Do[Print["No", i, ":=", \[Upsilon][[i]]], {i, 1, Length[\[Upsilon]]}]

Length[\[Beta]]

(*Check that everything is correct*)
Simplify[Sum[\[Beta][[i]]*\[Upsilon][[i]], {i, 1, Length[\[Beta]]}] +
    \[Upsilon][[-1]] - Eq3]
```

LISTING C.3: Mathematica code that takes as input a polynomial in t, with exponents that are functions of some parameter s. It equates each pair of exponents to each other and attemps to solve for s, returning any solutions.

```
Eq3 :=
(*Provide the relevant equation here, in expanded form. Exponents
   should not be factorised, and if they contain multiple terms,
   these should not be placed over a common denominator*)

\[Alpha]1 := Position[Eq3, t^_]
\[Alpha]2 := Position[Eq3, t]

\[Beta] := If[Length[\[Alpha]1] == Length[\[Alpha]2],
   DeleteDuplicates[Extract[Eq3, \[Alpha]1]],
   DeleteDuplicates[Join[Extract[Eq3, \[Alpha]1], {t}]]]
\[Beta]
(*Returns a list of all powers of t that appear in Eq3*)

\[Digamma] := Position[Eq3, t];
\[Lambda] := Total[Flatten[DeleteCases[Reap[Do[Sow[Extract[Eq3, {\[
   Digamma][[i,1]]}]], {i, 1, Length[\[Digamma]]}]], Null]]];
\[Omicron] := {Simplify[Eq3 - \[Lambda]]};
\[Koppa] := If[ContainsExactly[\[Omicron], {0}],
   Flatten[DeleteCases[Reap[Do[Sow[Exponent[\[Beta][[i]], t]], {i, 1,
       Length[\[Beta]]}]], Null]],
   Join[Flatten[DeleteCases[Reap[Do[Sow[Exponent[\[Beta][[i]], t]], {
      i, 1, Length[\[Beta]]}]], Null]], {0}]]
\[Koppa]
(*Extracts the exponents of elements of \[Beta]. Also checks if Eq3
   contains any constant terms, and adds 0 to the list of exponents
   if it does*)

\[Sampi]1 := Do[{\[Stigma]1 := Solve[{\[Koppa][[i]] == \[Koppa][[j
   ]]}, {s}]; If[\[Stigma]1 != {}, Sow[s /. \[Stigma]1, tag1],
      Sow[s /. \[Stigma]1, tagnull]]}, {i, 1, Length[\[Koppa]] - 1},
         {j, i + 1, Length[\[Koppa]]}]
```

```
(*Equates each pair of exponents to each other, and if possible,
   solves for s*)

\[Gamma]1 := DeleteDuplicates[Flatten[DeleteCases[Reap[\[Sampi]1,
   tag1], Null]]]
\[Gamma]1
```

LISTING C.4: Mathematica code that takes as input a polynomial in t, with exponents that are functions of s and/or m. It equates each pair of exponents to each other and attemps to solve for s, then for m, returning any solutions.

```
Eq3 :=
(*Provide the relevant equation here, in expanded form. Exponents
   should not be factorised, and if they contain multiple terms,
   these should not be placed over a common denominator*)

\[Alpha]1 := Position[Eq3, t^_]
\[Alpha]2 := Position[Eq3, t]

\[Beta] := If[Length[\[Alpha]1] == Length[\[Alpha]2],
   DeleteDuplicates[Extract[Eq3, \[Alpha]1]], DeleteDuplicates[Join[
   Extract[Eq3, \[Alpha]1], {t}]]]
\[Beta]
(*Returns a list of all powers of t that appear in Eq3*)

\[Digamma] := Position[Eq3, t];
\[Lambda] := Total[Flatten[DeleteCases[Reap[Do[Sow[Extract[Eq3, {\[
   Digamma][[i,1]]}]], {i, 1, Length[\[Digamma]]}]], Null]]];
\[Omicron] := {Simplify[Eq3 - \[Lambda]]};
\[Koppa] := If[ContainsExactly[\[Omicron], {0}], Flatten[DeleteCases[
   Reap[Do[Sow[Exponent[\[Beta][[i]], t]], {i, 1, Length[\[Beta
   ]]}]], Null]],
   Join[Flatten[DeleteCases[Reap[Do[Sow[Exponent[\[Beta][[i]], t]], {
      i, 1, Length[\[Beta]]}]], Null]], {0}]]
\[Koppa]
(*Extracts the exponents of elements of \[Beta]. Also checks if Eq3
   contains any constant terms, and adds 0 to the list of exponents
   if it does*)

\[Sampi]2 := Do[{\[Stigma]1 := Solve[{\[Koppa][[i]] == \[Koppa][[j
   ]]}, {s}]; \[Stigma]2 := Solve[{\[Koppa][[i]] == \[Koppa][[j]]},
   {m}]; If[\[Stigma]1 != {}, Sow[s /. \[Stigma]1, tag1],
      If[\[Stigma]2 != {}, Sow[m /. \[Stigma]2, tag2]]]}, {i, 1,
         Length[\[Koppa]] - 1}, {j, i + 1, Length[\[Koppa]]}]
```

```
(*Equates each pair of exponents to each other,and if possible,solves
    for s or m*)

\[Gamma]1 := DeleteDuplicates[Flatten[DeleteCases[Reap[\[Sampi]2,
   tag1], Null]]]
\[Gamma]1

\[Gamma]2 := DeleteDuplicates[Flatten[DeleteCases[Reap[\[Sampi]2,
   tag2], Null]]]
\[Gamma]2
```

APPENDIX D

Markov Chain Monte–Carlo Sampling

The name *Markov Chain Monte-Carlo (MCMC)* reflects two important properties of this sampling technique. The Monte-Carlo part refers to the practice of making inferences about a distribution by analysing random samples from it. Each new sample provides a 'stepping stone' to the next one (which is why we talk of Markov *chains*) [386]. More specifically, the Markov nature of these chains means that given a sampled point x_s, the next element of the sequence (x_{s+1}) is conditionally independent of x_1, $x_2, \ldots, x_{s-1}$ [387].[97]

MCMC is especially useful in Bayesian statistics. This is because one of the main features of the latter – the posterior distribution – is often difficult to study analytically. It is important to keep in mind, however, that MCMC is a sampler, and as such is not well-suited to search the parameter space for good models, or to optimise posterior distributions [388].

Bayes' theorem

According to the Bayesian point of view, the probability that a theory or model is correct is a subjective 'degree of belief' [390]. Bayes' theorem essentially tells us how to update and improve our initial beliefs using new information [387]. It may be expressed in the form:[98]

$$P(\theta_M|D) = \frac{\pi(\theta_M)P(D|\theta_M)}{P(D)} \ , \tag{D.1}$$

[97] Conditional independence of two events A and B given another event C means that, if C is true, knowledge about A does not influence our belief about B (and vice-versa) [387].

[98] A bar denotes conditional probability: in general, $P(A|B)$ is the probability for event A to happen, given event B.

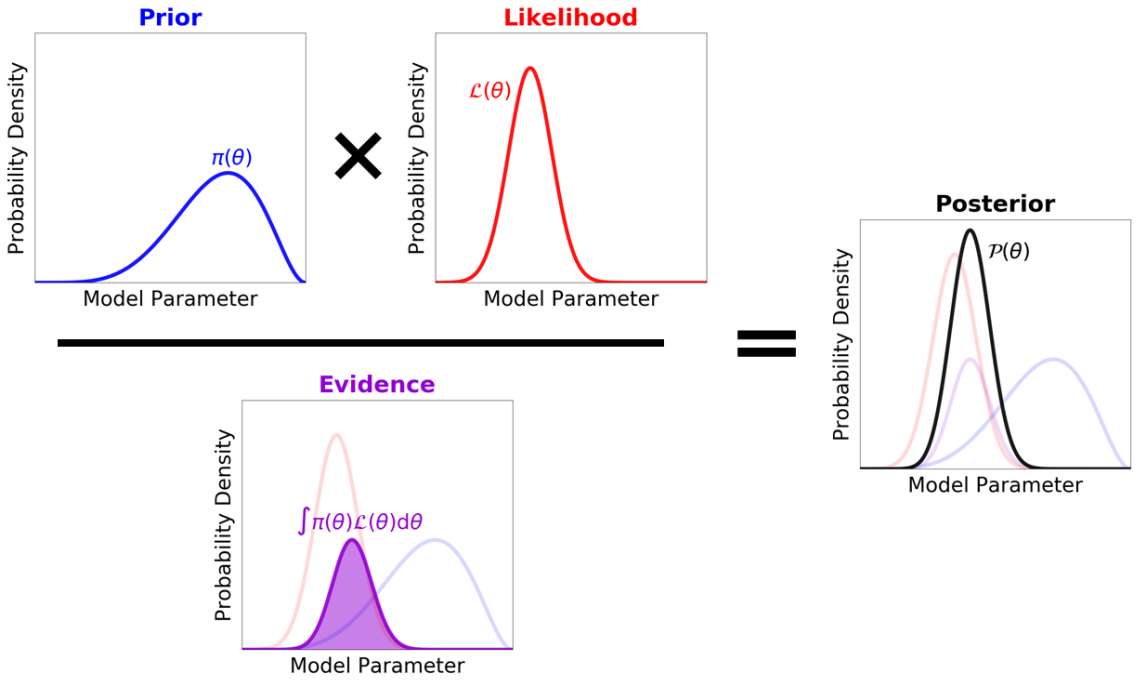

FIGURE D.1: Illustration of Bayes' theorem [389].

where θ_M represents a set of values for the parameters of model M, D is our data, and the different probability distributions are described below [389, 391]:

- The *prior* $\pi(\theta_M)$ is independent of D – it incorporates our initial beliefs about what θ_M should be. These beliefs are usually based on physical considerations or on the results of previous studies.
- $P(D|\theta_M)$ establishes how probable it is for D to have resulted from our particular θ_M. It may thus be said to quantify the likelihood of θ_M being the true set of parameter values, although when interpreted in this way it is commonly referred to as the *likelihood* $\mathscr{L}$ [$\mathscr{L}(\theta_M|D) = P(D|\theta_M)$].
- The *evidence* $P(D)$ indicates how well the model M describes D if we take into account all the possibilities for θ_M [i.e. if we integrate over the full parameter space: $P(D) = \int \pi(\theta_M)P(D|\theta_M)\mathrm{d}\theta_M$]. In other words, it reflects how good a fit the predictions of M provide for D. If only one model is considered, $P(D)$ is a fixed quantity and may be treated as a normalising factor.
- The *posterior probability* $P(\theta_M|D)$ is a measure of our belief in θ_M after we have combined $\pi(\theta_M)$, our prior intuition, with the data D and normalised by the overall evidence, $P(D)$.

The Metropolis-Hastings algorithm

Even when our knowledge of the mathematical properties of a probability distribution function (pdf) is limited, attributes like the mean and median may be inferred by analysing a large number of samples drawn randomly from the distribution. This makes MCMC an indispensable tool to extract information from posterior pdfs. It is often the case that the evidence $P(D)$ is very difficult to calculate, so that one can construct the posterior pdf solely up to a constant. The good news about MCMC is that it is insensitive to the normalising factor, and only requires us to calculate *ratios* of the pdf at arbitrary points of the parameter space. Furthermore, in its simplest form MCMC sampling can be carried out without having to integrate or differentiate the pdf [388].

The default MCMC algorithm implemented in Monte Python is known as *Metropolis-Hastings*. Let us suppose that we have already generated a number of samples, the last of which is θ_k. The next sample, θ_{k+1}, is obtained as follows [387, 388]:

- A point $\tilde{\theta}$ is drawn from the proposal distribution, which we shall denote by $q(\tilde{\theta}|\theta_k)$; $q(\tilde{\theta}|\theta_k)$ may be, for instance, a multi-variate Gaussian for $\tilde{\theta}$ with mean θ_k. The Markov property requires that the proposal function is independent of any values of θ that precede θ_k in the chain.
- A number u is chosen randomly from a top-hat distribution that is non-zero over the range $(0, 1)$.
- The function $f(\theta_M) \equiv \pi(\theta_M) \times P(D|\theta_M)$ is evaluated at $\theta_M = \tilde{\theta}$ and $\theta_M = \theta_k$. Then one computes the acceptance ratio r:

$$r = \frac{f(\tilde{\theta})}{f(\theta_k)} \times \frac{q(\theta_k|\tilde{\theta})}{q(\tilde{\theta}|\theta_k)} \ . \tag{D.2}$$

  If $u < r$, $\tilde{\theta}$ is accepted and incorporated into the chain. Otherwise, θ_{k+1} is set equal to θ_k.

Bibliography

[1] A. G. Riess et al. *Astron. J.* **116**, 1009 (1998).

[2] B. P. Schmidt et al. *Astrophys. J.* **507**, 46 (1998).

[3] The Supernova Cosmology Project, S. Perlmutter et al. *Astrophys. J.* **517**, 565 (1999).

[4] NobelPrize.org. Nobel Media AB 2019, *The Nobel Prize in Physics 2011.* www.nobelprize.org/prizes/physics/2011/summary/. Accessed on 30 Jul. 2019.

[5] S. Perlmutter. *Phys. Today* **56**, 53 (2003).

[6] M. S. Longair, *High Energy Astrophysics.* Cambridge University Press, New York, 3rd ed., 2011.

[7] B. Katz, S. Dong and D. Kushnir, *What Causes Supernovae Explosions?* www.ias.edu/ideas/2013/katz-dong-kushnir-1a-supernovae. Published in *The Institute Letter – Summer 2013* by the Institute for Advanced Study.

[8] S. Carroll, *Spacetime and Geometry: An Introduction to General Relativity.* Addison Wesley, San Francisco, 2004.

[9] E. Harrison. *Astrophys. J.* **403**, 28 (1993).

[10] S. M. Carroll. *Living Rev. Relativ.* **4**, 1 (2001).

[11] M. Inglis, *Astrophysics Is Easy!: An Introduction for the Amateur Astronomer*, The Patrick Moore Practical Astronomy Series. Springer, Switzerland, 2nd ed., 2015.

[12] S. Das et al. *Phys. Rev. Lett.* **107**, 021301 (2011).

[13] B. D. Sherwin et al. *Phys. Rev. Lett.* **107**, 021302 (2011).

[14] I. Szapudi et al. *Mon. Not. R. Astron. Soc.* **450**, 288 (2015).

[15] R. K. Sachs and A. M. Wolfe. *Astrophys. J.* **147**, 73 (1967).

[16] F. X. Dupé et al. *Astron. Astrophys.* **534**, A51 (2011).

[17] S. Gottlöber et al. In *NIC Symposium 2014 - Proceedings* (K. Binder, G. Münster and M. Kremer, eds.), vol. 47 of *The NIC Publication Series*, p. 69, Forschungszentrum Jülich, Jülich, Germany, 2014.

[18] M. P. Hobson, G. P. Efstathiou and A. N. Lasenby, *General Relativity: An Introduction for Physicists*. Cambridge University Press, New York, 2006.

[19] C. L. Bennett et al. *Astrophys. J. Suppl. S.* **208**, 20 (2013).

[20] Planck Collaboration, N. Aghanim et al. arXiv:1807.06209.

[21] T. Davis and B. Griffen. *Scholarpedia* **5**:9, 4473 (2010). www.scholarpedia.org/article/Cosmological_constant#einstein17.

[22] Planck Collaboration, P. A. R. Ade et al. *Astron. Astrophys.* **594**, A13 (2016).

[23] BOSS Collaboration, J. N. Grieb et al. *Mon. Not. R. Astron. Soc.* **467**, 2085 (2017).

[24] R. D. Klauber, *Student Friendly Quantum Field Theory*. Sandtrove Press, Iowa, 2nd ed., 2013.

[25] V. M. Mostepanenko and G. L. Klimchitskaya. *Symmetry* **11**, 314 (2019).

[26] A. G. Riess et al. *Astrophys. J.* **855**, 136 (2018).

[27] T. Nakama, J. Chluba and M. Kamionkowski. *Phys. Rev. D* **95**, 121302 (2017).

[28] L. Miao et al. *Commun. Theor. Phys.* **56**, 525 (2011).

[29] J. Yoo and Y. Watanabe. *Int. J. Mod. Phys. D* **21**, 1230002 (2012).

[30] B. Ratra and P. J. E. Peebles. *Phys. Rev. D* **37**, 3406 (1988).

[31] R. R. Caldwell, R. Dave and P. J. Steinhardt. *Phys. Rev. Lett.* **80**, 1582 (1998).

[32] V. Faraoni. *Phys. Rev. D* **85**, 024040 (2012).

[33] J.-B. Durrive et al. *Phys. Rev. D* **97**, 043503 (2018).

[34] S. Tsujikawa. *Class. Quant. Grav.* **30**, 214003 (2013).

[35] Y. Fujii and K.-I. Maeda, *The Scalar-Tensor Theory of Gravitation*. Cambridge University Press, Cambridge, U.K., 2004.

[36] V. Faraoni, *Cosmology in Scalar-Tensor Gravity*. Kluwer Academic, Dordrecht, The Netherlands, 2004.

[37] R. R. Caldwell. *Phys. Lett. B* **545**, 23 (2002).

[38] S. M. Carroll, M. Hoffman and M. Trodden. *Phys. Rev. D* **68**, 023509 (2003).

[39] R. R. Caldwell, M. Kamionkowski and N. N. Weinberg. *Phys. Rev. Lett.* **91**, 071301 (2003).

[40] K. J. Ludwick. *Phys. Rev. D* **92**, 063019 (2015).

[41] T. Chiba, T. Okabe and M. Yamaguchi. *Phys. Rev. D* **62**, 023511 (2000).

[42] M. Malquarti et al. *Phys. Rev. D* **67**, 123503 (2003).

[43] R. Saitou and S. Nojiri. *Eur. Phys. J. C* **71**, 1712 (2011).

[44] C. Armendáriz-Picón, D. Damour and V. Mukhanov. *Phys. Lett. B* **458**, 209 (1999).

[45] C. Deffayet et al. *J. Cosmol. Astropart. Phys.* **2010**:10, 026.

[46] R. Kimura and K. Yamamoto. *J. Cosmol. Astropart. Phys.* **2011**:04, 025.

[47] D. Maity. *Phys. Lett. B* **720**, 389 (2013).

[48] N. Arkani-Hamed et al. *J. High Energy Phys.* **2004**:05, 074.

[49] S. Peirone et al. *Phys. Rev. D* **100**, 063540 (2019).

[50] A. Kamenshchik, U. Moschella and V. Pasquier. *Phys. Lett. B* **511**, 265 (2001).

[51] M. C. Bento, O. Bertolami and A. A. Sen. *Phys. Rev. D* **66**, 043507 (2002).

[52] Z. H. Zhu. *Astron. Astrophys.* **423**, 421 (2004).

[53] H. B. Sandvik et al. *Phys. Rev. D* **69**, 123524 (2004).

[54] M. E. Taylor, *Partial Differential Equations II – Qualitative Studies of Linear Equations*. Springer Science+Business Media, New York, 1996.

[55] S. Kopeikin, M. Efroimsky and G. Kaplan, *Relativistic Celestial Mechanics of the Solar System*. Wiley-VCH, Weinheim, Germany, 2011.

[56] T. P. Sotiriou and V. Faraoni. *Rev. Mod. Phys.* **82**, 451 (2010).

[57] V. Faraoni. arXiv:0810.2602v1.

[58] E. V. Linder. *Phys. Rev. D* **81**, 127301 (2010). [Erratum: *Phys. Rev. D* **82**, 109902 (2010)].

[59] G. R. Bengochea and R. Ferraro. *Phys. Rev. D* **79**, 124019 (2009).

[60] Y.-F. Cai et al. *Rep. Prog. Phys.* **79**:10, 106901 (2016).

[61] M. Milgrom. *Astrophys. J.* **270**, 365 (1983).

[62] J. Bekenstein and M. Milgrom. *Astrophys. J.* **286**, 7 (1984).

[63] J. D. Bekenstein. *Phys. Rev. D* **70**, 083509 (2004).

[64] B. Zwiebach. *Phys. Lett.* **156**, 315 (1985).

[65] A. De Felice, D. F. Mota and S. Tsujikawa. *Phys. Rev. D* **81**, 023532 (2010).

[66] D. Lovelock. *J. Math. Phys.* **12**, 498 (1971).

[67] J. Kastikainen. *Class. Quant. Grav.* **37**, 025001 (2020).

[68] M. H. Dehghani and S. Assyyaee. *Phys. Lett. B* **676**, 16 (2009).

[69] P. Hořava. *Phys. Rev. D* **79**, 084008 (2009).

[70] A. Burnel, *Noncovariant Gauges in Canonical Formalism*, Lect. Notes Phys. 761. Springer, Berlin/Heidelberg, 2009.

[71] E. N. Saridakis. *Eur. Phys. J. C* **67**, 229 (2010).

[72] P. D. Mannheim. *Prog. Part. Nucl. Phys.* **56**, 340 (2006).

[73] C. Lanczos. *Ann. Math.* **39**, 842 (1938).

[74] P. D. Mannheim and J. G. O'Brien. *Phys. Rev. D* **85**, 124020 (2012).

[75] P. D. Mannheim. *Phys. Rev. D* **93**, 068501 (2016).

[76] Y. Yoon. *Phys. Rev. D* **88**, 027504 (2013).

[77] P. D. Mannheim and D. Kazanas. *Astrophys. J.* **342**, 635 (1989).

[78] D. Cutajar and K. Zarb Adami. *Mon. Not. R. Astron. Soc.* **441**, 1291 (2014).

[79] A. Hakimov, A. Abdujabbarov and B. Narzilloev. *Int. J. Mod. Phys. A* **32**, 1750116 (2017).

[80] M. C. Campigotto, A. Diaferio and L. Fatibene. *Class. Quant. Grav.* **36**, 245014 (2019).

[81] J. Sultana, D. Kazanas and J. L. Said. *Phys. Rev. D* **86**, 084008 (2012).

[82] O. Kaşıkçı and C. Deliduman. *Phys. Rev. D* **100**, 024019 (2019).

[83] Y.-K. Lim and Q.-h. Wang. *Phys. Rev. D* **95**, 024004 (2017).

[84] J. Sultana and D. Kazanas. *Phys. Rev. D* **81**, 127502 (2010).

[85] C. Cattani et al. *Phys. Rev. D* **87**, 047503 (2013).

[86] J. D. Bekenstein. *Lett. Nuovo Cimento* **4**, 737 (1972).

[87] J. D. Bekenstein. *Phys. Rev. D* **7**, 2333 (1973).

[88] S. W. Hawking. *Commun. Math. Phys.* **43**, 199 (1975).

[89] G. 't Hooft. arXiv:gr-qc/9310026v2.

[90] L. Susskind. *J. Math. Phys.* **36**, 6377 (1995).

[91] L. Susskind, *The Black Hole War: My Battle with Stephen Hawking to Make the World Safe for Quantum Mechanics*. Back Bay Books, New York, 2008.

[92] S. D. H. Hsu. *Phys. Lett. B* **594**, 13 (2004).

[93] A. G. Cohen, D. B. Kaplan and A. E. Nelson. *Phys. Rev. Lett.* **82**, 4971 (1999).

[94] C. P. Singh and P. Kumar. *Astrophys. Space Sci.* **361**, 157 (2016).

[95] S. del Campo et al. *Phys. Rev. D* **83**, 123006 (2011).

[96] M. Li. *Phys. Lett. B* **603**, 1 (2004).

[97] A. Pontzen. *Scholarpedia* **11**:4, 32340. Revision #153559. www.scholarpedia.org/article/Bianchi_universes.

[98] S. Räsänen. *J. Cosmol. Astropart. Phys.* **2006**:11, 003.

[99] S. W. Hawking. In *Field Theory, Quantum Gravity and Strings* (H. J. de Vega and N. Sánchez, eds.), vol. 246 of *Lecture Notes in Physics*, p. 1, Springer-Verlag, Berlin, 1988.

[100] B. S. DeWitt. *Phys. Rev.* **160**, 1113 (1967).

[101] C. DeWitt-Morette and J. A. Wheeler, eds., *Battelle Rencontres: 1967 Lectures in Mathematics and Physics*. W. A. Benjamin, New York, 1968.

[102] J. B. Hartle and S. W. Hawking. *Phys. Rev. D* **28**, 2960 (1983).

[103] M. McGuigan. *Phys. Rev. D* **41**, 418 (1990).

[104] M. McGuigan. arXiv:hep-th/0602112v1.

[105] S. H. H. Tye. arXiv:hep-th/0611148v3.

[106] A. G. Sánchez et al. *Mon. Not. R. Astron. Soc.* **400**, 1643 (2009).

[107] M. Moresco et al. *J. Cosmol. Astropart. Phys.* **2016**:12, 039.

[108] Y. Gong and Y. Z. Zhang. *Phys. Rev. D* **72**, 043518 (2005).

[109] K. Ichikawa and T. Takahashi. *Phys. Rev. D* **73**, 083526 (2006).

[110] G. B. Zhao et al. *Phys. Lett. B* **648**, 8 (2007).

[111] A. Bonilla Rivera and J. E. García-Farieta. *Int. J. Mod. Phys. D* **28**, 1950118 (2019).

[112] K. Ichikawa and T. Takahashi. *J. Cosmol. Astropart. Phys.* **2007**:02, 001.

[113] K. Ichikawa et al. *J. Cosmol. Astropart. Phys.* **2006**:12, 005.

[114] C.-G. Park and B. Ratra. *Astrophys. Space Sci.* **364**, 134 (2019).

[115] J. M. Virey et al. *J. Cosmol. Astropart. Phys.* **2008**:12, 008.

[116] Y. Wang and P. Mukherjee. *Phys. Rev. D* **76**, 103533 (2007).

[117] J. N. Dossett and M. Ishak. *Phys. Rev. D* **86**, 103008 (2012).

[118] S. Del Campo, M. Cataldo and F. Peña. *Gen. Relativ. Gravit.* **37**, 675 (2005).

[119] E. Di Dio et al. *J. Cosmol. Astropart. Phys.* **2016**:06, 013.

[120] A. Rest et al. *Astrophys. J.* **795**, 44 (2014).

[121] A. R. Liddle and M. Cortês. *Phys. Rev. Lett.* **111**, 111302 (2013).

[122] T. Delubac et al. *Astron. Astrophys.* **574**, A59 (2015).

[123] K. Bolejko. *Class. Quant. Grav.* **35**, 024003 (2018).

[124] K. Bolejko. *Phys. Rev. D* **97**, 103529 (2018).

[125] A. G. Riess et al. *Astrophys. J.* **876**, 85 (2019).

[126] A. R. Liddle and D. H. Lyth, *Cosmological Inflation and Large-Scale Structure*. Cambridge University Press, Cambridge, UK, 2000.

[127] S. Weinberg, *Gravitation and Cosmology: Principles and Applications of the General Theory of Relativity*. John Wiley & Sons, New York, 1972.

[128] B. Si Lakhal and A. Guezmir. *J. Phys.: Conf. Ser.* **1269**, 012017 (2019).

[129] A. H. Guth. *Phys. Rev. D* **23**, 347 (1981).

[130] G. Nordström. *Phys. Z.* **13**, 1126 (1912). *English translation available in:* J. Renn, ed., vol. 3 of *The Genesis of General Relativity,* p. 1412, Springer, Dordrecht, The Netherlands, 2007.

[131] P. A. M. Dirac. *Nature* **139**, 323 (1937).

[132] P. Jordan and C. Müller. *Z. Naturforsch. A* **2**, 1 (1947).

[133] C. Brans and R. H. Dicke. *Phys. Rev.* **124**, 925 (1961).

[134] CMS Collaboration, S. Chatrchyan et al. *Phys. Lett. B* **716**, 30 (2012).

[135] F. Englert and R. Brout. *Phys. Rev. Lett.* **13**, 321 (1964).

[136] P. W. Higgs. *Phys. Rev. Lett.* **13**, 508 (1964).

[137] ATLAS Collaboration, G. Aad et al. *Phys. Lett. B* **716**, 1 (2012).

[138] E. S. Fradkin and A. A. Tseytlin. *Nucl. Phys. B* **261**, 1 (1985). [Erratum: *Nucl. Phys. B* **269**, 745 (1986)].

[139] R. D. Reasenberg et al. *Astrophys. J.* **234**, L219 (1979).

[140] C. M. Will. *Living Rev. Relativ.* **17**, 4 (2014).

[141] P. J. Steinhardt and F. S. Accetta. *Phys. Rev. Lett.* **64**, 2740 (1990).

[142] J. D. Barrow and K.-i. Maeda. *Nucl. Phys. B* **341**, 294 (1990).

[143] LIGO Scientific Collaboration and Virgo Collaboration, B. P. Abbott et al. *Phys. Rev. Lett.* **119**, 161101 (2017).

[144] B. P. Abbott et al. *Astrophys. J. Lett.* **848**, L13 (2017).

[145] J. M. Ezquiaga and M. Zumalacárregui. *Phys. Rev. Lett.* **119**, 251304 (2017).

[146] C. Charmousis et al. *Phys. Rev. Lett.* **108**, 051101 (2012).

[147] A. Nicolis, R. Rattazzi and E. Trincherini. *Phys. Rev. D* **79**, 064036 (2009).

[148] C. Deffayet, G. Esposito-Farèse and A. Vikman. *Phys. Rev. D* **79**, 084003 (2009).

[149] J. Gleyzes et al. *Phys. Rev. Lett.* **114**, 211101 (2015).

[150] D. Langlois and K. Noui. *J. Cosmol. Astropart. Phys.* **2016**:02, 034.

[151] J. Ben Achour et al. *J. High Energy Phys.* **2016**:12, 100.

[152] K. Koyama. *Rep. Prog. Phys.* **79**, 046902 (2016).

[153] P. J. E. Peebles and A. Vilenkin. *Phys. Rev. D* **59**, 063505 (1999).

[154] M. Sami and N. Dadhich. *TSPU Bulletin* **44N7**, 25 (2004).

[155] E. J. Copeland, A. R. Liddle and J. E. Lidsey. *Phys. Rev. D* **64**, 023509 (2001).

[156] A. S. Majumdar. *Phys. Rev. D* **64**, 083503 (2001).

[157] S. Tsujikawa et al. *Phys. Rev. D* **77**, 103009 (2008).

[158] B. J. Barros et al. *J. Cosmol. Astropart. Phys.* **2019**:01, 007.

[159] L. N. Granda and D. F. Jimenez. *Eur. Phys. J. C* **79**, 772 (2019).

[160] F. Beyer and L. Escobar. *Class. Quant. Grav.* **30**, 195020 (2013).

[161] R. A. Daly and E. J. Guerra. *Astron. J.* **124**, 1831 (2002).

[162] X. Chen, R. J. Scherrer and G. Steigman. *Phys. Rev. D* **63**, 123504 (2001).

[163] S. Sonego and V. Faraoni. *Class. Quant. Grav.* **10**, 1185 (1993).

[164] C. G. Callan Jr., S. Coleman and R. Jackiw. *Ann. Phys.* **59**, 42 (1970).

[165] R. H. Dicke. *Phys. Rev.* **125**, 2163 (1962).

[166] G. K. Karananas and A. Monin. *Phys. Lett. B* **757**, 257 (2016).

[167] A. N. Schellekens. *Fortschr. Phys.* **44**, 605 (1996).

[168] J. D. Bekenstein and A. Meisels. *Phys. Rev. D* **22**, 1313 (1980).

[169] H. Stephani, D. Kramer, M. Maccallum, C. Hoenselaers and E. Herlt, *Exact Solutions to Einstein's Field Equations*. Cambridge University Press, New York, 2nd ed., 2003.

[170] U. von der Gönna and D. Kramer. *Class. Quant. Grav.* **15**, 215 (1998).

[171] R. M. Wald, *General Relativity*. The University of Chicago Press, Chicago, 1984.

[172] B. F. Roukema et al. *Astron. Astrophys.* **598**, A111 (2017).

[173] N. Dauphas. *Nature* **435**, 1203 (2005).

[174] S. Wanajo et al. *Astrophys. J.* **577**, 853 (2002).

[175] I. Ferreras, A. Melchiorri and J. Silk. *Mon. Not. R. Astron. Soc.* **327**, L47 (2001).

[176] G. M. Kremer. *Phys. Rev. D* **68**, 123507 (2003).

[177] D. C. Johnston, *Advances in Thermodynamics of the van der Waals Fluid*. Morgan & Claypool, San Rafael, California, 2014.

[178] H. B. Callen, *Thermodynamics and an Introduction to Thermostatistics*. John Wiley & Sons, New York, 2nd ed., 1985.

[179] G. M. Kremer. *Gen. Relativ. Gravit.* **36**, 1423 (2004).

[180] A. D. Linde. *Phys. Lett. B* **108**, 389 (1982).

[181] A. Albrecht and P. J. Steinhardt. *Phys. Rev. Lett.* **48**, 1220 (1982).

[182] M. S. Turner and A. G. Riess. *Astrophys. J.* **569**, 18 (2002).

[183] C. Shapiro and M. S. Turner. *Astrophys. J.* **649**, 563 (2006).

[184] Y. Gong and A. Wang. *Phys. Rev. D* **73**, 083506 (2006).

[185] R. R. Caldwell and M. Kamionkowski. *Annu. Rev. Nucl. Part. S.* **59**, 397 (2009).

[186] S. Chakraborty and S. Saha. *Phys. Rev. D* **90**, 123505 (2014).

[187] G. M. Kremer and M. C. N. Teixeira da Silva. *Braz. J. Phys.* **34**:3b, 1204 (2004).

[188] W. Zimdahl. *Phys. Rev. D* **57**, 2245 (1998).

[189] V. N. Pokrovskii. *Int. Sch. Res. Notices* **2013**, 906136.

[190] W. Israel and J. M. Stewart. *Ann. Phys.* **118**, 341 (1979).

[191] G. L. Murphy. *Phys. Rev. D* **8**, 4231 (1973).

[192] V. A. Belinskiĭ, E. S. Nikomarov and I. M. Khalatnikov. *Sov. Phys. JETP* **50**, 213 (1979).

[193] H. Weyl. *Sitzungsber. Preuss. Akad. Wiss. Berlin* **1918**, 465. *English translation available in:*
L. O'Raifeartaigh, *The Dawning of Gauge Theory,* p. 121, Princeton University Press, Princeton, New Jersey, 1997.

[194] W. D. Halford. *Aust. J. Phys.* **23**, 863 (1970).

[195] G. Lyra. *Math. Z.* **54**, 52 (1951).

[196] H. H. Soleng. *Gen. Relativ. Gravit.* **19**, 1213 (1987).

[197] M. Khurshudyan et al. *Adv. High Energy Phys.* **2014**, 878092.

[198] M. A. Jafarizadeh et al. *Phys. Rev. D* **60**, 063514 (1999).

[199] J. A. S. Lima, E. L. D. Perico and G. J. M. Zilioti. *Int. J. Mod. Phys. D.* **24**, 1541006 (2015).

[200] J. A. S. Lima and M. Trodden. *Phys. Rev. D* **53**, 4280 (1996).

[201] E. L. D. Perico et al. *Phys. Rev. D* **88**, 063531 (2013).

[202] J. A. S. Lima, S. Basilakos and J. Solà. *Mon. Not. R. Astron. Soc.* **431**, 923 (2013).

[203] C. Moreno and J. E. Madriz Aguilar. *J. Phys. Conf. Ser.* **545**, 012010 (2014).

[204] Planck Collaboration, P. A. R. Ade et al. *Astron. Astrophys.* **594**, A14 (2016).

[205] S. Joudaki et al. *Mon. Not. R. Astron. Soc.* **471**, 1259 (2017).

[206] A. Einstein. *Sitzungsber. Preuss. Akad. Wiss. Berlin* **1915**, 831. *English translation available in:*
The Collected Papers of Albert Einstein, Volume 6: The Berlin Years: Writings, 1914–1917, p. 112, Princeton University Press, Princeton, New Jersey, 1997. Translated by A. Engel. With E. Schucking as consultant.

[207] I. i. Shapiro, *Solar system tests of general relativity: recent results and present plans*, In *General Relativity and Gravitation, 1989: Proceedings of the 12th International Conference on General Relativity and Gravitation* (N. Ashby, D. F. Bartlett and W. Wyss, eds.), p. 313. Cambridge University Press, Cambridge, New York, 1990.

[208] D. J. Eisenstein et al. *Astrophys. J.* **633**, 560 (2005).

[209] S. Weinberg. In *Sources and Detection of Dark Matter and Dark Energy in the Universe* (D. B. Cline, ed.), p. 18, Springer-Verlag, Berlin/Heidelberg, 2001.

[210] W. Hu and I. Sawicki. *Phys. Rev. D* **76**, 064004 (2007).

[211] J. Khoury. *Class. Quant. Grav.* **30**, 214004 (2013).

[212] S. Basilakos, D. Polarski and J. Solà. *Phys. Rev. D* **86**, 043010 (2012).

[213] I. L. Shapiro et al. *Phys. Lett. B* **574**, 149 (2003).

[214] A. Gómez-Valent, J. Solà and S. Basilakos. *J. Cosmol. Astropart. Phys.* **2015**:01, 004.

[215] J. Solà Peracaula, J. de Cruz Pérez and A. Gómez-Valent. *Mon. Not. R. Astron. Soc.* **478**, 4357 (2018).

[216] S. Basilakos, M. Plionis and J. Solà. *Phys. Rev. D* **80**, 083511 (2009).

[217] J. Grande et al. *J. Cosmol. Astropart. Phys.* **2011**:08, 007.

[218] C.-Q. Geng, C.-C. Lee and L. Yin. *J. Cosmol. Astropart. Phys.* **2017**:08, 032.

[219] A. Gómez-Valent, E. Karimkhani and J. Solà. *J. Cosmol. Astropart. Phys.* **2015**:12, 048.

[220] I. L. Shapiro and J. Solà. *Phys. Lett. B* **475**, 236 (2000).

[221] I. L. Shapiro and J. Solà. *J. High Energy Phys.* **2002**:02, 006.

[222] I. L. Shapiro and J. Solà. *Nucl. Phys. B* **127**, 71 (2004).

[223] J. Solà. *J. Phys. A-Math. Theor.* **41**, 164066 (2008).

[224] J. Solà, A. Gómez-Valent and J. de Cruz Pérez. *Phys. Lett. B* **774**, 317 (2017).

[225] J. Solà Peracaula, J. de Cruz Pérez and A. Gómez-Valent. *Europhys. Lett.* **121**, 39001 (2018).

[226] J. Solà, A. Gómez-Valent and J. de Cruz Pérez. *Astrophys. J.* **836**, 43 (2017).

[227] M. S. Berman. *Phys. Rev. D* **43**, 1075 (1991).

[228] A. Beesham. *Phys. Rev. D* **48**, 3539 (1993).

[229] O. Bertolami. *Nuovo Ciment. B* **93**, 36 (1986).

[230] D. Kalligas, P. Wesson and C. W. F. Everitt. *Gen. Relativ. Gravit.* **24**, 351 (1992).

[231] J. L. Lopez and D. V. Nanopoulos. *Mod. Phys. Lett. A* **11**, 1 (1996).

[232] A. I. Arbab. *Gen. Relativ. Gravit.* **29**, 61 (1997).

[233] Y. Fujii and T. Nishioka. *Phys. Rev. D* **42**, 361 (1990).

[234] A. Beesham. *Gen. Relativ. Gravit.* **26**, 159 (1994).

[235] M. S. Berman and M. M. Som. *Int. J. Theor. Phys.* **29**, 1411 (1990).

[236] M. Endō and T. Fukui. *Gen. Relativ. Gravit.* **8**, 833 (1977).

[237] P. Spindel and R. Brout. *Phys. Lett. B* **320**, 241 (1994).

[238] A. B. Dussattar and R. G. Vishwakarma. *Pramana* **47**, 41 (1996).

[239] M. V. John and K. Babu Joseph. *Class. Quant. Grav.* **14**, 1115 (1997).

[240] J. C. Carvalho, J. A. S. Lima and I. Waga. *Phys. Rev. D* **46**, 2404 (1992).

[241] I. Waga. *Astrophys. J.* **414**, 436 (1993).

[242] R. F. Sisteró. *Gen. Relativ. Gravit.* **23**, 1265 (1991).

[243] J. M. Overduin and F. I. Cooperstock. *Phys. Rev. D* **58**, 043506 (1998).

[244] A. I. Arbab and A.-M. M. Abdel-Rahman. *Phys. Rev. D* **50**, 7725 (1994).

[245] A.-M. M. Abdel-Rahman. *Phys. Rev. D* **45**, 3497 (1992).

[246] V. Méndez and D. Pavón. *Gen. Relativ. Gravit.* **28**, 679 (1996).

[247] M. O. Calvao et al. *Phys. Rev. D* **45**, 3869 (1992).

[248] V. Silveira and I. Waga. *Phys. Rev. D* **56**, 4625 (1997).

[249] W. Chen and Y.-S. Wu. *Phys. Rev. D* **41**, 695 (1990).

[250] M. Özer and M. O. Taha. *Phys. Lett. B* **171**, 363 (1986).

[251] K. Freese et al. *Nucl. Phys. B* **287**, 797 (1987).

[252] P. Wang and X.-H. Meng. *Class. Quant. Grav.* **22**, 283 (2005).

[253] J. A. S. Lima and J. C. Carvalho. *Gen. Relativ. Gravit.* **26**, 909 (1994).

[254] C. Wetterich. *Astron. Astrophys.* **301**, 321 (1995).

[255] S. Ray, U. Mukhopadhyay and X.-H. Meng. *Gravit. Cosmol.* **13**, 142 (2007).

[256] S. Ray et al. *Int. J. Theor. Phys.* **50**, 2687 (2011).

[257] D. A. Easson, P. H. Frampton and G. F. Smoot. *Phys. Lett. B* **696**, 273 (2011).

[258] S. Basilakos and J. Solà. *Phys. Rev. D* **90**:023008, (2014).

[259] J. Solà. *J. Phys. Conf. Ser.* **283**, 012033 (2011).

[260] I. L. Shapiro. *Class. Quant. Grav.* **25**, 103001 (2008).

[261] I. L. Shapiro, J. Solà and H. Štefančić. *J. Cosmol. Astropart. Phys.* **2005**:01, 012.

[262] J. Solà, A. Gómez-Valent and J. de Cruz Pérez. *Astrophys. J. Lett.* **811**, L14 (2015).

[263] D. Blas, J. Lesgourgues and T. Tram. *J. Cosmol. Astropart. Phys.* **2011**:07, 034.

[264] B. Audren et al. *J. Cosmol. Astropart. Phys.* **2013**:02, 001.

[265] M. Betoule et al. *Astron. Astrophys.* **568**, A22 (2014).

[266] X.-B. Zou et al. *Phys. Lett. B* **776**, 284 (2018).

[267] C. Zhang et al. *Res. Astron. Astrophys.* **14**, 1221 (2014).

[268] M. Moresco et al. *J. Cosmol. Astropart. Phys.* **2016**:05, 014.

[269] D. Stern et al. *J. Cosmol. Astropart. Phys.* **2010**:02, 008.

[270] J. Simon, L. Verde and R. Jimenez. *Phys. Rev. D* **71**, 123001 (2005).

[271] M. Moresco et al. *J. Cosmol. Astropart. Phys.* **2012**:08, 006.

[272] M. Moresco. *Mon. Not. R. Astron. Soc.: Lett.* **450**, L16 (2015).

[273] A. L. Ratsimbazafy et al. *Mon. Not. R. Astron. Soc.* **467**, 3239 (2017).

[274] R. Jimenez and A. Loeb. *Astrophys. J.* **573**, 37 (2002).

[275] G. Bruzual and S. Charlot. *Mon. Not. R. Astron. Soc.* **344**, 1000 (2003).

[276] E. Komatsu et al. *Astrophys. J. Suppl. Ser.* **180**, 330 (2009).

[277] Q.-G. Huang, K. Wang and S. Wang. *J. Cosmol. Astropart. Phys.* **2015**:12, 022.

[278] BOSS Collaboration, É. Aubourg et al. *Phys. Rev. D* **92**, 123516 (2015).

[279] F. Beutler et al. *Mon. Not. R. Astron. Soc.* **416**, 3017 (2011).

[280] A. J. Ross et al. *Mon. Not. R. Astron. Soc.* **449**, 835 (2015).

[281] M. Ata et al. *Mon. Not. R. Astron. Soc.* **473**, 4773 (2018).

[282] J. E. Bautista et al. *Astron. Astrophys.* **603**, A12 (2017).

[283] S. Alam et al. *Mon. Not. R. Astron. Soc.* **470**, 2617 (2017).

[284] H. du Mas des Bourboux et al. *Astron. Astrophys.* **608**, A130 (2017).

[285] J. Bautista, *Baryon Acoustic Oscillations in the Large Scale Structures of the Universe as seen by the Sloan Digital Sky Survey*, Ph.D. thesis, Université Paris Diderot, 2014.

[286] W. J. Percival et al. *Phil. Trans. R. Soc. A* **369**, 5058 (2011).

[287] J. Kwan, G. F. Lewis and E. V. Linder. *Astrophys. J.* **748**, 78 (2012).

[288] B. Sagredo, S. Nesseris and D. Sapone. *Phys. Rev. D* **98**, 083543 (2018).

[289] H. Mo, F. van den Bosch and S. White, *Galaxy Formation and Evolution.* Cambridge University Press, New York, 2010.

[290] A. Gómez-Valent and J. Solà Peracaula. *Mon. Not. R. Astron. Soc.* **478**, 126 (2018).

[291] A. de la Cruz-Dombriz, A. Dobado and A. L. Maroto. *Phys. Rev. D* **77**, 123515 (2008).

[292] K. Koyama, R. Maartens and Y.-S. Song. *J. Cosmol. Astropart. Phys.* **2009**:10, 017.

[293] D. J. Eisenstein and W. Hu. *Astrophys. J.* **511**, 5 (1999).

[294] Planck Collaboration, P. A. R. Ade et al. *Astron. Astrophys.* **594**, A20 (2016).

[295] D. J. Eisenstein and W. Hu. *Astrophys. J.* **496**, 605 (1998).

[296] S. Dodelson, *Modern Cosmology.* Academic Press, San Diego, California, 2003.

[297] M. J. Hudson and S. J. Turnbull. *Astrophys. J. Lett.* **751**, L30 (2012).

[298] Y.-S. Song and W. J. Percival. *J. Cosmol. Astropart. Phys.* **2009**:10, 004.

[299] C. Blake et al. *Mon. Not. R. Astron. Soc.* **415**, 2892 (2011).

[300] L. Samushia, W. J. Percival and A. Raccanelli. *Mon. Not. R. Astron. Soc.* **420**, 2102 (2012).

[301] C. Blake et al. *Mon. Not. R. Astron. Soc.* **425**, 405 (2012).

[302] A. Pezzotta et al. *Astron. Astrophys.* **604**, A33 (2017).

[303] T. Okumura et al. *Publ. Astron. Soc. Japan* **68**, 38 (2016).

[304] S. Nesseris, G. Pantazis and L. Perivolaropoulos. *Phys. Rev. D* **96**, 023542 (2017).

[305] L. Kazantzidis and L. Perivolaropoulos. *Phys. Rev. D* **97**, 103503 (2018).

[306] C. Alcock and B. Paczyński. *Nature* **281**, 358 (1979).

[307] E. Macaulay, I. K. Wehus and H. K. Eriksen. *Phys. Rev. Lett.* **111**, 161301 (2013).

[308] G. Efstathiou. *Mon. Not. R. Astron. Soc.* **440**, 1138 (2014).

[309] E. Mörtsell and S. Dhawan. *J. Cosmol. Astropart. Phys.* **2018**:09, 025.

[310] E. Di Valentino, E. V. Linder and A. Melchiorri. *Phys. Rev. D* **97**, 043528 (2018).

[311] V. Poulin et al. *Phys. Rev. Lett.* **122**, 221301 (2019).

[312] G. Mangano et al. *Nucl. Phys. B* **729**, 221 (2005).

[313] D. J. Fixsen. *Astrophys. J.* **707**, 916 (2009).

[314] A. Lewis. arXiv:1910.13970.

[315] A. Avgoustidis et al. *J. Cosmol. Astropart. Phys.* **2012**:02, 013.

[316] G. Luzzi et al. *J. Cosmol. Astropart. Phys.* **2015**:09, 011.

[317] P. Noterdaeme et al. *Astron. Astrophys.* **526**, L7 (2011).

[318] A. Avgoustidis et al. *Phys. Rev. D* **93**, 043521 (2016).

[319] H.-N. Lin, M.-H. Li and X. Li. *Mon. Not. R. Astron. Soc.* **480**, 3117 (2018).

[320] F. De Bernardis, E. Giusarma and A. Melchiorri. *Int. J. Mod. Phys. D* **15**, 759 (2006).

[321] R. F. L. Holanda, V. C. Busti and J. S. Alcaniz. *J. Cosmol. Astropart. Phys.* **2016**:02, 054.

[322] C. Ma and P.-S. Corasaniti. *Astrophys. J.* **861**, 124 (2018).

[323] S. S. McGaugh. *Astrophys. J.* **611**, 26 (2004).

[324] S. S. McGaugh. *Can. J. Phys.* **93**, 250 (2015).

[325] M. Douspis, L. Salvati and N. Aghanim. *PoS Proc. Sci.* **335**, 037 (2018).

[326] H. Akaike. *IEEE Trans. Automat. Contr.* **19**, 716 (1974).

[327] G. Schwarz. *Ann. Stat.* **6**, 461 (1978).

[328] C. J. Schwarz, *Sampling, Regression, Experimental Design and Analysis for Environmental Scientists, Biologists, and Resource Managers*. Lecture notes; Simon Fraser University: British Columbia, Canada, 2011. people.stat.sfu.ca/\%7Ecschwarz/Stat-650/Notes/PDF/MLE-AIC.pdf.

[329] W. A. Link and R. J. Barker, *Bayesian Inference: With Ecological Applications*. Academic Press, London, 2010.

[330] J. Kuha. *Sociol. Methods Res.* **33**, 188 (2004).

[331] A. R. Liddle. *Mon. Not. R. Astron. Soc.: Lett.* **377**, L74 (2007).

[332] L. A. Jordanger and D. Tjøstheim. *Stat. Probabil. Lett.* **92**, 249 (2014).

[333] S. Nesseris, A. De Felice and S. Tsujikawa. *Phys. Rev. D* **82**, 124054 (2010).

[334] A. R. Liddle. *Mon. Not. R. Astron. Soc.* **351**, L49 (2004).

[335] H.-J. Schmidt. *Int. J. Geom. Methods Mod. Phys.* **04**, 209 (2007).

[336] R. Utiyama and B. S. DeWitt. *J. Math. Phys.* **3**, 608 (1962).

[337] S. Capozziello and A. Stabile. arXiv:1009.3441v1.

[338] A. Stabile. *Phys. Rev. D* **82**, 124026 (2010).

[339] J. Sultana, F. Melia and D. Kazanas. *Phys. Rev. D* **99**, 103505 (2019).

[340] S. Capozziello, S. Carloni and A. Troisi. *Recent Res. Dev. Astron. Astrophys.* **1**, 625 (2003).

[341] S. M. Carroll et al. *Phys. Rev. D* **70**, 043528 (2004).

[342] A. Dolgov and M. Kawasaki. *Phys. Lett. B* **573**, 1 (2003).

[343] T. Chiba. *Phys. Lett. B* **575**, 1 (2003).

[344] L. Amendola et al. *Phys. Rev. D* **75**, 083504 (2007).

[345] A. A. Starobinsky. *Phys. Lett. B* **91**, 99 (1980).

[346] G. Cognola et al. *Phys. Rev. D* **77**, 046009 (2008).

[347] A. De Felice and S. Tsujikawa. *Living Rev. Relativ.* **13**, 3 (2010).

[348] R. C. Nunes et al. *J. Cosmol. Astropart. Phys.* **2017**:01, 005.

[349] V. Faraoni. *Phys. Rev. D* **74**, 104017 (2006).

[350] J. Khoury and A. Weltman. *Phys. Rev. Lett.* **93**, 171104 (2004).

[351] P. Brax et al. *Phys. Rev. D* **78**, 104021 (2008).

[352] A. de la Cruz-Dombriz et al. *Phys. Rev. D* **93**, 084016 (2016).

[353] S. D. Odintsov, D. Sáez-Chillón Gómez and G. S. Sharov. *Eur. Phys. J. C* **77**, 862 (2017).

[354] A. A. Starobinsky. *J. Exp. Theor. Phys.* **86**, 157 (2007).

[355] S. Tsujikawa. *Phys. Rev. D* **77**, 023507 (2008).

[356] J. Pérez-Romero and S. Nesseris. *Phys. Rev. D* **97**, 023525 (2018).

[357] S. Basilakos, S. Nesseris and L. Perivolaropoulos. *Phys. Rev. D* **87**, 123529 (2013).

[358] K. Bamba et al. *Class. Quant. Grav.* **30**, 015008 (2013).

[359] D. M. Scolnic et al. *Astrophys. J.* **859**, 101 (2018).

[360] G.-B. Zhao et al. *Mon. Not. R. Astron. Soc.* **482**, 3497 (2019).

[361] T. Brinckmann and J. Lesgourgues. arXiv:1804.07261.

[362] S. Capozziello et al. *J. Cosmol. Astropart. Phys.* **2005**:04, 005.

[363] G.-J. Wang et al. *Astrophys. J.* **847**, 45 (2017).

[364] A. R. Liddle and D. H. Lyth. *Phys. Rep.* **231**, 1 (1993).

[365] A. L. Coil. In *Planets, Stars and Stellar Systems* (T. D. Oswalt and W. C. Keel, eds.), p. 387, Springer, Dordrecht, 2013.

[366] J. A. Wheeler and K. Ford, *Geons, Black Holes, and Quantum Foam: A Life in Physics*. W. W. Norton & Co., New York, 1998.

[367] V. F. Mukhanov, H. A. Feldman and R. H. Brandenberger. *Phys. Rep.* **215**, 203 (1992).

[368] J. M. Bardeen. *Phys. Rev. D* **22**, 1882 (1980).

[369] C.-P. Ma and E. Bertschinger. *Astrophys. J.* **455**, 7 (1995).

[370] E. Bertschinger. In *Cosmology and Large Scale Structure: Proceedings of the "Les Houches École d'Été de Physique Théorique"* (R. Schaeffer, J. Silk, M. Spiro and J. Zinn-Justin, eds.), p. 273, Elsevier Scientific, Amsterdam, 1996.

[371] H. Kurki-Suonio, *Cosmological Perturbation Theory, part 1.* Lecture notes; University of Helsinki: Helsinki, Finland, 2020. www.courses.physics.helsinki.fi/teor/cpt/.

[372] J.-c. Hwang and H. Noh. *Phys. Rev. D* **65**, 023512 (2001).

[373] A. A. Asgari, A. H. Abbassi and J. Khodagholizadeh. *Eur. Phys. J. C* **74**, 2917 (2014).

[374] L. Amendola and S. Tsujikawa, *Dark Energy: Theory and Observations.* Cambridge University Press, New York, 2010.

[375] L. F. Abbott and R. K. Schaefer. *Astrophys. J.* **308**, 546 (1986).

[376] P. G. Ferreira. *Annu. Rev. Astron. Astrophys.* **57**, 335 (2019).

[377] L. Pogosian and A. Silvestri. *Phys. Rev. D* **94**, 104014 (2016).

[378] W. Hu and I. Sawicki. *Phys. Rev. D* **76**, 104043 (2007).

[379] M. Ishak. *Living Rev. Relativ.* **22**, 1 (2018).

[380] S. Tsujikawa, K. Uddin and R. Tavakol. *Phys. Rev. D* **77**, 043007 (2008).

[381] M.-C. Chiu et al. *Phys. Rev. D* **92**, 103514 (2015).

[382] G. Esposito-Farèse and D. Polarski. *Phys. Rev. D* **63**, 063504 (2001).

[383] L. Amendola et al. *Living Rev. Relativ.* **21**, 2 (2018).

[384] Dark Energy Survey Collaboration, T. M. C. Abbott et al. *Phys. Rev. D* **98**, 043526 (2018).

[385] C. Pallis. In *The Identification of Dark Matter* (M. Axenides, G. Fanourakis and J. Vergados, eds.), p. 602, World Scientific, Singapore, 2007.

[386] D. van Ravenzwaaij, P. Cassey and S. D. Brown. *Psychon. Bull. Rev.* **25**, 143 (2018).

[387] P. D. Hoff, *A First Course in Bayesian Statistical Methods*. Springer Science+Business Media, New York, 2009.

[388] D. W. Hogg and D. Foreman-Mackey. *Astrophys. J. Suppl. S.* **236**, 11 (2018).

[389] J. S. Speagle. arXiv:1909.12313v2.

[390] R. J. Barlow, *Statistics – A Guide to the Use of Statistical Methods in the Physical Sciences*. John Wiley & Sons, Chichester, England, 1989.

[391] G. Bohm and G. Zech, *Introduction to Statistics and Data Analysis for Physicists*. Verlag Deutsches Elektronen-Synchrotron, Hamburg, 2010.